Census and Characterization of Nearby Infrared Excess Stars

by

Tara Hufford Cotten

(Under the Direction of Inseok Song)

Abstract

Debris disk stars are the workshops for planetary formation and evolution and excess emission in the infrared serves as the signpost. The disk of tenuous dust surrounding a main-sequence star is analogous to our own Solar System. The goal of this study is to understand the evolution of a star and its relationship to the circumstellar dust as well as develop connections to planetary formation. Since there exist a plethora of conjectures which tie the disk to stellar properties albeit with weak statistical influence, this work provides an unprecedented number of sources to explore these relationships.

A comprehensive collection of stars which display infrared excess were first compiled from many published studies over the past three decades. Concurrent to the literature sources, a new search for excess using the recent release of the AllWISE catalog resulted in an extensive catalog of stars. The development of algorithms to identify and exclude stars masquerading as infrared excess emission ensured the highest fidelity that these stars host a debris disk.

Some of the unanswered questions regarding relationships between a star and its circumstellar material include: How does the dust evolve?; Does the angular momentum of the star affect the debris disk phase?; Is it true that the amount of metals contained in the star suggests the amount of material in the disk?; Does the presence of a stellar compan-

ion hinder or promote the formation and evolution of a debris disk? In order to begin to address these claims, a large number of debris disk stars with reliable stellar parameters is needed. Archival optical spectroscopy and new observations for over 500 stars yielded many stellar parameters including rotational velocity, equivalent width of Hα and Li 6708Å, radial velocity, metallicity, activity indicators (Ca II H & K), and age. This investigation sought confirmation of the nature in which infrared excess decays over time and if there are observational signatures to confirm the idea that a stellar companion is expected to disrupt the star's ability to host a debris disk. In addition, the search for stars with debris disks offered an ideal sample to investigate the unanswered questions of whether a large stellar metal content inherently produces a large amount of circumstellar material that is ideal for planet formation or whether there is a direct connection between the debris disk and the stellar rotation where the disk serves as a means to remove angular momentum from the host star. The comprehensive catalog of debris disk stars confirms the nature of the evolution as dust decreases over time, but negated assertions regarding rotation, metallicity, and multiplicity of the star as primary influences on the dustiness of a disk. Thus, this work suggests that collisional grinding accounts for the main method of dust production and the initiator of these collisions must be tied to planetary evolution.

INDEX WORDS: Main Sequence Stars, Infrared Astronomy, Circumstellar Disks

Census and Characterization of Nearby Infrared Excess Stars

by

Tara Hufford Cotten

B.S., Loyola University Chicago, 2010

A Dissertation Submitted to the Graduate Faculty
of The University of Georgia in Partial Fulfillment
of the
Requirements for the Degree

Doctor of Philosophy

Athens, Georgia

2016

Census and Characterization of Nearby Infrared Excess Stars

by

Tara Hufford Cotten

Approved:

Major Professor: Inseok Song

Committee: Jean-Pierre Caillault
Loris Magnani

Electronic Version Approved:

Suzanne Barbour
Dean of the Graduate School
The University of Georgia
December 2016

Dedication

I dedicate this work to my

incredible parents

and husband.

Acknowledgments

I first want to acknowledge the unwaivering support of my advisors at the University of Georgia. Prof. Inseok Song has guided me and challenged me to become the best astronomer, student, and mentor that I can. I would not have learned as much as I did without him. A sincere thanks goes to Prof. Loris Magnani and Prof. J. P. Caillault who provided me with meaningful discussions and advice to help with all of the challenges of graduate school.

Next, I want to thank my husband, David Cotten, for all of his encouragement. I would not be where I am today without his support, love, and selflessness. His constant praise and humor continue to make every day enjoyable and help me strive to be better.

Without my parents, I would never achieved all of my dreams so far. Besides being able to provide for the amazing opportunities that graduate school has enabled me, their support gave me the motivation to keep growing and learning. I love them tremendously and cannot say thank you enough.

Finally, I would be remiss to exclude the friends and colleagues who have meant so much to me during my time at UGA. I am extremely grateful for Dr. Adam Schneider, whose mentorship blossomed into an amazing friendship. I want to thank him especially for the helpful suggestions and recommendations for ongoing projects and future work. I also want to thank Jinhee Lee for being an amazing friend, conference partner, and office mate. Our astronomy discussions were always insightful and I enjoy all of our time together. Additional thanks to my other office mate, Lauren Sgro, who has helped me develop confidence in understanding astronomy through our many discussions. Lastly, I thank Dr. Kyle Walker for a friendship that continues to grow stronger. His support, jokes and comics, encouragement, and discussions have helped me through my entire graduate career and I look forward to many more in the future.

Table of Contents

List of Figures

List of Tables

Chapter 1

Introduction

What is our place in the Universe? Is it unique? Our understanding of planetary systems has grown significantly in the last few decades upon the discovery of over 3000 confirmed planets around other stars in our galaxy[1]. Current exoplanet searches are limited by planet size, and the technology to directly image an exo-Earth is still many years in the future. Until that time, debris disks play a key role in the detection of planetary systems as they provide a variety of host stars and planetesimal environments.

The discovery of the debris disk surrounding Vega using the *Infrared Astronomical Satellite* (IRAS) by Aumann et al. (1984) inspired the ability to use excess emission in the infrared to identify circumstellar disks. Starlight is absorbed by dust grains and reradiated (Wyatt 2008), and thus detected as emission in excess above the expected stellar photosphere at thermal wavelengths. Figure 1.1 displays the spectral energy distribution (SED) for Vega using all of the current photometry available to emphasize the ability to distinguish dust due to a circumstellar disk above the stellar photosphere. The dust is generally optically thin and found surrounding mature stars in locations analogous to our Solar System's Asteroid and Kuiper belts. Following planetary formation, small dust grains and gas are efficiently removed from the protoplanetary disk, and Backman & Paresce (1993) infer that debris disks must originate from recent collisional activity between planetestimals, asteroids, and comets (Kenyon & Bromley 2004). Thus, debris disks are intimately linked to the formation and evolution of planetary systems and addresses investigations into the conditions that are necessary to form planets, especially terrestrial planets.

[1]NASA Exoplanet Archive: http://exoplanetarchive.ipac.caltech.edu

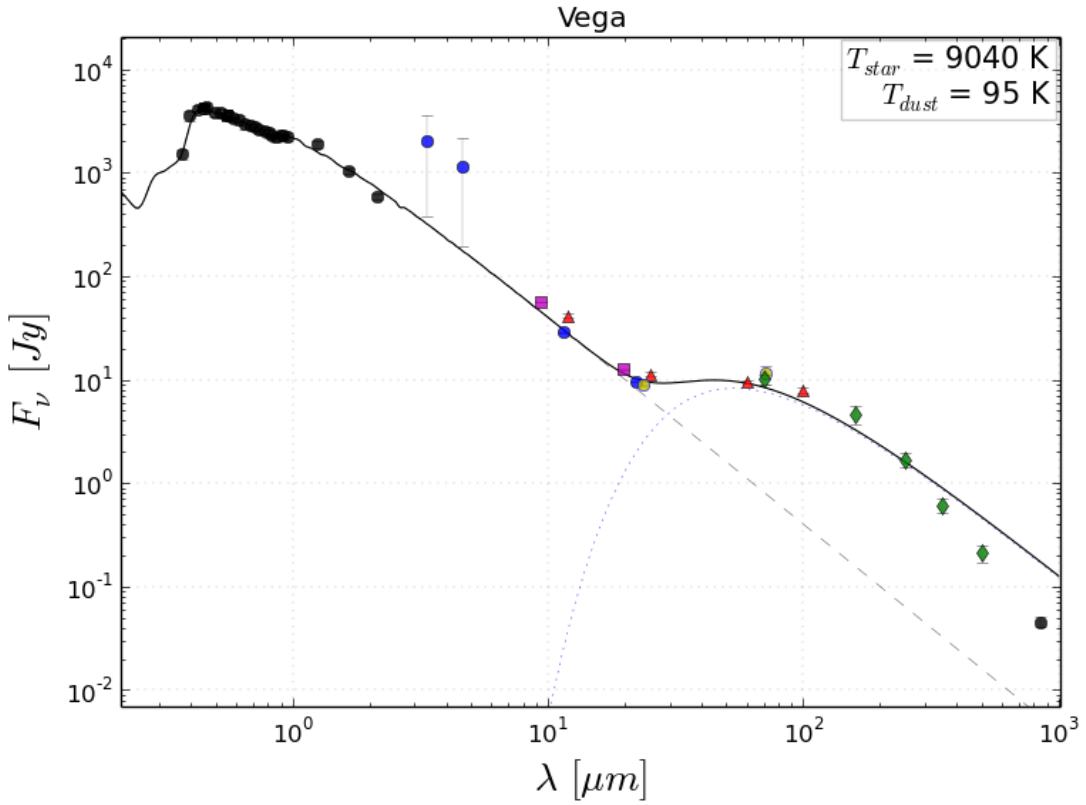

Figure 1.1: Spectral energy distribution of Vega displayed as the flux (in janskys) versus the wavelength in log scale. The black data points represent optical photometry from various instruments and near-infrared photometry from the Two-Micron All-Sky Survey (2MASS). The blue circles are AllWISE data, magenta are from AKARI, red from IRAS, yellow from *Spitzer* MIPS, and green from *Herschel* PACS and SPIRE. Sub-millimeter data from the SCUBA instrument is plotted as a black circle as well. The original discovery of Vega was found using only the red triangles from IRAS, but has since been confirmed out to far-infrared and sub-millimeter wavelengths.

Following its discovery in 1984, Smith & Terrile (1984) investigated the disk around β Pictoris using direct imaging and were able to confirm the findings of IRAS and the use of infrared excess. Imaging techniques have become even more precise in recent years, and Apai et al. (2015) have discussed structures such as warps and gaps within the disk itself. However, the true amalgamation of exoplanet and debris disk science comes from the discovery of planets in addition to the debris disk around β Pictoris as was reconfirmed by Millar-Blanchaer et al. (2015). Similar to β Pictoris, Fomalhaut has been observed to have an inner and outer component to its debris disk (Kalas et al. 2005; Mennesson et al. 2013) as well as a planet embedded in the disk (Kalas et al. 2008). Kalas et al. (2013) have traced the motion of the planet and believe it will interact with the dust belt within the next two decades. Thus, infrared excess indicates circumstellar material and can be linked to planetary formation and evolution.

Many studies have confirmed the use of excess emission in the infrared to identify debris disk stars (Beichman et al. 2006b; Bryden et al. 2006b; Su et al. 2006; Gautier et al. 2007; Moro-Martin et al. 2007a; Rhee et al. 2007; Hillenbrand et al. 2008; Trilling et al. 2008; Carpenter et al. 2009; Greaves et al. 2009; Morales et al. 2012; Bulger et al. 2013; Eiroa et al. 2013; Patel et al. 2014). The infrared missions and instruments that have enabled these discoveries include *Infrared Astronomical Satellite* (IRAS), *Infrared Space Observatory* (ISO), *Spitzer Space Telescope* MIPS and IRS, *AKARI*, *Herschel Space Observatory* PACS and SPIRE, *Wide-Field Infrared Survey Explorer* (WISE) and all-sky release, AllWISE, as well as more recent sub-millimeter instruments such as *Atacama Large Millimeter/Sub-millimeter Array* (ALMA). Progress in the field of debris disk science and its use as a signpost for planetary formation can be identified in the thousands of debris disk candidates reported in over 200 literature sources displayed in Figure 1.2. However, the conclusion of the WISE mission, which provides observations of over 700 million sources, may be the final opportunity to create the largest, all-sky infrared survey to facilitate the creation of a

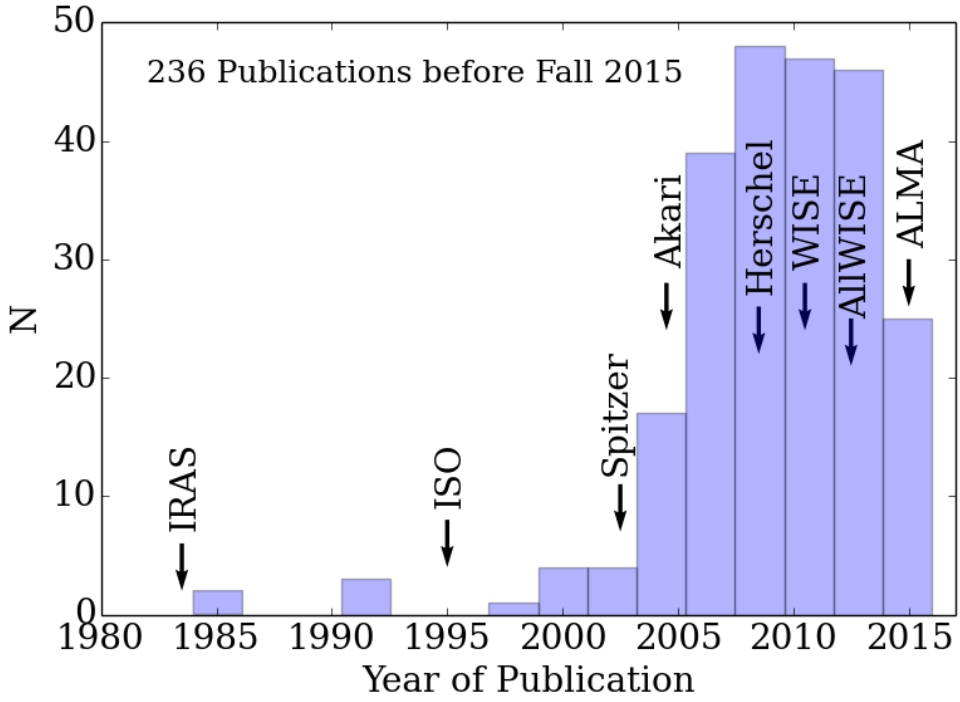

Figure 1.2: Number of publications involving infrared excess and debris disks published following the IRAS survey and the discovery of the debris disk around Vega (Aumann et al. 1984). Surveys which were instrumental to debris disk science are labeled according to the year of their data release (See Section 2.2 for more details regarding this figure). Publications released in 2016 were not included in this study.

comprehensive catalog of debris disk stars using infrared excess. In combination with the catalog of the Two Million Brightest Stars (Tycho-2; Høg et al. 2000), this project seeks a uniform analysis of infrared excess and to thoroughly characterize the sources in the solar neighborhood discovered to have circumstellar disks.

1.1 Difficulties in Debris Disk Identification

While it seems straightforward to use infrared excess to identify stars with debris disks, difficulty arises in uniting these efforts due to a number of reasons. First, Song et al. (2002) and Bulger et al. (2013) point out that studies have been plagued by false infrared excess (IR excess) stars. False excess occurs due to discrepancies between imaging and

photometric measurements as the result of the instrument beam size and background object contamination (source confusion). Even the most recent mission by WISE with a beam size of $\sim 12.''0$ at 22μm (WISE band W4) is unable to resolve the disk from the star at distances of only a few parsecs and so the image of the star and any existing circumstellar disk appears as a point source. Studies such as Krivov et al. (2013) notice this issue and point out the contamination rate of colder IR excess (due to larger grains) is higher due to less sensitivity of far-IR instruments. In addition, Rhee et al. (2007) described that a star's distance causes contamination since cirrus and heated dust in the interstellar medium (ISM) outside of the Local Bubble (a region of very low gas density compared to the galactic ISM; Galeazzi et al. 2014) can artificially enhance a detection of infrared excess. Kalas et al. (2002) examined five stellar sources surrounded by reflection nebulosity masquerading as IR excess that should not be attributed to the same phenomenon as a dusty debris disk and conclude that stars beyond 100 pc should be accepted as disk candidate stars with caution. Techniques to remove false excess stars have previously been lacking.

Second, investigations throughout the past decades use various criteria to identify debris disk stars through excess emission. In particular, Gorlova et al. (2004), Avenhaus et al. (2012), Wu et al. (2013), and Patel et al. (2014) select debris disk stars using a color criterion that involves multiple infrared passbands. Other studies prefer to use a comparison of flux in each individual passband to the stellar photosphere estimated using photometry and the spectral energy distribution, essentially comparing direct measurement to what is predicted or expected for that host star at a particular wavelength. The differences between these two methods can be seen in Figure 1.3 using a sample of stars from Wu et al. (2013).

Lastly, recent studies such as Schneider et al. (2013) and Kennedy & Wyatt (2013) highlight the necessity to distinguish between a protoplanetary and a post-protoplanetary disk since the impacts of understanding debris disk evolution is essential. Wyatt et al. (2015) describe in detail the properties and distinctions between protoplanetary disks and their evolution into optically thin debris disks. Such a distinction is crucial in interpreting

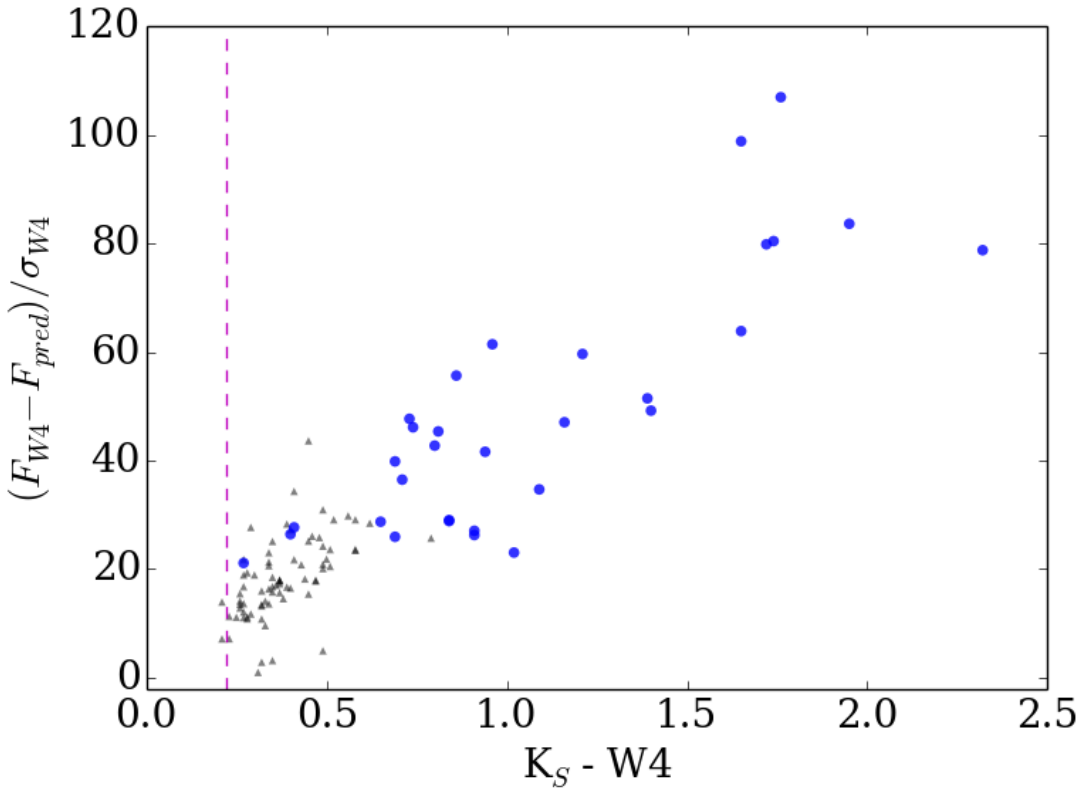

Figure 1.3: Example of different IR excess criteria using a sample of stars designated to have IR excess by Wu et al. (2013). The study by Wu et al. (2013) used a color comparison between the 2MASS K_S and WISE W4 passbands and selected stars to the right of the vertical dashed line in the figure. All the sources were reproduced in the study by Cotten & Song (2016), however, only those shown as blue circles were reproduced as true IR excess stars using the comparison between measured and predicted fluxes at W4.

the evolutionary state of the system and putting the dust grain size and environment into the perspective of planetary formation. Therefore, this work focuses on using IR excess as a tool but hinges on the identification of these systems as true IR excess sources indicative of hosting a debris disk through confirming evidence of excess emission at more than one wavelength. Along with a number of image contamination procedures, we compile stars with the highest reliability of hosting a debris disk.

1.2 Assessing The Connection Between Stars and Disks

Debris disks are believed to be in a steady state of evolution (Wyatt 2008). This implies a collisional grinding of planetestimals that leads to a distribution of grain sizes throughout the disk (Backman & Paresce 1993). Zuckerman (2001) describe this understanding in the context of young, optically thick disks that still maintain primordial material from the formation of the star. The primordial dust will experience effects from radiation pressure, Poynting-Robertson drag, as well as collisions that gradually diminish grain sizes and allow smaller grains to feel the effects of the aforementioned forces Wyatt (2008). Backman & Paresce (1993) derive timescales for each of these processes in order to determine that typically grains within 100 AU of the star would be removed on the order of 10^5 years. Thus, stars older than 1 Myr are most likely to have dust formed from regenerative procedures, namely, collisions, and research postulates a decline of IR excess with time. The exact nature of the decline of dust from second generation collisions requires observational evidence. Early studies such as Dominik & Decin (2003) and Rieke et al. (2005) established that the age of a star and the amount of IR excess are inversely related. More recent investigations point out that different spectral types will have a different evolutionary influence on the circumstellar material and Siegler et al. (2007) and Carpenter et al. (2009) suggest a faster rate of evolution for later spectral types. Kains et al. (2011) further identify the necessity to specify the location of the dust in solidifying a relationship with age. Debris disks provide the key to constraining the evolutionary context of dust in planetary systems.

Besides the time constraint in developing planetary systems, parameters that describe the environment of the formation of the star and disk are believed to yield evidence to how our Solar System formed. One parameter in particular, metallicity, identifies the amount of elements heavier than hydrogen and helium available during the star's collapse since they are difficult to form through fusion alone. Fischer & Valenti (2005) established a correlation between high metallicity stars and gas giant planets such that if a star is born with a higher metal content then it possesses a higher probability for hosting giant planets. Wyatt et al. (2007) recognized that the Core Condensation Planet Formation Theory predicts this relationship between metallicity and giant planets. The theory suggests that if more material is available during the formation of the star and disk, this leads to larger reservoirs of material necessary for the formation of the cores of giant planets. This theory was in competition at the time with ideas that the planets themselves were polluting the atmospheres of the host star (Gonzalez 1997). Since the circumstellar disk participates in the formation of reservoirs of material, this led to the search for a relationship between metallicity and debris disks. However, Beichman et al. (2006b), Greaves et al. (2006), Kospal et al. (2009), and Maldonado et al. (2012) were unable to identify a correlation between high metallicity stars and IR excess indicative of a debris disk.

Stellar angular momentum and its connection to the evolution of the disk has become a recent topic in debris disk studies due to the "angular momentum problem" (Kundurthy et al. 2006). Herbst et al. (2007) states that there is a significant discrepancy between observations of the angular momentum of protostellar clouds rotating much faster than stars on the main-sequence. Since the evolution of a star typically involves a circumstellar disk of material, Herbst et al. (2007) and Bouvier et al. (2014) and references therein identify a theoretical connection between the star and the disk such that the disk contributes to the slowing of the host star. The theory of "disk-locking" suggested by many (Shu et al. 1994; Bouvier et al. 1997) is understood to create the correlation such that rapidly rotating stars are less likely to host a circumstellar disk while slow rotators are more likely to maintain

significant disk mass in relation to the primordial disk mass. However, the applications of this theory to the effects on debris disk dust are not fully understood. Rebull et al. (2006) and Kundurthy et al. (2006) confirmed the disk-locking theory with observations of pre-main-sequence disks that were found to have larger mid-IR excesses around slowly rotating stars. Discrepancies arose between the findings of Sierchio et al. (2010) who corroborated the results of Rebull et al. (2006) and Kundurthy et al. (2006) using debris disk stars while Mizusawa et al. (2012) found a sample of dustier debris disk stars that are rotating faster than expected. While trying to focus on the entire range of spectral types and dust removal mechanisms, the investigation presented here pursues whether rotation can be directly linked to the aid or hindrance of the dustiness of a mature debris disk star.

Finally, models predict that the stellar environment involving companions should effect the development and/or evolution of debris disks around stars. Fischer & Marcy (1992) found that nearby stars with companions are more prevalent than single stars, especially amongst late-type stars. Many studies then went on to investigate whether a companion would hinder or promote planetary growth (Duchêne & Kraus 2013); however, understanding these complex environments can be extremely challenging. Providing more incentive to understand binary systems, Horch et al. (2014) found that nearly half of the systems they investigated from the Kepler mission (Borucki et al. 2010) had gravitationally bound companion stars. Trilling et al. (2007) found a marginally higher incidence for IR excess in binary star systems and began a discussion regarding whether the companion system contains more material for planetary formation from birth or whether the stellar companion instigates the collisions that produce dust. However, Rodriguez & Zuckerman (2012) pointed out that debris disks were less common around multiple stars and implied the companion encourages more efficient clearing times for dust grains around multiple star systems. Consequently, Armstrong et al. (2014) discussed the important implications of finding low mass planets around binary systems as a result of gas dispersal which leaves more rocky material for the development of terrestrial-like planets.

Debris disks represent a significant epoch of planetary formation and evolution, especially in understanding the evolution of our Solar System. Analogous in structure, except for the amount of dust since technology limits the detection of faint, cold dust, debris disks are believed to be the closest comparison to the Asteroid and Kuiper belts. Therefore, in order to advance our understanding of stellar and planetary formation and evolution, infrared excess and debris disks are essential. While many studies have made progress with regard to debris disk evolution, often the number of stars with debris disks is limited. The number of debris disk stars presented in this work is unprecedented. This project highlights the historical influence of these investigations through the collection of previously claimed debris disk stars, but also strives to establish relationships between the host star and the circumstellar material by including newly found infrared excess stars.

The second chapter of this thesis contains a description of the creation of a comprehensive census including a summary of the history of debris disk science and a new search for IR excess stars. Importantly, the second chapter describes the methods used to remove contaminators and false positive IR excess sources and identify the most reliable stars that host a debris disk. Observations of several census stars and the derivation of key fundamental parameters including age, metallicity, rotation, and multiplicity are contained in Chapter 3. The remainder of Chapter 3 discusses the investigation into the relationships between the star and its circumstellar material. Chapters 4 and 5 describe the applications for future work to enhance the understanding of debris disk stars as well as the conclusions of this project.

Chapter 2

A Comprehensive Census of Nearby Infrared Excess Stars[1]

[1]Cotten, T. H. and Song, I., 2016, *The Astrophysical Journal Supplement Series*, Vol. 225, No. 15. Reprinted here with permission of publisher and authors.

2.1 Introduction

Excess emission in the infrared (IR excess, hereafter) provides a useful tracer of the dust in a circumstellar disk due to the process by which the dust grains are heated by the starlight and reemit at longer wavelengths. Identifying each distinct evolutionary phase can be challenging but is possible since the shape of the IR excess depends on the size, temperature, and composition of the emitting dust grains. While it is understood that as the protoplanetary disk evolves, the gas and dust is cleared from the inner region closest to the star and then from the outer regions (Wyatt et al. 2015), the discovery of the first debris disk around Vega (Aumann et al. 1984) using the *Infrared Astronomical Satellite* (*IRAS*; Beichman et al. 1988), provided evidence for a secondary generation of dust. The secondary origin of this dust around a mature stellar system must be the result of the collisional grinding of planetesimals, comets, and asteroids (Kenyon & Bromley 2008). The information gathered from IR excess stars provides a link to the formation and evolution of exoplanets (Wyatt 2008).

Many studies (Beichman et al. 2006b, Bryden et al. 2006a, Su et al. 2006, Gautier et al. 2007, Moro-Martin et al. 2007b, Rhee et al. 2007, Hillenbrand et al. 2008, Trilling et al. 2008, Carpenter et al. 2009, Greaves et al. 2009, Morales et al. 2012, Bulger et al. 2013, Eiroa et al. 2013, Patel et al. 2014) have confirmed the use of excess emission in the infrared as an indicator for circumstellar dust. Table 2.1 shows the notable infrared surveys that were developed to improve the sensitivity of *IRAS* and were used in the detection of debris disk stars. Circumstellar material in locations analogous to our Kuiper and Asteroid belts can be detected by excess emission at $\geq 10 \mu m$ wavelengths, and the past few decades have allowed for the exploration of disk properties such as dust temperature ranging from very cold ($\sim$ 10 K) to warm ($\sim$ 500 K). At the current time, all major mid- to far-infrared space missions have finished operations, including the most recent *Herschel Space Observatory* (Pilbratt et al. 2010) and the *Wide-Field Infrared Survey Explorer* (*WISE*; Wright et al. 2010). Studies have shifted to analyze data available through archives. With the advent of

Table 2.1: Completed Infrared Space Mission Instruments.

Instrument	Filter Wavelength (μm)	Ang Res (arcsec)	Year of Launch	Comments
IRAS	12, 25, 60, 100	30 - 120	1983	all-sky, 96%, 250,000 sources
ISO	2.5 - 240	1.5 - 90	1995	30,000 pointed obs.
Spitzer MIPS	24, 70, 160	6 - 40	2003	$\sim$42 million pointed obs.
AKARI	9, 18	$\sim$60	2006	all-sky, 870,000 sources
Herschel PACS	70, 100, 160	5 - 13	2008	$\sim$40,000 pointed obs.
Herschel SPIRE	250, 350, 500	18 - 36	2008	$\sim$40,000 pointed obs.
WISE	3.5, 4.6, 12, 22	6.1 - 12	2009	all-sky, >500 million sources
AllWISE	3.5, 4.6, 12, 22	6.1 - 12	2009	all-sky, >740 million sources

new infrared missions still a couple years in the future (e.g. *James Webb Space Telescope* [*JWST*]; Gardner et al. 2006), we are at a unique time in which we can devote adequate effort to thoroughly characterizing known IR excess stars in the solar neighborhood.

The use of IR excess has generated hundreds of publications, as well as thousands of claimed IR excess stars. Focusing specifically on sources that attest to dust undergoing recent collisional activity, as in the case of debris disks, each of these studies presented various source selection and infrared excess criteria. However, many problematic IR excess candidate stars present conflicting evidence based on these different criteria. Therefore, a vetted list of IR excess stars is needed to maximize the scientific return of imminent next-generation missions (*JWST* and *Wide-Field Infrared Survey Telescope* [*WFIRST*]) and currently ongoing missions with new extreme adaptive optics instruments such as Gemini Planet Imager (Macintosh et al. 2006) and Spectro-Polarimetric High-contrast Exoplanet REsearch (Beuzit et al. 2008). Yet, we need to unify the search for IR excess stars through simultaneous examination of both previous and new findings of IR excess.

The most comprehensive catalog of nearby IR excess stars is created here through the combination of (1) a literature search for far-IR excess stars discovered with the *Spitzer Space Telescope*, *Herschel Space Observatory,* and *IRAS* (Section 2.2) and (2) a new search for mid-IR excess stars using the all-sky *Wide-Field Infrared Survey Explorer* catalog (AllWISE, Wright et al. 2010; Section 2.3). The paper begins with a description of our literature search

of over 200 published articles that present many IR excess and debris disk stars, and we describe our reanalysis of the claimed IR excess. Section 2.3 recounts our new investigation IR excess stars with warm dust radiating at $\geq 10\mu$m through the cross-correlation between the Tycho-2 catalog (Høg et al. 2000) and the AllWISE catalog, providing significant additions to historical infrared studies. We compare our Tycho-2/AllWISE cross-match to similar warm dust studies performed recently in Section 2.4. Characteristics of the final IR excess catalog are provided in Sections 2.5 and 2.6, followed by our conclusions and future work described in Section 2.7.

2.2 Literature Search

Following Aumann et al. (1984), many studies reported new discoveries of IR excess stars. To summarize known IR excess stars from the literature, we select a few pivotal investigations involving *IRAS* and *Spitzer* as well as a review article: Rieke et al. (2005), Rhee et al. (2007), and Wyatt (2008). Besides the lists of authentic excess stars in each of these reports, citations included in these articles provide the basis of our literature search. We meticulously comb over 230 articles (displayed in Table 2.2) that cite at least one of these three pivotal papers for stars claimed to have IR excess and compile a database of these objects. The collection of previous publications excludes any searches for IR excess candidates that singularly used *WISE*, since this was the intent of our new infrared search presented later in Section 2.3.

Table 2.2: Summary of References Used in Literature Search for Previously Claimed IR Excess Stars

Author	Year	Author	Year	Author	Year
Aumann et al.	1984	Sadakane & Nishida	1986	Jura	1991
Patten & Willson	1991	Oudmaijer et al.	1992	Mannings & Barlow	1998
Decin et al.	2000	Song et al.	2001	Spangler et al.	2001
Sylvester et al.	2001	Laureijs et al.	2002	Song et al.	2002
Weinberger et al.	2003	Wyatt et al.	2003	Gorlova et al.	2004
Greaves et al.	2004	Jura et al.	2004	Liu et al.	2004
Metchev et al.	2004	Zuckerman & Song	2004a	Zuckerman & Song	2004b

Continued on Next Page...

Table 2.2 – Continued

Author	Year	Author	Year	Author	Year
Beichman et al.	2005	Chen et al.	2005a	Chen et al.	2005b
Greaves et al.	2005	Kim et al.	2005	Low et al.	2005
Najita & Williams	2005	Rieke et al.	2005	Song et al.	2005
Su et al.	2005	Beichman et al.	2006a	Beichman et al.	2006b
Bryden et al.	2006a	Bryden et al.	2006b	Carpenter et al.	2006
Chen et al.	2006	Gorlova et al.	2006	Goto et al.	2006
Hernandez et al.	2006	Hines et al.	2006	Kalas et al.	2006
Lestrade et al.	2006	Moor et al.	2006	Riaz et al.	2006
Silverstone et al.	2006	Smith et al.	2006	Su et al.	2006
Williams & Andrews	2006	Cieza et al.	2007	Gautier et al.	2007
Gorlova et al.	2007	Guieu et al.	2007	Hernandez et al.	2007
Kalas et al.	2007a	Kalas et al.	2007b	Lafreniere et al.	2007
Lisse et al.	2007	Luhman et al.	2007	Matthews et al.	2007a
Matthews et al.	2007b	Moerchen et al.	2007a	Moerchen et al.	2007b
Moro-Martin et al.	2007	Rhee et al.	2007	Rhee et al.	2007b
Siegler et al.	2007	Trilling et al.	2007	Wyatt et al.	2007a
Wyatt et al.	2007	Absil et al.	2008	Brown et al.	2008
Chen et al.	2008	Cieza et al.	2008	Gautier et al.	2008
Hernandez et al.	2008	Hillenbrand et al.	2008	Kastner et al.	2008
Marois et al.	2008	Merin et al.	2008	Meyer et al.	2008
Rebull et al.	2008	Rhee et al.	2008	Roberge & Weinberger	2008
Smith et al.	2008	Su et al.	2008	Trilling et al.	2008
Weinberger	2008	Wyatt	2008	Akeson et al.	2009
Balog et al.	2009	Booth et al.	2009	Brown et al.	2009
Bryden et al.	2009	Carpenter et al.	2009	Fujiwara et al.	2009a
Fujiwara et al.	2009b	Gáspár et al.	2009	Greaves et al.	2009
Gutermuth et al.	2009	Hernandez et al.	2009	Kospal et al.	2009
Lawler et al.	2009	Lestrade et al.	2009	Maness et al.	2009
Melis et al.	2009	Metchev et al.	2009	Moor et al.	2009
Morales et al.	2009	Nilsson et al.	2009	Plavchan et al.	2009
Roccatagliata et al.	2009	Schneider et al.	2009	Sicilia-Aguilar et al.	2009
Smith et al.	2009	Smith et al.	2009	Su et al.	2009
Tanner et al.	2009	Ardila et al.	2010	Bonsor & Wyatt	2010
Buenzli et al.	2010	Cieza et al.	2010	Duchêne et al.	2010
Eiroa et al.	2010	Gizis	2010	Greaves et al.	2010
Grinin et al.	2010	Kastner et al.	2010	Kennedy et al.	2010
Koerner et al.	2010	Krivov et al.	2010	Lagrange et al.	2010
Liseau et al.	2010	Matthews et al.	2010	Melis et al.	2010
Moerchen et al.	2010	Monin et al.	2010	Moro-Martin et al.	2010

Continued on Next Page...

Table 2.2 – Continued

Author	Year	Author	Year	Author	Year
Nilsson et al.	2010	Rebull et al.	2010	Sierchio et al.	2010
Smith & Wyatt	2010	Stock et al.	2010	Thompson et al.	2010
Vandenbussche et al.	2010	Wahhaj et al.	2010	Chen et al.	2011
Churcher et al.	2011	Churcher et al.	2011	Currie et al.	2011
Desidera et al.	2011	Eiroa et al.	2011	Golimowski et al.	2011
Heng	2011	Kennedy et al.	2011	Marshall et al.	2011
Millan-Gabet et al.	2011	Moor et al.	2011	Morales et al.	2011
Patience et al.	2011	Peterson et al.	2011	Smith et al.	2011
Williams & Cieza	2011	Wilner et al.	2011	Zuckerman et al.	2011
Acke et al.	2012	Avenhaus et al.	2012	Chen et al.	2012
Cieza et al.	2012	Dahm et al.	2012	Donaldson et al.	2012
Ertel et al.	2012	Kennedy et al.	2012	Lawler & Gladman	2012
Lebreton et al.	2012	Lestrade et al.	2012	Luhman & Mamajek	2012
Maldonado et al.	2012	Melis et al.	2012	Meng et al.	2012
Mizusawa et al.	2012	Morales et al.	2012	Riaz & Gizis	2012
Riviere-Marichalar et al.	2012	Riviere-Marichalar et al.	2012	Rodigas et al.	2012
Rodriguez & Zuckerman	2012	Schneider et al.	2012	Smith & Jeffries	2012
Urban et al.	2012	Wyatt et al.	2012	Zuckerman & Song	2012
Zuckerman et al.	2012	Ballering et al.	2013	Bonsor et al.	2013
Booth et al.	2013	Broekhoven-Fiene et al.	2013	Bulger et al.	2013
Eiroa et al.	2013	Fujiwara et al.	2013	Gáspár et al.	2013
Janson et al.	2013	Mathews et al.	2013	Melis et al.	2013
Moor et al.	2013	Morales et al.	2013	Olofsson et al.	2013
Panic et al.	2013	Riviere-Marichalar et al.	2013	Schneider et al.	2013
Thalmann et al.	2013	Wahhaj et al.	2013	Bailey et al.	2014
Ballering et al.	2014	Bonsor et al.	2014	Carpenter et al.	2014
Esplin et al.	2014	Greaves et al.	2014	Greaves et al.	2014
Kennedy et al.	2014	Kennedy et al.	2014	Liu et al.	2014
Marshall et al.	2014	Panic et al.	2014	Pawellek et al.	2014
Ricci et al.	2014	Riviere-Marichalar et al.	2014	Rodigas et al.	2014
Soummer et al.	2014	Thureau et al.	2014	Wittenmyer et al.	2014
Hung et al.	2015	Jang-Condell et al.	2015	Maldonado et al.	2015
Moor et al.	2015	Rodigas et al.	2015		

In our creation of the main IR excess star catalog, we focus on identifying nearby, main-sequence stars with post-protoplanetary disks. However, without available age information,

we select disks through a characteristic inspection of the shape of the spectral energy distribution (SED). We assume that stars having photospheric AllWISE fluxes at W1 (3.5μm) and W2 (4.6μm) bands with clear excess emission at mid- to far-IR are sources involved in secondary dust generation. We reserve a discussion of the ages of these systems for a forthcoming paper using optical spectroscopy to characterize our primary target IR excess stars. Using these criteria, it is reasonable to assume that we will be missing the youngest disk counterparts, including many T Tauri and Herbig Ae/Be disks. Furthermore, we avoid publications that focused on circumstellar disks around very distant stars ($>$ 500 pc; e.g. Cloutier et al. 2014) or white dwarfs (e.g. Barber et al. 2012). For example, we keep only stars from Luhman & Mamajek (2012) that can be matched best to an "older", inner cleared disk with no excess emission at W1 or W2. Moreover, some studies provide lists of rejected sources (Rhee et al. 2007, Ballering et al. 2013) that enabled us to avoid stars confirmed to be non-excess.

To investigate the nature of apparent IR excess emission, we create an SED of all compiled candidate IR excess stars and perform several procedures to prevent including any false positives. The SED displays flux density versus wavelength from measured photometry, which is then fit to a Phoenix NextGen main-sequence stellar model (Hauschildt et al. 1999). For more details regarding the SED models and fitting, refer to Rhee et al. (2007). Roughly 820 stars were compiled and assessed from the literature search. However, since previous publications include evolved stars whose IR excess mechanism is different from that of main-sequence stars, we checked all IR excess candidate stars using SIMBAD and remove 20 stars with luminosity classes of I, II or III. Lastly, two key procedures for eliminating false-positive excess stars include the visual inspection of the SED and AllWISE images to remove possible contaminated sources (explained in full detail in Section 2.3.2). We use the VizieR database to gather additional photometry from optical to far-IR wavelengths if available. The multitude of photometric measurements ensures a reliable SED fit to the stellar photosphere and enables us to quantify the number of passbands that display IR excess

('Num_Excess'). Section 2.3.2 has more details regarding the parameter "Num_Excess". We remove 65 stars having photospheric flux at far-IR wavelengths (i.e. showing no IR excess).

Among IR excess publications, the work of Chen et al. (2014) is notable because they provided *Spitzer* IRS spectra of over 300 stars. When available, they also reported MIPS 24 and 70 μm measurements. Because the evidence of excess determined from infrared spectroscopy aids in the reliability of IR excess from photometry alone, we retain most stars from Chen et al. (2014) unless the IRS spectra are consistent with the photosphere.

To create the most useful catalog of IR excess stars for more efficient future follow-up observations, we implement additional restrictions for a star to be included in the "Prime" table: (1) AllWISE W3 (12 μm) or W4 (22 μm) flux being greater than 10 mJy, (2) distance within 120 pc and (3) either multiple passbands demonstrating IR excess ("Num_Excess">1) or one passband of IR excess and IRS spectroscopic confirmation of the photometric excess. These requirements ensure that stars in our final catalog are bright enough to be fully characterized. The distance restriction is sometimes relaxed to include few interesting stars with corroborating IRS spectra; however, no star beyond 150 pc was included. Our choice of distance cut, 120 pc, is mainly to remain inside of the local bubble in order to ignore interstellar reddening and nearby star-forming regions.

After all removals and restrictions, the literature sample of "Prime" IR excess stars (Table 2.3) contains ∼430 unique targets. Distant, faint, and marginal excess candidates are maintained in our "Reserved" star catalog (Table 2.4, an additional ∼300 stars). Hereafter, we shall refer to this list as the "literature IR excess stars." The catalog of literature IR excess stars and information regarding the star and disk parameters for this sample of stars are included in Tables 2.3 and 2.4. Each table's details are explained fully in Section 2.3.2.

Table 2.3: Prime IR Excess Stars from the Literature and Tycho-2 cross-correlation with AllWISE

Name	R.A. and Decl.	Spectral Type	$T_{*,SED}$ (K)	$R_{*,SED}$ ($R_\odot$)	T_{dust} (K)	R_{disk} (au)	T_{dust2} (K)	R_{disk2} (au)	$\frac{L_{IR}}{L_{star}}$ ($\times 10^{-4}$)	Dist. (pc)	Num Excess	λ_{start} (μm)	Has IRS?	Known Reference
HR 9102	00:04:20.3 -29:16:07	A0V	8820	2.58	200	11.6	70	95.5	1.37	124.84	2	22	N	Su et al. (2006)
HD 105	00:05:52.6 -41:45:11	G0V	6070	1.01	390	0.5	50	34.6	4.53	39.38	3	22	Y	Zuckerman & Song (2004a)
HD 166	00:06:37.1 +29:01:15	K0V	5700	0.78	300	0.6	70	12.1	3.56	13.67	4	22	Y	Bryden et al. (2006b)
HD 203	00:06:50.1 -23:06:27	F3V	6710	1.48	160	6.0	–	–	1.69	39.38	3	22	Y	Rebull et al. (2008)
HD 377[b]	00:08:25.8 +06:37:00	G2V	5910	1.03	200	2.1	60	23.4	5.31	39.07	3	22	Y	Moor et al. (2006)
sig And	00:18:19.6 +36:47:06	A2V	8780	2.00	155	14.9	–	–	0.19	41.32	3	22	Y	Morales et al. (2009)
HD 1466	00:18:26.2 -63:28:39	F8V	6140	1.06	140	4.7	–	–	1.68	41.54	2	22	Y	Smith et al. (2006)
HD 1461	00:18:42.1 -08:03:12	G3V	5880	1.07	65	20.5	–	–	0.50	23.24	1	22	Y	Lawler et al. (2009)
9 Cet	00:22:51.7 -12:12:33	G3V	5920	0.95	40	48.5	–	–	0.09	20.86	2	60	Y	Chen et al. (2014)
kap Phe	00:26:12.3 -43:40:46	A5IVn	8010	1.76	170	9.0	–	–	0.18	23.80	3	22	Y	Rieke et al. (2005)
HD 2834	00:31:24.9 -48:48:12	A1Va	8950	2.24	95	46.3	–	–	0.17	52.96	1	22	Y	Chen et al. (2014)
HD 2772	00:31:46.3 +54:31:20	B8Vn	12230	3.50	400	7.6	35	995.0	2.29	115.74	4	11	N	Chen et al. (2005a)
bet03 Tuc	00:32:44.0 -63:01:53	A0V	9050	1.63	300	3.4	150	13.8	2.73	45.55	5	11	Y	Song et al. (2001)
HD 3126	00:34:27.1 -06:30:14	F4V	6380	1.23	200	2.9	45	57.8	1.91	40.91	1	22	Y	Trilling et al. (2008)
HD 3296	00:36:02.0 -05:34:15	:F5	6450	1.46	60	39.2	–	–	0.23	45.04	1	22	Y	Trilling et al. (2008)
HD 3670	00:38:56.7 -52:32:03	F5V	6440	1.35	290	1.5	55	43.1	6.47	83.12[a]	1	22	Y	Moor et al. (2011)
64 Psc	00:48:58.7 +16:56:26	F8V	6570	1.52	300	1.7	–	–	1.38	23.45	2	60	N	Koerner et al. (2010)
HD 5133	00:53:01.1 -30:21:24	K2.5V	5170	0.66	30	45.7	–	–	0.11	14.17	3	60	N	Lawler et al. (2009)
66 Psc	00:54:35.2 +19:11:18	A1Vn	9340	2.70	250	8.7	35	447.8	2.20	108.10	2	22	Y	Rhee et al. (2007)
TYC2278-834-1	01:04:25.3 +31:18:27	:K0	5310	0.78	260	0.7	–	–	6.19	62.89[a]	2	11	N	–
V443 And	01:10:41.9 +42:55:54	G7V	5660	0.78	200	1.4	50	23.3	1.96	27.07	1	22	Y	Kim et al. (2005)
HR 333	01:12:17.3 +79:40:26	A3V	8920	2.41	80	69.7	–	–	1.88	82.84	2	22	N	Jura et al. (2004)
HD 7570	01:15:11.1 -45:31:54	F9VFe	6170	1.19	85	14.5	–	–	0.08	15.11	2	22	Y	Beichman et al. (2006a)
HD 7590	01:16:29.1 +42:56:21	G0V	6090	0.90	200	1.9	40	48.8	3.13	23.19	1	22	Y	Plavchan et al. (2009)
2MASS J01203226-1128035	01:20:32.3 -11:28:05	G9V	5500	0.75	300	0.5	–	–	1.96	34.39	1	22	Y	Carpenter et al. (2009)
HD 8907	01:28:34.4 +42:16:02	:F7	6250	1.23	50	45.0	–	–	2.85	34.77	1	22	Y	Zuckerman & Song (2004a)
EO Psc	01:29:04.9 +21:43:23	K2.5V	4930	0.96	70	11.1	–	–	0.44	23.73	1	22	Y	Ballering et al. (2013)
49 Cet	01:34:37.8 -15:40:34	A1V	8670	1.77	180	9.6	65	73.6	11.14	59.38	8	22	Y	Oudmaijer et al. (1992)
EX Cet	01:37:35.5 -06:45:38	G5V	5440	0.75	200	1.3	60	14.5	1.95	23.95	2	22	Y	Plavchan et al. (2009)
HD 10472	01:40:24.1 -60:59:56	F2IV/V	6610	1.34	200	3.4	60	37.9	5.47	67.24	2	22	Y	Zuckerman & Song (2004a)
HD 10647[b]	01:42:29.5 -53:44:27	F9V	6280	1.01	300	1.0	55	30.9	5.80	17.43	7	22	Y	Zuckerman & Song (2004a)

Notes: The spectral types are taken from SIMBAD unless designated by a ':'. The Num_Excess parameter describes the number of passbands that demonstrate IR excess. The λ_{start} column offers an approximate starting wavelength for the IR excess. The IRS column designates whether this study was able to acquire IRS spectra from the Enhanced Products Archive, which in many

cases supplements the IR excess we report.

[a] : This flag indicates that the disk has been resolved through scattered light and plotted in Figure 18.

[b] : This flag indicates that the distance shown is from the SED, as described in detail in the text (Section 2.3.2)

(This table is available in its entirety in machine-readable form.)[2]

[2]It is also included in the Appendix B.

Table 2.4: Reserved IR Excess Stars from the Literature and Tycho-2 cross-correlation with AllWISE

Name	R.A. and Decl.	Spectral Type	$T_{*,SED}$ (K)	$R_{*,SED}$ ($R_\odot$)	T_{dust} (K)	R_{disk} (au)	T_{dust2} (K)	R_{disk2} (au)	$\frac{L_{IR}}{L_{star}}$ ($\times 10^{-4}$)	Dist. (pc)	Num Excess	λ_{start} (μm)	Has IRS?	Known Reference
TYC3660-183-1	00:00:11.5 +57:52:20	:A8	7130	1.470	150	7.70	–	–	0.910	132.41 [a]	1	22	N	–
TYC4026-379-1	00:01:18.6 +66:50:12	:F4	6540	1.350	260	1.90	–	–	3.100	116.38 [a]	2	11	N	–
TYC2789-507-1	00:03:08.3 +42:44:52	:A2	8430	3.080	70	103.90	–	–	2.690	162.33	2	22	N	–
TYC4294-584-1	00:05:20.0 +68:53:04	:A1	9130	2.410	140	23.80	–	–	0.490	169.49	1	22	N	–
TYC4667-1078-1	00:11:34.8 -03:04:38	:F8	6240	1.130	180	3.10	–	–	2.660	101.46 [a]	1	22	N	–
HD 870	00:12:50.0 -57:54:45	K0V	5550	0.750	300	0.60	45	26.630	1.570	20.18	1	60	Y	Lawler et al. (2009)
TYC4026-208-1	00:13:03.4 +67:14:46	:K1	5190	0.760	170	1.60	–	–	17.270	184.32 [a]	2	11	N	–
HD 987	00:13:53.2 -74:41:18	G8V	5670	0.780	125	3.70	–	–	0.830	44.40	1	22	N	Zuckerman et al. (2011)
HD 1237	00:16:12.6 -79:51:04	G8V	5650	0.820	300	0.60	–	–	1.630	17.49	1	60	Y	Beichman et al. (2005b)
TYC2272-1059-1	00:16:42.9 +36:37:47	:A2	8300	2.110	140	17.20	–	–	0.610	126.41	1	22	N	–
39 Psc	00:17:50.1 +16:19:51	F6V	6400	1.180	200	2.80	–	–	0.320	44.82	1	22	N	Mizusawa et al. (2012)
26 And	00:18:42.1 +43:47:27	B8V	10850	3.760	75	169.30	–	–	2.450	202.83	2	22	N	Wyatt (2008)
HD 1562	00:20:00.2 +38:13:35	G1V	5910	0.930	75	13.40	–	–	0.580	24.79	1	60	N	Koerner et al. (2010)
TYC4015-1052-1	00:20:53.9 +61:27:42	:K6	4320	0.600	120	1.80	–	–	5.160	32.11 [a]	1	22	N	–
TYC8846-897-1	00:21:33.4 -66:18:16	A0V	9330	1.720	120	24.20	–	–	0.500	142.86	1	22	N	–
TYC4019-3245-1	00:22:05.1 +62:13:13	:K4	4850	0.690	165	1.30	–	–	8.240	93.56 [a]	1	22	N	–
TYC1186-730-1	00:23:11.9 +20:05:09	:A8	7190	1.230	140	7.50	–	–	1.090	105.26	1	22	N	–
TYC9135-268-1	00:34:53.4 -68:35:48	A0V	6940	2.230	340	2.10	–	–	2.300	182.81	2	11	N	–
TYC16-83-1[c]	00:37:19.2 +07:29:10	:M	2830	0.130	300	0.03	–	–	47.830	1.75 [a]	1	22	N	–
eta Phe	00:43:21.1 -57:27:47	A0IV	9080	3.760	65	170.80	–	–	0.010	75.52	1	60	N	Su et al. (2006)
HR 189	00:44:26.1 +47:51:50	B5V	13000	3.690	175	47.40	55	480.070	5.190	191.20	4	11	N	Chen et al. (2014)
TYC3667-527-1	00:50:59.5 +59:41:35	:F5	6470	1.300	180	3.90	–	–	2.280	165.10 [a]	1	22	N	–
TYC8034-360-1	00:51:58.7 -49:47:04	:G2	5900	0.960	290	0.90	–	–	7.680	170.27 [a]	2	11	N	–
TYC4017-1710-1	00:53:28.1 +60:39:56	A0V	8250	3.030	140	24.40	–	–	0.690	253.16	1	22	N	–
HD 5349	00:55:11.7 -16:58:17	K0IV	5170	1.600	250	1.60	–	–	1.180	48.94	1	22	Y	Chen et al. (2014)
TYC2802-1387-1	00:59:26.2 +40:09:18	:A3	7950	1.580	150	10.30	–	–	0.550	110.37	1	22	N	–
TYC3680-352-1	01:03:48.4 +58:09:36	:A3	8300	1.580	160	9.90	–	–	1.130	186.47 [a]	1	22	N	–
HD 6434	01:04:40.1 -39:29:17	G2/3V	5920	1.090	120	6.10	–	–	0.080	41.37	1	60	Y	Reid et al. (2007)
TYC4021-1605-1	01:05:13.8 +62:25:26	:K6	4340	0.610	150	1.10	–	–	4.240	36.90 [a]	1	22	N	–
TYC25-152-1	01:05:38.5 +06:38:50	:G2	5890	0.960	180	2.40	–	–	60.130	259.96 [a]	2	11	N	–
TYC4021-680-1	01:07:35.5 +63:21:11	:G5	5660	0.880	300	0.70	–	–	4.340	71.15 [a]	2	11	N	–

Notes: The spectral types are taken from SIMBAD unless designated by a ':'. The Num_Excess parameter describes the number of passbands that demonstrate IR excess. The λ_{start} column offers an approximate starting wavelength for the IR excess. The IRS column designates whether this study was able to acquire IRS spectra from the Enhanced Products Archive, which in many

cases supplements the IR excess we report.

[a] : This flag indicates the distance shown is from the SED as described in detail in the text (Section 2.3.2).

[b] : This flag indicates that the disk has been resolved through scattered light and plotted in Figure 2.17.

[c] : This star is most likely a giant based on the difference between the proper motion magnitude (distance proxy) and SED distance. Needs spectroscopic/astrometric confirmation.

(This table is available in its entirety in machine-readable form.)

2.3 Tycho-2 and AllWISE

2.3.1 Total Proper Motion and Cross-Correlation

Analysis of photometric excess based on stellar SEDs requires precise optical photometry in order to constrain the spectral shape (i.e., the stellar effective temperature). Thus, we cross-correlate a large optical survey (the Tycho-2 Catalog of the 2.5 Million Brightest Stars as released in 2000; Høg et al. 2000) and the most comprehensive all-sky mid-infrared survey (the AllWISE all-sky catalog; Cutri et al. 2013) to create a massive list of sources. Lacking accurate parallax measurements for most Tycho-2 stars, we implement a restriction on the proper-motion magnitude defined by

$$\mu_{total} = \sqrt{(\mu_\alpha)^2 + (\mu_\delta)^2} \geq 25.0 \ (mas/yr), \tag{2.1}$$

as a proxy for distance corresponding to stars within 200 pc. The stars with total proper motion greater than 25 mas yr^{-1} recover 91% of stars with measured distances less than 100 pc. The proper-motion criterion solely applied to the Tycho-2 catalog assembles 515,518 stars.

We perform a cross-match of the proper-motion-selected Tycho-2 sample and the AllWISE survey comparing the catalog positions. Considering the 20 yr baseline between these two catalogs implies that an object with a large proper motion ($\gtrsim 0.''1$ yr^{-1}) would be displaced by $2.''0$; therefore, we execute a proper-motion correction to Tycho-2 positions using the Tycho-2 proper motions in order to mitigate this effect. We select sources with a $5.''0$ match radius between the two catalogs, and the cross-match returns 99.6% of the Tycho-2 sample. The cross-correlated sample contains 513,478 objects.

2.3.2 IR Excess Selection Procedures

This section provides our algorithm to reduce the starting sample from over 500,000 stars to a reliable sample of main-sequence, IR excess candidate stars. A number of criteria are used to remove evolved stars, poor photometric quality data, and false positives. A summary of the procedure can be found in the flowchart shown in Figure 2.1.

Giants

A non-negligible fraction of the cross-correlated sample will inherently be evolved stars that are not discernible from main-sequence stars. Although there are some interesting exceptions of giants with IR excess (i.e. Phoenix giants; see Melis et al. 2009), we will focus only on main-sequence stars where IR excess points to circumstellar material suggestive of planetary relevance.

To gain insight into the contamination fraction of giant stars in our sample, we cross-match our sample of 513,478 Tycho-2/AllWISE sources with the *Hipparcos* catalog (van Leeuwen 2007). A 5.″0 search radius ensures the closest match with the *Hipparcos* catalog and returns 54,016 stars with measured parallax. A similar color-magnitude diagram (CMD) method of excluding evolved stars using the *Hipparcos* catalog was performed by Rhee et al. (2007) and more recently by Patel et al. (2014). We convert the Tycho-2 B_T and V_T magnitudes to the Johnson system using correction factors (Bessell 2000). We choose $(V - W2)$ for the color of our CMD since our sources have AllWISE data and this color provides the longest, useful color baseline. Figure 2.2 displays $(V - W2)$ color versus the absolute visual magnitude for the 54,016 Tycho-2/AllWISE/*Hipparcos* sources and the well-structured evolutionary separations between the white dwarfs, main-sequence stars, and giant branch stars. Our choice of excluding giants and white dwarfs is shown by the dashed red lines and blue crosses in Figure 2.2 defined by

$$(V - W2) > 2.0 \; and \; M_V \leq 5.0 \tag{2.2}$$

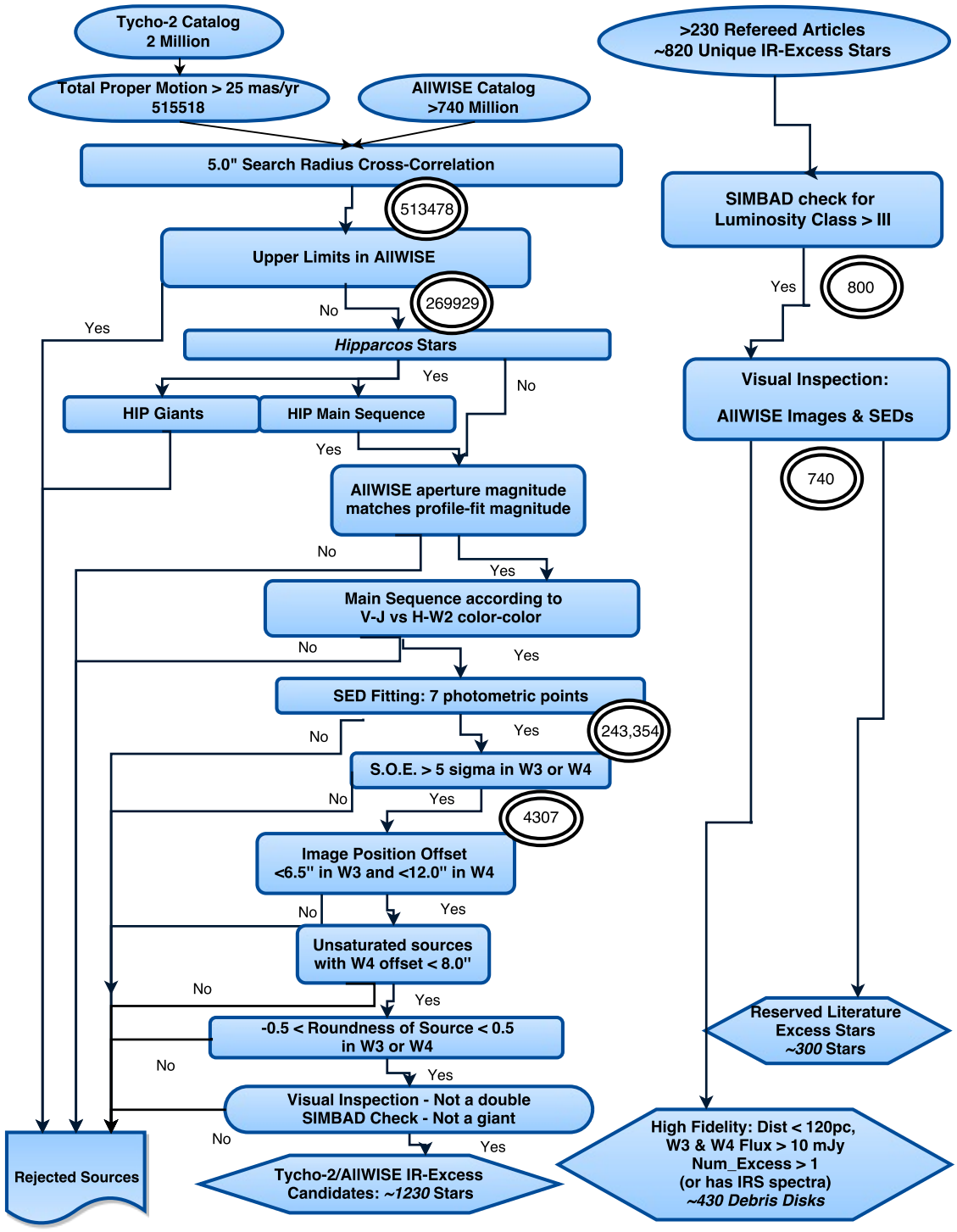

Figure 2.1: Flowchart description of the initial sample selection used to collect the Tycho-2/AllWISE cross-correlated IR excess candidates and a summary of literature IR excess star selection.

$$M_V \geq 2.5 \times (V - W2) + 1.8 \tag{2.3}$$

This procedure identifies 15,071 stars as giants and 581 white dwarf stars among 54,016 Tycho-2/AllWISE/*Hipparcos* stars. The fraction of evolved stars from a sample of about 54,000 is about 30% and we expect this same contamination rate of the Tycho-2/AllWISE sample that lacks *Hipparcos* data. We anticipate the majority of remaining giant stars to belong to K and M spectral types since early-type giants are rare due to their short lifetimes.

Since the CMD method requires *Hipparcos* data, we also investigate a method to remove evolved stars based on various color-color diagrams. Bessell & Brett (1988) demonstrated the use of color-color diagrams to identify the divergence of late-type main-sequence and giant tracks, which appear to diverge at approximately early M type. For our study, we want to identify colors that are able to distinguish G- and K-type dwarfs from giants. We compare dwarf and giant model fluxes at various passbands to determine a useful color that bifurcates the evolved branch at spectral types earlier than M. We find that the broadband colors of $H - W2$ versus $V - J$ show this distinction most clearly (Figure 2.3). We define the conservative polynomial to remove objects falling within the green dashed curves

$$y = 0.05x^3 - 0.19x^2 + 0.23x + 0.13 \tag{2.4}$$

where $x = (V - J)$ and $y = (H - W2)$. The selection using the dashed lines removes 77% of the known *Hipparcos* giant sample and 82% of the literature giant sample. Using the $V - J$ and $H - W2$ color-color cut, it demonstrates that about 80% of known giants can be flagged while only about 2% of main-sequence stars are lost. So, by applying this color-color cut in combination with the expected contamination rate from the CMD, we expect that only $\sim 6\%$ of the final Tycho-2/AllWISE sample will be giants.

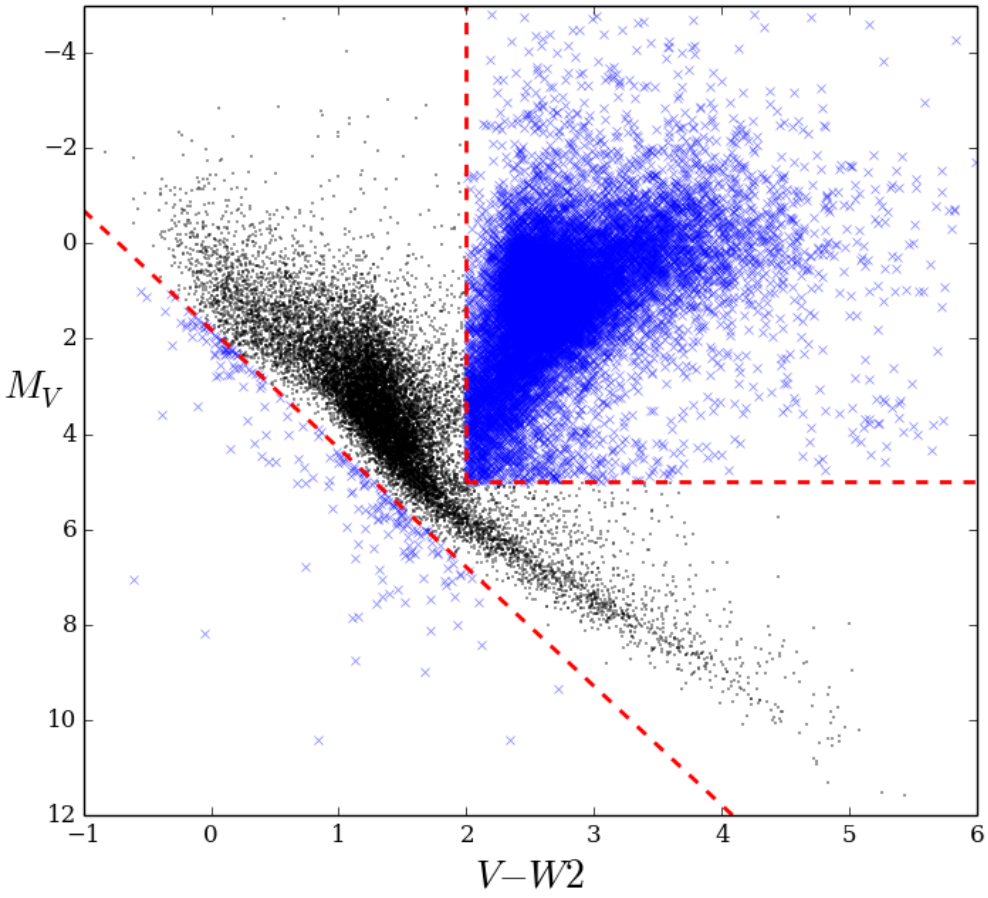

Figure 2.2: Color-magnitude diagram for the Tycho-2/AllWISE stars with *Hipparcos* parallax information. The dashed lines designate the cuts for removing giants and white dwarfs. We have selected these lines to ensure that we do not lose many main-sequence dwarfs. The blue crosses constitute over 15,000 stars rejected from the cross-correlated sample for being giants or white dwarfs.

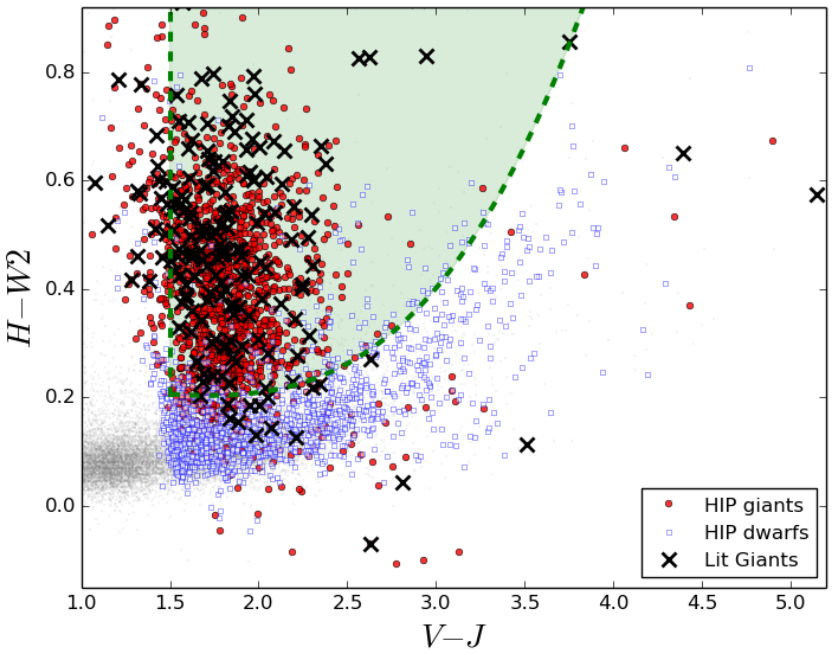

Figure 2.3: Color-color diagram used to distinguish giant stars. The green dashed curves and the enclosed shaded region display the cuts used in removing additional late-type evolved stars from our main-sequence sample (see Section 2.3.2 for the functional form of the curved line). The small gray dots are the remaining sample of $> 200,000$ Tycho-2 stars. The red circles are the *Hipparcos* giants removed from the sample using the CMD (see Figure 2.2), while the open blue squares are the *Hipparcos* main-sequence sample selected in the CMD that have well-measured parallax (error <10%). The large crosses are giants selected from SIMBAD that have a luminosity class of I, II, or III.

AllWISE Photometry

We compare the profile-fit and aperture-derived photometry as an additional analysis of the reliability of the AllWISE photometric measurements. While the AllWISE explanatory supplement recommends using the profile-fit photometry to avoid the poor aperture photometry at the saturation limits (W1 > 8.0, W2 > 7.0, W3 > 3.8; Cutri et al. 2013), we believe that unsaturated, well-behaving stars should have similar photometry derived from both methods. We remove sources for which this is not the case by fitting a standard Gaussian to the differences between the aperture and profile-fit magnitudes at each AllWISE passband and excluding stars having differences in photometry outside of 2.5 σ. Nearly 6000 stars had photometry that we would term unreliable. These sources tend to be contaminated by nearby ($\lesssim$12″) brighter objects such as stars, galaxies, or nebulae or cases of strong cirrus contamination in either W3 or W4. The number of stars in our sample after removing the giants and poor photometry sources is 245,924.

For accurate SED fitting, we remove over 2000 stars without a complete set of measurements from Tycho-2, the Two Micron All Sky Survey (2MASS), and AllWISE. Some of the stars in our final sample may have poorer-quality data according to the flags from the individual catalogs. However, we continue to use these data rather than disregard those magnitudes as it improves the SED fitting. The only instances in which photometric measurements do not improve the SED fit are upper limits, and so we have eliminated stars with upper limits at these crucial wavelengths.

SED Fitting

In our SED fitting, NextGen (PHOENIX code version 9.1; Hauschildt et al. 1999) and Kurucz (Castelli & Kurucz 2004) model atmospheres are fit against observed photometric measurements. Between the two models, there is a systematic difference of about ∼120 K in the best-fit stellar temperature. Because of the small difference between the two models and to avoid mixing the two models in our analysis, we decide to use only the NextGen models

in our SED fitting. The SED fitting algorithm converts all the photometric measurements into flux and compares them to the grid of available temperatures and selects the best agreement between model and data using a χ^2 minimization technique (refer to Rhee et al. 2007 for complete details). After producing a good fit to the photosphere, the mid-infrared Rayleigh-Jeans tail provides a comparison for excess emission above the photosphere.

Spurious AllWISE Saturation Correction

Upon inspecting a number of SED fits using the procedure described in Section 2.3.2, we noticed an issue of overestimated fluxes in AllWISE measurements. Sources brighter than 8.1, 6.7, 3.8, and -0.4 mag at W1 through W4, respectively, are saturated, and thus the fluxes are overestimated (Cutri et al. 2013). Patel et al. (2014) present a similar discussion but a different analysis. The *WISE* team described this bias for W2 < 6.5 mag and illustrated this finding through their Figure 8 in Section VI.3.c.4 of Cutri et al. (2012); however, at the time of writing they did not offer a solution to the nearly 0.5 mag overestimate for the brightest objects. The bright candidates in our sample demonstrate this spurious flux mainly at W2. Since this effect is not intrinsic to the object, we develop a correction to the AllWISE W2 flux using over 26,000 early A and F stars ($T_{*,SED} \geq 6000$ K) selected by their best-fit stellar temperature from the SED. These earlier-type stars have a smooth Rayleigh-Jeans tail at every AllWISE passband, while later-type stars develop strong carbon monoxide (CO) absorption features near W2 (4.6μm). Figure 2.4 displays the overestimation of the flux density specifically for magnitudes brighter than 7 in W2. The correction function involves a series of logarithms as described below:

$$\text{W2} \leq 7.0 \text{ mag:}$$

$$y = 3.28 - 168.55 \log(x + 0.084)^{-1} + 164.78 \log(x + 0.003)^{-1} \tag{2.5}$$

where the value of y refers to the difference between the measured and predicted W2 flux in jansky and the value of x refers to the AllWISE catalog magnitude.

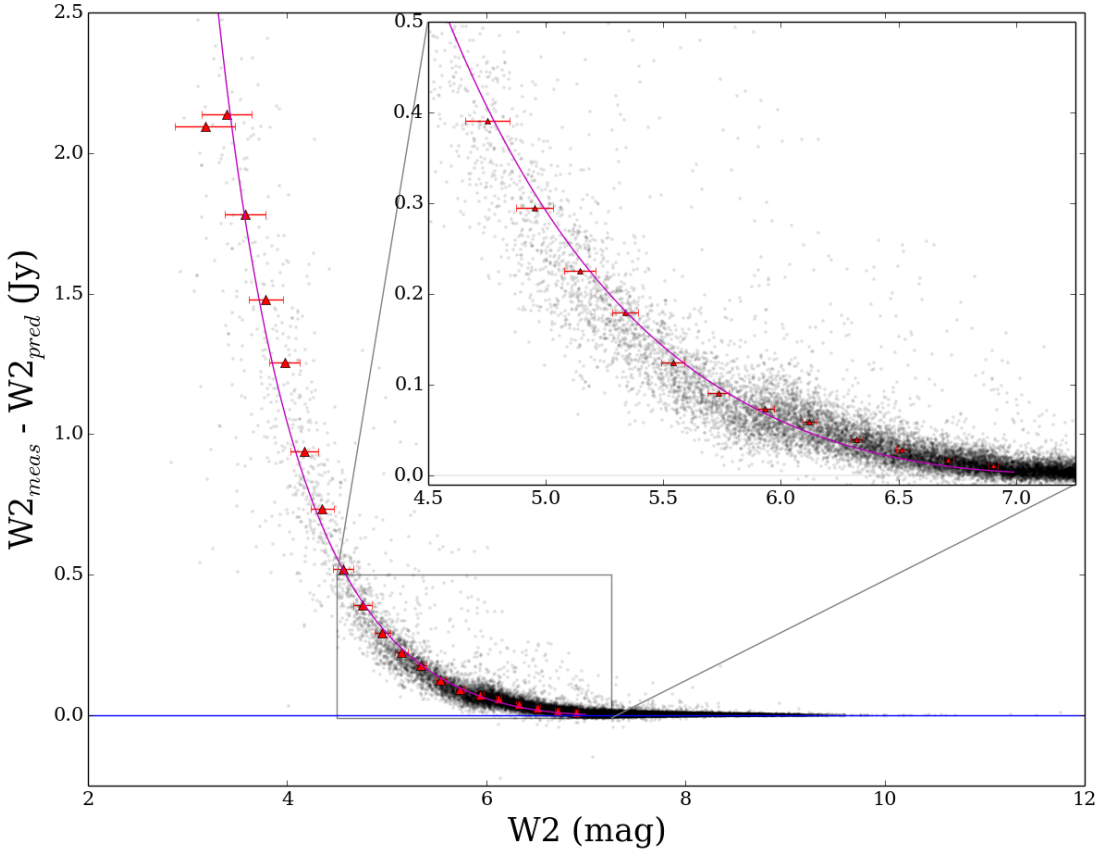

Figure 2.4: The function displayed is designed to correct the flux overestimation effect in the AllWISE W2 passband. The data plotted contain stars with effective temperatures from the SED fitting greater than 6000K, binned by ∼0.2 magnitudes, and fit using a series of logarithms in the saturation region. A solid (blue) horizontal line has been displayed at zero for reference. The correction function is of the form $y(Jy) = 3.28 - 168.55 \times \log(x + 0.084)^{-1} + 164.78 \times \log(x + 0.003)^{-1}$ and applies to W2 magnitudes less than 7.

Qualification of Excess

Our infrared excess qualifications use the predicted flux values at the AllWISE passbands determined by the best-fit SED after applying the saturation correction. We define the amount of IR excess in terms of a 'Significance of Excess' as

$$\text{Significance of Excess} \equiv \frac{F_{AllWISE} - F_{predicted}}{\sqrt{(\sigma^2_{AllWISE} + \sigma^2_{cal})}} \tag{2.6}$$

where $F_{AllWISE}$ is the measured flux at a given AllWISE passband and $\sigma_{AllWISE}$ is the uncertainty in that measurement combined with an absolute calibration uncertainty (σ_{cal}) defined by Jarrett et al. (2011) and Cruz-Saenz de Miera et al. (2014) to be 4.5% in W3 and 5.7% in W4. The calibration uncertainty was derived by Jarrett et al. (2011) through comparison of AllWISE photometry and *Spitzer* data for a set of standard stars. $F_{predicted}$ represents the photospheric flux value from the SED fit predicted at each AllWISE passband. As mentioned previously, we expect W1 and W2 to be consistent with the stellar photosphere and use W3 and W4 excess for our final IR excess candidates. In our analysis, we do not include a color correction of AllWISE measurements because the effects are small.

Figure 2.5 displays the significance of excess versus stellar temperature for the 243,354 stars in our sample. The figure shows a significant decreasing trend in the significance of excess with decreasing stellar temperature, in particular, for stars with $T_{*,SED} < 4000$ K. AllWISE W3 shows a steeper decline, and we believe that this is inherently due to the larger passband of W3 than W4. Wright et al. (2010) mention that a color correction applied to the flux in W3 would be larger than for any other passband and is exacerbated by the variability and activity found around nearby late-type stars. Further, Wright et al. (2010) describe the in-flight discrepancy found between red and blue sources that implies that the coolest stars will have a W3 flux that is measured to be fainter than models (i.e. a negative significance of excess). To remove this effect, we fit a curve to this trend for stars with temperature

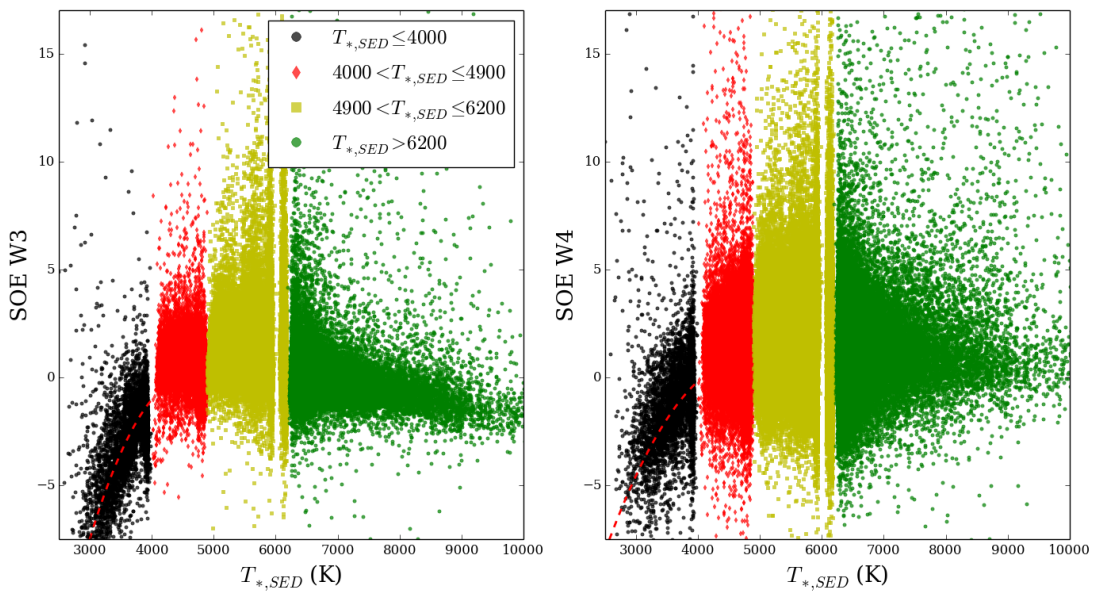

Figure 2.5: *Left:* significance of excess (SOE) in AllWISE W3 flux for stars in the cross-correlated sample (243,354) versus the best-fit stellar temperature from the SED. The colors represent four different regions pointing out the trend toward "negative excess" of the coolest stars in our sample. This trend is seen for stars with SED temperatures less than 4000K and is fitted with a function shown as the dashed line (refer to Section 2.3.2: Equations 7 and 8 for the functional form of the corrections). *Right:* same as the left panel, but for AllWISE W4.

less than 4000K. The functional form of the curve for the W3 and W4 significance of excess (SOE) correction is

$$W3: \ SOE = -2.9 \times 10^{-6} \times T_*^2 + 0.03 \times T_* - 62.22 \tag{2.7}$$

$$W4: \ SOE = -1.7 \times 10^{-6} \times T_*^2 + 0.02 \times T_* - 37.92 \tag{2.8}$$

where T_* refers the the best-fit stellar temperature from the SED. The stars in the other temperature regions do not show any significant trend requiring a correction.

After applying the correction to the stars with the coolest temperatures ($T_{*,SED} < 4000$ K), histograms of the significance of excess are displayed in Figure 2.6 for each temperature division for W3 and W4. Our selection of significant IR excess uses a Gaussian fit to each

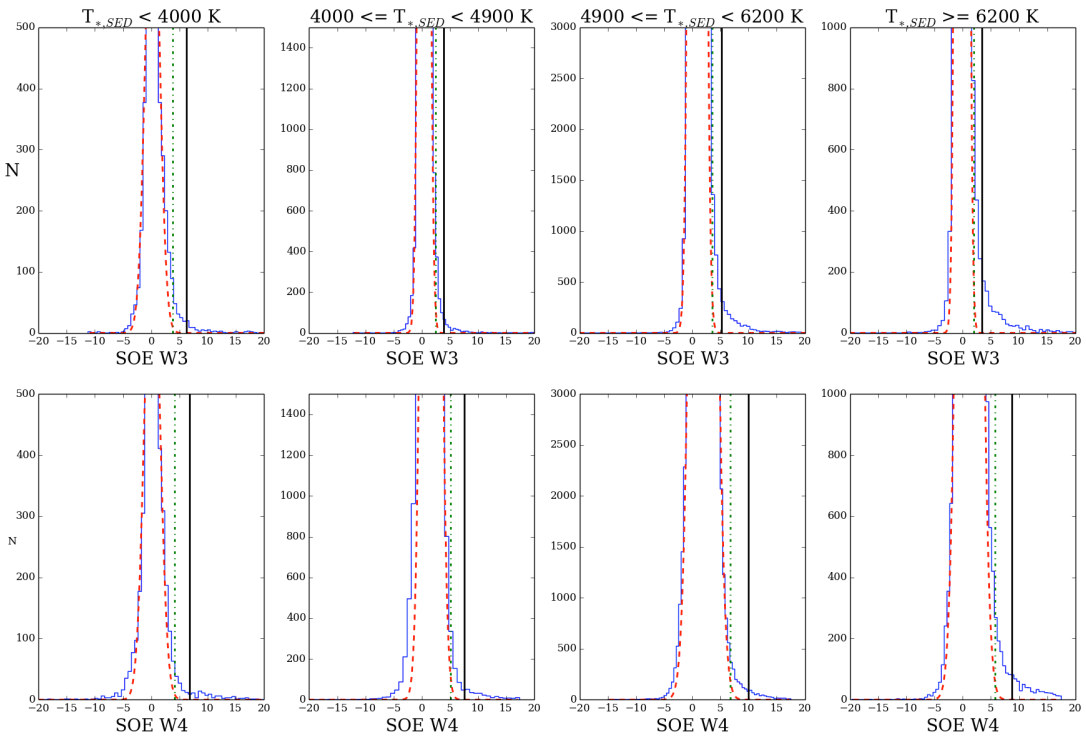

Figure 2.6: Significance of excess (SOE) for the temperature divisions shown in Figure 2.5. Each histogram portrays our significance of excess defined in Section 2.3.2 and is fitted with a Gaussian, and the green (dot-dashed) and black (solid) vertical lines represent the 3σ and 5σ selection criteria for excess stars, respectively. The histograms have been magnified to show the true distribution of stars within each temperature division.

apparent population of non-excess stars, shown by the red dashed curve. The mode of the significance of excess is offset from zero in the positive direction in many histograms, likely due to a combination of model uncertainties, Malmquist bias, and other unknown uncertainties. We initially select the best excess candidates using the Gaussian fits and retain stars beyond the solid, vertical, black lines representing 5σ in W3 or W4 for each temperature division; however, recognizing that many past studies (Patel et al. 2014, Vican & Schneider 2014) isolated cases of marginal W4 excess, which may in fact prove to be true detections of IR excess, we also include the sample of stars with W3 or W4 greater than 3σ, shown by the vertical dashed line in Figure 2.6. This procedure identifies nearly 4300 stars with significant IR excess.

Contamination Inspection

Given the likelihood that many false-positive stars are due to source confusion in AllWISE images due to a large mid-IR beam size, we present a series of quantitative image analyses. These sources of contamination include cirrus or foreground infrared sources, adjacent stronger IR sources affecting the AllWISE photometry, background galaxies, nebulosity surrounding the source (see Pleiades phenomenon; Herbig & Simon 2001; Kalas et al. 2002), and optical/near-infrared binary stars that cannot be resolved with the beam size of *WISE*. The goal of the image analysis is to eliminate the contamination issues in a quantitative fashion.

The first methodology aims to compare the expected central, cross-correlation position with the position found through isolating the brightest central source in each AllWISE image. When a contamination source is present (at W1 and W2) adjacent to a candidate IR excess star and is unresolved in the AllWISE image, the centroid position of the candidate star shifts. The second methodology is to analyze the isolated source's shape to determine whether the object is extended or noncircular. We use a criterion of roundness defined through comparison of the bilateral symmetry of each source determined by fitting a two-dimensional Gaussian to the source point-spread function defined similar to

$$Roundness \propto \frac{(\sigma_x - \sigma_y)}{\frac{(\sigma_x + \sigma_y)}{2}} \tag{2.9}$$

where σ_x and σ_y are the standard deviations of those Gaussians. A roundness criterion of zero would appear circular, while a roundness of -1.0 or 1.0 would be noticeably elliptical. Further, since we expect W3 and/or W4 excess to be from the dust grains, the disks should be unresolved at the W3 and W4 passbands (except for the nearest stars); hence, their roundness values should be close to zero.

To implement the image inspection, we download $2' \times 2'$ images at each AllWISE passband followed by the source detections on these images using IRAF's program *daofind*. We

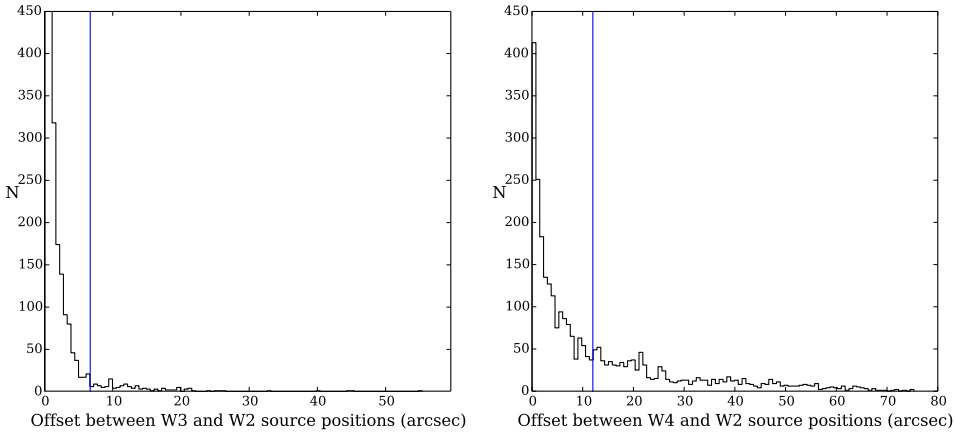

Figure 2.7: Offset in the main source position between AllWISE W2 and W3 (left) and W2 and W4 (right). The difference between W2 and W3 does not show a significant variation from which to distinguish contamination. The difference between W2 and W4 shows a larger spread and can easily distinguish cases of image contamination. We have initially removed stars further separated than 6.″7 in W3 or 12.″0 in W4 using the resolution of *WISE* as a cutoff. The vertical lines indicate this location. (See text for more details.)

compare detected source positions and shapes against the expected stellar positions. All sources were detected in W3, but 770 targets went undetected in W4. Of these nondetections, 92% are cirrus contamination leading to spurious excess fluxes, while the remaining are extended sources indicating large nearby objects, most likely galaxies. The remaining sample contains 3530 sources with identified *daofind* positions in each AllWISE passband, which are plotted in Figure 2.7 displaying the detected offset between the source position in W3 or W4 compared to W2 since W2 most accurately reflects the Tycho-2 source position. First, we remove sources with positional offsets greater than the resolution of W3 (6.″7) or W4 (12.″0) in AllWISE. Upon further inspection, however, sources offset in W4 greater than 8.″0 are also contaminated and so while the sources removed due to offsets in W3 (120) preserve 95% of the sample, 1180 additional targets are removed for large offset positions in W4. In this case, 44% of the sources appear to be cirrus, 25% are due to background sources, and the remaining 30% are sources unresolved in the AllWISE images in which the secondary object is brighter at this passband and so shifts the detected source position.

Further, excess candidates were inspected for potential ellipticity. Of the 150 sources we remove, 64% appear to be cirrus, 22% are some sort of background object or nebula, and 14% are likely double stars of similar brightness that are unresolved at W3 or W4. The double stars are removed here because the secondary source will contribute additional flux to the target star and act as a false-positive IR excess candidate. The candidate IR excess stars now total ∼2100. Examples of some contaminated targets are displayed in Figure 2.8.

As mentioned previously, we expect $\sim 6\%$ of the remaining candidates to be giants based on our discussion in Section 2.3.2. With the sample now reduced, we search each candidate position in SIMBAD to identify a published luminosity class or a contaminating object nearby such as a background galaxy. We remove 81 stars with luminosity class of I, II, or III. Through this endeavor, we also remove 46 other contentious objects such as Cepheid variables, white dwarfs, nebulae, novae, and known galaxies (within $10''$). Additionally, we eliminate 523 sources through inspection of the 2MASS images that are likely double- or multiple-star systems (within $10''$) unconfirmed in the AllWISE images, especially W4. Double stars that are unresolved in *WISE* display excess above the photosphere in all passbands, mimicking the Rayleigh-Jeans tail. Thus, inspecting the SED for each star and eliminating likely binary-related false excess, reduces to 1430 stars.

In order to affirm the SED fit and IR excess, we also gathered additional photometry through VizieR from the ultraviolet to the far-IR (including data from *Spitzer* MIPS and the *Herschel* PACS or SPIRE instruments; Griffin et al. 2010; Poglitsch et al. 2010) and performed a reevaluation of the candidate SEDs. Additional photometry did one of three things in terms of contamination or true source identification: (1) it shifts the stellar photosphere slightly such that a star's significance of excess, now no longer passes our criteria, (2) it provides additional far-IR photospheric data which refutes the AllWISE excess, or (3) it corroborates previous excess detections. Far-IR data from the *Spitzer* MIPS instrument provide better sensitivity through pointed observations; therefore, we treat the *Spitzer*

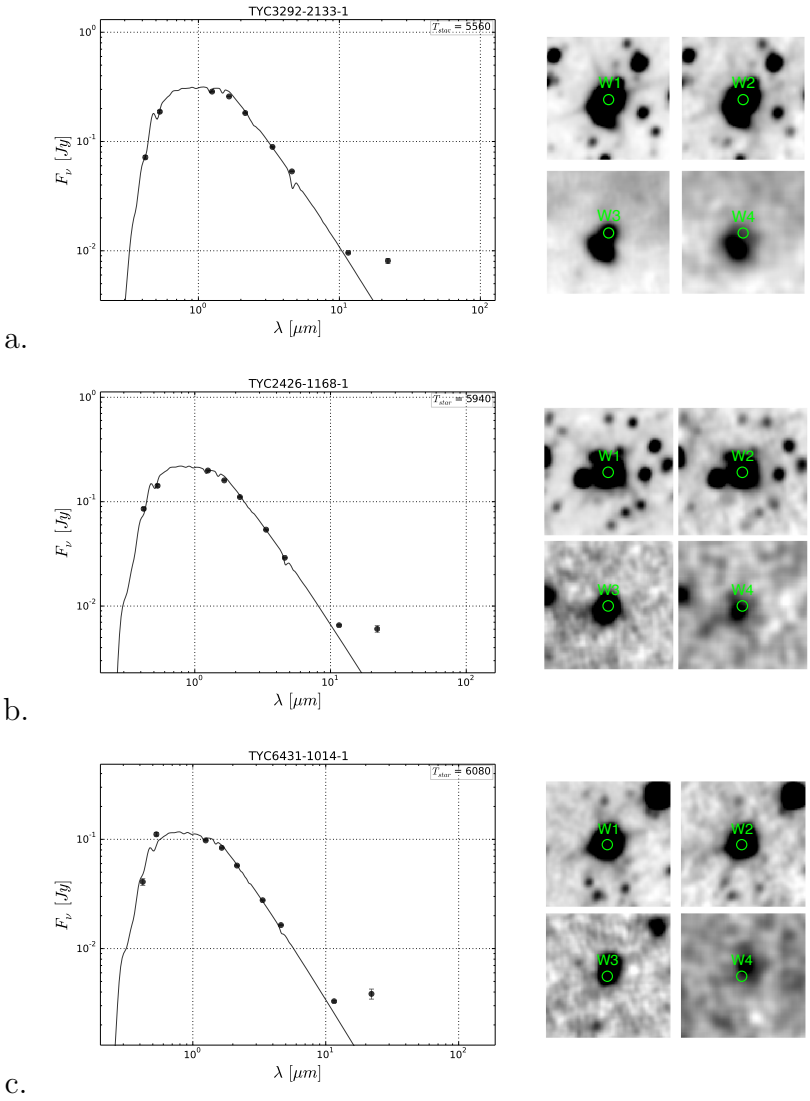

Figure 2.8: Examples of stars removed during the image vetting procedures. The left panels display the SED for each star with the photosphere fit to Tycho-2 B_T, V_T and 2MASS J, H and K_S. The right panels show the AllWISE images taken from the NASA/IPAC Infrared Science Archive and are $2'$ by $2'$, scaled linearly. The images also contain a $5.''0$ circle centered on the search position. (a.) Due to both the background contaminating cirrus and the large offset to the brightest source in W4, this source is likely a background galaxy found through our offset criteria. (b.) This source passed the initial offset criteria, but further inspection proved sources with W4 offsets $>8.''0$ need to be removed as well. The object shown in the W4 image is offset from the W2 position by $9.''1$ and yet the amount of W4 excess emission cannot be due to a center source alone. (c.) This source demonstrates an elliptical shape in W3; it is rejected based on the roundness criteria and is likely a background IR source. See Section 2.3.2 for more details regarding these images.

data as representative of the true measurement of far-IR flux. The third case of additional photometry is the only example of beneficial photometry, and so we will examine the other cases in more detail. First, for $\sim$ 80 stars, the inclusion of more data to improve the fit to the stellar photosphere shifts the photosphere and the infrared Rayleigh-Jeans tail, and a reevaluation of the significance of excess makes these sources non-excess. Second, additional photometric measurements at far-IR wavelengths (MIPS, PACS, SPIRE) can reject marginal cases of mid-IR excess. We removed 60 objects with photospheric detections at MIPS 24 and no IR excess at 70μm. However, one interesting case, HD 69830, found by Beichman et al. (2005b) has mid-IR excess around 10μm confirmed using interferometric evidence by Smith et al. (2009b) without the presence of any far-IR excess detection. This rare and unique circumstellar disk is also host to three exoplanets (Lovis et al. 2006). While we do not want to miss any interesting cases, we removed 60 additional stars that have the potential to be HD 69830-like due to true mid-IR excess in W3 and/or W4 and far-IR photospheric detections, since we believe that the majority of these are likely bogus excess sources. Our IR excess candidate sample comprises 1230 sources.

Reliability of Excess and Final Distance Restriction

Proximity to our Sun serves as an initial quantifier for our 'Prime' targets. We initially selected stars using the total proper-motion magnitude as a proxy for a distance corresponding to $\sim$200 pc. Considering the size of the Local Bubble and the minor interstellar medium influence on the IR excess in this region, we place stars within 120 pc in our Prime catalog. This identified $\sim$300 stars from our Tycho-2/AllWISE IR excess sample with measured distances.

For the remaining 75% of stars without trigonometric parallaxes, we develop a more reliable distance restriction based on a photometric distance calculated by our SED fitting algorithm. The SED fit uses all photospheric photometry for which the brightnesses are highly covariant unlike a single photometric passband. This procedure is based on the

final step of the SED fitting algorithm, which multiplies the model fluxes by a scale factor, namely, $(\frac{R}{d})^2$, where R refers to the stellar radius in solar radii and d is the distance to the star in parsecs (see discussion in Cushing et al. 2008 for more details). We then investigate deducing a distance from this scale factor value using model isochrones to infer an expected stellar radius given the best-fit stellar temperature returned from the SED fit. Using the isochrones from Siess et al. (2000), Allard et al. (2011), and Dell'Omodarme et al. (2012), we construct a composite isochrone model that ranges between 2000 and 15,000 K (for more details regarding this model, see J. Lee & I. Song 2016, in preparation). SED distances are estimated for about 900 stars and the expected uncertainty is typically $\sim 12\%$.

The effort to include the SED distance for stars without trigonometric parallax identified 48 stars that are likely evolved M-type stars. Inspection of their SED distance within 15 pc and the total proper motion (less than 40 mas yr^{-1}) offers conflicting data regarding the location of these stars. Although there are two small regions (solar apex and anti-apex) where nearby stars exhibit very small proper motions, if the total proper motion is $\sim$40 mas yr^{-1}, we expect the distance to be on the order of 100 pc. However, for these 48 stars in our sample the SED distances of less than 15 pc are very unrealistic. We retain these stars in the Reserved sample with an accompanying note until spectroscopy can confirm that they have indeed evolved away from the main-sequence.

Finally, to aid in the reliability of our IR excess stellar sample, we generate a parameter called "Num_Excess" in Tables 2.3 and 2.4, which represents the number of passbands that display excess above the photosphere. We designate the following wavelength ranges as our IR excess passbands: 5 - 13μm, 17 - 30μm, 55 - 75μm, 90 - 110μm, 120 - 170μm, 200 - 300μm, 300 - 400μm, 400 - 500μm, 500 - 600μm, 700 - 900μm, and >1000μm. Thus, instruments with similar wavelength photometry such as *WISE* W4 (22μm), *Spitzer* MIPS 24μm, and *IRAS* 25μm are maintained as corroborative evidence of the same excess near 25μm. Besides being a more reliable indication of excess, multiple excess detections reduce the inherent degeneracy in fitting a blackbody temperature to the dust, thereby allowing for a

more detailed dust analysis. Tables 2.3 and 2.4 display Num_Excess, the starting wavelength of the IR excess in microns, and a flag if the *Spitzer* IRS spectra are available. These columns should provide a full description of the nature of the excess. We also include in the online materials a table of photometric measurements and model predictions at key stellar fitting passbands for all the stars in Tables 2.3 and 2.4 as well as the measured photometry from *Spitzer* and/or *Herschel* if available from the literature. An example of the content and form of the photometry table is provided here in Table 2.5.

We compare our final tables of Tycho-2/AllWISE Prime IR excess stars and Reserved IR excess candidates with the literature sample found in Section 2.2 in order to exclude duplicate entries. Then, the following reliability criteria are used as in Section 2.2 to select reliable IR sources from the Tycho-2/AllWISE sample for our Prime catalog:

1. at least two passbands demonstrating IR excess ("Num_Excess" > 1), AllWISE W3 or W4 flux greater than 10 mJy (for more efficient follow-up observations), and proximity such that distance is within 120 pc; or

2. at least one passband demonstrating IR excess, AllWISE W3 or W4 flux greater than 10 mJy, has IRS spectra confirming photometric IR excess identification, and distance $<$120 pc.

Passing the above criteria, we compile just about 500 stars from the Tycho-2/AllWISE search and the literature search for the Prime IR excess catalog. The Reserved table contains over 1200 stars[3].

[3]The full extents of Tables 2.3 and 2.4 are available as online material for this manuscript, as well as stored locally on a public server through the University of Georgia entitled Debris Disk Database (www.debrisdisks.org).

Table 2.5: Photometry Information for Prime and Reserved Catalog Stars.

Column	Explanation
1	Source identifier
2-8	R.A./Dcl. (J2000)
9	Catalog embership
10	SED effective temperature
11	Stellar radius ($R_{\odot}$)
12-14	W1 measurement (Jy), Uncertainty, Predicted photospheric measurement
15-17	W2 measurement (Jy), Uncertainty, Predicted photospheric measurement
18-20	W3 measurement (Jy), Uncertainty, Predicted photospheric measurement
21-23	W4 measurement (Jy), Uncertainty, Predicted photospheric measurement
24-26	*IRAS* 12μm measurement (Jy), Uncertainty, Predicted photospheric measurement
27-29	*IRAS* 25μm measurement (Jy), Uncertainty, Predicted photospheric measurement
30-32	*IRAS* 60μm measurement (Jy), Uncertainty, Predicted photospheric measurement
33-35	*IRAS* 100μm measurement (Jy), Uncertainty, Predicted photospheric measurement
36-39	MIPS 24μm measurement (Jy), Uncertainty, Reference, Predicted photospheric measurement
40-43	MIPS 70μm measurement (Jy), Uncertainty, Reference, Predicted photospheric measurement
44-47	MIPS 160μm measurement (Jy), Uncertainty, Reference, Predicted photospheric measurement
48-51	PACS 70μm measurement (Jy), Uncertainty, Reference, Predicted photospheric measurement
52-55	PACS 100μm measurement (Jy), Uncertainty, Reference, Predicted photospheric measurement
56-59	PACS 160μm measurement (Jy), Uncertainty, Reference, Predicted photospheric measurement
60-63	SPIRE 250μm measurement (Jy), Uncertainty, Reference, Predicted photospheric measurement
64-67	SPIRE 350μm measurement (Jy), Uncertainty, Reference, Predicted photospheric measurement
68-71	SPIRE 500μm measurement (Jy), Uncertainty, Reference, Predicted photospheric measurement

(This table is available in its entirety in machine-readable form.)

2.4 Previous WISE Excess Searches

This study is not the first use of the *WISE* survey to search for IR excess; therefore, we compare our results to the debris disk candidates discovered by Wu et al. (2013), Cruz-Saenz de Miera et al. (2014), Patel et al. (2014), Theissen & West (2014) and Vican & Schneider (2014). We will avoid a comparison between our final samples and Rizzuto et al. (2012) since they made use of data from the preliminary *WISE* catalog data only, which is now obsolete once the full catalog was released and many of their stars were reassessed through other studies. Each of these searches maintains a similar sample criterion to our new Tycho-2/AllWISE cross-correlation; however, each study presents a different standard of significance of excess and final analysis of the candidates.

First, Wu et al. (2013) were specifically searching for 22 μm excess using *Hipparcos* stars within 200 pc. They selected candidate excess stars using a color criterion of $[K_S - W4]$ and produced a sample of 141 candidate IR excess stars. Our study was able to reproduce 63 stars from the final Wu et al. (2013) IR excess sample. From the remaining stars that were not matched, 44% have total proper motions according to the Tycho-2 catalog that are less

than 25 mas yr^{-1} (the initial sample selection that we used), and the rest (56%) do not pass our significance of excess.

Patel et al. (2014) found 220 stars showing W3 and/or W4 excess. We confirmed 114 ($\sim$ 52%) of their IR excess stars. The majority (85%) of the remaining 106 IR excess candidates do not pass our significance of excess criteria, and the rest (15%) show total proper motions less than 25 mas yr^{-1}.

Constraining their sample using SIMBAD, Cruz-Saenz de Miera et al. (2014) selected only main-sequence dwarfs and any distance. They use a comparison between the predicted and measured ratio of fluxes (W4/W2) divided by the calibration-weighted uncertainty. Through the typical (and somewhat subjective) process of visual inspection of *WISE* images to remove false-positive IR excess candidates, Cruz-Saenz de Miera et al. (2014) report 197 IR excess stars. We confirmed 40 of these sources as IR excess stars in our Prime or Reserved catalog. A total of 60% of the Cruz-Saenz de Miera et al. (2014) sample does not pass our significance of excess cut, and the rest (40%) do not pass our total proper-motion criteria.

Previous searches for M stars with IR excess by Avenhaus et al. (2012), who used the AllWISE catalog and the RECONS sample from Henry et al. (2006), did not find any new cases of M stars with IR excess indicating a debris disk. Theissen & West (2014) were able to expand this search using the Sloan Digital Sky Survey (SDSS) spectroscopically selected M-type stars out to a distance of nearly 2000 pc. While they executed a series of contamination checks to ensure that their sample contains only M dwarfs, only 36% of their 175 IR excess stars are within 200 pc. None of these stars were reproduced by our search. The main reason for the dissimilar results with respect to our sample is distance. Moreover, of the 63 M dwarfs within 200 pc, none of them have Tycho-2 catalog matches. The faintness limit of Tycho-2 would exclude many M dwarfs at these distances.

Vican & Schneider (2014) searched the literature for stars with chromospheric activity indicators in order to constrain the age of their sample before using *WISE* to determine whether these stars had IR excess. Their criterion for excess is very similar to our significance

of excess using the comparison between measured and photospheric fluxes, and they found 98 IR excess candidates. Twenty-four of these sources can be found in our Tables 2.3 and 2.4. Eight stars were not selected to our sample due to very low total proper-motion and the rest (66) were not selected based on our significance of excess criteria.

2.5 Sample Characteristics

The Prime IR excess star catalog (Table 2.3) contains ∼500 stars and information regarding the best-fit SED stellar effective temperature, the number of excess passbands, distance, and disk parameters such as temperature, radius, and fractional dust luminosity. We have marked the previously published IR excess stars using the column "known" that designates one of the star's first claims of IR excess in the literature. Table 2.4 mimics the display of the Prime catalog. Most notably, this study has produced >70 new Prime IR excess stars, which is almost a 20% increase in notable IR excess stars, as well as a handful of very dusty disks ($L_{IR}/L_* \equiv \tau > 10^{-2}$). Further, the number of marginal IR excess stars has quadrupled with this new Tycho-2/AllWISE search.

For the disk parameters, we choose the most simplistic model to define the disk temperature and radius. We assume that the SED can first be fit with a single-blackbody function. If the single-blackbody model does not fit the dust, then a two-blackbody disk model is applied. Stars with *Spitzer* IRS spectroscopy have disk models that match the spectroscopic evidence. In addition, for stars in the Reserved catalog with IR excess in only one passband and without *Spitzer* IRS spectroscopy, we assume a warm dust disk whose dust flux peaks at the single excess wavelength. The fitting parameters are listed in Tables 2.3 and 2.4.

Past studies presented several estimates on the occurrence rate of excess stars focusing on nearby, main-sequence stars and in some cases focusing on a specific cluster, region, or spectral type. Su et al. (2006) report a debris disk fraction of $\geq 33\% \pm 5\%$ surrounding A stars using *Spitzer* MIPS measurements of excess emission at 24 or 7 0μm, while Beichman et al. (2006b) combined their results with the Bryden et al. (2006a) and Gautier et al. (2007)

studies to report that 15% ± 3% of F0- to K0-type stars have debris disks detected at 70 μm. Gorlova et al. (2006) surveyed the 30 Myr old cluster NGC 2547 and report that incidences of 40% of B- to F-type stars demonstrate excess at 24 μm. More recently, Eiroa et al. (2013) discussed the overall prevalence of far-IR detection of circumstellar dust around nearby solar-type stars to be nearly 23%. This can be contrasted with larger all-sky searches for nearby solar-type stars with mid-IR excess such as those performed by Wu et al. (2013) and Patel et al. (2014) who found incidence rates of mid-IR excess specifically at 22μm solar-type stars of 2.21% and 1.8%, respectively. To create a comparable sample of stars that are not contaminated by nearby objects, we filter the starting sample of 250, 000 Tycho-2/AllWISE stars to exclude giants (originally ∼30%) and then eliminate the expected number of sources with nearby contamination (∼50% of 200,000 stars) extrapolated from the results in Section 2.3.2. This procedure interprets ∼120,000 main-sequence stars from various sources that have the potential to contain IR excess stars without any contaminating influences. From this sample, we determine that the occurrence of IR excess for Tycho-2/AllWISE stars with W4 excess from the parent sample is 1.0% (1200/120,000). In order to best compare with past IR excess studies, we focus on the incidence of 22 μm (W4) excess around A-type or earlier stars and solar-type stars only. Excluding the literature sample from this analysis, we find that 15.6% (∼320 of 2100 stars with SED temperatures that reflect A type from the 120,000-star sample) have infrared excess at W4, while the solar-type stars have an incidence rate for W4 excess of 0.7% (∼850/115,000). This value is in agreement with the values put forth by Wu et al. (2013) and Patel et al. (2014), but still less. We will avoid a discussion of M-type IR excess incidence until spectroscopic evidence indicates a main-sequence age.

Considering the spectral types of the Prime and Reserved catalogs, Figure 2.9 shows the range of the best-fit SED stellar temperature. F- and G-type stars show the largest prevalence of IR excess in these catalogs. Given that the sensitivity to detect infrared excess depends on spectral type and distance, the distribution of Prime IR excess stars, especially the apparent concentration of F- and G-type stars, is likely an observational bias. However, F and G stars

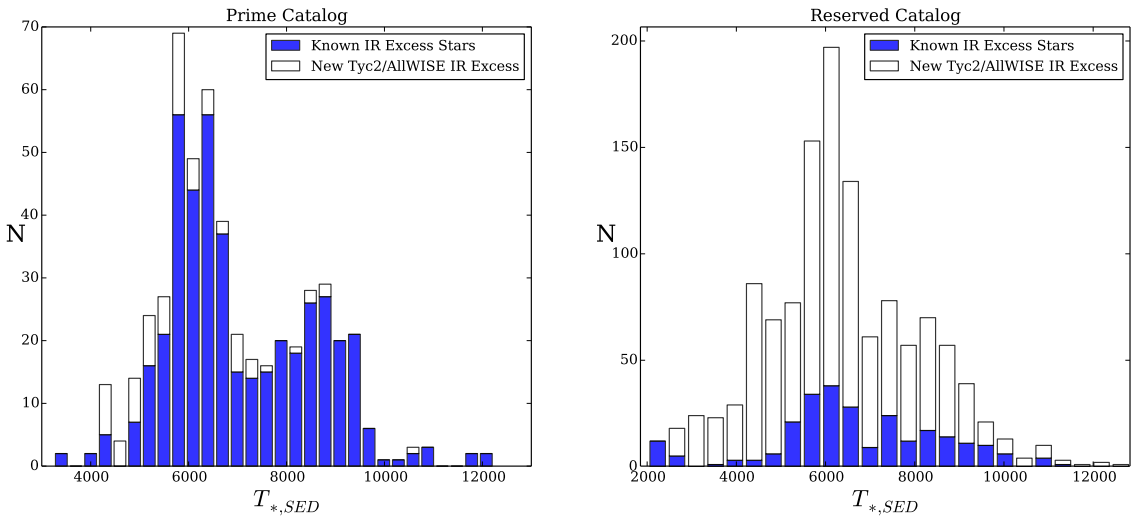

Figure 2.9: Distribution of best-fit stellar temperature in the final, Prime IR excess sample (left) and the Reserved sample (right). The filled histogram contains stars previously claimed to display IR excess and reproduced in this study. The unshaded histogram contains stars that are new IR excess detections from our Tycho-2/AllWISE search. Refer to Section 2.5 for more details.

are important for understanding the formation and evolution of stellar systems analogous to our solar system. As a secondary check for our use of the SED effective temperature as a spectral type, we gather spectral type information from SIMBAD, where the luminosity class has already been determined (82% of the Prime IR excess catalog). We use the relationship between the spectral type and the SED stellar temperature in order to extrapolate a spectral type for the remaining stars. Without significant outliers, we conclude that our SED fitting algorithm is working effectively. Both Tables 2.3 and 2.4 will display the spectral type either with a luminosity class from SIMBAD or with a ':' signifying that it is an interpolated spectral type from SED fits.

We confirm in Figure 2.10 the representation of IR excess stars across the entire sky. The dashed curve indicates the galactic plane. Stars centered on the galactic plane may show IR excess as the a result of source confusion and likely introduce false positives into the sample. However, since the new IR excess stars are not crowded around the galactic plane, we reason that the source confusion did not jeopardize our final catalogs. The two different symbols

represent the literature excess sample (triangles) and the new IR excess stars (circles) found here. The small open symbols represent the entire Reserved catalog from Table 2.4. We note in Figure 2.10 that there are more candidate IR excess stars at declinations less than -10° and at right ascensions between 150° and 250°. This region highlights the Scorpius-Centaurus Association (ScoCen, hereafter). Based on the age of $\sim$ 11 Myr approximated by Pecaut et al. (2012), we expect this region to have an enhanced density of younger stars with circumstellar material; however, the ages of the ScoCen subregions are still not fully settled (see Herczeg & Hillenbrand 2015). The new IR excess stars that are located near the ScoCen region may be on the forefront of this massive population of young stars.

2.6 Discussion

We have begun a detailed characterization study of the Prime stars by gathering optical spectroscopy and the details will be described in a future manuscript focused on the relationship between star and dust parameters. Here, we examine the dust parameters in order to investigate relationships between the SED fitting parameters: stellar temperature, dust temperature, dust radius, and the fractional dust luminosity. Lastly, we discuss the relationship between the SED disk radius and the true size of the disk for those disks resolved with scattered light imaging.

2.6.1 Fractional Dust Luminosity

The fractional dust luminosity, defined as $\tau \equiv L_{IR}/L_{star}$, provides an estimate for the amount of dust surrounding each of the IR excess stars regardless of the number of blackbody fits to the dust. Figure 2.11 shows the distribution of fractional dust luminosity for the Prime catalog (left) and the Reserved catalog (right). From this distribution, we see that the majority of our main-sequence IR excess stars have τ values between 10^{-5} and 10^{-3}. The Reserved sample shows a more central peak around 10^{-3}, although this peak should be evaluated with caution since many of the reserved IR excess stars only display one passband of

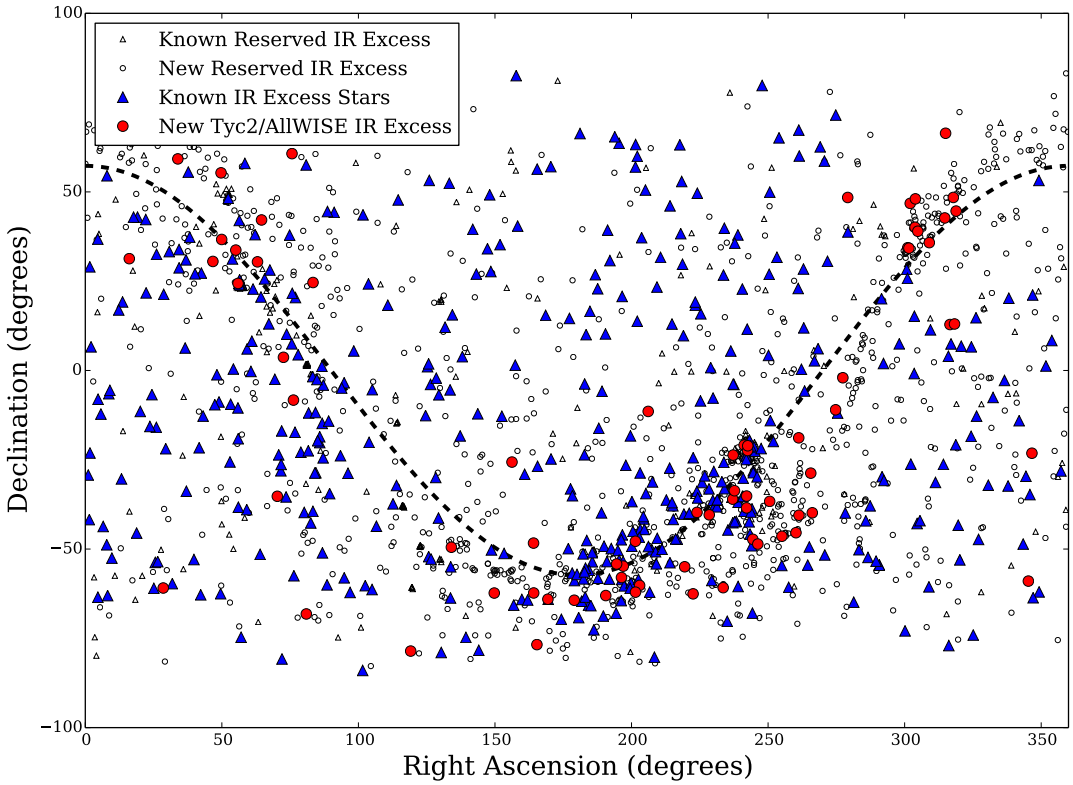

Figure 2.10: Spatial distribution of IR excess stars in R.A. and decl. Red circles represent the new, Prime Tycho-2/AllWISE IR excess stars, and blue triangles show the sample of known, Prime IR excess stars. The gray symbols are from the Reserved catalog that did not qualify for the Prime targets. The symbol shapes are the same for the literature and new IR excess stars in the Reserved sample. For reference, the dashed curve signifies the galactic plane.

excess, which increases the likelihood of degeneracy in the SED fit to the dust and may select dust temperatures that suggest a higher fractional dust luminosity. Reflecting on our sample, Roberge et al. (2012) explored the sensitivity limits of the fractional dust luminosity of past instruments. However, the investigation of the limiting detectable fractional dust luminosity assumes that each IR excess star has the same amount of dust and is representative of IR excess at far-IR wavelengths. The detectability at mid-IR wavelengths is complicated by the necessity for precise photospheric detections from which to distinguish IR excess, and so the limit of mid-IR surveys is more challenging to assess. While not found in our sample and outside of the currently detectable range (i.e. $\tau < 10^{-7}$), we would expect extremely dust-poor debris disk systems similar to our solar system ($\tau \sim 10^{-7}$; Moro-Martin et al. 2008; Wyatt 2008; Nesvorný et al. 2010; Vitense et al. 2012). Yet, the other extreme in Figure 2.11 (i.e. $\tau > 10^{-3}$) provides interesting objects since the amount of dust either can be the result of a large, destructive, transient event such as a period of Late Heavy Bombardment (LHB) or is sustained by the support generated due to the presence of gas. A period such as LHB would indicate a mature system that we are able to observe at a crucial planet evolution epoch, while the gas may indicate extreme youth.

To compare our new Tycho-2/AllWISE IR excess search with the literature, we plot the fractional dust luminosity against the Johnson visual magnitude in Figure 2.12. Figure 2.12 shows that our study extends the number of faint stars detected with IR excess. The figure also displays a trend in which these fainter magnitude stars have a higher value of τ. This trend is indicative of later spectral types (K and M) and confirms the observational bias of our survey. The Reserved catalog (right panel of Figure 2.12) displays the same trend.

Because there are a number of IR excess stars in our catalog with significantly dusty disks ($\tau > 10^{-2}$), we will take a moment just to mention these Prime catalog targets and some of the associated parameters.

Three stars from the Prime catalog are well-known IR excess sources: HD 98800 (HIP 55505), BD +20 307 (HIP 8920), and HD 141569 (HIP 77542). These stars are within 100

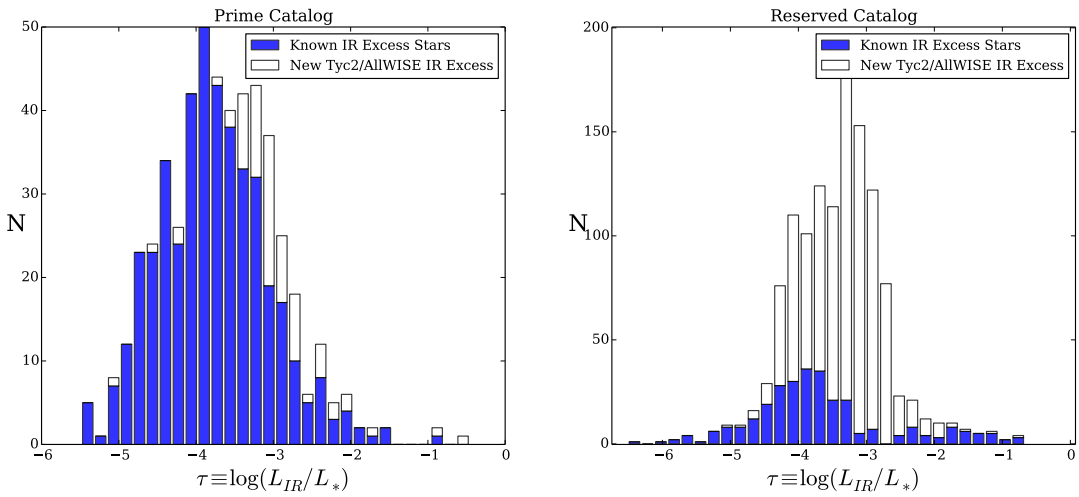

Figure 2.11: Histogram of the fractional dust luminosity displayed in logarithmic scale for the Prime IR excess catalog (left) and the Reserved catalog (right). The average fractional dust luminosity for the Prime catalog has a value of $10^{-3.8}$ where low-τ stars were not detected due to limited sensitivities of IR excess surveys. There are a handful of extremely dusty disks ($\tau > 10^{-2}$), which will be interesting for further understanding the formation and evolution of dust around a star.

pc, and our SED parameters agree with literature values. In particular, HD 98800 was first discovered by Walker & Wolstencroft (1988) and later qualified to be a member of the TW Hydrae association (Zuckerman & Song 2004b), thereby implying that the system has an age of roughly 8 Myr but still presents an inner region cleared of gas and dust (Dent et al. 2013). BD +20 307 was first discovered by Song et al. (2005) and then a thorough follow-up of mid-IR photometry revealed strong silicate features (Weinberger et al. 2011). The rarity of having a significant amount of warm dust (> 120 K) at > 1 Gyr is indicative of a recent, large collisional event (Song et al. 2005). Finally, HD 141569 is a Herbig Ae star, although the nature of the IR excess is still under debate as to whether the disk is more debris disk like even with the detection of gas in the disk. Either way, the disk was confirmed by Weinberger et al. (1999) using the *Hubble Space Telescope* and so remains one of a few dozen stars that have been resolved through imaging the scattered light.

Besides the very well known stars, a few other stars have been studied by Chen et al. (2011) and Olofsson et al. (2013). Chen et al. (2006, 2011) reported on the IR excess around

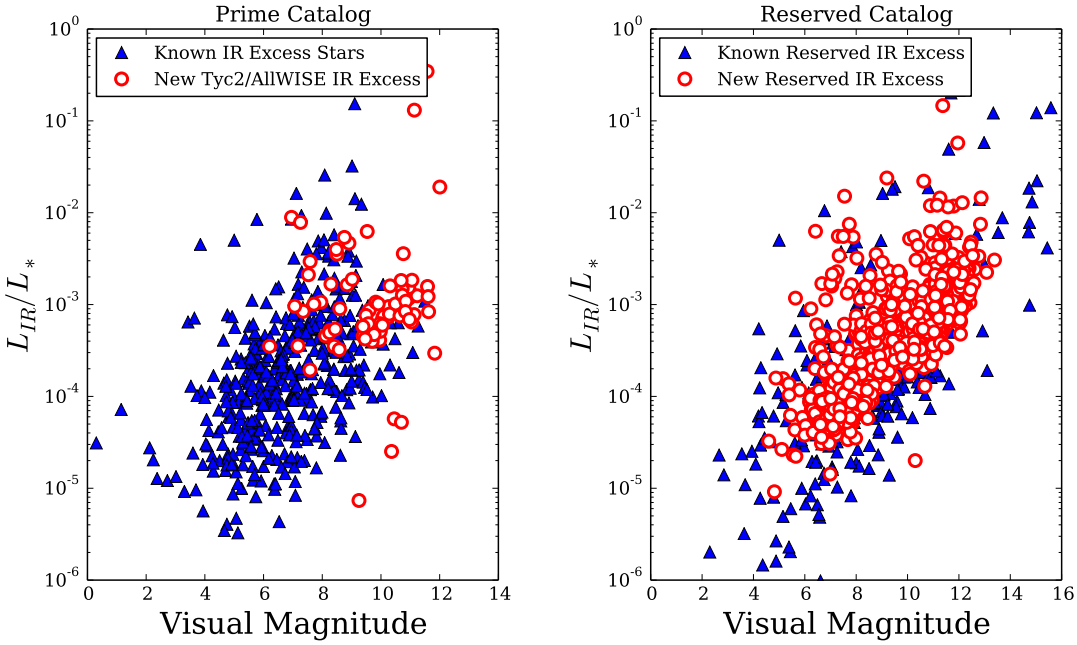

Figure 2.12: Visual magnitude versus the fractional dust luminosity for the Prime IR excess stars (left) and the Reserved catalog (right). This plot demonstrates that our new Prime IR excess stars extend to fainter magnitudes as the sensitivity of instruments has improved. The Reserved catalog covers the same range of magnitudes. There are a handful of very dusty disks ($\tau > 10^{-1}$) in the Reserved catalog; however, the majority of these stars are likely the population of remaining late-type giants in the sample based on an SED distance within 15 pc (see Section 2.3.2).

HD 146897 (HIP 79977) and HD 129590 (HIP 72070). These solar-type stars are on the edge of our distance restriction but with values of fractional dust luminosity greater than 10^{-2} making them significantly dusty compared to the rest of our Prime catalog stars. In addition, HD 129590 has IRS spectroscopy (Chen et al. 2014) that confirms the amount of dust around this star and the use of a two-component disk model fit to the dust. HD 113766 is also best fit with two separate dust temperatures (500 K, 230 K) and Olofsson et al. (2013) performed a full mineralogical investigation into the composition of grains in these disks.

In what follows, we will address the stars with new detections of IR excess individually.

TYC 6213-1122-1: This new Tycho-2 IR excess star currently does not have an entry in SIMBAD. It was best fit with a stellar temperature of 4370 K, making it a spectral type of ∼K6. The projected SED distance places this star 60.5 pc from the Earth. In combination with its position at 16 hr right ascension and a declination of -21°, we hypothesize that this star may be a new member of the Upper Scorpius-Centaurus region. Figure 2.13 displays the SED for TYC 6213-1122-1. The young age of this region (∼5 Myr; Preibisch & Zinnecker 1999; or ∼11 Myr; Pecaut et al. 2012) means that the large dust emission, $\tau = 23.2 \times 10^{-2}$, may in part be attributed to young age; however, optical spectroscopy is necessary to confirm the age of this system.

TYC 7851-810-1: This star is another new discovery with a similarly dusty disk to TYC 6213-1122-1 and a similar sky position (R.A. of 16 hr, decl. of -38°) possibly belonging to the Scorpius-Centaurus region. A recent study by Merin et al. (2008) using the *Spitzer* c2d survey, which studied "From Molecular Cores to Planet-Forming Disks," found this object near the ScoCen region and, using the MIPS instrument at 24 and 70μm, qualified the disk to be a young, Class II circumstellar disk. However, based on the shape of the SED, the disk shows a large inner cleared cavity, and without information regarding the gas content of the disk, we are led to believe that this object is definitely undergoing an interesting transient phase regardless of its age. This object will be discussed further in T. Cotten et al. (2016; in preparation). The SED provides a stellar temperature of 4590K (∼K6 spectral

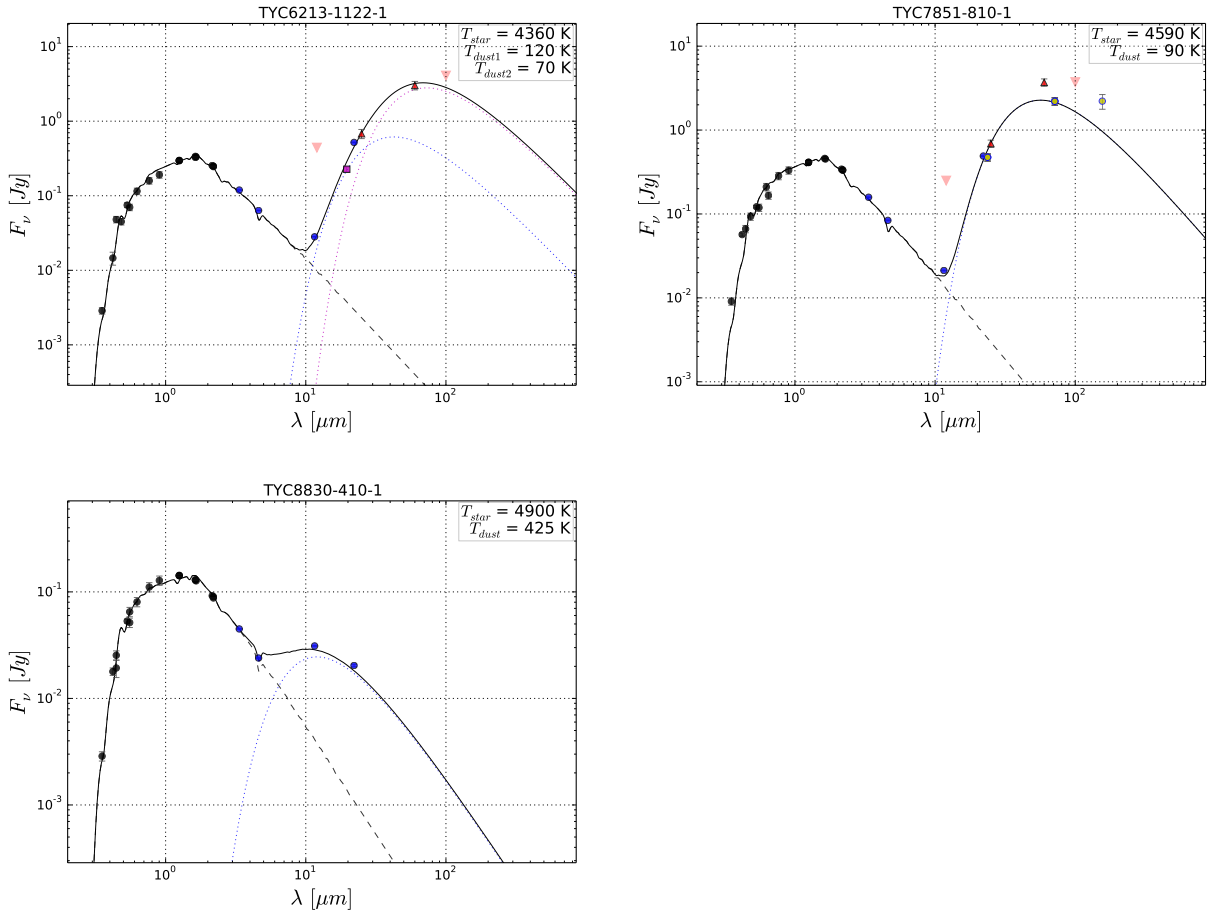

Figure 2.13: Newly discovered, dustiest disks in the Prime IR excess catalog. All of these targets display a fractional dust luminosity $> 10^{-2}$. The photometry plotted in each SED includes (not necessarily in every case) Johnson B, V (black circles), Tycho-2 B_T, V_T (black circles), *Sloan* g', r', i', z' (black circles), 2MASS J, H, K (black circles), *WISE* W1, W2, W3, and W4 (blue circles), *AKARI* 9 and 18μm (magenta squares), MIPS 24 and 70μm (yellow circles), and *IRAS* 12, 25, 60, and 100μm (red triangles) from the optical to the far-IR. A description of each star can be found in Section 2.6.1.

type), $\tau = 13.1 \times 10^{-2}$, and a distance of 57.6 pc. From Figure 2.13, the IR excess is corroborated by photometry at AllWISE W3 and W4, *IRAS* 25, 60, and 100μm, *Spitzer* MIPS 24, 70, and 160μm.

TYC 8830-410-1: This star does not have any available information or references from SIMBAD. It is best fit using a 4900 K stellar temperature, and so we assign it a spectral type of K3. The dust displays a luminosity of $\tau = 1.90 \times 10^{-2}$ in the warm inner region near the star and is best fit using a single disk with a dust temperature of 425 K. Our SED returned a distance of 120 pc for this source. Based on the evidence we have for this star, the IR excess is indicative of the rare case of warm debris such as with BD +20 307. Based on the knowledge that silicates are expected to emit around 10μm, the peak of this star's IR excess at W3 (see Figure 2.13) could indicate a transient event that is generating the destruction of planetesimals, comets, and/or asteroids. Current ongoing observations using SOFIA (Stratospheric Observatory for Infrared Astronomy; Young et al. 2012; cycle 3 and 4 programs 03_0099, 04_0126, 04_0130) should provide more evidence regarding the nature of the dust.

2.6.2 Dust Temperatures and Disk Radii

The parameters of the dust fits can be used to derive an orbital dust radius (R_{disk}) as in Rhee et al. (2007). This implies that $R_{disk}(R_{\odot}) = (\frac{R_{*,SED}}{2})(\frac{T_{*,SED}}{T_{disk}})^2$, which is then converted into AU. If the true dust grains are smaller than the model blackbody grains, they would be located farther away than blackbody grains. Figure 2.14 displays the dust temperature and radius of the disk. The symbol shapes distinguish between a single- and two-component disk fit by using a connecting solid line. Over one-third ($\sim 37\%$) of the Prime IR excess stars have disks that are best fit using two-blackbody curves. The left panels display the Prime catalog stars, while the right panels show the Reserved catalog restricted to stars that have more than one IR excess passband. These top panels show no recognizable trend for spectral type and dust temperature, which directly agrees with the reports mentioned in the

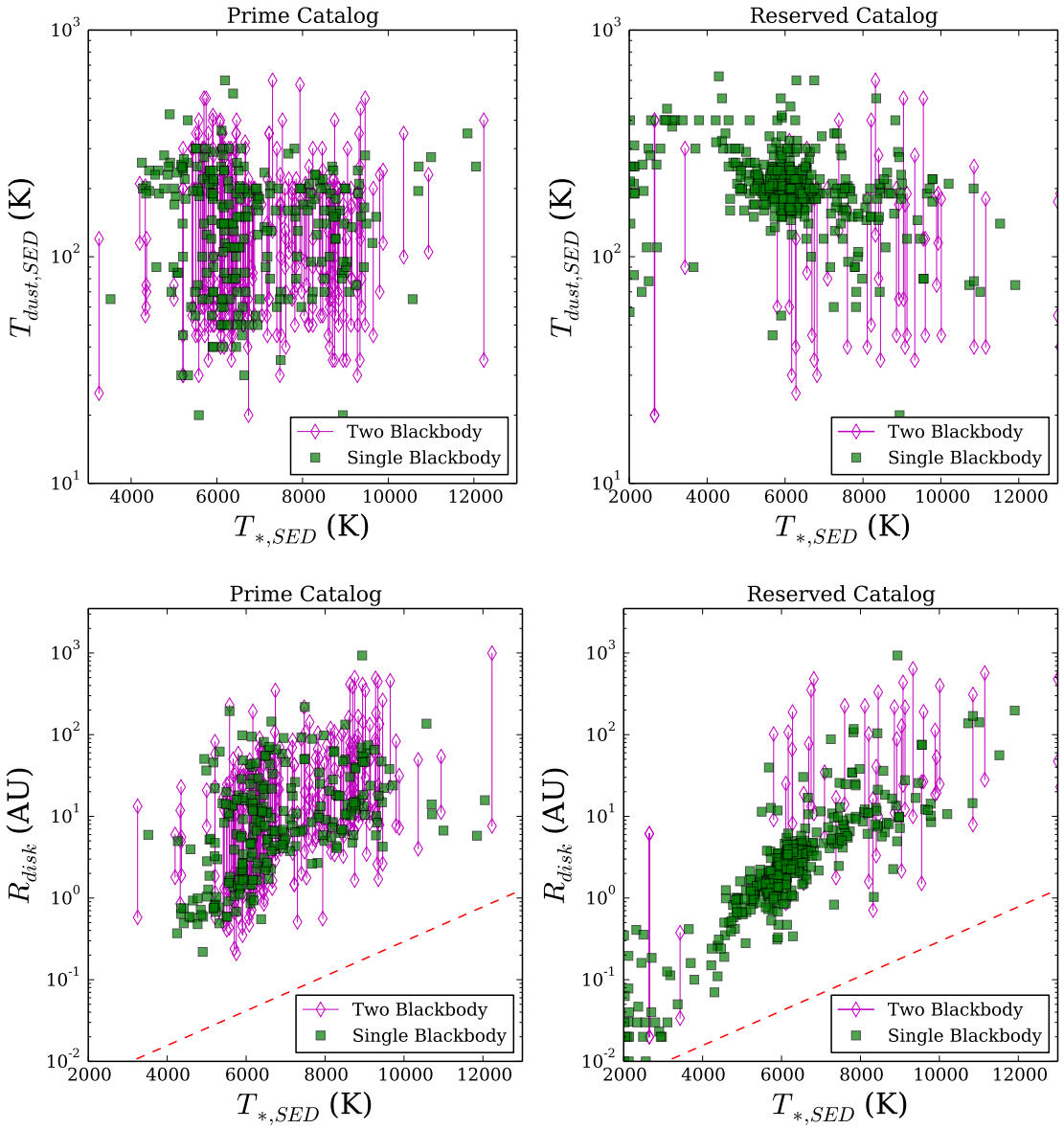

Figure 2.14: (Top) Dust temperature for the range of spectral types included in the Prime IR excess catalog (left; Table 2.3) and the Reserved IR excess catalog (right; Table 2.4). The filled squares correspond to a single-blackbody dust fit. The open diamonds are the IR excess stars that are best fit with two-blackbody fits, and the line connects the two. The sample of the Reserved catalog that is plotted displays excess at more than one passband, as without this criterion, the disk fitting procedure remains unconstrained. (Bottom) Disk radius in AU for the single- and two-blackbody fits comparing the spectral type of the star using the best-fit SED temperature for the Prime catalog (left) and the Reserved catalog (right). The dashed red line indicates the dust sublimation radius for silicate grains behaving as blackbodies at a sublimation temperature of 1500 K (Moro-Martin 2013).

review article by Matthews et al. (2014). Thus, we conclude that the luminosity and mass of the host star do not predict the temperature expected for the micron-sized grains creating the IR excess. However, the dust temperature is not the complete picture and is intimately linked to the disk radius.

Considering the results shown in the top panels of Figure 2.14, the bottom panels confirm a trend of late-type stars having the smallest disk radii. If all spectral types sustain disks of similar dust temperatures, then the late-type stars would need to have dust closer to the star to reradiate IR excess at the same temperature as early-type stars. In addition, the estimated silicate grain sublimation range ($\sim$1500 K estimated by Moro-Martin 2013) is plotted as the red dashed line in Figure 2.14. Because dust grains will be sublimated inside of this range, we do not see any IR excess stars with disk size smaller than this in our catalogs. We note, however, that for a given stellar spectral type, the smallest disk size is at least an order of magnitude larger than the dust sublimation limit. This implies either that grains far from the sublimation distance are efficiently removed by other mechanisms or that hot disks are not identifiable observationally because of the various limits (e.g., photospheric flux estimate, poor photometric measurement of excess emission, etc.).

The dust temperature for the stars fit with a single dust temperature using multiple passbands of IR excess from the Prime and Reserved catalogs is shown in Figure 2.15. The distribution of dust temperatures appears to be evenly spread, with a peak around 200 K. This peak mostly reflects the IR excess stars whose excess begins around W3 and peaks in the mid-IR. Since many of these disks are new discoveries using AllWISE and may not have far-IR photometry, our distribution may be biased in that many disks may only show the warm tail end of the dust disk. Separately, previous discoveries of IR excess make up the majority of the population of disks with cooler dust temperatures around 80 K. This is due to the fact that the known IR excess stars were mainly discovered at far-IR wavelengths where the excess begins at or after W4.

Figure 2.16 compares the fractional dust luminosity to the dust radius. The temperatures

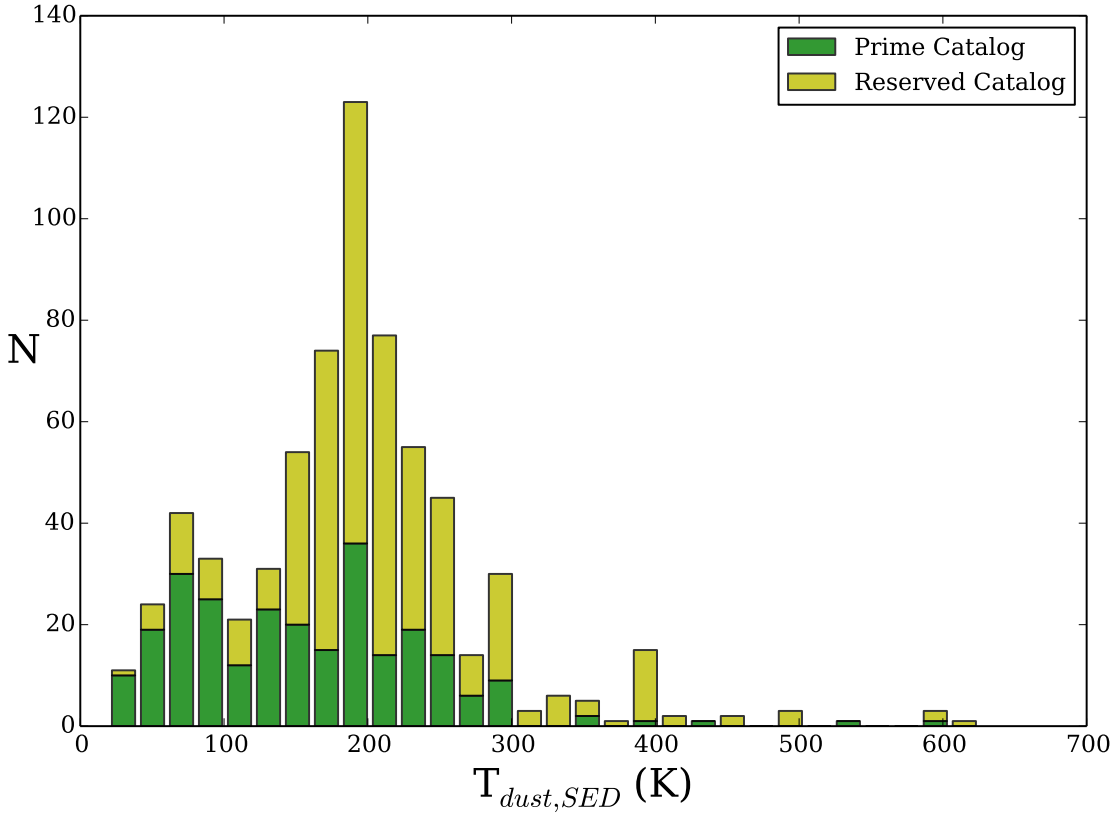

Figure 2.15: Distribution of dust temperatures for stars best fit using a single-blackbody fit in the Prime and Reserved catalogs. Only stars with multiple passbands that display IR excess are included in this figure.

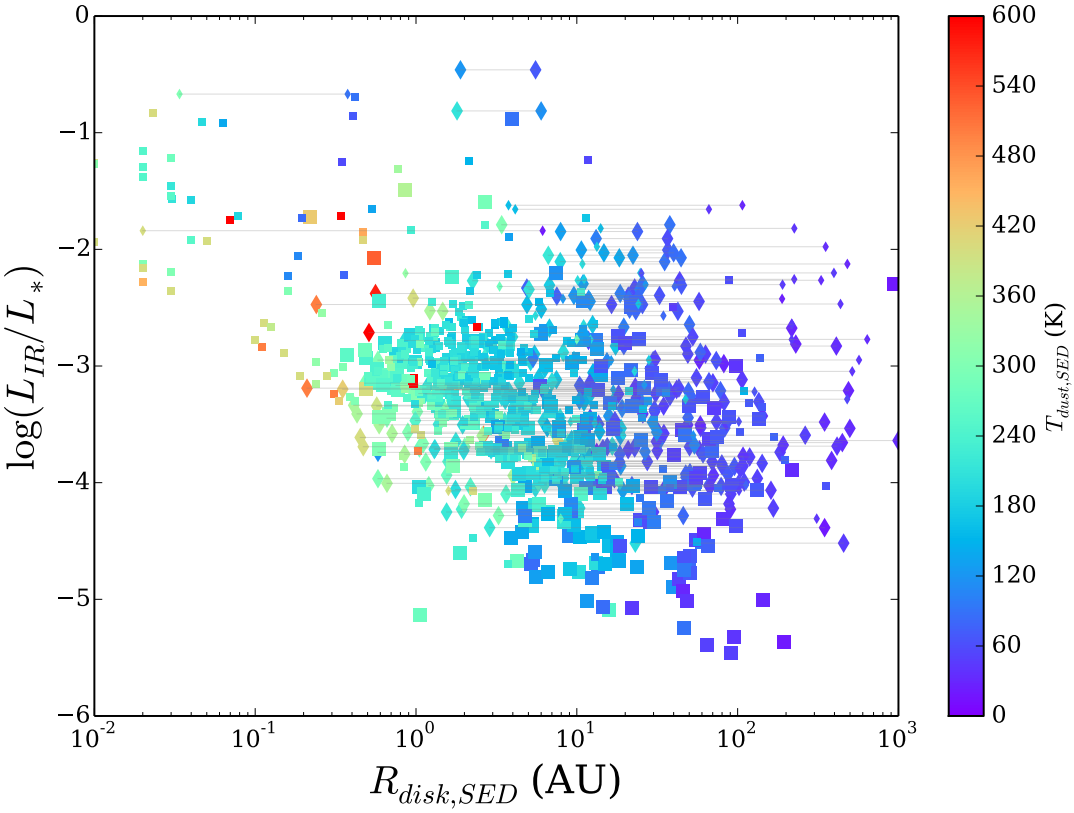

Figure 2.16: Disk radius in AU versus the fractional dust luminosity (τ) for the Prime (large symbols) and Reserved (small symbols) IR excess catalogs. The squares correspond to a single-blackbody dust fit. The diamonds are the stars that are best fit with two-blackbody fits, and the line connects the two. The color corresponds to the temperature of the dust.

of the single-blackbody fits and the two-component fits of the dust are plotted as the color in the figure. One may expect that an IR excess star with multiple disk components would exhibit a higher fractional dust luminosity, but Figure 2.16 does not display such a trend. Additionally, this figure confirms that the warm disk components are closer to the star, while the cooler components are farther away. This plot does display an apparent void of low fractional dust luminosity and small disk radius. As referenced earlier, this deficit of stars is likely an observational bias due to the difficulty in assessing IR excess from the photosphere at wavelengths shorter than 10μm, which may produce a collection of marginal, warm IR excess stars.

Studies of thermally resolved disks by Booth et al. (2013) and Rodriguez & Zuckerman (2012) found that the predicted disk radius from the SED blackbody fit was 1-5 times smaller than the size of the disk resolved in thermal imaging. They conclude from their results that the dust grains studied using different techniques must be of different sizes and compositions and, in particular, thermal imaging better traces the larger grains. Scattered light imaging probes a small grain size (submicron) and yet this ratio has been used to compare this method to the SED disk radius. In Figure 2.17, we display the predicted disk radius from our blackbody SED fit to the disk radius for stars that have been resolved through scattered light. There are over two dozen of these stars in our catalogs, and they have been identified in the tables. A few of the most well-known debris disk stars have been labeled in the figure, including AU Mic, Fomalhaut, and beta Pictoris. Figure 2.17 shows that we can make a prediction regarding the relationship between different dust detection methods. The SED disk radii (shown as black squares) displays the trend shown by the best-fit solid black line and the additional lines shown in this figure are multiplicative factors of this line. Since many of the disks are extended, we include the inner and outer components of the continuous disk rather than an average or peak location of the dust. This plot demonstrates that the resolved inner disk boundary ranges from 1 to 4 times the blackbody disk radius, in agreement with the results from Rodriguez & Zuckerman (2012) and Booth et al. (2013). Further, we extend this relationship to the outer edge of the dust disks and estimate that the outer edge of the circumstellar material can extend to nearly 20 times the blackbody dust radius.

Biases between the disks resolved through scattered light and SED blackbody modeling complicate the comparison made in Figure 2.17. For many disks imaged in scattered light, the inner portion of the disk suffers from self-subtraction due to the large stellar flux, and so an inner rim is difficult to measure. On the far side, the dust grains tend to fade out of view of the central star's flux at large distances, and so an outer rim is difficult to determine as well. Further, the inclination angle of the disk presents difficulties in determining an inner and outer edge, especially if the disk is edge-on like AU Mic. In these cases, the inner rim

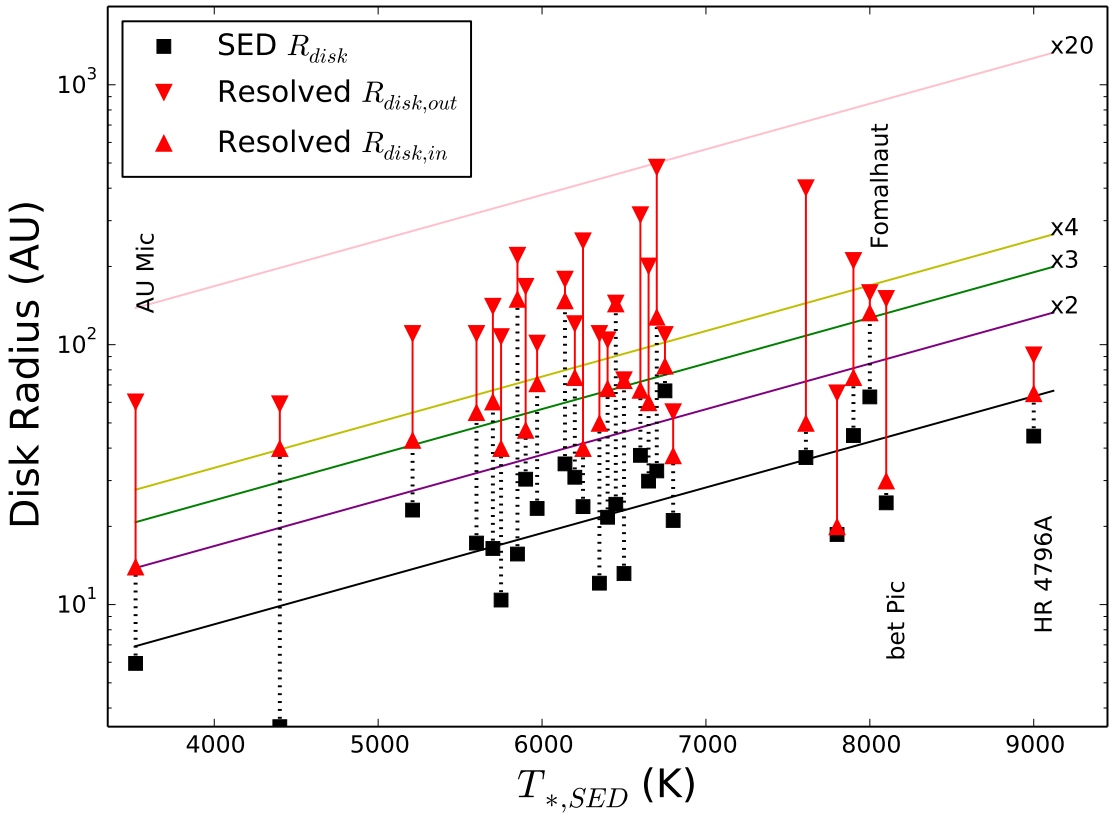

Figure 2.17: Comparison of the disk radius predicted by the SED blackbody model fit and the radius resolved through scattered light. The black squares are the SED disk radius in AU, and the red triangles connected with the solid line are the extended dust range from inner to outer radius in AU. The names of some of the most well-known debris disks are shown. All stars plotted here are flagged in Tables 2.3 and 2.4. The solid black line indicates the fit to the SED disk radius (squares), and the consecutive lines indicate the amount of increase to that fit. The purple, green, yellow, and pink lines show twice, three times, four times, and 20 times the original fit, respectively.

of the dust is approximated by the closest the scattered light technique can probe to the central star. The comparison shown in Figure 2.17 is still useful as it can be extrapolated to the entire Prime catalog and used as a method to identify targets for future observations and improve predictions regarding the expected dust location.

2.7 Conclusion

We have conducted an extensive search and collection of IR excess stars from two sources: a new Tycho-2 cross-correlation with the AllWISE catalog, and a literature search for previously claimed IR excess stars. We recognize a need for a saturation correction in AllWISE W2 and develop a simple polynomial correction. Using an SED fitting algorithm, we determine the amount of excess above the photosphere comparing the measured and the photospheric fluxes. We select new IR excess candidates by requiring an excess of $> 3\sigma$ or $> 5\sigma$ in either W3 or W4 and infrared bright in either W3 or W4 (>10 mJy). Further, extensive analysis of the AllWISE images removed a large number of false positives. We then implement a series of criteria involving brightness, number of passbands showing excess, and distance in order to ensure a sample of the highest-fidelity IR excess stars displaying an SED indicative of a post-protoplanetary disk. For stars lacking an accurate *Hipparcos* parallax, we perform an estimate of distance using the best-fit SED temperature and extrapolating a typical stellar radius from a composite isochrone. This is similar to a photometric distance, but with improved accuracy using all the available photometric data from the optical to infrared wavelengths. Finally, the inclusion of catalogs such as *AKARI*, AllWISE, *Spitzer* MIPS, *IRAS*, and *Herschel* PACS and SPIRE improves the reliability of the Prime catalog, especially when the measurements corroborate and reduce the degeneracy of the SED fitting algorithm.

Specifically focusing on our Prime sample of ∼500 nearby (< 120 pc) IR excess stars, we have compiled the largest, most reliable IR excess star catalog to date. In addition, the new Tycho-2/AllWISE search for IR excess increased the known, reliable IR excess sample by ∼20%. Moreover, a few IR excess stars appear to be new, extremely dusty systems requiring follow-up observations to better understand the evolution of the dust and/or the transient nature of the dust. The literature IR excess sample represents mainly the cold, less dusty disks, while the newly discovered Tycho-2/AllWISE IR excess stars are typically warmer and more dusty. Considering the Reserved sample, this study more than doubled the number of

known IR excess stars, and these stars are maintained for more sensitive future surveys.

We offer a discussion of the relationship between the dust parameters and stellar parameters obtained during the SED fitting procedure and a portrayal of many two disk systems that span the entire spectral type range. Our findings affirm that a two-component dust disk does not suggest any particular stellar or dust temperature, but also that the activity that generates the dust around these stars can be assumed to be analogous to either the Asteroid or the Kuiper belt and operates regardless of the luminosity or mass of the host star. Future work should strive for a complete catalog of submillimeter data, which has been shown to be more suggestive of the true amount of dust in these systems and thus the mass of dust in each system. In addition, we investigate the relationship between the disk radius assumed using a blackbody disk model and the disk radius resolved using scattered light. Since scattered light reveals the actual location of dust in the disk, the SED disk radius can be used to indicate that the true inner disk radius is roughly four times larger and the outer disk radius is 20 times larger than predicted by the SED.

2.7.1 *Acknowledgments*

We thank the referee for their very helpful comments and suggestions that have improved this manuscript. Support for this work was provided by NASA (NNN12AA01C, NAS2-97001) through an award issued by JPL/Caltech and USRA, as well as partially supported by a grant issued by SOFIA and USRA to UGA. The authors would also like to acknowledge J. Lee, A. Schneider, and L. Sgro for their helpful suggestions. This study has made extensive use of the NASA/ IPAC Infrared Science Archive, data products from the *Wide-field Infrared Survey Explorer*, the *Herschel* Science archive, the *Spitzer* Heritage Archive, SIMBAD, and VizieR (operated at CDS).

Chapter 3

Characterization of Nearby Infrared Excess Stars[1]

[1]Cotten, T. H., Song, I., Melis, C. et al. 2016, *The Astrophysical Journal*, To be submitted.

3.1 Introduction

Debris disks are important to identify relationships between the stellar properties and the presence of dusty material in order to understand the physical processes that influence the creation of our Solar System. Following the confirmations and discoveries of nearby stars with significant infrared excess (IR excess, hereafter) indicative of debris disk stars made by Cotten & Song (2016), we investigate the nature of relationships between many fundamental stellar parameters and their disks.

This chapter seeks to address relationships involving age, metallicity, rotation, and multiplicity and their effects on stars with circumstellar disks. Therefore, we first establish our observations using optical spectroscopy as well as our archival spectroscopic analysis in Section 3.3. We then describe how we obtain the fundamental parameters in Sections 3.4, 3.5, 3.6, and 3.7. These sections are followed by a discussion of observational trends and the implications, focusing specifically on the IR excess stars which are most likely to have a debris disk. In addition, due to the recent release of Gaia parallax measurements for sources from the *Hipparcos* catalog and the Two Million Brightest Stars Catalog (Tycho-2; Høg et al. 2000), we include a discussion of corrections to the Prime and Reserved catalogs of Cotten & Song (2016) (Chapter 2) with respect to giant contaminators.

3.2 Updates to Chapter 2 with Gaia Data

The recent release of the Gaia Data Release 1 catalog (Gaia Collaboration 2016a; Lindegren et al. 2016) of sources from the Tycho-Gaia Astrometric Solution inspired a reinvestigation of the Cotten & Song (2016) infrared excess sources for spurious evolved sources. A cross-match using a search radius of $5.''0$ and proper-motion corrected positions (since the positions from the Tycho-2 catalog and the Gaia release are nearly 20 years apart) returned 1222 stars from the Prime and Reserved catalogs with Gaia parallax measurements. Over 55% of these stars have no previously reported parallax measurements. This is a good representation since the

vast majority of stars from Cotten & Song (2016) were required to be Tycho-2 sources. We create an updated $(V-W2)$ versus M_V color-magnitude diagram (CMD). Using the previous criteria with updated parallax information, 17 stars from the Prime catalog and 168 stars from the Reserved catalog would be considered giants. Therefore, we consider the fraction of new giants to be 5.1% and 13.0% for the Prime and Reserved samples, respectfully. Chapter 2 reported the expected giant contamination rate of the final catalogs to be ∼6%. We believe these new values fall within this range and remain flexible since the next data release from the Gaia mission should report more accurate astrometrical observations. Still, the 17 Prime stars that are found to be giants here are excluded from our analysis of ages and dust parameters since we are uncertain regarding whether the IR excess is due to circumstellar dust or generated by stellar dynamics[2]. These stars include: TYC8991-3324-1, TYC8995-2386-1, TYC8653-1256-1, TYC8981-4034-1, TYC8962-532-1, TYC9385-93-1, TYC4079-687-1, TYC2359-1127-1, TYC8850-1468-1, TYC7358-1468-1, TYC8850-1468-1, TYC4259-1185-1, HD 278507, HD 190228, HD 210277, HD 131496, and HD 283759. In addition, we include the new disk parameters in Table A.1 in the Appendix.

3.3 Data Acquisition

Our primary objective is to obtain high-resolution optical spectroscopy of the Prime and Reserved targets from Chapter 2 to increase the number of objects with spectroscopic stellar information. As mentioned in Chapter 2, these targets are believed to be debris disks based on the classification of their spectral energy distribution displaying an obvious disk with an inner cleared region separated from the star. The parameters of interest for many debris disk star studies are temporal evolution, metallicity, multiplicity, and rotation. Since stars of spectral type ∼F3 or earlier do not provide useful age indicators through optical spectroscopy, we focus on observations of mid-F type stars or later. In addition, stars with multiple observations are presented only if stellar parameters were measured from multiple spectra,

[2]The new giants from the Reserved catalog are flagged in the online database available at www.debrisdisks.org.

Table 3.1: Optical Spectroscopy Instruments and the Number of Stars Observed

Instrument Name	Telescope	Resolution	Wavelength Range	No. of Stars
HARPS	3.6m ESO La Silla Observatory	100000	3800-7000	86
FEROS	2.2m ESO/MPI Telescope	48000	3600-9200	16
UVES	8.2m Very Large Telescope	115000	3000-6800	68
ELODIE	1.93m Observatoire de Haute-Provence	42000	3850-6800	111
SOPHIE	1.93m Observatoire de Haute-Provence	75000	3820-6930	32
Hamilton	3m Shane Telescope	60000	3500-10000	49
SSO-Echelle	2.3m Australian National University Telescope	60000	3300-9300	53
SSO-WiFeS	2.3m Australian National University Telescope	7000	5400-7000	116
DAO	1.2m Dominian Astrophysical Observatory	∼4000	6100-6770	84

otherwise, we select measurements from the highest resolution spectra available.

3.3.1 Archival Data

We examine the publicly available databases of high-resolution optical spectra for target stars. These archives include the following instruments: ELODIE, SOPHIE, UVES, HARPS, and FEROS. ELODIE echelle spectrograph offers a resolution of $\sim$ 42000 and the SOPHIE echelle spectrograph (R $\sim$ 70000) was commissioned to replace ELODIE in 2006 and continues to perform accurate radial velocity measurements (Baranne et al. 1996; Moultaka et al. 2004; Bouchy et al. 2013). The data available in these archives have been observed in similar format and therefore, reduced through similar automatic pipelines. The UVES, FEROS, and HARPS data are available through the European Southern Observatory (ESO) Science archive[3] (Delmotte et al. 2006). In particular, the UVES data (Dekker et al. 2000) have been reprocessed using the ESO pipeline. The HARPS and FEROS instruments have a readily used standard pipeline that performs the typical routines such as flat fielding and a proper dispersion solution following the observation run. A summary of the spectroscopic instruments and the number of archival spectra selected is shown in Table 3.1.

[3]http://archive.eso.org/cms.html

3.3.2 New Observations

We observed a number of stars through various facilities from 2012 to 2016. These facilities include the Lick Observatory, Siding Spring Observatory (SSO), and the Dominion Astrophysical Observatory (DAO). The high-resolution optical echelle spectrograph (Hamilton) on the Shane telescope and on the Australian National University 2.3 meter telescope provides age-related information as well as metallicity for the observed sources. The lower resolution spectroscopy obtained through the DAO 1.2 meter telescope using the McKellar spectrograph and the SSO WiFeS integral-field spectrograph is analyzed primarily for the age indicators provided by the Hα (6563Å) and Li 6708Å lines (see Section 3.4 for more details).

The echelle data reduction for the SSO instrument and the Lick Hamilton instrument is performed through a standard routine using the Image Reduction and Analysis Facility (IRAF). The spectra are trimmed, bias subtracted, and flat fielded except in the cases in which the flat fielding procedure significantly reduces the signal to noise. We derive a wavelength solution using Thorium-Argon (ThAr) calibration lamp exposures following each object observation. The Hamilton spectra include a wavelength range of ∼3900Å to 7000Å while the SSO echelle instrument covers ∼3900Å to 6750Å based on our choice of the 316/7500 cross-disperser.

Observations using the DAO McKellar spectrograph cover a small wavelength range (6150 - 6759Å) particularly defined by the 1200H grating to obtain information about Hα and Li (6708Å). The spectra are reduced in a standard 1D spectroscopy routine using IRAF and a ThAr lamp for calibration of the wavelength solution.

The SSO WiFeS instrument offers two different wavelength channels for observation and we select the red spectrum covering ∼5400 - 7000Å to identify key age diagnostic lines. WiFeS creates a spectrum for each pixel in the image, and SSO provides a reduction pipeline called PyWiFeS, described in detail by Childress et al. (2013). As Childress et al. (2013) describes, the "slitlet" spectra are extracted after detecting the main source and then they

are bias subtracted, flat fielded, and wavelength and flux calibrated. The output returns a 3D cube of the finalized spectra and the pipeline offers a simple routine to extract a final one-dimensional spectra.

3.4 Age

Age is one of the most fundamental parameters of a star and the most difficult to measure (Zuckerman & Song 2004b). Understanding the temporal evolution of debris disk stars can provide knowledge regarding the nature of the dust and the potential of planetary formation and evolution. Early studies such as Dominik & Decin (2003), Rieke et al. (2005), and Wyatt (2008) predict a power law relationship between the amount of dust in a debris disk and time such that the amount of dust falls off at a rate of t^{-1}. Other researchers, including Rhee et al. (2007) and Su et al. (2006), compiled additional evidence reflecting this same trend. More recently, however, the inversely related temporal evolution of dust was questioned in studies such as Hillenbrand et al. (2008), Trilling et al. (2008), and Lawler et al. (2009). The previously defined relationship holds for early-type stars in which the disk is undergoing a collisional cascade in timescales where the effect of PR drag is negligible (Dominik & Decin 2003). In solar-type and late-type stars, the argument can be made that due to the additional influence of strong stellar winds, the material will dissipate even more rapidly at a rate of t^{-2} (Siegler et al. 2007; Wyatt 2008), although the exact form is still uncertain. Further, investigators such as Kains et al. (2011) distinguish between a warm disk and cold disk sample in describing the evolution of debris disk stars. Given the extensive catalog of stars with IR excess indicative of being stars with debris disks provided by Cotten & Song (2016), we intend to further investigate this relationship and discuss implications for the differences in evolution with disk temperature.

Table 3.2 offers a description of the appropriate age diagnostic that we employ for various spectral types in our sample. First, we consider the likelihood that many of our objects may be open cluster members or known moving group members and apply this set age

Table 3.2: Age Diagnostic Criteria By Spectral Type

Age	M3-K5	K5-G5	G5-F5	>F5
≤10 Myr	Li, CMD	Li, CMD	Li, CMD	CMD
10-100 Myr	Li, CMD	Li, X-ray, Ca II	Li, X-ray	CMD
100-100 Myr	Li, X-ray	Li, X-ray, Ca II	Li, X-ray	CMD

Note: The criteria are listed in order of importance.

based on coevality. Otherwise we derive ages from spectroscopic information or location on a CMD. Since the age methods described may provide constraints on the particular age method selected for that spectral type, we use the additional age information as uncertainties. Therefore, Table 3.3 provides the age with upper and lower limits determined by additional age diagnostics and a note describing which method is reported. Specific details regarding the observations are also included in Table 3.3.

3.4.1 Cluster Membership

A crucial age-dating technique relies on the membership of an individual star to a number of known open clusters. Since the age of the individual member star is expected to be coeval (Zuckerman & Song 2004b), this method is often very useful as an age indicator. Recent work by Soderblom et al. (2014) and references therein point out that ages identified in this way are only reliable for ≤20 Myr; however, we continue with this method until thorough age-dating techniques are established. We compile lists of accepted members of the Pleiades from Stauffer et al. (2007), the Hyades from Perryman et al. (1998), IC 2391 from Platais et al. (2007), and η Cha from Mamajek et al. (1999) that maintain the stars have a high probability (usually > 80% for stars identified here) of being true members. Thus, we cross-match the Prime and Reserved catalogs with the member list using a 5.″0 search radius to ensure a best match. In addition, we investigate the potential membership of our stars to the Scorpius-Centaurus Association (ScoCen, hereafter), since this association contains stars of an estimated age range between 5 Myr and 17 Myr (Pecaut & Mamajek 2016).

Table 3.3: Measurements and Methods of Age-Dating for Prime and Reserved Catalog Stars

Name	Catalog	Obs. MJD	Instr.	EW Hα (mÅ)	EW Li6708 (mÅ)	$v \sin(i)$ (kms^{-1})	RV (kms^{-1})	[Fe/H] (dex)	log (g)	log ($\frac{L_X}{L_{bol}}$)	log (R'_{HK})	Multiple Ref.	Age (Myr)	Age-Dating Method	Refs	Notes
HR 9102	P	–	–	–	–	341.00	18.40±1	–	–	–	–	–	485^{+110}_{-60}	CMD	62,13,-,-	–
HD 105	P	54249.40950	VUA	1196	146	15.84	2.29±0.60	-0.12±0.01	4.46±0.02	-4.41	-4.60	–	30^{+345}_{-0}	Tuc-Hor(X-ray)	1,1,1,10/30	–
HD 166	P	53253.12860	OEA	1040	76	5.40	1.88±1.32	0.15±0.02	–	-4.39	–	WDS	375^{+0}_{-0}	Li	1,1,29,-	X-ray agreement
HD 203	P	57323.49316 SEO 57320.46287 SWO		3238	0	96.75	-0.28±11.15	-0.87±0.02	3.65±0.18	–	–	–	15^{+610}_{-0}	β Pic (Li)	1,1,1,30	–
HD 377	P	56561.92090	OSA	1116	145	15.96	1.62±21.75	-0.06±0.02	4.34±0.04	-4.20	-4.54	–	125^{+250}_{-0}	Li(X-ray)	1,1,1,-	–
sig And	P	–	–	–	–	123.00	-8.20±1	–	–	–	–	WDS,10	665^{+65}_{-120}	CMD	61,13,-,-	–
HD 1466	P	53311.16184	EHA	1381	134	20.60	7.06±2.84	-0.13±0.04	4.44±0.09	-4.18	-4.60	WDS	30^{+345}_{-0}	Tuc-Hor(X-ray)	1,1,1,10/30	Li agreement
HD 1461	P	51150.78318	OEA	1132	11	3.09	-8.32±1.31	0.16±0.03	–	–	–	–	0^{+0}_{-625}	Li	1,1,29,-	–
9 Cet	P	53624.24352	EHA	1233	82	7.88	-2.36±0.44	0.19±0.01	4.58±0.03	-4.64	-4.69	WDS	625^{+0}_{-0}	Li	1,1,1,-	X-ray agreement
kap Phe	P	–	–	–	–	213.00	11.30±3	-0.04±-99.00	–	–	–	–	940^{+30}_{-140}	CMD	21,13,4,-	–
HD 2834	P	–	–	–	–	111.00	-2.00±4	–	–	–	–	WDS	520^{+55}_{-120}	CMD	12,13,-,-	–
HD 2772	P	–	–	–	–	253.00	-12.20±1	–	–	–	–	WDS	195^{+30}_{-40}	CMD	61,13-,-,-	–
bet03 Tuc	P	53278.33238	EHA	4505	0	82.45	7.70±1	–	–	–	–	CCDM	30^{+170}_{-0}	Tuc-Hor(CMD)	1,13,-,10/30	–
HD 3126	P	53358.03861	EHA	1599	58	24.15	12.25±3.86	0.09±0.08	4.08±0.14	-4.53	-4.68	–	625^{+0}_{-0}	Li	1,1,1,-	X-ray agreement
HD 3296	P	57293.62442 SWO 57358.44166 SEO		1986	18	22.49	6.69±3.65	0.07±0.02	4.10±0.04	-5.10	–	–	625^{+0}_{-0}	Li	1,1,1,-	X-ray agreement
HD 3670	P	57293.59045 SWO 57358.45082 SEO		2142	90	29.30	5.26±5.08	0.10±0.02	4.15±0.05	-4.46	–	–	125^{+250}_{-0}	Li(X-ray)	1,1,1,-	–
64 Psc	P	56138.43972	EHA	1665	59	2.97	3.76±0	-0.20±0.02	4.25±0.07	-6.41	–	CCDM	625^{+4000}_{-0}	Li(X-ray)	1,13,1,-	spectroscopic binary
HD 5133	P	53359.03329	EHA	934	0	4.94	-13.05±0.22	0.11±0.02	4.60±0.03	-5.29	-4.80	–	100^{+50}_{-50}	CMD	1,1,1,-	–
66 Psc	P	–	–	–	–	144.00	8.50±3	–	–	–	–	CCDM	375^{+95}_{-60}	CMD	62,13,-,-	–
V443 And	P	57272.42065	DMO	1121	0	12.24	-34.10±1	-0.15±0.03	–	-5.23	–	WDS	0^{+2000}_{-0}	X-ray	1,13,49,-	–
HR 333	P	–	–	–	–	207.00	10.00±4	–	–	–	–	–	595^{+90}_{-50}	CMD	62,13,-,-	–

Only a portion of the table is contained here. The full table can be found in Appendix C.

Observation Keys: VUA: Very Large Telescope, UVES, Archival Data; OEA: OHP Telescope, ELODIE, Archival Data; OSA: OHP Telescope, SOPHIE, Archival Data; EHA: ESO La Silla Observatory, HARPS, Archival Data; MFA: MPI/ESO Telescope, FEROS, Archival Data; SWO: Siding Spring Observatory, WiFeS, Observed: S. Murphy; SEO: Siding Spring Observatory, Echelle, Observed: S. Murphy; DMO: Dominian Astrophysical Observatory, McKellar, Observed: T. Cotten; LHO: Lick Observatory, Hamilton, Observed: C. Melis, A. Schneider *Notes*: Measurements of Hα, Li 6708Å, R'_{HK}, and L_X/L_{bol} were calculated in this study. The age method included in () was used for the upper/lower limit. References column lists the reference for $v \sin i$, radial velocity, [Fe/H], and Cluster membership in this order if applicable. *References for Table 3.3:*

1 This work.

4 Anderson & Francis (2012)

10 Chen et al. (2014)

13 de Bruijne & Eilers (2012)

29 Maldonado et al. (2015)

30 Malo et al. (2013)

62 Royer et al. (2007)

49 Soubiran et al. (2016)

61 Zorec & Royer (2012)

We selected highly likely members to the ScoCen regions including Upper Scorpius (UpperSco), Upper Centaurus-Lupus (UCL), and Lower Centaurus-Crux (LCC) using de Zeeuw et al. (1999), Luhman & Mamajek (2012), and Pecaut & Mamajek (2016). Over 200 stars from our sample are believed members of the aforementioned clusters and thus a cluster age can be applied to these sources.

In order to perform a Bayesian statistical analysis on the probability of membership to known moving groups, we required the full set of parameters including parallax measurements from *Hipparcos* or Gaia, radial velocity, position, and proper-motions. For stars that were not successfully cross-matched to a member star described earlier and with high-resolution optical spectroscopy available, we measure the radial velocity using iSpec (Blanco-Cuaresma et al. 2014). Rather than using the very high-resolution solar template spectra available in iSpec, we cross correlate a number of radial velocity standards observed by the same instrument (or downloaded from the archives) with our star and report the weighted average of the individual radial velocity measurements.

The Bayesian method will be described in complete detail by Lee & Song (2016), however, we explain the procedure and our selection criteria briefly. The algorithm designed by Lee & Song (2016) is theoretically similar to the work begun in 2013 by Gagné et al. (2014) except for some information used as a "prior" such as the spatial distribution of nearby stars. Given the astrometric parameters collected as described above, the algorithm calculates the UVW and XYZ space motions of the star and, for an estimated age of the individual stars, generates a probability of membership to the following moving groups that are defined only by highly probable membership stars: AB Doradus, Argus, beta Pictoris, Carina, Tucana-Horologium, Columba, TW Hydrae, and a field star population. A total of 62 stars returned high probabilities of membership to these groups and 42 of these turned out to be already accepted members by investigators such as Malo et al. (2013) and used in the calculation of the probability itself. The remaining 20 stars were analyzed for additional criteria for ages beyond kinematics such as those techniques described above. We report here these 20

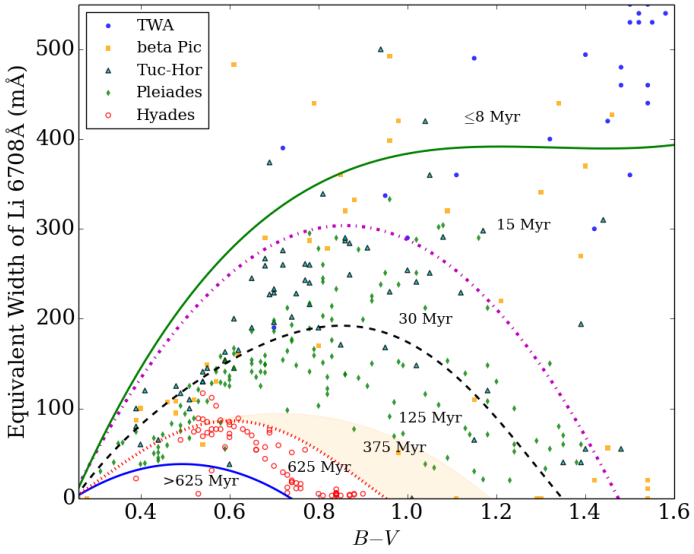

Figure 3.1: Demonstration of the age diagnostic using the EW of Li 6708Å and B-V. TWA, beta Pictoris, Tuc-Hor, Pleiades, and Hyades cluster members are displayed as blue circles, yellow squares, cyan triangles, green diamonds, and red unfilled circles, respectively. The boundaries are defined: TWA: $y = 325.8x^3 - 1296.0x^2 + 1704.6x - 350.74$, beta Pictoris: $y = -805.8x^2 + 1385.9x - 292.3$, Tuc-Hor: $y = 1122.8x^5 - 4344.5x^4 + 6131.1x^3 - 4458.5x^2 + 2034.9x - 311.7$, Pleiades: $y = 1721.3x^4 - 4186.9x^3 + 2908.1x^2 - 448.4x - 10.4$, Hyades: $y = -638.4x^2 + 630.5x - 117.6$.

member candidates based on their probabilities >80%, 13 of which have probabilities >95% and for these stars we have assigned the moving group age.

3.4.2 Lithium and Hydrogen

Ages can be estimated by measuring the equivalent width (EW) at 6708Å and comparing this value to open cluster members over a range of ages. Zuckerman & Song (2004b) discuss the caveat of age measurement using the lithium absorption due to the degeneracy between late-F and early-G type stars. The spread in the EW is much more distinguishable beyond mid-G type stars for ages between 5-200 Myr. To put a star into a Lithium age bin defined by several canonical groups of stars, we apply a series of boundaries between the different clusters that include TW Hydrae (TWA), beta Pictoris, Tucana-Horologium (Tuc-Hor), Pleiades, and Hyades. Figure 3.1 displays the boundaries as well as numerous cluster members with

measurements of the Li 6708Å line. The boundary for stars older than the Hyades is included due to the interpretation of this plot suggesting that there are likely stars within our sample that are older than even the Hyades 625 million years. Further, we consider the region slightly shaded orange to contain stars between the ages of Hyades and Pleiades members (375 Myr would be a median age) since the difference in age is so significant in this region. Ages were identified for stars with $0.3 < B - V < 1.4$ color depending upon the region that enclose the star.

Emission in Hα has been shown to indicate youth, especially in late-type stars (Song et al. 2004). Figure 5 from Zuckerman & Song (2004b) displays the ability to distinguish between main-sequence and pre-main-sequence stars based on emission of Hα. Therefore, in the case of a disk star displaying Hα emission, we believe this can potentially indicate a youthful disk, however, none of the stars in our sample display emission in Hα.

3.4.3 Calcium II H & K

Many studies have shown the usefulness in measuring the Ca II activity index to distinguish chromospheric activity and thus calculating an age for field stars and cluster members (Wright et al. 2004, White et al. 2007, Mamajek & Hillenbrand 2008). The measurement involves the calculation of the 'S-index' that subtracts the photospheric contribution from the emission. This index is often converted to the original Mount Wilson system originated by Wilson (1968) and described in detail by Duncan et al. (1991).

As mentioned previously, the archival spectra of this investigation are generated from a heterogeneous collection of archives. In order to calibrate the S-index, we first cross-match the Duncan et al. (1991) sample with each archival instrument to gather a sample of comparison measurements. We select the SOPHIE instrument as the best calibrator due to the number of matching sources (57 stars) to the catalog presented by Duncan et al. (1991). Using the standard technique described in Duncan et al. (1991) and Wright et al. (2004), the spectra are continuum normalized and a rectangular bandpass covers 20Å centered on

3901Å and 4001Å for measurement of the photospheric contribution. A triangular bandpass is used with a FWHM (full width at half maximum) of 1.09Å centered on the emission cores of the Ca II H and K lines (3933Å and 3968Å()). The flux in the triangular bandpasses is compared to the photospheric measurements such that $S_{SOPHIE} = \frac{(N_H+N_K)}{(N_R+N_V)}$ where R and V are the photospheric regions on either side of the H and K lines. The SOPHIE S-index and the Mount Wilson values (S_{MW}) are compared and the relationship is defined by: $S_{MW} = 6.792 \times S_{SOPHIE} + 0.0314$. We apply this function to the remaining sample of spectra which display the Ca II H and K features and have derived temperatures from the spectral energy distribution (SED) $4800K \leqq T_{SED} \leqq 6400K$ following the mass range investigated by Mamajek & Hillenbrand (2008) and then calculate the R'_{HK} parameter following the description in Noyes et al. (1984). Finally, while some investigators have produced age relationships for the Ca II activity index, we use the formula provided by Mamajek & Hillenbrand (2008) based on its simplicity and ability to reproduce cluster ages. Mamajek & Hillenbrand (2008) suggest

$$\log t = -38.053 - 17.912 \log R'_{HK} - 1.6675 \log (R'_{HK})^2 \tag{3.1}$$

where t is the age in years. This formula is appropriate for $-5.1 < \log (R'_{HK}) < -4.0$. We convert the prescribed ages to units of millions of years and report these in Table 3.3 if necessary. Based on the uncertainty required in continuum normalization, converting the S-index to Mount Wilson values, and using a simple polynomial function to obtain an age, we use Ca II H and K only when no other age indicator provided useful ages.

3.4.4 Rotational Period

Barnes (2007) streamlined the method of using "gyrochonology" established by Barnes (2003) which relates the rotation of the star to open clusters and the Sun. Recently, Mamajek & Hillenbrand (2008) revised the isochrones used to report ages using updated cluster infor-

mation. While many studies have used this method for age-dating purposes, the precision of gyrochonology is severely limited as Vican (2012) point out uncertainties of $\sim 20\%$ and the ambiguity in treating a star as either a fast/convective or slow/interface group can severely limit the usefulness of gyrochonology for individual stars. With the intent to use this method for the entire catalog of IR excess stars, we first cross-match the Prime catalog (506 stars) with the publicly available SuperWASP archive (Street et al. 2004) using a $30.''0$ search radius. We identify 212 stars that match sources in the SuperWASP database; however, only 74 have data with high quality (established though magnitude uncertainties $\leq 25\%$ and a statistically significant number of photometric points). We choose to use the Lomb-Scargle technique included in the Period04 package created by Lenz & Breger (2005) since the time-series data included here contain many gaps and non-uniformities. Initial results show that only a dozen stars produced a period distinguishable from the intrinsic aliasing and with an obvious sinusoidal curve after scrutinizing the data further to exclude data points with magnitude uncertainties $\geq 3\%$. Therefore, we do not maintain this information, nor use the data to produce age information from stellar rotation. Including other stellar variability catalogs may be a useful addition in future studies.

3.4.5 X-ray Emission

We cross-match the entire Prime and Reserved catalogs with the ROSAT All-Sky Survey (RASS) catalog (Voges et al. 1999). In total, 268 stars of mid-F or later spectral type returned X-ray data within $1'$ of the searched position. We convert the RASS catalog count rates to $\log(L_X/L_{bol})$ using

$$\log(L_X/L_{bol}) = \log f_X + 4.493 + (0.26 + m_V + BC)/2.5 \tag{3.2}$$

where $\log f_X = (5.3 \times \mathrm{HR1} + 8.31) \times 10^{-12} \times \mathrm{Counts}$. Here, HR1 is the hardness ratio from the RASS catalog, BC is the bolometric correction, and m_V is the apparent visual magnitude.

Finally, using the plotting space displayed in Figure 4 of Zuckerman & Song (2004b) including Pleiades and Hyades X-ray data, we identify a more likely age for individual sources using these two ages. Without extensive X-ray data at additional age bins, we perform a sufficient analysis using these two canonical clusters.

An age is estimated by the boundary shown in Figure 3.2 as Pleiades age ($\sim$ 125 Myr) or Hyades age ($\sim$ 625 Myr). We highlight a region that within $\sim$5% from the red dashed lines such that intermediate ages, assumed here to be the median of 375 Myr, can be imposed as well. We show the location of the Sun using the minimum and maximum estimated X-ray luminosity over many solar cycles from Judge et al. (2003). This allows us to shift the original boundary to an older population of stars closer to a field star age. So, we interpret stars beyond the gray dotted line segments to be older than 1 Gyr. The X-ray age is not meant to be a strict indicator, but rather to enhance the age identified from other age diagnostic techniques.

3.4.6 CMD of Early-Type Stars

A specific, although model-dependent, way to identify age is to locate the star on a Hertsprung-Russell diagram (HR diagram); however, this requires accurate distance information which is often lacking for many stars and meaningfully applicable to a limited range of certain spectral types and ages. Early-type stars do not provide the same measurement capabilities for age diagnostics as solar-type stars besides model isochrone comparison. In many cases, degeneracies exist between different isochrones at various temperatures and luminosities. Further, Brandt et al. (2015) point out that the model isochrones themselves are subject to the uncertainties in the measurement of distance, effective temperature, metallicity, and binarity along with David & Hillenbrand (2015) who describe that these models and age inferences often lack validation.

In particular, the effect of rotation on early-type stars with respect to the length of time spent on the main-sequence is important for age-dating stars $\geq 1.3\ M_{\odot}$ (Brandt et al. 2015).

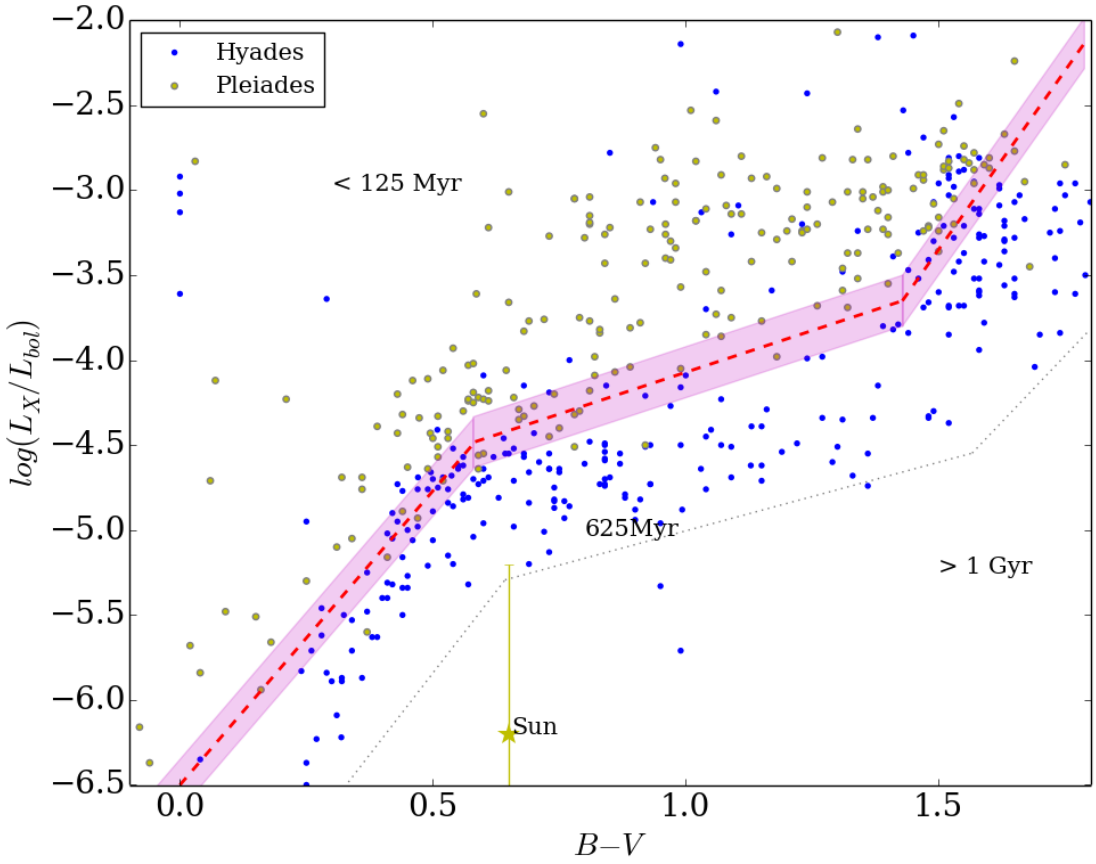

Figure 3.2: Age diagnostic using the X-ray luminosity. Members of the Pleiades are displayed as yellow circles and the Hyades members are shown in blue. The magenta dashed curve provides an empirical separation between the two clusters and the shaded region designates a region within 3σ. The red dashed curve mimics the magenta curve but is shifted to indicate the region of field stars.

We use rotating and non-rotating models from Georgy et al. (2013) and Ekstrøm et al. (2012) that provide a range of rotation rates, metallicities, and stellar masses. The models selected from Georgy et al. (2013) provide a range of equatorial velocities proportional to the critical velocity or break-up velocity and are applicable to masses between $1.7M_{\odot}$ and $15M_{\odot}$ with solar metallicity. For early F-type stars, we use the non-rotating models of Ekstrøm et al. (2012) who provide models for masses between $0.8M_{\odot}$ and $120M_{\odot}$ and solar metallicity.

Since we do not have equatorial velocity measurements for the majority of stars in our sample, we investigate the proportion of early-type stars that may be fast or intermediate rotators using the sample of stars provided by Royer et al. (2002) and applying a conversion factor. Royer et al. (2002) measured the rotational velocities for A-type stars and combined their results with work by Abt & Morrell (1995) to provide data for thousands of stars. We select 1830 main-sequence stars ranging from B5 to K5 and convert their rotational velocity measurement ($v \sin i$) to equatorial velocity using the factor $4/\pi$ as implemented by Zorec & Royer (2012) and derived by Chandrasekhar & Münch (1950) as the true statistical distribution of rotational velocities based on the unknown inclination angle. The break-up speeds are calculated for a range of spectral types and shown in Figure 3.3. This interpretation of the break-up velocity is similar to that investigated by Ekstrøm et al. (2012) and Georgy et al. (2013) except for considering the oblateness (R_{eq}) from rapid rotation. From Figure 3.3, a fast rotating early-type star is considered one in which the equatorial velocity is greater than 40% of the critical value which corresponds to an angular velocity of $\Omega/\Omega_{crit} \sim 0.6$ (Georgy et al. 2013). We regard early-type stars rotating at an intermediate speed to be rotating with an equatorial velocity greater than 20% of the critical value and so $\Omega/\Omega_{crit} \sim 0.3$.

The references for the $v \sin i$ values are provided in Table 3.3 and we convert the $v \sin i$ values to equatorial velocity using the statistical correction factor $4/\pi$ (Zorec & Royer 2012) in order to select the appropriate model isochrones. Examples of the model isochrones from Ekstrøm et al. (2012) and Georgy et al. (2013) are displayed in Figure 3.4 with stars selected

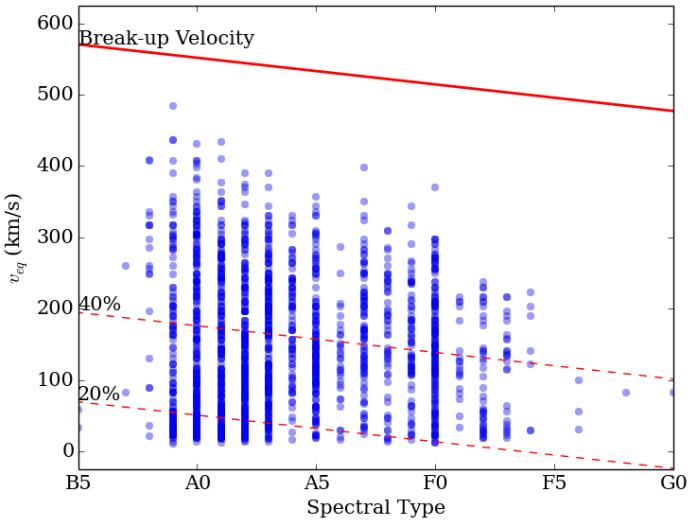

Figure 3.3: Equatorial velocities of early-type stars from Zorec & Royer (2012) converted from $v \sin(i)$ using the factor $4/\pi$ Chandrasekhar & Münch (1950). The red solid line designates the expected break-up velocity theoretically calculated through comparison of the gravitational and centrifugal forces assuming model radii for a range of spectral types. The two dashed lines represent 20% and 40% of the break-up speed.

to be fast, intermediate, and non-rotators with ages displayed as the color index ranging from $\log(\text{Age}) = 6.0$ to 10.0 in increments of $10^{0.1}$ years. For the remainder of stars in our sample that do not have literature values for the rotational velocity, we interpret that they are likely intermediate rotators and use the intermediate models. The parallax information is first selected from Gaia DR1 measurements if available and otherwise selected from measurements by *Hipparcos*. Ages were estimated through a two-dimensional interpolation using the nearest isochrones. Error bars are displayed through quadrature calculations involving the uncertainty in parallax measurements and apparent magnitudes. Using the plotted error bars, we also extrapolate this analysis to obtain an upper and lower estimate of the age. If the star is positioned close to the degenerate region or the zero-age main-sequence (ZAMS), we include a note in Table 3.3 since these stars have more uncertainty in identifying a specific age. This age is converted into millions of years and included in Table 3.3.

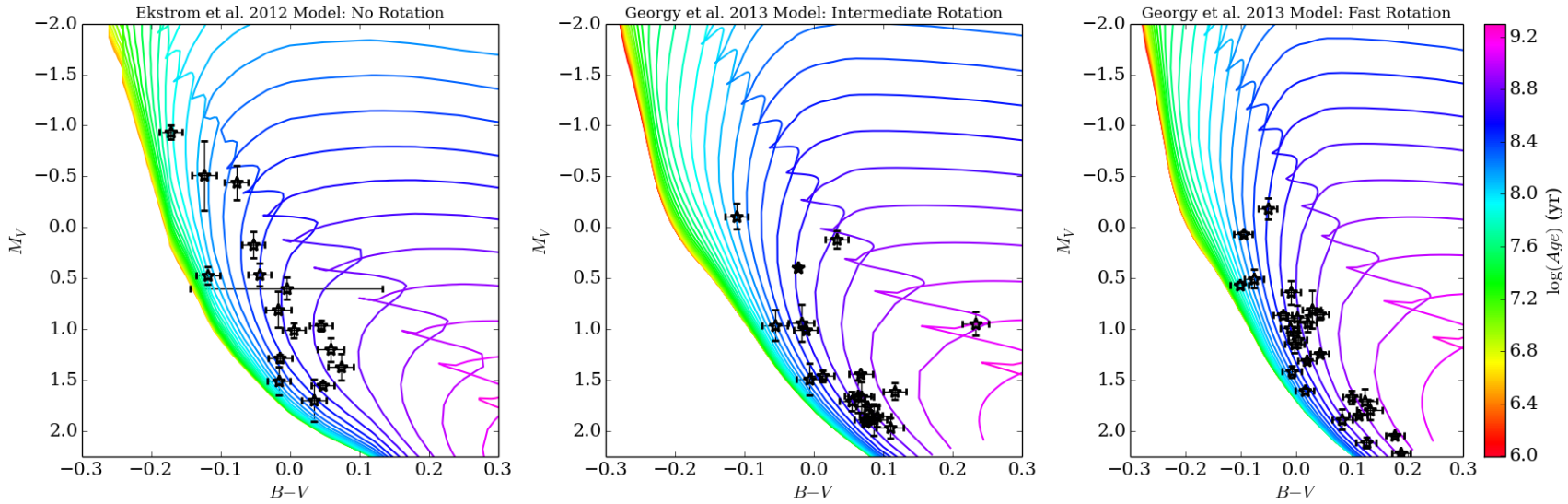

Figure 3.4: Isochrones from Ekstrøm et al. (2012) and Georgy et al. (2013) for no rotation, intermediate ($V/V_c = 0.3$) rotation, and fast ($V/V_c = 0.6$) rotation. The ages are displayed using color in the range of 1 Myr to ∼2 Gyr. A sample of early-type stars whose velocities correspond to the different plots are displayed as black stars with calculated uncertainties.

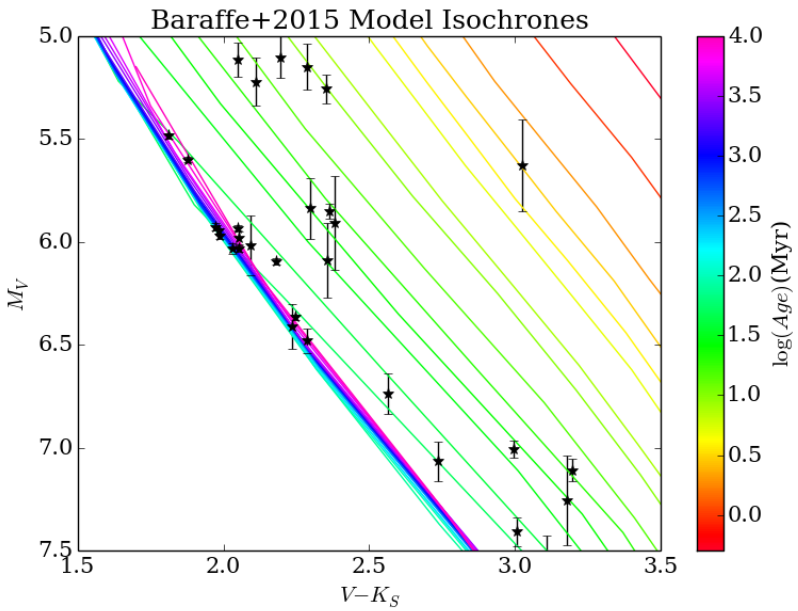

Figure 3.5: Model isochrones from Baraffe et al. (2015) with a sample of late-type stars. The ages are displayed using color in the range of 1 Myr to 10 Gyr.

3.4.7 CMD of Late-Type Stars

We select late-type stars for which we were able to ascertain Hipparcos or Gaia parallax measurements and the models of Baraffe et al. (2015) that contain improved atmospheric parameters specifically for late-type stars. Figure 3.5 displays the model isochrones using a color scale that ranges from 0.5 Myr to 10 Gyr and a sample of late-type infrared excess stars. We interpolate an age using the technique as described in Section 3.4.6 involving a two-dimensional interpolation between the closest isochrones then the same procedure applied to the error bars. For stars which fall in the degenerate region of the isochrones (i.e. error bar reaches the ZAMS region) we set the age to ZAMS which for late-G type stars is approximately 100 Myr and make a note in Table 3.3 since the ZAMS age would be a lower limit. These ages using this method are presented and identified in Table 3.3 if no other age identifiers are available.

3.4.8 Discussion: Age

To address findings regarding the inverse relationship between IR excess and time, Figure 3.6 displays the significance of excess found in Cotten & Song (2016) to the ages adopted in this investigation for the Prime catalog. We have distinguished between various spectral types and normalized the amount of excess according to spectral type. In addition, we have distinguished between stars with IR excess best fit by a single warm disk ($T_{dust} > 150$K), a single cold disk ($T_{dust} \leq 150$K), or two disk components. This is due to the fact that warm dust close to the star is expected to evolve faster than the outer, cold, Kuiper belt analogues. Further, we note that the excess at W4 (22μm) for a warm disk is close to the peak while it is close to the beginning tail of a cold disk in the case of single disk fits, but there is some uncertainty with the location of W4 excess when two disks are present.

Comparison between the top and middle panels of Figure 3.6 demonstrates the dust in the warm, inner regions of the disk does not undergo evolution on the same timescale as the dust further from the host star. However, the A stars appear to show trend in both plots since their evolution proceeds due to different mechanisms than solar-type stars. The solid curve and the dashed curve trace an inverse relationship with time and an inverse squared relationship with time, respectively. In agreement with the previously mentioned studies, the early-type stars behave similar to t^{-1} and the solar-type and later stars behave as t^{-2}. In the bottom panel of Figure 3.6, we find the significance of excess in W4 for disks with two-components behaves more similarly to the single cold disk case. These findings for a cold, outer disk confirms that these objects are likely undergoing a steady-state evolution due to collisions. While it may be possible that the W4 excess is merely tracing the cold dust component, it is also possible that the disks have evolved from a similar grain composition such that an object leading to the separation of the two disks perturbs the dust. This encourages the prediction even further that planetary objects may be embedded in these debris disks. We caution that this interpretation does not take into account the fact that collisions will produce a distribution of grain sizes. Focusing on the single warm disks, the

dust is expected to be closer to the star and thus, experience stronger dissipative forces due to the central star rather than evolve through steady-state processes. The top panel of Figure 3.6 displays several age populations of stars covering the entire range of dust emission and suggests that warm dust is transient. Thus, single warm disks may either be undergoing a significant event such as the period of Late Heavy Bombardment (LHB; Strom et al. 2005) or are recently perturbed dynamically possibly due to a planetary origin.

Kains et al. (2011) sought to compare the steady-state model of Wyatt et al. (2007) formulated for early-type stars on a collection of solar-type stars. Using observational data from Beichman et al. (2006b), Trilling et al. (2008), and Hillenbrand et al. (2008), Kains et al. (2011) showed that theoretically the relationship between age and amount of dust converted to fractional dust luminosity using this model should behave as $\tau \propto t^{-0.47}$. Figure 3.7 displays the fractional dust luminosity as a function of age for our Prime sample. We display only the Prime stars since the fractional dust luminosity is significantly constrained by multiple photometric confirmations of IR excess. Spectral types have been distinguished by different colors and symbols as described in the figure caption. In addition, we portray the age ranges as reported in Table 3.3 as error bars and stars with only upper or lower limits to the age as arrows. The stars with only limits on the age are not included in our fits. A fit to the entire population yields a power law function such that $\tau \propto t^{-0.34}$, however, there is a known spectral type dependency on dust removal mechanisms and time scales. Thus, power laws of the following forms give fits to the individual spectral types:

$$\begin{aligned} \mathrm{A} &: \tau \propto t^{-0.20} \\ \mathrm{F} &: \tau \propto t^{-0.35} \\ \mathrm{G} &: \tau \propto t^{-0.42} \\ \mathrm{K} &: \tau \propto t^{-0.44} \\ \mathrm{M} &: \tau \propto t^{-1.48} \end{aligned} \tag{3.3}$$

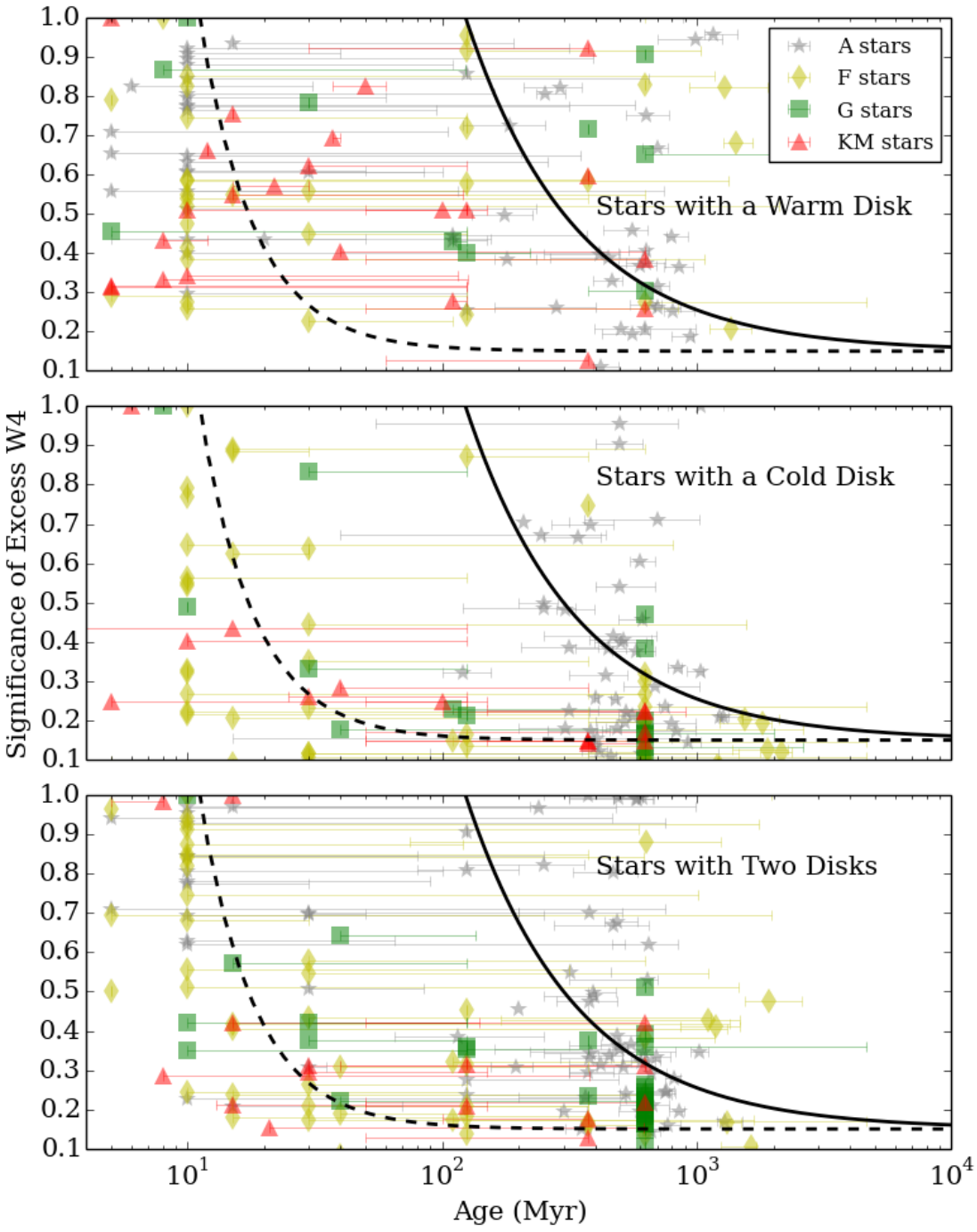

Figure 3.6: Significance of excess in W4 compared to age for stars with a single warm disk, single cold disk, or two disks. Spectral types A, F, G, and K and M are shown as grey stars, yellow diamonds, green squares, and red triangles accordingly. The panels display a solid curve corresponding to inverse time and a dashed curve corresponding to the inverse square of time.

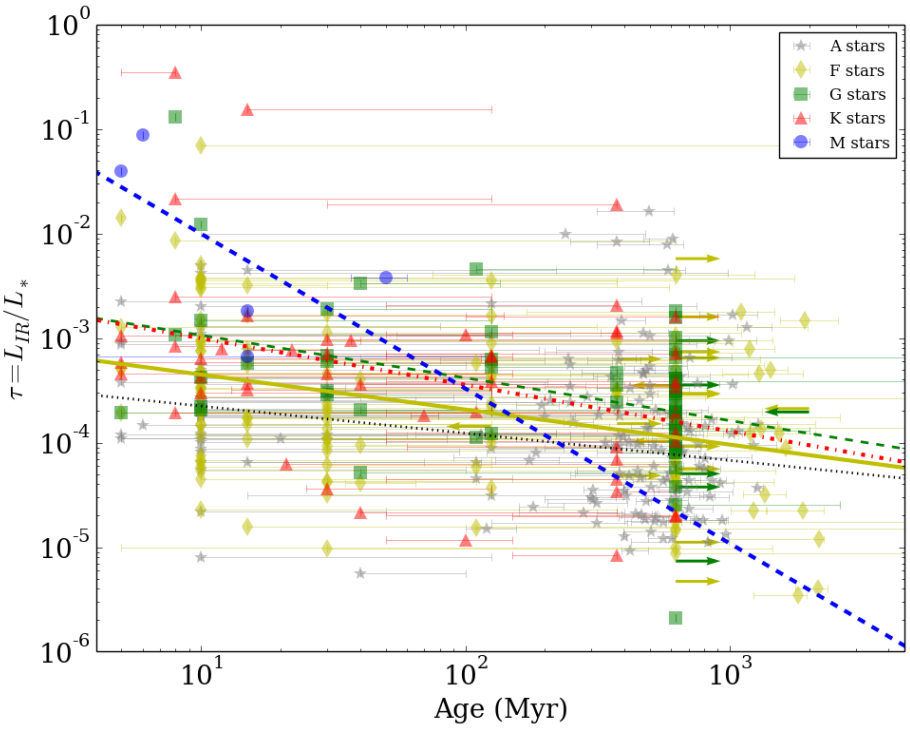

Figure 3.7: Fractional dust luminosity compared to age in Myr. The spectral types have been plotted similar to Figure 3.6 with the exception of M stars which are shown here as blue circles. The solid arrows identify stars with either upper limits or lower limits on the age. The black dotted line corresponds to A stars, the yellow solid line corresponds to F stars, the green dashed line corresponds to G stars, the red dot-dashed line corresponds to K stars, and the thick blue dashed line corresponds to M stars.

These fits are displayed in Figure 3.7 as lines of color matching the spectral type symbols. Focusing on the FGK stars, our fit agrees very well with the model fit suggested by Kains et al. (2011) that implies a steady-state evolution of dust for these objects. This comparison also confirms the prediction that solar-type stars dissipate disks faster than A-type stars and late-type stars are the fastest, although we note that the fit to the M star population suffers from a very small sample size.

3.5 Metallicity

The metallicity of a star is a parameter that describes the amount of metals present in the atmosphere of a star. Findings from Fischer & Valenti (2005) that stars with higher

metallicities are more likely to be hot giant planet host stars, led to the suspicion that debris disks may have the same trend. Theories speculate a high metallicity could either originate from birth or through the atmospheric pollution due to disk material falling on to the star during its evolution (Greaves et al. 2006). Wyatt (2008) explained this speculation using the Core Condensation Planet Formation theory suggesting that if more material is available during the formation of the star and disk, this leads to larger reservoirs of material necessary for the formation of the cores of giant planets. Either way, since debris disks are intimately tied to planetary material, these studies are key to characterizing stellar evolution and planet formation. Recently, Maldonado et al. (2012) challenged these ideas following the findings which suggest that low-mass planets are not found preferentially around metal-rich stars. Limited by observational constraints, Beichman et al. (2005), Bryden et al. (2006a), Greaves et al. (2006), and Kospal et al. (2009) found no correlation between metallicity and infrared excess in their samples, yet this relationship requires further confirmation. Challenges to this hypothesis suggest investigations requiring a more thorough abundance analysis of refractory elements other than iron (Ritchey et al. 2014, Gonzalez et al. 2014). Further, Gáspár et al. (2016) investigated the relationship between metallicity and dust mass specifically and found agreement with the core accretion model in that massive disks are less likely to have a low metallicity, although the study mentions the few objects used in the comparison. These interesting results suggest that ideas regarding the role of metallicity in stellar evolution are incomplete.

In our study, derivation of metallicity requires high-resolution optical spectra spanning the range of 400 - 670 nm. We implement a pipeline metallicity derivation using the iSpec tool (Blanco-Cuaresma et al. 2014). The iSpec code is based on the SPECTRUM code by Gray & Corbally (1994) and we refer the reader to Blanco-Cuaresma et al. (2014) for a full description of this tool, but we summarize the pipeline steps briefly. Following the continuum normalization, barycentric velocity correction, and radial velocity correction, the telluric regions were identified and flagged for avoidance during the line fitting procedure.

The algorithm automatically identifies a series of iron line masks (FeI and FeII) and measures the equivalent width for over 300 individual lines. iSpec performs an iterative spectral comparison using a least squares fit over the following free parameters: $\log(g)$, [Fe/H], v_{mic}, and v_{mac} where v_{mic} and v_{mac} are the microturbulent and macroturbulent velocity, respectively. We fix the rotational velocity ($v \sin i$) to 3 kms^{-1} and the other velocities are free to vary. T_{eff} is also fixed to the best-fit stellar temperature from the SED since our initial investigation found that fixing the temperature ensured dwarf constraints on $\log(g)$. We select the model atmospheres from MARCS GES/APOGEE models which assume Local Thermal Equilibrium (LTE) and provide effectives temperatures in the range of 2500 to 8000 K, $\log(g)$ values in the range of 0.0 to 5.0, and metallicities in the range of -5.0 to 1.0 (Gustafsson et al. 2008). In addition, we choose the solar abundances for comparison from Asplund et al. (2009). 161 stars have recalculated metallicity measurements using our spectra and 56 measurements reported here were previously unknown. We mention that stars observed with the SSO Echelle produced very poor quality spectroscopic measurements due to clouds, brightness, and technical issues during observations and, therefore, should be interpreted with caution.

For stars in our sample which we were unable to observe or locate archival spectra, we searched the VizieR database for measurements of [Fe/H]. We were careful to select actual measurements that were reported rather than estimated or photometrically derived metallicities. In this way, the literature data and our new measurements of metallicity can be compared. In particular, we believe our measurements should correlate well with those in the literature since we compare the measurements using iSpec to literature values for >120 stars with $T_{eff} < 6300$ K and found a nearly 1-to-1 relationship between the two sources. We collect metallicity information for over 400 infrared excess stars from 20 different literature references. The metallicity values and references are provided in Table 3.3.

3.5.1 Discussion: Metallicity

While many studies were unable to establish a firm relationship between higher metallicity stars and debris disk stars (Beichman et al. 2005, Bryden et al. 2006a, Greaves et al. 2006, Kospal et al. 2009), Maldonado et al. 2012 identified a deficit of debris disk stars with [Fe/H] $<$ -0.1. Similarly, Gáspár et al. (2016) reported that larger disks were less likely to be found at [Fe/H] $<$ -0.2. We display the distribution of metallicities amongst our Prime and Reserved sample in Figure 3.8. We do not find a noticeable deficit of stars at any subsolar metallicity displayed as the shaded region in the figure, especially given the distribution is centered at [Fe/H]$\sim$-0.1. The proposition that metal-rich stars (as measured by [Fe/H]) would have more material to develop gas giant planets (Fischer & Valenti 2005) seems to suggest that stars with disks should also follow such a trend since the circumstellar material is intimately tied to the formation and evolution of planets and planetesimals. However, the distribution of Figure 3.8 seems to conclude otherwise. We do note that the collection of metallicity values presented here are heterogeneous in source. Although, we collect only metallicity which is actually measured from spectroscopy. Also, Blanco-Cuaresma et al. (2014) compare the synthetic spectrum fitting using iSpec to reference values and find very small differences and so the heterogeneity of this study should be acceptable.

To investigate the lack of trend, we compare the fractional dust luminosity (i.e. the amount of dust) to the metallicity of Prime stars in Figure 3.9. The triangles reflect stars that lack uncertainties for the metallicity reported in the literature and so we do not include them in our fit. We fit the data using a Theil-Sen linear regression analysis to eliminate significant outliers and show this as the green solid line in the figure. The lack of trend negates the prediction that dustier disks may also have a higher metallicity since the slope of this line is $\sim$0. Additionally, the Pearson correlation coefficient for this data is 0.05, confirming the lack of any significant trend. Recently, Gáspár et al. (2016) mentioned that the investigation into a trend involving debris disks should distinguish between whether or not the disk has a single component or two components. A disk with multiple components

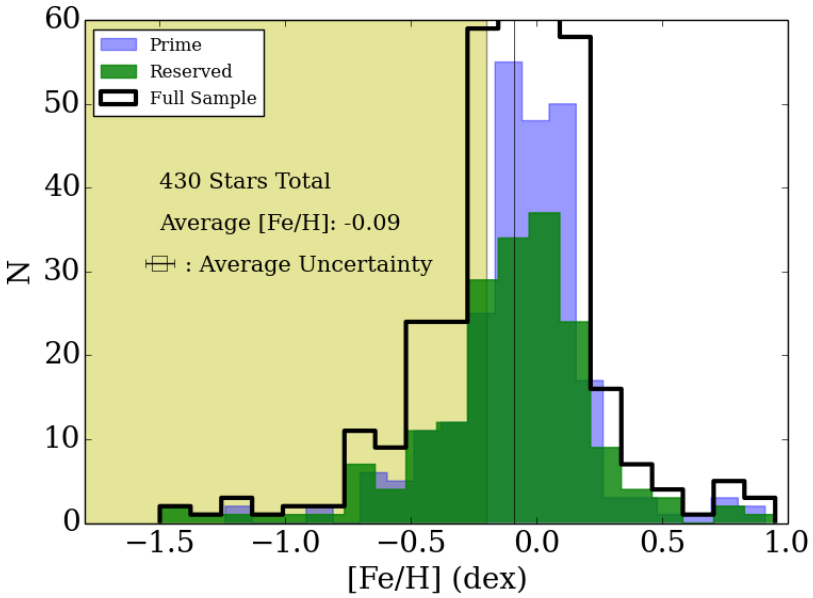

Figure 3.8: Distribution of [Fe/H] values for the Prime, Reserved, and combined catalogs. The average value of metallicity for the full sample is -0.09 plotted as the solid vertical line and the full sample is distributed about this line. The shaded region highlights the area of expected deficiency identified by Maldonado et al. (2012) and Gáspár et al. (2016).

could be more closely linked to the formation and evolution of giant planets since the planet could be the perturber that carves out a region between the two disks such as in the case of our Solar System. Figure 3.9 also shows our Prime sample with a single disk as the blue points and the stars with two component disks as red points. Using the suggestion of Gáspár et al. (2016), our sample does not show a deficit of the dustiest stars ($\tau > 10^{-3}$) at low metallicities.

There is, however, a dearth of stars across the entire sample with [Fe/H]>0.25 which seems to agree with previous studies such as Greaves et al. (2006). Only 36% of the stars with a single component disk and 30% of stars with two disk components have supersolar metallicities. We note that for these stars with IR excess we have not considered whether they are known planet hosts or undetected planet hosts. Greaves et al. (2006) explain the correlation of giant planets and high metallicity using the core accretion model and point out that the planets can form rapidly, migrate inwards, and clear their disks of detectable debris.

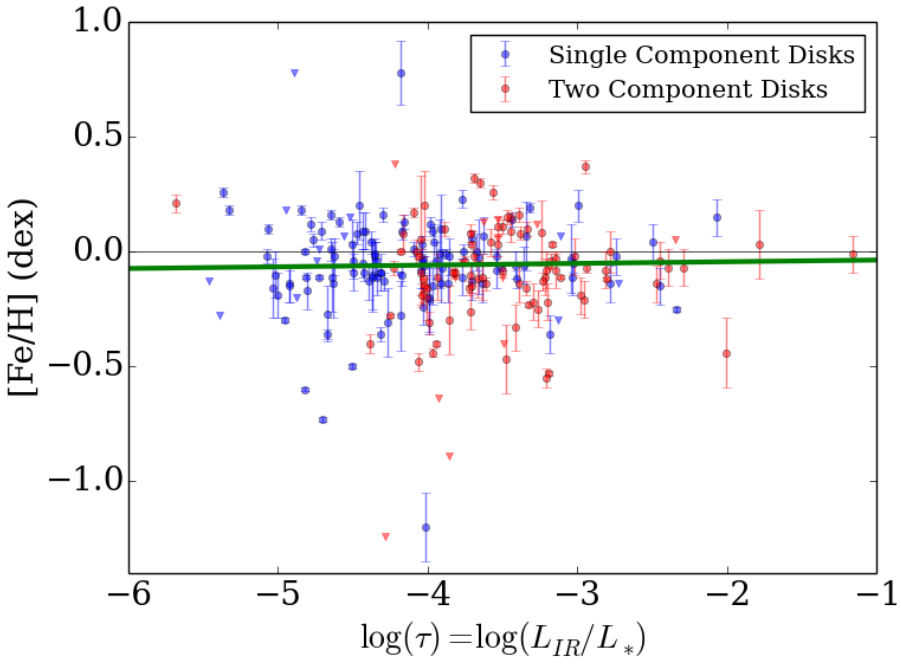

Figure 3.9: Metallicity for Prime catalog stars compared to the fractional dust luminosity. Circles designate stars with measured uncertainties and triangles are upper limits. The blue points are IR excess stars best fit with a single disk and red points have two dust components. A horizontal solid line is included to indicate solar metallicity. The green solid line is the best fit using a Theil-Sen Regression analysis to exclude outliers.

In line with this argument, Maldonado et al. (2012) reported that the stars found to have disks and planets were more likely to host low-mass planets. Our findings can then be viewed in the context of low-mass planet formation such that even a low metallicity environment can still form rocky, solid bodies which are capable of producing the dustiest debris disks from collisions. We conclude that the metallicity must play a role in the type of planets that are able to form and thus the lifetime of the gas in a circumstellar disk if low-mass planets are more likely to form. A complete survey of planets found around stars with debris disks will provide a more complete answer to this question.

3.6 Rotation

In discussing the relationship between a star and its disk, stellar rotation is a key parameter of interest to understand the relationship between angular momentum and circumstellar disk evolution. The review article by Herbst et al. (2007) identifies what has become known as the "angular momentum problem" that describes the fact that the angular momentum of main-sequence stars is 5 to 6 times less than measurements of protostellar cloud cores (Bodenheimer 1995). Therefore, theorists and observers have sought solutions to the additional mechanism that transports angular momentum from the core and recognized a link between pre-main-sequence stars and their circumstellar material. Initial studies by Kundurthy et al. (2006), Rebull et al. (2006), and Currie et al. (2008) of pre-main-sequence stars and T-Tauri stars suggested that massive primordial disks became massive debris disks and found that the slower rotating stars had larger amounts of IR excess. This relationship describes what is referred to as "disk-locking" explained in detail in the review article by Bouvier et al. (2014). Essentially, the stellar magnetosphere is locked to the disk and slows the star's rotation, thus Herbst et al. (2007) summarizes that rapidly rotating stars are presumed unlikely to have disks while slowly rotating stars may or may not have a disk. The extrapolation of this finding from pre-main-sequence disks to debris disks is still uncertain.

Herbst et al. (2007) cautions that it is an oversimplification to assume that the star's rotation is completely controlled by disk-locking. In particular, the spectral type plays a role since Plavchan et al. (2005) predict that stellar winds of late-type stars efficiently remove dust grains as an explanation for the dearth of M-type stars with mature debris disks. The observational evidence suggests that late-type stars might not display the same trend of massive primordial disks becoming massive debris disks. Although Sierchio et al. (2010) corroborated the results of Kundurthy et al. (2006) and Rebull et al. (2006) with a sample of solar-type stars with mature debris disk stars and suggested that the wind strength is overestimated, Mizusawa et al. (2012) isolated the effects of the stellar wind by dividing their sample at F5. Mizusawa et al. (2012) unexpectedly found that the late F-type, rapidly

rotating stars had the highest incidence of infrared excess. We seek to determine these effects using a large sample size across a range of rotational velocities and spectral types.

We measure the rotational velocity using $v \sin i$ as a rough observational constraint since the inclination angle is unknown. For stars which have new optical spectroscopy, we derive $v \sin i$ values following the method outlined in Fekel (1997) applied to a number of Fe I, Fe II, and Ca I lines near 6400Å. We measure $v \sin i$ for 386 stars in our sample with optical spectra. In addition to new measurements, we searched the VizieR database using our entire Prime and Reserved samples. Over 25 references offer $v \sin i$ measurements for 571 stars. Our discussions using $v \sin i$ will use the new measurements in place of literature values if applicable.

3.6.1 Discussion: Rotation

To investigate the findings of Mizusawa et al. (2012) we compare the fractional dust luminosity of various spectral types to $v \sin i$ in Figure 3.10. The vertical line designates the separation between fast and slow rotators by Mizusawa et al. (2012) at 15 kms^{-1} which they select based on the saturation of the X-ray flux in G stars. This saturation would then correlate to the activity of G stars and hence, the rotation rate. Using a value of 15 kms^{-1}, our sample of FGK stars is nearly equally divided (114 fast-rotators and 120 slow-rotators) and so we maintain this criteria. We have also plotted the sample of A stars from the Prime catalog. However, these stars are known to rotate faster than solar-type stars since their convective zone is shallow and they do not have magnetic fields to slow their rotation, so we focus our discussion of Figure 3.10 on the solar-type sample.

We expect that the fast rotating stars with the highest fractional dust luminosity should necessarily be young. The four stars with $\tau > 10^{-1.52}$ and rotating fast include HD 98800, HD 113766, TYC7851-810-1, and TYC6213-1122-1. These stars are all found to be younger than ∼20 Myr as shown in Table 3.3 based on their strong Li content. We ignore these stars in discussing the rest of the sample.

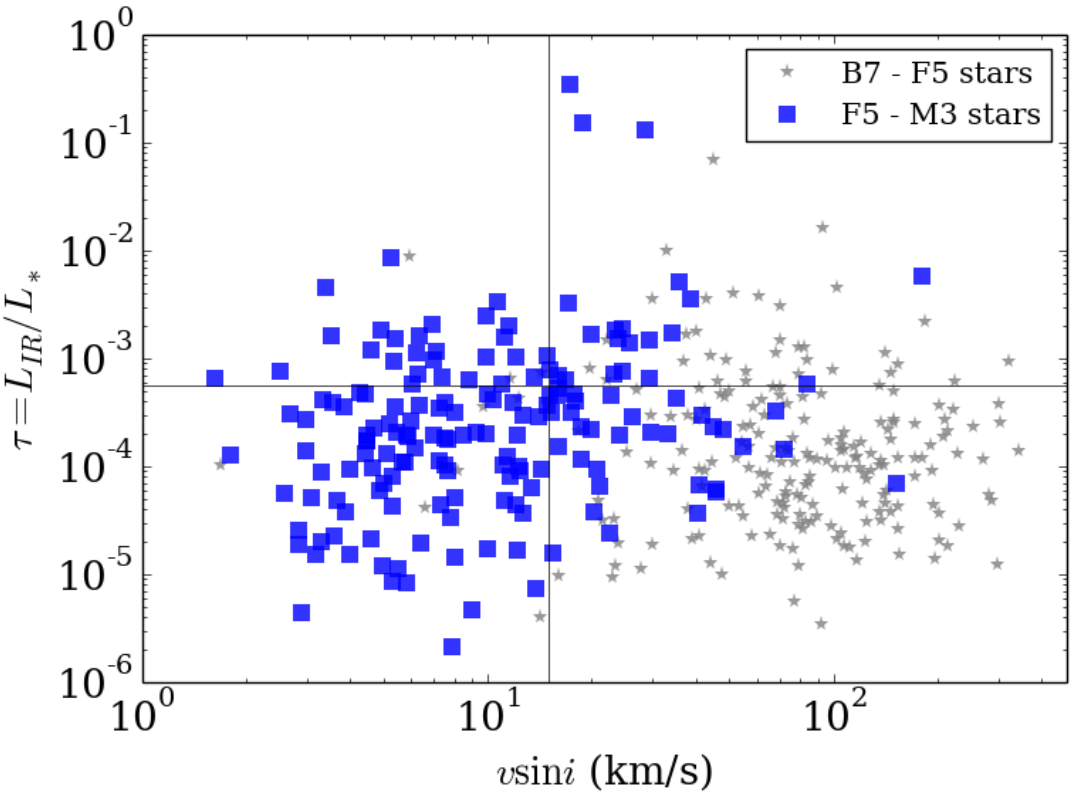

Figure 3.10: Fractional dust luminosity versus the rotational velocity of Prime catalog stars. Spectral types are separated into early-type and late-type at F5 based on the convective zone and magnetic field which greatly influence stars later than F5 (Schatzman 1962). The vertical solid line represents the split between fast and slow rotating stars at 15 kms^{-1}. Refer to Section 3.6.1 for more details.

Figure 3.10 also displays a horizontal line indicating the average value of fractional dust luminosity excluding the four dustiest stars. This line identifies stars that may be dustier than average with respect to the fast/slow designation and we do not identify a trend from this figure. Using a Spearman correlation for the sample of stars of spectral type later than F5, we find a coefficient value of 0.15. This implies that there is no correlation we can make between stellar rotation and the dustiness of a debris disk and this result contradicts the findings of Mizusawa et al. (2012) and Sierchio et al. (2010) who confirmed angular momentum trends using samples of debris disk stars. The evolution of the disk to an optically thin debris disk and the evolution of the stellar angular momentum do not appear to be directly related. We note that the slowly rotating stars across all spectral types span the entire range of fractional dust luminosity as expected; however, this may not be a correspondence to the postulates discussed above. A massive primordial disk slowing stars in their early lifetime does not directly link to the debris disk phase. It also does not appear to be true that the mass of the primordial disk translates into the mass of the debris disk (estimated here as the fractional dust luminosity).

A lack of trend could result from using debris disks for this investigation since the relationship between angular momentum and the amount of dust is recognized for primordial disks which are still gas-rich. In addition, Kundurthy et al. (2006) point out that including binary stars could also influence the amount of dust and misidentify a trend. However, the sample presented in Figure 3.10 contains nearly equal numbers of single stars and binary or multiple star systems (54% are single stars), and we do not distinguish a difference in the distribution of these stars. Finally, we point out that these findings contain an inherent ambiguity in using $v \sin i$ without knowledge of the inclination angle or the true rotation rate.

3.7 Multiplicity

Based on the understanding that multiple star systems are more prevalent than single stars (Fischer & Marcy 1992), Duchêne & Kraus (2013) inquired whether the circumstellar environment of multiple star systems is conducive to planetary growth. Researchers including Pascucci et al. (2008) and Kraus et al. (2012) investigated the effects of binarity on the growth and settling of dust grains in young, pre-main-sequence disks and found that binarity shortened the timescale of planetary formation and wide separation binaries are able to sustain dust beyond the protoplanetary phase. This implies that mature debris disks are still expected to form and evolve in multiple stellar systems. Armstrong et al. (2014) discussed the idea that circumbinary planets should be more common and low mass since companion interactions would effectively remove the gas in the system. Past work by Trilling et al. (2007) found a marginally higher incidence of excess for multiple systems rather than for single stars, suggesting that planetary formation is not necessarily a hindrance for multiple star systems. In contrast to these studies, Rodriguez & Zuckerman (2012) found that debris disks are less common around multiple stars and predict these results imply more rapid clearing times for dust in the disk. Confirmation of these ideas is timely and relevant for exoplanet investigations.

Similar to the approach of Rodriguez & Zuckerman (2012), we used the entire catalog of IR excess stars from Cotten & Song (2016) to search the literature for multiplicity information. We include the Washington Double Star Catalog (WDS; Mason et al. 2001), the Catalog of Components of Double and Multiple Stars (CCDM; Dommanget et al. 2002), and the Tycho Double Star Catalog (TDSC; Fabricius et al. 2002) in our search as well as individual binary star searches and those involving infrared excess (Trilling et al. 2007, Kennedy et al. 2012, Rodriguez & Zuckerman 2012, Su et al. 2013, Thalmann et al. 2013, Rodriguez et al. 2015, Draper et al. 2016, Perrot et al. 2016). Over 400 stars were found to have one or multiple companions at a range of separations.

3.7.1 Multiplicity Discussion

Figure 3.11 displays the companion separation (in AU) versus the disk radius (in AU) from the central star. The disk radius is calculated using the SED prescribed stellar temperature and stellar radius, the blackbody dust temperature and the distance to the star itself for the conversion into AU (see Chapter 2 for details). This value assumes a thin ring of material at this location. Our method of IR excess interprets the primary star to be the object with a disk, however, we recognize this may be misleading for close binaries which WISE is not able to resolve. The sample plotted represents only the Prime stars found to have a single companion (circle) or multiple companions (triangle). Data that are connected by a line display each disk component radius based on the two component disk fit to the IR excess while a single point implies a single disk fit. Discussion about the disk parameters is discussed in greater detail in Cotten & Song (2016) and these parameters are provided in the online materials (Table A.1).

In order to interpret the interaction of these systems and a dusty disk, we follow the method outlined by Trilling et al. (2007) and used by Rodriguez & Zuckerman (2012) to determine regions of interaction which can lead to stability or instability of the system. This work stems from Holman & Wiegert (1999) who simulated the stability of individual particles in a variety of environments. Choosing a mass ratio of 0.5 and an eccentricity of 0.5, the results of Holman & Wiegert (1999) predict critical radii for the stable environment to be outside of 0.12 and 3.76 times the radius for circumstellar and circumbinary disks, respectively. We display these as red dashed lines in Figure 3.11 and note that this interpretation is only valid for the binary star systems in our sample (circles).

We first note an interesting object according to this figure, DK Cet, displayed as the yellow star. According to our analysis, this object has a companion as well as two disk components which implies that it has maintained a circumstellar disk in addition to a circumbinary disk. Table 3.3 reflects membership to the Tucana-Horologium association according to Chen et al. (2014) and Malo et al. (2013) and so this star is likely in the epoch of terrestrial

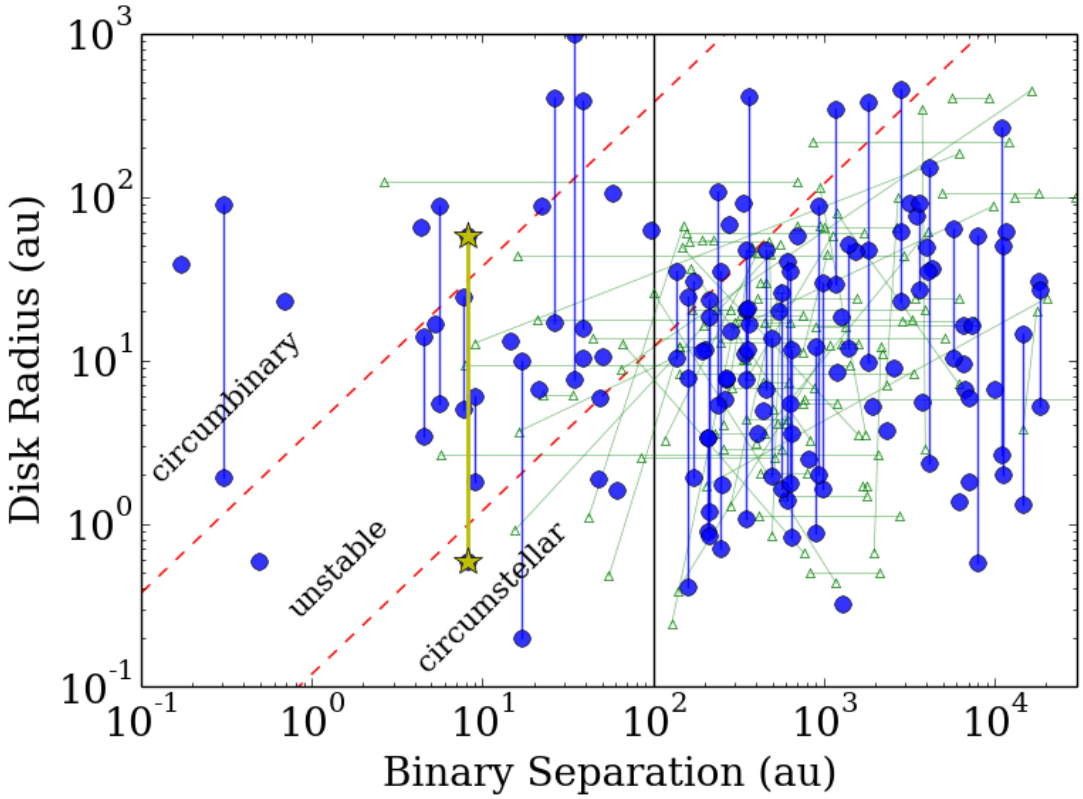

Figure 3.11: Binary separation versus the disk radius in AU. Stars with a binary companion are plotted as blue circles and multiple systems are shown as unfilled green triangles. The red dashed lines identify the theoretical limits of Holman & Wiegert (1999) described in Section 3.7.1 as a region of instability in circumstellar material due to a binary companion. DK Cet, displayed as the yellow star, identifies an object that straddles the unstable boundary. Stars that are best fit with two dust components are connected by solid lines to show the regions likely to have the presence of dust.

planet formation (30-100 Myr; Melis et al. (2010)) and would be an interesting object for exoplanet direct imaging studies as well as far-infrared disk studies.

As seen in Figure 3.11, the majority of the stars lie in the region of circumstellar disks around the primary star, including both components of the multiple disk systems. There are 43 disks (24%) that lie in the unstable region which could indicate a transience of dustiness in the system due to the interaction of the primary and secondary companions or possibly the migration of dust (Trilling et al. 2007). Rodriguez & Zuckerman (2012) examine the likelihood that stars in the unstable region are the result of unaddressed parameters such as the companion projection given the position angle, dust grain size, and the fitted disk parameters. While Rodriguez & Zuckerman (2012) conclude the companion projection effect would be minor, they suggest the interpretation of the dust temperature assuming blackbody grains would have a larger effect and shift systems to the right. We agree that the largest contamination to this relationship is the interpretation of the dust location from the assumption of blackbody grains. As discussed in Rodriguez & Zuckerman (2012) and Cotten & Song (2016), the inner disk radius assuming blackbody dust grains underpredicts the disk location compared to disks resolved in scattered light by more than four times. This effect cannot be addressed without information regarding the true dust location and the continuous nature of the dust; however, this information would shift some disks beyond the unstable region and many more disks into this region, especially considering multiple disk components. A shift in the dust location would nearly double the number of stars in the unstable region. The results found here suggest that the simplified model for disks around binary systems is incomplete, especially without consideration of two-component disks.

We investigated the age of the systems located in the unstable area and the majority of the stars are less than 100 Myr. The young age in combination with the gravitational influence of the companion could in part support the hypothesis that the companion is affecting the disk, although the result that so many of these debris disks are transient due to these interactions is unexpected.

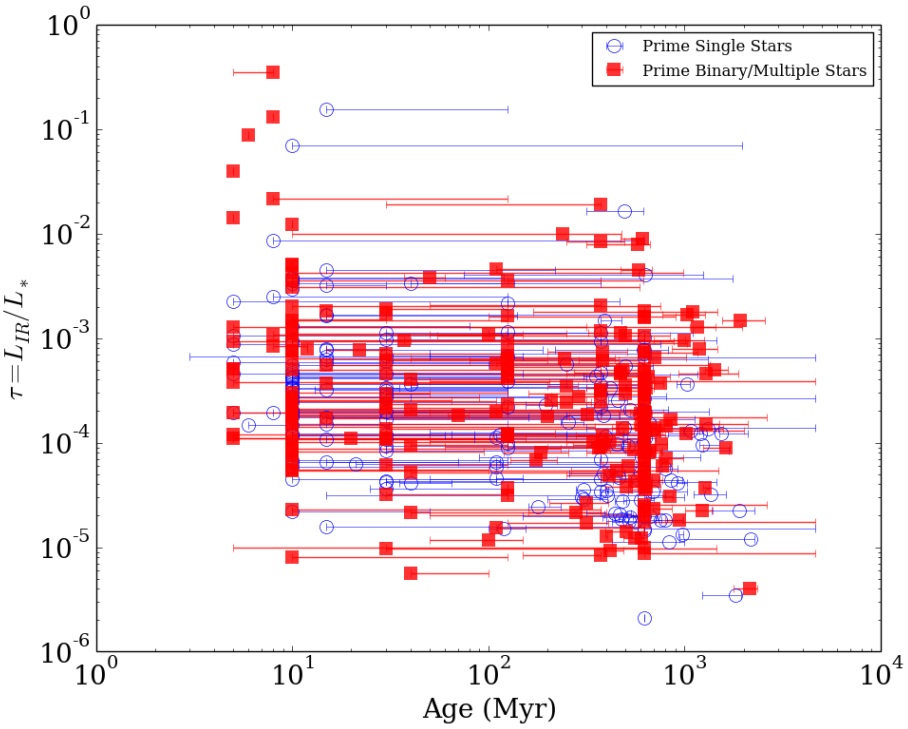

Figure 3.12: Evolution of the fractional dust luminosity for stars in the Prime catalog that are either single (unfilled blue circles) or multiple (filled red squares) stars. This figure shows no trend in identifying the effect of multiplicity on the evolution of the dust.

Finally, we consider the effects of the presence of a companion on the evolution of the dust. Results of Rodriguez & Zuckerman (2012) indicated that binary systems had some effect on the amount of dust, but a more recent study including more debris disk stars by Rodriguez et al. (2015) found there was no statistically significant difference. The data in Figure 3.12 corroborate the findings of Rodriguez et al. (2015): there does not appear to be a difference between single stars and multiple star systems that host a disk. Thus, at any particular age, the presence of a companion does not increase or decrease the amount of dust expected around the primary star. Further, Figure 3.12 shows that the multiple star systems have not cleared their systems of dust faster than single stars since the two populations cannot be separated. We conclude that the companion is influencing the disk and possibly generating the amount of dust in that debris disk, but it is not enhancing the dustiness or decreasing the timescale of dust production compared the single star systems.

3.8 Conclusion

We have collected over 600 spectra from new observations and archival data for F and later spectral type stars from the Prime and Reserved Catalogs (Cotten & Song 2016). Various age-dating techniques were applied for the measured quantities using the optical spectra and CMD age-dating was performed for early-type stars. A total of 1102 stars have age data presented here. In addition, we use the highest resolution spectra to measure metallicity using the iSpec code (Blanco-Cuaresma et al. 2014) to specifically focus on the iron content of these stars. Finally, we measure the rotational velocity ($v \sin i$) for stars with available spectra. Each quantity derived is investigated to further understanding about stars with debris disks and the influence on planetary formation and evolution.

Our findings regarding the evolution of the disks in our sample confirms the t^{-1} behavior for early-type stars (Wyatt 2008) and the t^{-2} behavior for F-type or later stars (Carpenter et al. 2009). These results are mainly identified through inspection of the cold, outer disks or stars with multiple disk components. Thus, stars with a single cold disk or a disk with two components may be undergoing similar evolutionary conditions or it may be that the fractional dust luminosity is dominated by the cold disk component. Contrastingly, a single warm disk close to the star may evolve at an even more rapid pace due to its proximity to the star. It is interesting to note that there are stars with a warm disk at many different ages which could indicate recent extreme events. Lastly, exploration into the evolution of the amount of dust in these disks leads us to concur with the model of steady-state evolution through collisional cascades for this debris disk sample.

We find our debris disk sample extends over a range of metallicities which negates previous suggestions of a dearth of low-metallicity stars with debris disks (Maldonado et al. 2012). Instead, there appears to be a dearth of debris disks around high-metallicity stars ([Fe/H] > 0.25). However, even the low-metallicity environment is still conducive to dust formation and possibly planet formation. This indicates a star with metallicity above solar value can form gas giant planets, undergo migration, and clear a debris disk rapidly such that we do

not find large debris disks around high metallicity stars, and that the low-metallicity star can still produce dust and rocky debris indicative of low-mass planet formation.

We do not find any trend between rotational velocity and the dustiness of the debris disk. The stars in our sample are presumed to be main-sequence and earlier discussions report a variety of ages. Therefore, besides the four dustiest, young disks in our sample, the remainders suggest a lack of connection between the host star's angular momentum and the disk. We point out the difficulty in making this assumption based on a line-of-sight velocity, however, it appears the secondary generation of dust in debris disk stars is not significantly influenced by the angular momentum of the system.

Lastly, we investigate the effect of a binary star or multiple companions on the location and amount of dust in a debris disk. We find that many disks lie in a region of instability caused by the companion(s) and if we compensate for the underproduction of the disk radius assuming blackbody dust grains, then even more disks would be included. The proposal regarding the location of instability is challenged by our inclusion of disks with multiple components since previous studies only investigated single disk systems. Therefore, we conclude that multiplicity must influence the dust in the disk, however, it does not cause these systems to have properties distinct from the case of a single star with a debris disk.

Previous investigations into the relationships between a disk and the host star have been limited by the number of sources available. Through the compilation of large catalogs of IR excess (Cotten & Song 2016), we were able to gather observational data for the largest input sample. We recognize age as the most influential factor in the evolution of dust although a more homogeneous derivation of stellar parameters will fully solidify this result. Another strong factor is not evident. We also point out that direct imaging of debris disks in scattered light for accurate dust locations as well as observations using optical spectroscopy for the entire Prime and Reserved catalogs will offer a more complete observational set of data for theoretical modelling.

3.8.1 *Acknowledgments*

This work is in part based on spectral data retrieved from the ELODIE and SOPHIE archives at Observatoire de Haute-Provence (OHP), and data obtained from the ESO Science Archive Facility. This research has made use of the Washington Double Star Catalog maintained at the U.S. Naval Observatory as well as data from the European Space Agency (ESA) mission *Gaia* (http://www.cosmos.esa.int/gaia), processed by the *Gaia* Data Processing and Analysis Consortium (DPAC, http://www.cosmos.esa.int/web/gaia/dpac/consortium). Funding for the DPAC has been provided by national institutions, in particular the institutions participating in the *Gaia* Multilateral Agreement. We also recognize P. Copenhaver (an undergraduate student at the University of Georgia) and C. McFerren (a local High School student performing research through the Young Dawgs program at the University of Georgia) for their work in extracting some of the stellar parameters and analysis of stellar spectra.

Chapter 4

Potential Applications and Directions

4.1 Imaging of Debris Disks

One discrepancy in the study of debris disks is the lack of complete information regarding the true location of the dust. The use of IR excess to identify debris disk stars assumes a spherical grain (micron-size) in thermal equilibrium which behaves as a blackbody and therefore, offers a temperature and an inferred location around the star. A number of studies, including Cotten & Song (2016), have shown the difference between the disk radius as a result of blackbody grains versus direct imaging techniques and the blackbody model points to disk radii that are much less than a realistic grain population would identify. So, while assuming that grains behave as blackbodies is convenient, the direct imaging of debris disks targets small grains that scatter starlight from the host star, thereby directly identifying the location of the dust. New instruments such as Gemini Planet Imager (GPI; Macintosh et al. 2006) and Spectro-Polarimetric High-contrast Exoplanet REsearch (SPHERE; Beuzit et al. 2008) now provide the techniques to be able to observe the nearest debris disk stars. In particular, Perrin et al. (2015) and Millar-Blanchaer et al. (2015) offer two examples of resolving the disk radius of HR 4796 and β Pictoris, which are two important exoplanet host stars. Most notably, Perrin et al. (2015) discuss the goal of GPI to be able to image debris disk stars with fractional luminosities down to 10^{-5} which would contain a significant fraction of the stars presented in this catalog.

Observations of debris disks in the sub-millimeter provide a map of the population of larger dust grains ($\sim$cm). Larger grains imply a more direct connection to planetesimals and so knowledge regarding the location of this dust can link these studies to planetary

evolution. In addition, the larger, cold grains can trace the outer edges of the circumstellar material and describe the planetesimal population as well as the underlying strength of the forces in the system. Steele et al. (2016) was able to constrain the dust temperatures and disk structure even at a modest resolution using the Submillimeter Array (SMA). However, the ALMA sub-millimeter array and the *Herschel Space Observatory* currently provide the most sensitive instruments for this study. Increasing the number of objects observed at this wavelength will enable comparison between the multitude of different systems and disk architectures.

4.2 Mineralogical Studies

Besides knowledge of the location and morphology of debris disks, a key parameter of interest for these systems is the type of grains and their composition. Song et al. (2005) through the use of infrared spectroscopy identified that the grains that constitute the warm dust surrounding BD+20 307 must be composed of silicates and, thus, located a significant population of asteroids. A similar investigation by Olofsson et al. (2013) on the debris disk star, HD 113766, modelled several grain compositions in order to understand the emission features observed through infrared spectroscopy. The limitation of these investigations is due to the difficulty in obtaining spectroscopic observations of stars in the infrared since ground-based techniques are nearly impossible as a result of the Earth's atmosphere. Improvements in this field will likely come from the use of instruments aboard the Stratospheric Observatory for Infrared Astronomy (SOFIA; Young et al. 2012) which has a 2.5 meter telescope attached to a Boeing 747SP aircraft flying at 12 km, although the number of observations so far have been small. The development of models regarding the evolution of the Solar System and analogous disk systems requires understanding not just "where", but "what" is a dust grain.

4.3 Debris Disks around M Dwarfs

The dearth of late-type stars discovered to host a debris disk is the biggest difficiency amongst debris disk studies. A number of studies (Plavchan et al. 2005; Avenhaus et al. 2012; Theissen & West 2014) sought a sample of mature M dwarfs which host a debris disk, although there has been only one confirmed true debris disk around an M star, AU Microscopii (AU Mic). Theissen & West (2014) present a number of debris disk candidates around confirmed M-type stars, however, their location at hundreds of parsecs from the Sun increases the likelihood of contamination by interstellar dust emission and excludes the possibility of future follow-up missions. The inherent faintness of M dwarfs originally presented challenges to past studies without sensitive infrared observations. Plavchan et al. (2005) explained the rarity of detecting an M-type debris disk star by claiming that the environment around M dwarfs is not conducive to sustaining a disk due to strong stellar winds. Despite the fact that the AllWISE mission provides the most sensitive, all-sky infrared instrument available to identify infrared excess around M stars, issues with contamination in the sample selection still persist. The most recognizable contaminator is the inclusion of evolved M stars since giants display infrared excess due to dust grain condesation from the stellar winds. Therefore, the upcoming release of astrometric data for the billions of stars to be observed by Gaia (Gaia Collaboration 2016a) will enable researchers to eliminate the evolved star population using a CMD and various color criteria to constrain a nearby sample of M dwarfs from which the amount of infrared excess can be examined. The cross-match between the Gaia data release ($>$ 1 billion sources) and the AllWISE catalog ($\sim$740 million sources) will provide a more reliable starting sample than previous studies. The inclusion of late-type stars with debris disks is paramount to understanding the evolution of stars and disks.

Chapter 5

Conclusions

Through the collection of stars with known debris disks and a comprehensive search for new IR excess stars using the two largest surveys, Tycho-2 and AllWISE, we compile over 500 reliable IR excess stars indicative of hosting a debris disk and over 1200 stars with candidate debris disks. Using an algorithm designed to recognize oblong sources and scrutinize all available image sources and photometry from optical to far-infrared, we eliminate the majority of false excess cases. The stars in this census reflect the entire range of spectral types, dust temperatures, and disk locations. This comprehensive census increased the reliable debris disk sample by $\sim 20\%$.

Analysis regarding the dust parameters suggests there is no particular type, temperature, or location of dust with respect to the type of host star. We recognize that many of these objects are analogous to the Solar System's Asteroid and Kuiper belts, attributing the dust to planetary formation and evolution. Most importantly, since mid- to far-IR excess identifies micron- to centimeter-sized grains and direct observations of dust using scattered-light imaging reveals the true location of much smaller dust grains, we constrain the limits of fitting a blackbody model to the dust. These findings offer target information for future direct imaging missions and searches for exoplanets embedded within debris disks.

Suppositions regarding stellar evolution and disk evolution were addressed with an unprecedented numbers of sources. New observations using optical spectroscopy of 263 unique stars are reported here along with 255 unique archival observations. Parameters were extracted such that age, metallicity, and rotation were derived in addition to the collection of multiplicity information from the literature. We confirm that the age of the star behaves in

an inverse relationship to the dust when there is an outer, cold belt of material, whereas the presence of an inner, warm disk does not behave according to any presumed function. Thus, the dominant mechanism for dust production in many of these systems is collisions and a steady-state of grinding of planetesimals, but the stars with a single warm disk must be undergoing a much more transient mechanism. There is neither a deficit of low-metallicity stars with debris disks nor the suggestion that a higher metallicity environment contributes to the amount of dust in a debris disk, but this may indicate an increased likelihood of hosting rocky planetesimals. The problem involving angular momentum is unanswered since we were limited to using $v \sin i$ as the rotation of the star. There is no direct link between the amount of dust in a debris disk and the rate of rotation as was seen by primordial disks around pre-main-sequence stars. Lastly, inferences regarding the gravitational influence of a companion star on a debris disk were challenged upon recognition of a star hosting two disk components. The true location of the dust would exist in a region of instability.

We have isolated an important and extensive catalog of IR excess stars. This catalog serves as both a historic context of using infrared excess to identify debris disk stars following the culmination of infrared space missions, as well as a future target list for directly observing planets embedded in mature disk systems. Debris disk stars present an indirect means of addressing many unanswered questions about planetary formation and evolution and the theories addressed will have a significant impact on models which attempt to reproduce a Solar System. Knowledge about the precise location of the disk observed through direct imaging using instruments such as GPI and SPHERE would improve this study greatly. Further, the upcoming release of Gaia astrometric information will enable a new sample of M-type or later stars with mature debris disks to be discovered and included in theoretical investigations into evolution. A comprehensive catalog of debris disks including stellar and disk parameters will benefit the theoretical and observational fields of astronomy as a legacy of decades of investigations as well as providing new targets for the direct detection of planets embedded within a disk.

Appendix A

Disk Parameters

The disk parameters were originally derived in Cotten & Song (2016) and remain the same except for stars with new Gaia parallax measurements. Distances to stars play an important role in understanding the size of the disk. Therefore, we note here that stars with new parallax measurements that have uncertainties less than 30% have updated disk parameters. In total, we updated this information for 1222 stars. These parameters can be found in the catalogs available through the website www.debrisdisks.org. We use the updated parameters throughout the entirety of this manuscript.

Table A.1: Updated Disk Parameters for Prime and Reserved Stars using Gaia DR1 Distances

Name	Catalog	$T_{*,SED}$ (K)	$R_{*,SED}$ ($R_\odot$)	T_{dust} (K)	R_{disk} (au)	T_{dust2} (K)	R_{disk2} (au)	$\frac{L_{IR}}{L_{star}}$ ($\times 10^{-4}$)
TYC3660-183-1	R	7130	3.99	150	21.01	–	–	0.916
TYC4026-379-1	R	6540	1.44	260	2.13	–	–	3.110
HD 105	P	6070	0.98	390	0.56	50	33.87	4.539
HD 166	P	5700	0.79	300	0.66	70	12.19	3.569
HD 203	P	6710	1.49	160	6.12	–	–	1.694
HD 377	P	5910	1.00	200	2.05	60	22.73	5.310
HD 870	R	5550	0.76	300	0.61	45	27.22	1.579
TYC4026-208-1	R	5190	1.32	170	2.88	–	–	17.279
HD 987	R	5670	0.82	125	3.96	–	–	0.831
HD 1237	R	5650	0.82	300	0.68	0	0.00	92.967
HD 1466	P	6140	1.09	140	4.90	–	–	0.936
HD 1562	R	5910	0.92	75	13.37	–	–	0.586
TYC4015-1052-1	R	4320	8.02	120	24.21	–	–	5.166
TYC8846-897-1	R	9330	1.97	120	27.73	–	–	0.504
9 Cet	P	5920	0.97	40	49.55	0	0.00	0.021
TYC1186-730-1	R	7190	1.50	140	9.25	–	–	1.092
HD 3126	P	6380	1.23	200	2.92	45	57.67	1.914
TYC9135-268-1	R	6940	3.09	340	2.99	–	–	2.302
HD 3296	P	6450	1.43	60	38.67	–	–	0.237
HD 3670	P	6440	1.25	290	1.44	55	40.03	6.478
TYC3667-527-1	R	6470	1.21	180	3.66	–	–	2.281
TYC8034-360-1	R	5900	1.18	290	1.14	–	–	7.682
HD 5133	P	5170	0.65	30	44.97	–	–	0.118
TYC4017-1710-1	R	8250	3.54	140	28.67	–	–	0.692

Continued on Next Page...

Table A.1 – Continued

Name	Catalog	$T_{*,SED}$ (K)	$R_{*,SED}$ ($R_\odot$)	T_{dust} (K)	R_{disk} (au)	T_{dust2} (K)	R_{disk2} (au)	$\frac{L_{IR}}{L_{star}}$ ($\times 10^{-4}$)
HD 5349	R	5170	1.93	250	1.93	–	–	1.184
TYC2802-1387-1	R	7950	1.62	150	10.60	–	–	0.558
HD 6434	R	5920	1.12	120	6.34	–	–	0.083
TYC4021-1605-1	R	4340	0.61	150	1.19	–	–	4.242
TYC25-152-1	R	5890	0.96	180	2.40	–	–	60.135
TYC4021-680-1	R	5660	0.88	300	0.73	–	–	4.347
TYC3681-405-1	R	2960	0.18	230	0.07	–	–	10.484
TYC8479-1036-1	R	6290	1.23	215	2.45	–	–	7.519
V443 And	P	5660	0.78	200	1.46	50	23.33	1.964
HR 333	P	8920	2.62	80	75.98	–	–	1.883
HD 7193	R	6240	1.12	200	2.55	–	–	0.287
CPD-64 120	R	5140	0.74	140	2.35	–	–	1.789
HD 7590	P	6090	0.94	200	2.04	40	51.04	3.131
2MASS J01203226-1128035	P	5500	0.77	300	0.60	–	–	1.961
TYC2813-111-1	R	4670	0.67	200	0.86	–	–	6.890
HD 8558	R	5690	0.85	170	2.24	–	–	0.598
TYC4038-493-1	R	4380	13.7	500	2.46	–	–	14.670
HD 8907	P	6250	1.18	50	43.02	–	–	2.856
EO Psc	P	4930	0.94	70	10.89	0	0.00	0.632
TYC28-219-1	R	5890	0.96	205	1.85	–	–	10.699
TYC4305-1804-1	R	6490	1.33	160	5.12	–	–	1.674
EX Cet	P	5440	0.76	200	1.31	60	14.53	1.957
TYC8478-902-1	R	6470	1.23	220	2.49	–	–	1.423
HD 10472	P	6610	1.41	200	3.60	60	39.97	5.473
HD 10647	P	6280	1.00	300	1.03	55	30.61	5.808
HD 10638	P	7470	1.56	65	47.96	–	–	4.585
TYC4036-1980-1	R	5920	1.49	220	2.52	–	–	5.666
HD 10939	P	8960	2.30	200	10.75	55	142.11	1.463
BD Phe	R	7670	2.45	65	79.65	–	–	0.289
TYC2824-15-1	R	7300	1.69	120	14.60	–	–	3.281
TYC8850-1468-1	P	5040	7.06	185	12.20	–	–	15.283
BD+20 307	P	6110	1.57	410	0.81	–	–	115.802
TYC7543-602-1	R	4410	0.69	200	0.79	–	–	3.447
TYC9360-1318-1	R	6760	1.90	180	6.26	–	–	0.616
DK Cet	P	5800	0.91	350	0.58	35	58.41	3.133
TYC7553-86-1	R	5880	1.60	195	3.40	–	–	20.446
TYC1757-1096-1	R	5870	0.91	195	1.93	–	–	12.435
TYC4689-810-1	R	6600	2.02	180	6.32	–	–	13.269
TYC2321-561-1	R	5200	4.21	150	11.77	–	–	574.200
HD 13246	P	6160	1.13	165	3.69	–	–	1.980
HD 12467	P	8140	2.09	200	8.06	50	128.99	1.660
TYC2838-2293-1	R	7570	1.53	160	8.02	–	–	3.633
TYC1765-924-1	R	4730	10.2	180	16.52	–	–	1.990
HD 14082B	P	5910	0.97	220	1.63	55	26.11	5.748
HD 14907	R	6390	1.19	200	2.83	–	–	0.174
TYC4046-1651-1	R	9060	2.31	120	30.70	–	–	0.688
HD 15115	P	6660	1.39	320	1.40	60	39.95	6.212
TYC1774-769-1	R	5890	0.86	250	1.11	–	–	7.958
AG Tri	P	4330	0.84	205	0.88	55	12.16	16.553
TYC638-129-1	R	6850	2.02	120	15.34	–	–	1.487
TYC2327-1909-1	R	7660	1.71	190	6.49	–	–	0.993
TYC2832-2209-1	R	8260	1.67	180	8.23	–	–	1.397
TYC2335-1086-1	R	8010	1.61	120	16.69	–	–	2.406
HD 15407	P	6380	1.45	525	0.50	–	–	85.083
TYC1222-1654-1	R	6580	4.40	180	13.69	–	–	1.424
HD 15745	P	6730	1.40	120	10.25	65	34.94	40.249
TYC4050-1212-1	R	5920	1.95	200	3.99	–	–	8.376
TYC4051-785-1	R	9290	2.16	140	22.22	–	–	0.307

Continued on Next Page...

Table A.1 – Continued

Name	Catalog	$T_{*,SED}$ (K)	$R_{*,SED}$ ($R_\odot$)	T_{dust} (K)	R_{disk} (au)	T_{dust2} (K)	R_{disk2} (au)	$\frac{L_{IR}}{L_{star}}$ ($\times 10^{-4}$)
TYC4051-1211-1	R	8450	1.66	200	6.90	–	–	1.150
HD 16743	P	6850	1.58	200	4.32	50	69.16	7.178
TYC1776-36-1	R	7900	1.67	140	12.38	–	–	0.838
TYC4047-531-1	R	6440	1.70	210	3.73	–	–	4.664
TYC5289-743-1	R	5660	1.11	190	2.30	–	–	8.421
HR 826	P	6760	1.53	50	65.12	–	–	2.360
BD+14 466	R	5230	2.07	40	82.71	–	–	13.811
TYC3704-1028-1	R	8140	1.79	160	10.83	–	–	0.584
HD 17848	P	8420	1.91	220	6.52	55	104.35	0.969
TYC8051-608-1	R	7590	2.11	200	7.09	–	–	1.422
TYC3701-937-1	R	7650	1.76	170	8.30	–	–	1.606
TYC3709-994-1	R	7650	1.78	160	9.49	–	–	1.462
TYC7015-583-1	R	5230	0.76	230	0.92	–	–	9.654
TYC3713-529-1	R	7280	2.73	120	23.41	–	–	1.014
TYC4060-490-1	R	5620	0.80	220	1.22	–	–	19.064
TYC4620-1949-1	R	6260	1.76	180	4.97	–	–	2.456
HD 19257	P	7110	1.63	235	3.49	–	–	9.591
TYC2847-544-1	R	7260	1.41	110	14.35	–	–	2.439
IS Eri	P	5590	0.77	180	1.75	–	–	1.132
BD+21 418	R	5890	0.89	280	0.92	–	–	1.526
HD 19624	R	9180	2.85	130	33.12	–	–	1.419
TYC4049-426-1	R	6380	2.32	130	13.02	–	–	7.124
HD 19893	R	8980	2.44	230	8.68	–	–	1.587
TYC7023-69-1	R	5910	0.89	240	1.26	–	–	5.381
TYC3706-340-1	P	5590	1.65	185	3.52	–	–	7.876
TYC4711-827-1	R	6130	1.35	175	3.86	–	–	3.358
TYC8860-1359-1	R	5900	1.02	245	1.39	–	–	17.691
HD 20759	R	6290	1.85	290	2.03	–	–	0.618
HD 278507	P	5570	3.17	195	6.03	–	–	10.148
V459 Per	R	7010	1.5	170	5.93	–	–	1.851
TYC3715-724-1	R	6290	6.44	110	48.99	–	–	32.779
TYC1809-78-1	R	8160	1.74	140	13.78	–	–	0.699
TYC3707-592-1	R	5730	1.40	210	2.43	–	–	7.472
TYC7027-1218-1	R	8490	2.18	160	14.29	–	–	0.653
HD 21091	R	9000	2.06	160	15.19	–	–	0.650
HD 21122	R	7790	1.79	150	11.27	–	–	0.890
TYC3316-489-1	R	7770	1.80	160	9.88	–	–	0.869
HD 21117	R	8330	2.19	160	13.82	–	–	0.847
HD 21375	R	8070	2.85	120	30.04	–	–	0.717
TYC3320-399-1	R	8110	2.84	180	13.45	–	–	0.572
BD+47 837	P	5920	1.53	220	2.59	–	–	1.763
TYC3316-2311-1	R	8220	4.07	160	25.01	–	–	0.955
HD 21480	R	7240	1.50	140	9.39	–	–	1.719
TYC4326-1934-1	R	9130	2.62	120	35.39	–	–	4.972
CD-46 1064	R	4840	0.79	110	3.60	–	–	2.043
TYC1806-170-1	R	8670	1.72	160	11.77	–	–	0.450
HR 1056	R	8300	3.28	70	107.57	–	–	0.196
HD 21641	R	9490	3.05	260	9.46	–	–	1.162
HD 21997	P	8220	1.56	65	58.14	–	–	5.411
TYC8870-626-1	R	6140	2.29	175	6.56	–	–	7.396
BD+50 784	R	6160	1.47	200	3.24	–	–	3.080
TYC663-317-1	R	5880	2.16	240	3.03	–	–	3.569
HD 22179	P	5920	1.02	70	17.09	–	–	2.889
HD 22705	R	5920	1.01	200	2.07	–	–	0.567
TYC2874-69-1	R	8300	1.79	145	13.66	–	–	1.150
TYC2359-1127-1	P	4350	11.9	75	93.83	–	–	25.729
TYC4723-932-1	R	7310	1.45	120	12.58	–	–	4.063
TYC5880-75-1	R	5510	0.92	200	1.63	–	–	3.049

Continued on Next Page...

Table A.1 – Continued

Name	Catalog	$T_{*,SED}$ (K)	$R_{*,SED}$ ($R_\odot$)	T_{dust} (K)	R_{disk} (au)	T_{dust2} (K)	R_{disk2} (au)	$\frac{L_{IR}}{L_{star}}$ ($\times 10^{-4}$)
TYC7031-220-1	R	6740	1.41	160	5.86	–	–	0.979
TYC1799-1062-1	R	6890	1.92	190	5.88	–	–	6.522
HD 23356	P	5210	0.70	45	21.99	–	–	0.084
TYC1803-486-1	R	8180	1.25	290	2.33	–	–	3.709
HD 23484	P	5400	0.77	60	14.61	–	–	1.035
TYC 1803-1061-1	R	5920	0.93	390	0.50	–	–	5.167
TYC1799-306-1	R	6890	1.45	170	5.55	–	–	1.981
HD 23361	P	7480	1.55	230	3.82	100	20.21	21.536
HD 23267	P	9490	2.27	140	24.32	–	–	0.942
HD 23430	P	7680	1.62	220	4.60	105	20.21	4.334
TYC1800-1908-1	R	8270	1.86	170	10.24	–	–	1.008
HD 23514	R	6290	1.36	600	0.35	–	–	192.128
HD 282954	P	5920	1.03	100	8.46	–	–	2.198
TYC1804-2081-1	R	8800	2.22	155	16.69	–	–	4.580
V1210 Tau	P	7150	1.70	300	2.25	85	28.05	1.192
TYC2875-1341-1	R	9230	1.94	170	13.31	–	–	0.690
HD 23632	P	8800	2.15	120	27.01	65	92.06	0.901
TYC1800-2201-1	R	9110	2.58	170	17.27	–	–	0.664
V1229 Tau	P	8510	2.35	80	62.01	–	–	0.195
HD 24636	P	6630	1.40	120	10.01	–	–	1.364
TYC2867-1126-1	R	7450	3.86	175	16.31	–	–	1.562
HD 23863	P	7610	1.53	170	7.17	–	–	0.314
TYC1804-2047-1	R	9640	2.30	190	13.81	–	–	1.113
TYC5884-1513-1	R	6850	1.33	150	6.47	–	–	4.197
TYC3725-758-1	R	8220	2.55	175	13.14	–	–	0.809
HR 1183	R	9770	2.53	190	15.62	–	–	0.566
TYC2360-286-1	R	6340	1.98	180	5.73	–	–	2.550
TYC1804-1545-1	R	8040	1.62	160	9.53	–	–	0.524
HD 24649	R	6250	1.13	110	8.53	–	–	0.792
TYC2361-2209-1	R	4420	3.05	130	8.20	–	–	11.590
TYC1813-734-1	R	7260	1.57	200	4.84	–	–	1.335
TYC4718-865-1	R	6300	2.30	300	2.36	–	–	2.556
TYC2876-1915-1	R	8870	1.80	160	12.91	–	–	1.569
TYC2868-941-1	R	6950	1.26	150	6.33	–	–	2.551
TYC7570-1523-1	R	4280	3.45	160	5.75	–	–	2.545
TYC2881-432-1	R	5730	2.47	150	8.41	–	–	22.522
TYC4731-1206-1	R	4790	11.1	120	41.18	–	–	1.692
TYC2889-298-1	R	8240	5.39	121	58.24	–	–	5.954
TYC2877-249-1	R	7030	1.62	150	8.28	–	–	3.196
TYC5312-2218-1	R	6490	1.67	155	6.84	–	–	2.094
50 Per	P	6360	1.21	270	1.57	40	71.58	1.159
TYC4728-802-1	R	4780	10.2	220	11.26	–	–	3.744
HD 26255	R	6160	4.76	240	7.31	–	–	15.053
TYC4072-576-1	R	6480	1.66	200	4.07	–	–	6.561
HD 281683	P	5670	2.16	220	3.34	–	–	4.526
HD 27346	R	6970	2.33	120	18.33	–	–	0.453
HD 26784	R	6260	1.30	90	14.67	–	–	0.355
HD 27026	P	10570	3.60	65	221.93	–	–	3.511
TYC81-1043-1	R	5910	0.92	130	4.44	–	–	15.857
HD 28069	R	6280	1.19	120	7.64	25	176.10	37.660
TYC7578-425-1	R	4350	0.88	120	2.70	–	–	2.058
TYC6463-1240-1	R	5360	0.71	300	0.53	–	–	4.060
TYC1816-668-1	R	3880	10.4	120	25.42	–	–	4.495
TYC81-1439-1	R	6770	1.59	120	11.84	–	–	2.573
TYC3346-555-1	R	6140	1.55	165	5.01	–	–	5.038
TYC2888-369-1	R	7710	1.54	120	14.83	–	–	1.761
TYC2385-896-1	R	5230	2.53	220	3.33	–	–	5.697
HD 283759	P	5560	1.46	70	21.54	–	–	99.365

Continued on Next Page...

Table A.1 – Continued

Name	Catalog	$T_{*,SED}$ (K)	$R_{*,SED}$ ($R_\odot$)	T_{dust} (K)	R_{disk} (au)	T_{dust2} (K)	R_{disk2} (au)	$\frac{L_{IR}}{L_{star}}$ ($\times 10^{-4}$)
TYC3346-806-1	R	6780	1.51	125	10.39	–	–	3.987
CPD-35 525	P	5550	0.79	250	0.91	–	–	7.137
TYC95-489-1	R	6420	1.37	130	7.78	–	–	3.864
TYC695-1074-1	R	6120	1.24	180	3.35	–	–	4.784
TYC4341-859-1	R	4870	0.65	120	2.52	–	–	16.615
TYC1835-1066-1	R	6820	2.85	200	7.73	30	343.72	74.935
EX Eri	P	7760	1.61	200	5.65	65	53.46	0.898
HD 30447	P	6670	1.41	300	1.63	70	29.88	11.133
HD 32195	P	6180	1.14	300	1.13	65	24.02	2.167
TYC88-1288-1	P	7470	2.70	170	12.14	30	389.90	21.127
TYC5322-663-1	R	4890	0.70	260	0.58	–	–	5.153
HD 31392	P	5560	0.79	300	0.64	40	35.80	4.112
TYC1280-246-1	R	5710	1.55	300	1.31	–	–	6.854
TYC7587-734-1	R	6450	1.26	220	2.52	–	–	3.895
TYC4342-270-1	R	8620	4.40	235	13.78	–	–	1.016
TYC2906-2792-1	R	4860	0.74	225	0.81	–	–	7.856
TYC2396-810-1	R	6670	2.58	190	7.41	–	–	2.054
TYC697-1673-1	R	5470	2.01	185	4.10	–	–	17.910
TYC7046-1264-1	R	6110	1.06	190	2.57	–	–	5.902
HD 32297	P	7610	1.62	130	12.94	70	44.63	98.712
TYC4079-687-1	P	4910	0.71	260	0.59	–	–	7.192
TYC1853-1069-1	R	7600	2.50	160	13.14	40	210.25	151.304
TYC5323-272-1	P	6300	2.03	220	3.88	50	75.08	53.839
HD 33081	P	6330	1.53	250	2.29	45	70.69	0.921
TYC7050-818-1	R	6850	1.51	120	11.50	–	–	8.130
TYC4511-575-1	R	7810	2.18	170	10.73	–	–	1.827
TYC9161-718-1	R	5020	0.82	260	0.72	–	–	8.493
HD 33636	P	5940	0.99	250	1.30	55	26.92	0.977
HD 34324	P	8040	1.60	190	6.68	55	79.66	3.338
TYC2398-384-1	R	6150	2.02	200	4.44	–	–	2.414
TYC8097-337-1	R	5910	1.78	200	3.62	–	–	14.284
TYC3747-1379-1	R	6440	2.09	190	5.61	–	–	8.235
TYC2896-391-1	R	6290	1.11	220	2.12	–	–	2.260
TYC8085-1019-1	R	4810	10.2	300	6.11	–	–	6.157
AS Col	P	6250	1.20	110	9.05	–	–	0.654
TYC699-987-1	R	4490	9.02	160	16.53	–	–	3.161
TYC8085-246-1	R	6650	1.39	160	5.61	–	–	1.030
TYC5331-856-1	R	4860	0.92	250	0.82	–	–	14.116
HD 35150	R	8540	1.74	220	6.13	–	–	4.171
HD 287787	R	7960	1.62	150	10.64	–	–	2.212
HD 35416	R	6500	1.33	120	9.12	–	–	0.707
TYC9162-586-1	P	4850	1.00	230	1.04	–	–	7.770
HD 35351	R	9630	2.11	135	25.00	–	–	0.620
HD 35367	R	8370	1.46	180	7.37	–	–	2.669
HD 35650	R	4400	0.59	90	3.28	–	–	2.666
TYC1847-1200-1	R	6080	1.59	170	4.75	–	–	8.715
HD 287861	R	8320	1.31	600	0.59	125	13.56	11.190
HD 287850	R	7280	1.67	180	6.39	–	–	1.871
TYC8089-513-1	R	4820	0.69	235	0.68	–	–	4.990
HD 287854	R	7340	1.37	135	9.44	–	–	3.752
HD 35625	R	9080	1.43	150	12.27	–	–	1.073
HD 35841	P	6470	1.20	70	24.03	–	–	17.078
AF Lep	P	6130	1.17	300	1.14	75	18.26	1.505
HD 290521	R	7430	1.36	140	8.93	–	–	7.108
TYC2411-2259-1	R	5700	1.69	240	2.23	–	–	4.476
VZ Col	R	4170	0.57	180	0.72	–	–	1.265
TYC126-1078-1	R	6490	1.34	145	6.27	–	–	1.759
HD 290540	R	9040	1.64	110	25.77	–	–	0.773

Continued on Next Page...

Table A.1 – Continued

Name	Catalog	$T_{*,SED}$ (K)	$R_{*,SED}$ ($R_\odot$)	T_{dust} (K)	R_{disk} (au)	T_{dust2} (K)	R_{disk2} (au)	$\frac{L_{IR}}{L_{star}}$ ($\times 10^{-4}$)
HD 36444	R	9600	2.59	120	38.59	45	274.40	49.856
HD 290598	R	9010	1.49	210	6.39	–	–	0.646
TYC8090-477-1	R	8030	2.24	110	27.82	–	–	3.173
TYC1860-185-1	R	3620	0.50	160	0.60	–	–	6.296
HD 36968	P	6880	1.43	200	3.95	55	52.19	17.780
TYC4089-1079-1	R	8110	3.03	180	14.35	40	290.64	55.391
HR 1915	P	7980	1.45	200	5.37	–	–	1.209
TYC709-241-1	R	5880	1.38	165	4.08	–	–	15.711
HD 37306	P	8750	1.67	400	1.87	100	29.85	1.850
HD 37484	P	6610	1.38	190	3.89	75	24.97	6.084
TYC2918-2067-1	R	7430	1.91	190	6.81	–	–	1.589
TYC4779-587-1	R	6540	1.35	120	9.37	–	–	1.647
HD 37564	P	7300	3.91	600	1.35	130	28.75	19.356
TYC722-21-1	R	6800	1.59	160	6.72	–	–	0.788
TYC4767-911-1	R	6310	1.68	170	5.41	–	–	1.862
AI Lep	R	5930	1.04	300	0.95	–	–	1.228
HR 1966	R	9890	2.20	185	14.63	75	89.03	0.954
TYC1873-26-1	R	7840	1.74	155	10.39	–	–	1.794
TYC4779-179-1	R	6380	1.21	160	4.49	–	–	1.512
HD 38207	P	6760	1.44	200	3.85	55	50.86	14.787
HR 1975	P	9800	1.69	230	7.14	70	77.11	2.941
TYC1303-1829-1	R	4590	3.97	140	9.95	–	–	1.750
TYC2405-551-1	R	8930	1.88	160	13.63	–	–	0.486
TYC4772-310-1	R	5910	1.44	140	5.99	–	–	8.631
HD 38949	R	6120	0.99	200	2.16	–	–	0.371
HD 38858	P	6100	0.84	65	17.30	–	–	45.816
TYC7069-536-1	R	4940	3.69	225	4.14	–	–	6.087
TYC6491-4-1	R	4340	0.61	140	1.36	–	–	2.730
HD 39415	P	6170	5.48	240	8.43	–	–	57.547
TYC3373-148-1	R	6160	2.27	160	7.85	–	–	2.149
TYC2912-46-1	R	5820	1.32	120	7.24	–	–	22.880
TYC9163-157-1	R	6110	1.51	325	1.24	60	36.48	62.394
HD 40540	P	7240	1.47	80	28.19	–	–	6.479
TYC1324-2723-1	R	5740	1.11	210	1.94	–	–	4.563
TYC8529-1004-1	R	5670	0.76	150	2.55	–	–	8.741
TYC1313-1482-1	R	4170	0.69	120	1.94	–	–	2.236
HD 40979	P	6160	1.19	80	16.54	–	–	0.144
TYC2431-746-1	R	4730	8.90	260	6.86	–	–	7.238
TYC1877-629-1	R	5930	1.02	115	6.32	–	–	13.260
TYC1322-312-1	R	5850	0.82	180	2.02	–	–	14.554
TYC5933-1801-1	R	4710	3.37	140	8.90	–	–	4.443
TYC8110-320-1	R	5930	1.04	260	1.26	–	–	8.739
HD 43162	P	5840	0.81	240	1.12	–	–	0.804
HD 43319	P	8590	1.78	200	7.65	–	–	0.173
TYC5371-1216-1	R	7000	1.60	160	7.14	–	–	0.981
V1358 Ori	P	6110	1.07	140	4.78	–	–	0.607
AB Pic	P	5330	0.92	30	67.65	–	–	0.365
TYC8110-1373-1	R	6800	1.81	180	6.03	–	–	3.831
TYC1878-756-1	R	6880	1.66	160	7.17	–	–	1.033
HD 45184	P	5920	1.01	280	1.05	60	22.96	1.983
TYC8107-500-1	R	5900	0.86	215	1.52	–	–	4.733
HD 46190	P	8400	1.63	120	18.63	–	–	0.170
TYC7622-1681-1	R	5880	1.63	160	5.12	–	–	13.834
HD 46317	R	6350	1.26	200	2.96	–	–	0.304
TYC754-2197-1	R	3700	0.45	180	0.44	–	–	4.309
TYC9177-1892-1	R	5910	1.72	200	3.50	–	–	3.548
HD 49855	R	5770	0.83	120	4.49	–	–	1.018
HR 2562	P	6480	1.41	50	55.10	–	–	1.103

Continued on Next Page...

Table A.1 – Continued

Name	Catalog	$T_{*,SED}$ (K)	$R_{*,SED}$ ($R_\odot$)	T_{dust} (K)	R_{disk} (au)	T_{dust2} (K)	R_{disk2} (au)	$\frac{L_{IR}}{L_{star}}$ ($\times 10^{-4}$)
HD 50499	R	6070	1.35	80	18.13	–	–	0.103
HD 50554	P	6110	1.05	60	25.47	–	–	0.481
TYC9493-1937-1	R	6310	1.81	325	1.59	–	–	4.852
HD 53143	P	5620	0.84	250	0.99	60	17.26	3.407
HD 52265	P	6150	1.29	55	37.76	–	–	0.227
TYC4818-1115-1	R	6290	1.37	190	3.52	–	–	3.842
TYC5385-1444-1	R	4380	0.62	325	0.27	–	–	28.543
TYC7633-97-1	R	5340	0.96	210	1.46	–	–	11.465
TYC4110-72-1	R	6160	0.89	190	2.18	–	–	6.500
TYC2951-819-1	R	4260	0.59	120	1.75	–	–	2.285
TYC8554-1604-1	R	4660	4.48	255	3.48	–	–	6.439
TYC5969-918-1	R	7300	1.48	165	6.78	–	–	42.161
TYC8559-1994-1	R	8240	1.37	120	15.13	–	–	3.251
HD 57703	P	6480	1.36	55	43.96	–	–	0.401
TYC5408-4281-1	R	4630	7.64	250	6.10	–	–	4.997
TYC7655-1804-1	R	4460	0.63	240	0.51	–	–	8.708
TYC8128-1966-1	R	6270	1.14	180	3.22	–	–	1.599
HD 59967	P	5900	0.88	400	0.45	80	11.24	2.441
TYC8137-2204-1	R	6390	1.53	240	2.54	–	–	6.108
TYC2958-831-1	R	8670	1.68	150	13.08	–	–	0.529
TYC6543-1535-1	R	5120	0.96	200	1.48	–	–	9.013
HD 60491	R	5270	0.66	350	0.35	–	–	4.363
TYC7648-583-1	R	5880	1.15	180	2.86	–	–	12.740
HD 60234	R	5900	3.64	60	81.93	–	–	4.145
HD 61005	P	5700	0.81	500	0.25	60	17.09	33.646
HD 60856	R	9840	3.18	180	22.15	–	–	0.585
TYC7109-1494-1	R	6140	0.92	200	2.03	–	–	7.385
HD 60737	R	5910	0.98	80	12.54	–	–	0.465
TYC7114-2140-1	R	6930	1.37	140	7.82	–	–	4.511
TYC1912-350-1	R	4250	3.51	250	2.36	–	–	3.901
HD 62938	R	9710	1.96	200	10.75	–	–	1.560
TYC188-407-1	R	7420	3.48	300	4.95	–	–	1.984
TYC7127-1800-1	R	5770	1.02	320	0.77	–	–	9.740
TYC9385-93-1	P	5170	3.25	255	3.11	–	–	6.450
CD-60 1960	R	8590	2.06	120	24.58	–	–	0.798
TYC1930-698-1	R	6130	0.64	180	1.74	–	–	19.142
CD-60 2007	R	6890	1.65	220	3.78	–	–	1.609
TYC7663-880-1	R	6490	2.25	200	5.52	–	–	5.538
TYC8570-1792-1	R	7600	3.31	180	13.75	–	–	0.899
HD 67985	R	10490	2.57	120	45.75	–	–	0.286
TYC9402-936-1	R	6140	1.02	205	2.13	–	–	7.493
TYC5417-177-1	R	6420	4.08	120	27.22	–	–	1.545
TYC8148-924-1	R	5280	1.11	220	1.50	–	–	10.724
HD 68558	R	8490	1.86	125	20.03	–	–	1.201
HD 68698	R	8660	1.52	275	3.52	–	–	1.347
TYC8144-571-1	R	7380	1.33	150	7.50	–	–	2.465
TYC8136-2725-1	R	6640	1.52	180	4.84	–	–	1.277
TYC7130-1982-1	R	6170	2.41	140	10.91	–	–	3.123
TYC9193-870-1	R	4990	0.80	230	0.88	–	–	12.138
HD 70298	P	6500	1.83	35	147.29	–	–	6.481
V478 Hya	R	5910	0.92	60	20.80	–	–	1.020
TYC8149-4422-1	R	8710	1.67	160	11.56	–	–	0.712
HD 71722	P	8630	1.66	160	11.24	70	58.74	1.766
TYC8572-94-1	R	8570	1.57	145	12.76	–	–	1.234
TYC1387-1215-1	R	7480	1.54	120	13.95	–	–	0.898
HD 72687	P	5890	0.88	220	1.47	–	–	1.221
TYC6582-1085-1	R	6460	1.36	245	2.21	–	–	5.675
HD 73526	P	5760	1.41	85	15.16	–	–	4.805

Continued on Next Page...

Table A.1 – Continued

Name	Catalog	$T_{*,SED}$ (K)	$R_{*,SED}$ ($R_\odot$)	T_{dust} (K)	R_{disk} (au)	T_{dust2} (K)	R_{disk2} (au)	$\frac{L_{IR}}{L_{star}}$ ($\times 10^{-4}$)
HD 73210	R	7490	4.54	70	121.15	–	–	0.124
V401 Hya	P	5900	0.97	150	3.52	40	49.46	1.937
HD 74009	R	6520	2.25	130	13.20	–	–	1.437
pi.01 UMa	P	6080	0.87	400	0.47	70	15.41	2.057
TYC4871-726-1	R	6370	1.23	160	4.54	–	–	6.038
HD 73890	R	7230	2.83	180	10.64	–	–	0.265
HD 74374	R	6560	1.18	300	1.32	85	16.47	4.492
TYC7687-1632-1	R	6360	1.65	120	10.82	–	–	4.414
TYC8930-536-1	R	6550	1.23	245	2.06	–	–	4.428
TYC9206-1719-1	R	6370	1.71	190	4.48	–	–	2.857
TYC1399-1353-1	R	4970	0.72	375	0.29	–	–	8.685
TYC8930-2250-1	R	8090	1.59	145	11.52	–	–	3.429
TYC216-386-1	R	5860	0.88	200	1.77	–	–	0.904
TYC4134-166-1	R	5660	0.79	250	0.95	–	–	14.321
TYC8938-1028-1	R	6640	3.06	200	7.85	–	–	1.368
GJ 322	R	4340	0.56	250	0.39	–	–	1.525
TYC8156-1297-1	R	6120	1.25	200	2.73	–	–	11.076
TYC8577-3016-1	R	9460	2.12	140	22.52	–	–	0.379
HD 75616	P	6230	1.12	50	40.48	–	–	0.485
HD 76748	P	5320	0.74	190	1.36	–	–	1.253
TYC213-542-1	R	5850	1.30	210	2.36	–	–	5.459
TYC2488-933-1	R	8240	2.54	140	20.48	–	–	0.555
HR 3570	P	6540	1.21	150	5.37	–	–	0.445
TYC8156-1384-1	R	6410	1.26	220	2.50	–	–	5.475
TYC8160-1896-1	P	5910	1.04	210	1.93	–	–	7.240
TYC8160-1758-1	R	5910	0.83	150	3.02	–	–	24.198
TYC8586-143-1	R	8800	1.76	140	16.26	–	–	0.539
TYC6022-1079-1	R	4510	0.78	220	0.77	–	–	2.703
TYC7681-2133-1	R	5850	0.94	300	0.84	–	–	6.852
TYC8169-371-1	R	6580	2.04	165	7.56	–	–	7.930
TYC8173-923-1	R	5590	0.80	200	1.46	–	–	5.804
TYC8169-1002-1	R	4270	0.81	240	0.60	–	–	11.986
TYC6587-1091-1	R	8090	1.78	180	8.36	–	–	0.610
TYC233-561-1	R	5890	1.53	190	3.43	–	–	6.150
TYC8587-2400-1	R	9030	2.14	190	11.26	–	–	0.849
TYC8170-855-1	R	5100	0.64	190	1.08	–	–	13.953
TYC7678-3447-1	R	8830	1.73	120	21.89	–	–	1.590
TYC8174-517-1	R	4780	11.0	200	14.64	–	–	3.594
TYC8170-948-1	R	4650	8.24	250	6.63	–	–	7.211
HD 80606	R	5680	1.01	75	13.60	–	–	1.039
TYC8948-1822-1	R	6670	1.41	180	4.53	–	–	1.238
TYC9408-1798-1	R	6520	3.32	200	8.21	–	–	1.039
TYC8588-2277-1	R	8620	1.63	210	6.40	–	–	1.093
BD+40 2208	R	4290	0.79	350	0.28	40	21.17	10.826
TYC4382-780-1	R	4860	6.85	195	9.91	–	–	4.080
TYC8588-463-1	R	6130	1.37	250	1.93	–	–	6.880
TYC8588-315-1	R	4200	0.58	220	0.49	–	–	5.089
TYC9208-272-1	R	6810	1.45	160	6.15	–	–	1.043
HD 82443	P	5570	0.73	350	0.43	45	26.21	3.887
TYC3426-581-1	R	7760	1.68	165	8.65	–	–	0.936
TYC7166-1923-1	R	6350	1.40	175	4.30	–	–	60.974
HD 82943	P	6120	1.11	50	38.96	–	–	1.702
TYC8949-1690-1	R	8330	1.75	190	7.84	–	–	0.684
HD 84075	P	6120	0.97	300	0.95	55	28.18	4.062
TYC8953-1669-1	R	7270	1.55	130	11.34	–	–	0.647
TYC6614-884-1	R	4360	0.87	120	2.68	–	–	5.366
TYC1962-511-1	R	5910	0.74	150	2.68	–	–	22.805
TYC7701-1621-1	R	8400	1.64	160	10.52	–	–	0.467

Continued on Next Page...

Table A.1 – Continued

Name	Catalog	$T_{*,SED}$ (K)	$R_{*,SED}$ ($R_\odot$)	T_{dust} (K)	R_{disk} (au)	T_{dust2} (K)	R_{disk2} (au)	$\frac{L_{IR}}{L_{star}}$ ($\times 10^{-4}$)
HD 84870	P	7500	1.54	170	7.01	45	100.01	7.644
TYC8598-1432-1	R	6450	1.34	210	2.94	–	–	3.230
TYC8598-2166-1	R	7190	1.65	160	7.78	–	–	0.845
TYC7698-2416-1	R	8490	1.71	165	10.58	–	–	1.693
TYC9221-1576-1	R	8190	2.13	180	10.30	–	–	0.607
HD 85301	P	5660	0.91	220	1.41	70	13.90	3.167
TYC6607-1725-1	R	6310	1.37	220	2.64	–	–	4.777
TYC8606-82-1	R	6300	1.24	180	3.55	–	–	23.700
HD 85672	P	7850	1.57	80	35.24	–	–	6.402
TYC1964-883-1	R	5900	1.00	200	2.03	–	–	32.598
TYC8602-649-1	R	6820	2.09	200	5.67	–	–	3.467
TYC8602-463-1	R	4680	0.66	220	0.70	–	–	3.898
TYC8946-1580-1	P	7220	3.63	350	3.60	65	104.38	29.438
TYC8606-1759-1	R	5910	1.48	190	3.33	–	–	5.537
TYC7711-312-1	R	9730	3.79	180	25.80	–	–	0.382
TYC8607-221-1	R	5900	2.22	200	4.51	–	–	2.989
TYC6046-407-1	R	6840	1.48	200	4.03	–	–	2.703
TYC8603-1612-1	R	4720	8.02	280	5.30	–	–	10.049
TYC7178-160-1	R	6660	2.01	160	8.13	–	–	1.076
TYC8608-1091-1	R	4480	0.63	240	0.51	–	–	4.979
TYC3004-313-1	R	5620	2.79	160	8.02	–	–	14.616
TYC8612-931-1	R	4660	10.1	300	5.70	–	–	12.286
TYC8604-2364-1	R	5740	0.79	200	1.53	–	–	13.141
TYC 4144-329-2	R	5500	3.42	170	8.33	–	–	187.126
HD 89846	R	7100	1.91	100	22.42	–	–	0.164
TYC8612-556-1	R	6620	1.64	200	4.20	–	–	1.860
TYC5497-1730-1	R	5930	0.97	240	1.39	–	–	5.337
TYC8608-1868-1	R	7450	1.59	280	2.62	–	–	2.061
TYC6623-942-1	P	5830	0.90	240	1.25	–	–	5.115
TYC8604-2419-1	R	6690	1.27	190	3.66	–	–	5.823
TYC8964-622-1	R	6110	2.70	240	4.08	–	–	7.384
TYC4912-802-1	R	5230	2.94	200	4.68	–	–	5.657
TYC9219-2494-1	R	3160	0.21	200	0.13	–	–	13.184
TYC6620-1350-1	R	9350	3.05	180	19.18	–	–	0.309
TYC8613-1042-1	R	3890	0.50	180	0.55	–	–	3.253
TYC9215-3039-1	R	8970	1.88	190	9.77	–	–	1.806
CCDM J10389-6430AB	R	8520	2.30	55	128.40	–	–	0.655
TYC8605-1553-1	R	6750	6.99	600	2.06	–	–	21.403
HD 92536	P	10710	2.46	250	10.52	–	–	0.805
V419 Hya	P	5210	0.75	200	1.18	45	23.39	6.609
TYC8969-738-1	R	6400	1.56	140	7.61	–	–	6.100
TYC8957-2919-1	R	8850	2.59	160	18.44	–	–	0.974
TYC4916-263-1	R	4310	0.60	180	0.81	–	–	7.823
TYC1434-1074-1	R	6250	1.08	290	1.17	–	–	4.502
TYC6635-823-1	R	7030	5.14	120	41.10	–	–	0.575
TYC8203-154-1	P	7110	1.54	135	9.99	–	–	10.621
TYC8962-532-1	P	4250	3.90	260	2.43	–	–	12.468
TYC9410-532-1	P	6120	1.64	170	4.96	–	–	10.619
TYC4146-806-1	R	5770	0.86	190	1.86	–	–	11.006
TYC7734-537-1	R	5460	0.76	300	0.59	–	–	4.386
TYC8628-1696-1	R	10300	2.00	160	19.31	–	–	0.338
TYC8959-2269-1	R	6120	1.71	230	2.83	–	–	4.229
TYC8628-1491-1	R	7340	1.52	200	4.77	–	–	1.859
HD 308379	P	5920	2.10	185	5.00	–	–	7.618
HD 98363	P	7890	1.69	350	2.01	130	14.54	20.161
TYC8624-403-1	R	5610	0.82	200	1.52	–	–	7.453
TYC7738-140-1	R	3080	0.19	400	0.03	–	–	44.652
TYC9233-1852-1	R	9040	2.86	500	2.18	65	129.04	6.021

Continued on Next Page...

Table A.1 – Continued

Name	Catalog	$T_{*,SED}$ (K)	$R_{*,SED}$ ($R_\odot$)	T_{dust} (K)	R_{disk} (au)	T_{dust2} (K)	R_{disk2} (au)	$\frac{L_{IR}}{L_{star}}$ ($\times 10^{-4}$)
TYC9415-2314-1	R	4290	0.85	170	1.27	–	–	2.839
HR 4388	P	7850	2.08	220	6.18	75	53.16	1.219
TYC8963-240-1	R	5720	2.77	230	3.99	–	–	7.945
TYC6091-2196-1	R	7760	1.74	140	12.46	–	–	0.746
TYC8625-1007-1	R	8900	4.93	290	10.82	–	–	1.173
TYC8963-903-1	R	4310	12.1	190	14.49	–	–	6.371
TYC9225-4802-1	R	7480	1.47	170	6.65	–	–	4.702
TYC9411-1506-1	R	6270	2.04	220	3.86	–	–	3.098
TYC8617-921-1	R	3130	0.20	200	0.12	–	–	6.380
TYC8226-510-1	R	6120	1.57	165	5.05	–	–	17.233
TYC863-731-1	R	6150	1.05	200	2.32	–	–	7.337
HD 101088	P	6170	7.07	200	15.66	40	391.52	0.684
HD 101259	R	5200	4.56	60	79.83	–	–	0.066
TYC9238-188-1	R	6250	2.74	225	4.93	–	–	4.559
TYC9415-992-1	R	4580	8.23	220	8.30	–	–	2.552
TYC8634-844-1	R	7220	1.49	210	4.11	–	–	1.624
TYC9419-30-1	R	7830	4.33	70	126.16	–	–	4.792
TYC8634-1258-1	R	7820	1.59	190	6.30	–	–	1.594
TYC8642-775-1	R	4470	7.47	230	6.56	–	–	4.631
TYC9411-1067-1	R	8450	2.00	200	8.33	35	271.89	54.319
HD 102458	P	5900	1.54	200	3.13	45	61.83	2.080
TYC8639-131-1	R	5110	5.69	180	10.67	–	–	8.767
TYC8635-1089-1	R	2900	0.18	401	0.02	–	–	1464.870
HD 103234	P	6640	1.47	200	3.78	–	–	1.505
HD 103266	P	8550	1.92	190	9.05	–	–	0.381
TYC1985-520-1	R	5330	1.60	225	2.10	–	–	20.389
TYC276-574-1	R	6170	1.92	160	6.66	–	–	2.549
TYC7750-554-1	R	5880	0.81	205	1.56	–	–	4.077
TYC8981-4034-1	P	4560	10.9	230	10.00	–	–	35.817
HD 103703	P	6510	1.49	240	2.56	–	–	4.652
HD 104067	R	5080	0.77	70	9.50	–	–	1.060
HD 104231	P	6470	1.42	260	2.05	–	–	3.335
HD 104860	P	6100	0.96	300	0.93	45	41.28	6.289
EF Cha	P	7050	1.90	295	2.53	–	–	12.689
TYC3017-2044-1	R	5840	1.27	240	1.76	–	–	5.287
TYC8241-3236-1	R	10080	2.01	190	13.20	–	–	0.839
TYC 8241-2652-1	P	4770	1.10	200	1.46	–	–	10.892
HD 105613	P	7940	1.56	200	5.72	–	–	1.082
TYC8982-3676-1	R	3800	0.48	200	0.41	–	–	4.095
HD 105857	P	8180	1.71	190	7.42	–	–	1.845
TYC8974-124-1	R	4540	8.07	200	9.68	–	–	3.536
HD 105994	R	6640	1.73	200	4.44	–	–	0.292
HD 106036	P	8420	1.65	200	6.83	–	–	4.116
CD-54 4621	P	5010	1.23	170	2.49	–	–	4.249
HD 106252	P	6070	1.03	120	6.14	–	–	0.376
TYC8974-1183-1	R	3930	0.51	180	0.57	–	–	4.478
HD 106389	P	6140	1.44	280	1.61	–	–	3.914
TYC7756-372-1	R	7480	1.50	190	5.43	–	–	18.629
TYC8645-2086-1	R	4630	0.66	230	0.62	–	–	6.567
HR 4669	P	9010	2.42	200	11.43	–	–	2.459
HD 106906	P	6450	2.00	120	13.50	55	64.25	35.747
TYC8641-2187-1	R	4870	1.75	240	1.69	–	–	4.675
HD 107146	P	5910	0.94	200	1.92	50	30.72	11.402
TYC8645-1337-1	R	5900	1.43	220	2.40	–	–	6.245
TYC6685-190-1	R	7090	1.98	160	9.06	–	–	1.731
HD 107649	P	6450	1.33	190	3.59	–	–	1.918
CD-52 5008	P	5880	1.66	145	6.36	–	–	2.194
TYC9240-1486-1	R	6120	1.58	180	4.27	–	–	3.227

Continued on Next Page...

Table A.1 – Continued

Name	Catalog	$T_{*,SED}$ (K)	$R_{*,SED}$ ($R_\odot$)	T_{dust} (K)	R_{disk} (au)	T_{dust2} (K)	R_{disk2} (au)	$\frac{L_{IR}}{L_{star}}$ ($\times 10^{-4}$)
HD 107947	P	9320	1.69	350	2.79	130	20.24	2.520
TYC6106-964-1	R	6590	1.48	190	4.15	–	–	2.161
TYC8654-2750-1	R	7470	1.45	160	7.38	–	–	4.314
TYC9236-2820-1	R	5880	1.15	180	2.88	–	–	9.878
TYC8243-284-1	R	8020	2.90	160	16.97	–	–	0.513
HD 108874	P	5710	1.00	300	0.84	50	30.38	2.710
TYC8658-946-1	R	4380	0.61	250	0.44	–	–	6.428
HD 108857	P	6110	1.78	225	3.06	–	–	7.631
TYC8231-2373-1	R	6270	1.67	180	4.73	–	–	1.499
TYC880-226-1	R	6180	1.62	190	3.99	–	–	5.051
TYC8654-1778-1	R	7900	1.62	220	4.86	–	–	0.923
TYC7255-1491-1	R	7190	1.68	120	14.07	–	–	1.152
HD 109832	P	6830	1.60	170	6.03	80	27.24	9.534
HD 110058	P	7940	2.23	575	0.99	100	32.71	41.817
TYC9240-479-1	R	5860	0.97	190	2.15	–	–	5.112
TYC8992-106-1	P	5860	0.92	190	2.04	–	–	8.682
10 CVn	P	6130	0.90	65	18.63	0	0.00	0.000
TYC9228-2332-1	R	8320	1.59	120	17.83	–	–	0.601
HD 111103	P	6410	1.31	110	10.35	–	–	3.257
V940 Cen	R	5220	1.25	400	0.50	–	–	4.462
HD 111347	P	6380	1.27	140	6.15	–	–	0.675
HD 111520	P	6360	1.41	160	5.20	70	27.14	33.598
TYC8997-604-1	R	7450	1.46	200	4.72	–	–	1.728
TYC9001-28-1	R	5610	1.78	280	1.67	–	–	5.598
TYC3845-612-1	R	5670	0.95	180	2.21	–	–	17.406
TYC8989-583-1	R	5310	1.24	380	0.57	–	–	8.796
HD 112383	P	8720	1.76	240	5.41	–	–	1.803
TYC9421-683-1	R	8670	1.61	190	7.83	–	–	1.654
HD 112810	P	6560	1.39	180	4.30	55	46.07	12.628
TYC8997-1940-1	R	4470	0.63	350	0.24	–	–	7.058
CPD-52 6110	P	5200	0.90	140	2.91	–	–	3.007
TYC8997-1223-1	R	4560	6.58	250	5.10	–	–	6.328
HD 113319	R	5860	0.89	200	1.80	–	–	0.465
TYC8660-689-1	R	7510	1.74	165	8.39	–	–	5.832
HD 113524	P	6440	1.49	200	3.61	–	–	1.461
HD 113457	P	9310	1.74	220	7.28	–	–	2.716
TYC8997-1155-1	R	5630	1.51	300	1.24	–	–	4.136
TYC8656-483-1	P	6100	1.07	250	1.49	–	–	4.100
HD 113556	P	6770	1.51	180	4.97	60	44.77	9.530
TYC8997-1088-1	R	5750	1.54	250	1.90	–	–	6.351
TYC8653-1256-1	P	4770	10.6	280	7.16	–	–	13.775
HD 114082	P	6520	1.48	110	12.13	–	–	35.842
TYC8990-1084-1	R	4380	13.1	250	9.36	–	–	7.420
TYC8661-216-1	R	5460	1.62	200	2.82	–	–	9.654
TYC7782-1057-1	R	6480	1.39	220	2.81	–	–	2.729
HD 115361	P	6470	1.33	150	5.79	–	–	3.021
TYC3460-2402-1	R	6130	1.16	210	2.30	–	–	7.617
HD 115116	R	7620	1.73	50	93.52	–	–	3.805
TYC8998-1208-1	R	5730	1.99	230	2.88	–	–	7.771
HD 115600	P	6800	1.55	120	11.63	90	20.68	37.267
HD 115820	P	7370	1.59	160	7.87	–	–	1.415
TYC8998-929-1	R	5650	0.87	250	1.04	–	–	17.958
TYC8674-2045-1	R	4770	2.90	210	3.48	–	–	13.381
TYC9002-1148-1	R	7980	1.63	190	6.72	–	–	1.706
TYC8260-287-1	R	6850	1.67	140	9.35	–	–	4.244
TYC6120-799-1	R	3640	0.42	400	0.08	–	–	15.616
TYC8248-1589-1	R	6290	1.16	190	2.98	–	–	3.272
TYC8662-2197-1	R	8690	1.78	160	12.24	–	–	0.515

Continued on Next Page...

Table A.1 – Continued

Name	Catalog	$T_{*,SED}$ (K)	$R_{*,SED}$ ($R_\odot$)	T_{dust} (K)	R_{disk} (au)	T_{dust2} (K)	R_{disk2} (au)	$\frac{L_{IR}}{L_{star}}$ ($\times 10^{-4}$)
HD 116402	R	5920	1.25	280	1.31	–	–	2.769
TYC8674-2480-1	R	5460	1.38	220	1.98	–	–	6.682
TYC7799-1047-1	R	7240	1.58	160	7.54	–	–	4.944
TYC8252-1917-1	P	8200	1.75	170	9.47	–	–	1.938
HD 116956	P	5530	0.79	70	11.54	–	–	0.196
TYC8995-2386-1	P	4630	8.93	240	7.74	–	–	9.504
HD 117043	P	5700	1.00	140	3.87	0	0.00	4.098
TYC8670-22-1	R	6460	3.52	265	4.88	–	–	2.995
TYC3462-848-1	R	7150	5.29	200	15.73	–	–	0.143
70 Vir	P	5660	1.83	100	13.69	–	–	0.188
HD 117214	P	6340	1.96	130	10.89	85	25.47	50.647
TYC9438-1004-1	R	6970	1.35	170	5.31	–	–	1.667
TYC8991-3324-1	P	4350	0.61	205	0.64	–	–	15.738
HD 117524	R	5460	1.61	400	0.70	–	–	4.692
TYC8666-700-1	R	6610	1.41	170	4.96	–	–	1.671
TYC8991-2436-1	R	4390	10.9	210	11.13	–	–	5.822
TYC8663-800-1	R	7380	1.57	240	3.46	–	–	0.804
TYC7788-806-1	R	5630	0.77	195	1.49	–	–	13.525
HD 118379	R	7870	1.63	100	23.54	–	–	2.301
CD-40 8031	P	5270	1.18	180	2.35	–	–	3.706
HD 119124	P	6130	1.11	200	2.43	50	38.89	1.024
HD 118972	P	5510	0.67	300	0.53	–	–	3.843
HD 119332	R	5370	0.76	80	7.98	–	–	0.777
TYC6130-223-1	R	6890	1.51	140	8.53	–	–	1.137
TYC7801-1120-1	R	7150	1.55	90	22.82	–	–	14.546
HD 119511	P	6640	1.74	270	2.45	–	–	0.762
TYC2540-406-1	R	4510	0.48	280	0.29	–	–	7.305
TYC8262-2554-1	R	7730	1.58	150	9.79	–	–	11.446
TYC9008-3742-1	R	4540	8.07	350	3.16	–	–	9.510
TYC8270-2110-1	R	6580	1.41	220	2.94	–	–	1.773
TYC7274-1776-1	R	7120	1.52	140	9.19	–	–	6.784
TYC9243-306-1	R	6260	1.27	130	6.86	–	–	7.513
HD 119718	P	6380	2.10	140	10.15	–	–	3.387
TYC6719-514-1	R	4550	0.69	250	0.53	–	–	7.017
TYC4171-34-1	R	6360	1.04	225	1.94	–	–	4.078
TYC7279-1292-1	R	5620	0.98	190	2.00	–	–	5.028
HD 120178	R	6260	1.79	205	3.89	–	–	1.855
TYC8664-713-1	R	6250	1.79	180	5.04	–	–	1.830
HD 120326	P	6840	1.49	160	6.34	85	22.46	30.694
TYC7802-1796-1	R	6400	1.31	190	3.48	–	–	2.376
TYC8664-1296-1	R	6260	1.29	170	4.10	–	–	3.441
HD 120160	P	6750	2.61	60	77.13	–	–	1.218
TYC8664-564-1	R	8260	2.17	180	10.66	–	–	0.777
TYC9438-722-1	R	5550	1.75	210	2.85	–	–	14.944
HD 121191	R	7530	1.60	200	5.28	–	–	25.211
HD 121812	P	5500	0.78	55	18.15	–	–	15.903
HD 121504	R	6080	1.04	45	44.35	–	–	0.777
HD 121617	P	8710	1.75	140	15.82	85	42.92	44.596
HR 5258	R	6360	3.08	70	59.26	–	–	1.536
TYC6149-284-1	R	6440	1.30	120	8.77	–	–	6.296
HD 122948	R	5880	0.81	300	0.73	–	–	1.118
TYC8268-3628-1	R	9410	1.88	130	23.03	–	–	3.410
TYC6149-753-1	R	3100	0.22	375	0.13	–	–	21.507
HD 123889	P	6710	1.57	120	11.43	–	–	0.449
TYC7812-108-1	R	6130	1.42	220	2.57	–	–	26.129
TYC9009-595-1	R	6110	1.64	200	3.57	–	–	14.849
HD 124469	R	7160	1.43	90	21.17	–	–	0.863
HD 124718	P	5810	0.94	65	17.53	–	–	18.041

Continued on Next Page...

Table A.1 – Continued

Name	Catalog	$T_{*,SED}$ (K)	$R_{*,SED}$ ($R_\odot$)	T_{dust} (K)	R_{disk} (au)	T_{dust2} (K)	R_{disk2} (au)	$\frac{L_{IR}}{L_{star}}$ ($\times 10^{-4}$)
TYC8690-1888-1	R	4840	1.90	200	2.60	–	–	8.172
TYC8678-260-1	R	6690	1.42	200	3.72	45	73.43	4.558
HD 124619	P	6720	1.42	190	4.15	–	–	1.184
TYC6743-252-1	R	4390	0.63	400	0.17	–	–	12.713
HD 125283	P	8510	1.86	200	7.87	–	–	0.280
HD 125541	P	7170	1.56	130	11.06	–	–	2.758
TYC5566-791-1	R	7950	1.86	140	13.99	–	–	0.649
TYC7805-1871-1	R	8390	1.37	145	10.72	–	–	4.820
BD+00 3170	R	4770	0.71	200	0.94	–	–	1.774
TYC8678-1032-1	R	6490	1.88	160	7.23	–	–	13.064
HD 126062	P	8770	1.76	150	14.05	55	104.49	4.919
TYC324-1006-1	R	6490	1.41	140	7.07	–	–	4.219
TYC9006-192-1	R	7180	1.56	155	7.83	–	–	11.741
CD-46 9327	P	5320	1.11	400	0.46	–	–	6.335
HD 127821	P	5210	1.16	200	1.84	30	81.90	10.478
HD 127236	R	6750	1.55	120	11.41	–	–	0.683
TYC2556-637-1	R	6150	2.42	200	5.34	–	–	5.992
HD 128165	P	5000	0.71	200	1.04	–	–	0.909
HD 128155	R	7480	1.55	120	14.03	–	–	0.231
TYC7308-2055-1	R	7240	1.68	100	20.53	–	–	0.352
TYC8683-242-1	P	5210	1.09	240	1.20	–	–	14.817
TYC7810-261-1	R	6490	1.57	180	4.77	–	–	2.007
HD 128788	R	7620	1.82	95	27.34	–	–	0.734
TYC9011-4622-1	R	7890	1.88	120	18.97	–	–	0.782
TYC326-428-1	R	8990	2.29	170	14.94	–	–	0.743
HD 129490	R	5920	1.99	200	4.07	–	–	0.609
HD 129590	P	5930	1.71	100	14.05	60	39.02	123.685
HD 129683	R	6160	1.45	180	3.97	–	–	4.229
TYC6754-604-1	R	5640	3.19	280	3.02	–	–	4.895
GJ 563.1	R	4250	0.66	80	4.39	–	–	1.628
TYC8684-2799-1	R	8110	2.64	180	12.50	–	–	1.268
TYC7297-1759-1	R	7280	1.79	190	6.12	–	–	1.826
TYC7823-1411-1	R	6320	1.30	235	2.20	–	–	9.797
TYC9011-3733-1	P	5780	1.31	225	2.01	–	–	6.187
HD 130656	R	7790	1.67	90	29.17	–	–	1.319
TYC2558-467-1	R	6130	2.54	200	5.56	–	–	3.676
HD 131496	P	4940	5.45	70	63.21	–	–	0.167
TYC7824-2717-1	P	6260	1.36	215	2.68	–	–	5.768
HD 132254	P	6270	1.43	140	6.68	–	–	0.173
HD 131835	P	7980	1.75	180	8.02	70	53.03	49.253
TYC6756-303-1	R	6790	1.47	180	4.89	–	–	14.287
TYC6176-925-1	R	6560	1.37	135	7.57	–	–	3.529
TYC922-865-1	R	6610	2.00	220	4.21	–	–	14.503
TYC8293-3733-1	R	6990	2.11	120	16.68	–	–	2.843
TYC8681-1601-1	R	5420	1.62	190	3.07	–	–	11.941
HD 133075	P	6150	3.56	120	21.81	–	–	0.657
TYC8293-3258-1	R	6990	1.42	120	11.24	–	–	16.285
TYC7821-299-1	R	7880	1.58	150	10.16	–	–	5.065
TYC6773-427-1	R	6140	2.87	190	6.98	–	–	3.051
HD 133803	P	6920	1.59	170	6.16	–	–	4.517
TYC8702-102-1	R	6310	1.45	175	4.39	–	–	6.789
TYC923-1568-1	R	8810	1.89	200	8.57	–	–	0.446
TYC7324-1668-1	R	7960	1.76	180	8.02	0	0.00	21.241
HD 134888	P	6480	1.48	200	3.61	75	25.71	14.957
TYC9025-1409-1	R	6260	1.77	195	4.25	–	–	2.665
TYC7826-2474-1	P	6190	1.40	115	9.44	–	–	62.481
TYC3051-1266-1	R	7540	2.45	200	8.12	–	–	0.810
HD 135599	P	5510	0.73	200	1.31	50	20.90	1.920

Continued on Next Page...

Table A.1 – Continued

Name	Catalog	$T_{*,SED}$ (K)	$R_{*,SED}$ ($R_\odot$)	T_{dust} (K)	R_{disk} (au)	T_{dust2} (K)	R_{disk2} (au)	$\frac{L_{IR}}{L_{star}}$ ($\times 10^{-4}$)
TYC8702-372-1	R	5320	0.95	220	1.31	–	–	5.801
TYC7834-2020-1	R	7550	1.50	150	8.86	–	–	4.157
TYC9021-457-1	R	4370	12.6	200	14.00	–	–	7.259
TYC6766-1629-1	R	7670	2.08	170	9.88	–	–	0.645
TYC5002-512-1	R	6550	1.96	180	6.05	–	–	1.588
HD 135953	P	6310	1.36	65	29.90	–	–	8.658
TYC7830-604-1	R	8480	1.71	160	11.23	–	–	0.557
TYC8694-1537-1	R	6440	2.99	200	7.22	–	–	2.330
GJ 581	P	3250	0.34	120	0.59	25	13.49	1.819
TYC8694-1771-1	R	5720	0.87	190	1.84	–	–	11.907
TYC7313-615-1	R	4230	1.69	320	0.69	–	–	10.858
HD 136246	P	8470	1.74	240	5.06	55	96.29	1.011
TYC8707-955-1	R	5240	1.32	230	1.60	–	–	145.163
TYC9021-6-1	R	4520	9.47	260	6.66	–	–	5.784
HR 5722	R	8550	2.58	200	11.00	–	–	0.171
HD 137057	R	6640	2.16	120	15.39	–	–	3.719
TYC8307-50-1	R	5660	0.97	220	1.51	–	–	7.483
TYC8303-30-1	R	7830	1.59	120	15.78	–	–	0.706
HD 137499	R	6420	1.38	140	6.79	–	–	2.993
TYC7326-638-1	R	4970	1.29	380	0.52	–	–	13.058
TYC7836-1284-1	R	6700	1.48	120	10.75	–	–	3.601
TYC9263-2262-1	R	6600	1.29	140	6.70	–	–	20.206
TYC9429-236-1	R	5940	1.38	175	3.71	–	–	12.056
TYC2567-151-1	R	8810	1.93	140	17.86	–	–	0.555
HD 138296	P	6490	1.72	120	11.73	–	–	0.228
TYC6764-1501-1	R	5910	1.50	220	2.53	–	–	4.818
TYC9022-1316-1	P	8770	1.78	150	14.21	–	–	3.542
TYC7836-1029-1	R	9780	1.85	175	13.45	–	–	1.054
TYC8708-405-1	R	7320	2.48	150	13.76	–	–	2.344
HD 138813	P	8660	1.85	170	11.17	85	44.69	22.678
HD 139323	P	5210	0.82	300	0.58	30	58.14	11.231
TYC7335-550-1	R	4430	1.44	210	1.50	–	–	10.583
TYC6197-174-1	R	3530	0.38	120	0.77	–	–	4.134
TYC941-1023-1	R	8670	2.28	180	12.33	–	–	0.929
HD 139590	R	6150	1.29	70	23.27	–	–	3.422
TYC6777-1626-1	R	8880	2.15	140	20.17	–	–	0.405
HR 5792	P	8630	1.64	200	7.12	65	67.42	7.341
TYC6781-652-1	R	6650	1.51	120	10.79	–	–	7.548
TYC8704-2004-1	R	6750	1.73	200	4.61	–	–	2.927
HD 140374	R	5510	1.54	500	0.44	–	–	4.419
TYC7327-365-1	R	6910	1.59	120	12.30	–	–	4.448
HD 140475	R	7980	1.81	80	42.07	–	–	0.902
TYC6781-328-1	R	5220	1.11	170	2.45	–	–	10.990
HD 140840	P	9380	2.01	200	10.32	80	64.50	3.607
TYC6782-1207-1	R	7630	1.78	190	6.70	–	–	1.000
TYC8701-236-1	R	4240	14.3	220	12.36	–	–	9.344
TYC7340-321-1	P	6170	1.51	240	2.33	–	–	3.985
HD 141011	P	6530	1.44	200	3.57	–	–	1.989
TYC8705-2248-1	R	4730	2.82	240	2.56	–	–	3.362
TYC7332-414-1	R	6680	1.84	200	4.78	–	–	1.952
HD 141227	P	5900	2.34	180	5.87	–	–	16.400
HD 141378	P	8240	1.86	190	8.18	60	82.01	1.448
TYC8321-382-1	R	6140	1.65	200	3.62	–	–	5.645
HD 141327	R	9050	2.57	180	15.14	–	–	0.576
HD 141569	P	8240	1.85	300	3.26	90	36.25	162.460
HD 141441	R	6160	1.70	225	2.98	–	–	2.496
TYC7332-2514-1	P	6630	1.41	250	2.32	–	–	3.231
HD 141521	R	5380	1.83	300	1.37	–	–	1.189

Continued on Next Page...

Table A.1 – Continued

Name	Catalog	$T_{*,SED}$ (K)	$R_{*,SED}$ ($R_\odot$)	T_{dust} (K)	R_{disk} (au)	T_{dust2} (K)	R_{disk2} (au)	$\frac{L_{IR}}{L_{star}}$ ($\times 10^{-4}$)
TYC6790-638-1	R	7280	1.46	130	10.69	–	–	20.689
HD 141943	P	5910	1.41	300	1.28	65	27.30	4.241
TYC7846-989-1	R	4410	0.62	300	0.31	–	–	8.667
HD 142315	R	8580	2.79	110	39.54	–	–	5.850
TYC9260-3624-1	R	6270	1.26	165	4.26	–	–	17.557
lam CrB	P	6990	2.12	320	2.36	40	150.80	0.843
TYC6199-673-1	R	6700	1.94	150	9.01	–	–	2.344
HD 142446	P	6670	1.47	70	31.08	–	–	7.611
TYC6779-1929-1	R	6740	1.58	160	6.56	–	–	2.468
TYC9031-3463-1	R	6100	1.37	250	1.91	–	–	7.120
TYC6783-296-1	R	6510	1.59	140	8.02	–	–	4.225
HD 142705	R	7500	2.24	120	20.37	–	–	0.387
TYC5031-413-1	R	7120	1.54	165	6.70	–	–	1.804
2MASS J15581270-2328364	R	5120	1.82	180	3.43	–	–	6.961
TYC9260-134-1	R	7530	1.62	160	8.35	–	–	0.858
2MASS J15584772-1757595	P	3860	1.86	450	0.32	–	–	10.635
TYC8310-1272-1	R	7690	2.46	150	15.09	–	–	1.885
TYC7851-91-1	R	9470	1.73	120	25.20	–	–	3.586
TYC6783-409-1	R	6170	1.12	125	6.40	–	–	21.123
LL Lup	R	7880	2.53	105	33.20	–	–	0.457
TYC5032-1033-1	R	7230	2.24	120	18.95	–	–	0.854
HD 143538	P	6880	1.50	240	2.87	–	–	0.585
TYC9285-1347-1	R	6800	1.46	130	9.35	–	–	1.779
HD 143675	P	7750	1.44	190	5.61	110	16.73	10.903
HD 143811	R	6360	1.63	140	7.86	–	–	0.850
HD 143956	R	7610	2.31	200	7.80	–	–	0.192
TYC7855-650-1	R	8500	1.80	140	15.44	–	–	0.585
TYC7855-1120-1	R	10850	1.73	250	7.58	40	296.11	0.492
LM Lup	P	10850	1.73	160	18.51	–	–	0.220
TYC6788-169-1	R	6110	1.06	180	2.85	–	–	2.598
TYC6212-349-1	P	6960	2.13	185	7.01	–	–	4.558
TYC7863-986-1	R	5470	1.05	185	2.14	–	–	15.818
TYC7851-1636-1	R	8410	1.51	150	11.11	–	–	5.982
HD 144569	R	7350	2.02	225	5.02	–	–	0.854
HD 144586	R	7950	1.86	215	5.94	–	–	0.753
HD 144587	P	6540	2.05	205	4.87	–	–	5.119
TYC7859-891-1	R	7330	2.00	175	8.17	–	–	8.705
TYC8714-791-1	R	4430	4.31	215	4.26	–	–	10.056
HD 144713	R	5870	2.03	500	0.65	–	–	5.886
HD 144729	P	6280	1.85	300	1.89	–	–	1.926
TYC7851-810-1	P	4590	1.70	90	10.34	–	–	1308.115
TYC7338-1156-1	P	7270	1.56	130	11.37	–	–	16.701
HD 144981	R	7380	1.95	400	1.55	130	14.64	6.271
HD 145229	P	5940	0.94	200	1.94	50	30.97	1.880
TYC4425-1270-1	R	5770	1.96	190	4.22	–	–	4.514
TYC5616-682-1	R	4590	0.65	330	0.29	–	–	7.109
TYC6213-12-1	P	6970	2.52	160	11.16	–	–	10.110
TYC6784-1422-1	R	8830	1.96	400	2.23	–	–	0.855
TYC6213-1122-1	P	4360	1.56	120	4.81	70	14.14	3458.429
HD 145263	R	6520	1.54	250	2.44	–	–	162.280
TYC2573-363-1	R	8050	1.73	180	8.06	–	–	0.522
TYC6793-681-1	R	6140	1.60	210	3.18	–	–	4.461
HD 145357	P	7240	1.61	190	5.47	–	–	1.214
HD 145554	P	7530	2.35	400	1.94	150	13.81	8.773
HD 145631	P	7430	2.33	200	7.51	–	–	1.185
HD 145655	R	5520	2.44	260	2.56	–	–	3.287
TYC8311-1761-1	R	6260	1.59	400	0.91	–	–	2.566
HD 145560	P	6460	1.40	400	0.85	80	21.29	38.213

Continued on Next Page...

Table A.1 – Continued

Name	Catalog	$T_{*,SED}$ (K)	$R_{*,SED}$ ($R_\odot$)	T_{dust} (K)	R_{disk} (au)	T_{dust2} (K)	R_{disk2} (au)	$\frac{L_{IR}}{L_{star}}$ ($\times 10^{-4}$)
TYC3880-518-1	R	5910	1.55	210	2.87	–	–	11.446
TYC8723-711-1	R	5660	4.83	215	7.79	–	–	5.288
TYC9048-2235-1	R	2860	0.17	200	0.08	–	–	14.087
HD 145880	P	8090	2.12	200	8.07	75	57.42	13.101
2MASS J16145918-2750230	P	5070	1.30	230	1.47	–	–	4.568
HD 146069	R	6110	1.61	220	2.90	–	–	2.175
HD 145984	R	6650	1.51	240	2.70	–	–	0.443
TYC8323-142-1	R	4250	22.5	130	56.00	–	–	5.685
HD 145972	P	6910	1.58	200	4.39	–	–	1.977
HD 146181	P	6450	1.36	350	1.08	80	20.58	29.731
TYC8315-1143-1	R	5610	3.89	200	7.12	–	–	5.747
HD 145689	P	8150	1.55	250	3.83	50	95.80	0.798
TYC6801-382-1	R	3900	5.91	180	6.46	–	–	5.972
HD 146606	P	9300	1.81	190	10.10	–	–	1.108
TYC8715-725-1	R	4070	0.54	200	0.53	–	–	5.134
TYC8711-3302-1	R	5870	0.81	190	1.82	–	–	7.051
TYC6798-340-1	R	5730	1.81	165	5.09	–	–	23.049
HD 147196	P	7260	2.97	210	8.27	–	–	9.362
TYC6798-35-1	R	3940	1.83	280	0.85	–	–	8.627
HD 147594	P	5910	1.70	240	2.41	–	–	1.941
TYC7348-847-1	R	6530	1.52	180	4.66	–	–	2.917
TYC6802-1242-1	R	7250	2.81	60	95.68	–	–	55.143
TYC2043-1337-1	R	3740	0.59	400	0.12	–	–	13.857
TYC8316-4073-1	P	6950	1.70	180	5.91	–	–	4.939
TYC5638-583-1	R	6140	1.25	170	3.80	–	–	3.516
HD 148040	R	6120	2.02	240	3.07	–	–	0.577
HD 148055	R	7640	1.50	60	56.77	–	–	2.500
TYC8324-3258-1	R	4850	10.1	230	10.53	–	–	6.402
TYC9274-4091-1	R	9330	3.74	280	9.66	35	618.44	16.918
TYC7861-1025-1	R	5210	2.16	195	3.59	–	–	21.254
TYC9037-1879-1	R	7860	3.96	140	29.09	–	–	0.826
TYC6799-933-1	R	6550	3.45	120	23.94	–	–	3.436
HD 150706	P	5940	0.96	350	0.65	55	26.17	1.474
HD 328333	R	6100	1.90	170	5.70	–	–	4.603
TYC6807-85-1	R	5460	0.63	160	1.72	–	–	25.040
TYC390-217-1	R	7270	1.56	140	9.82	–	–	0.946
TYC7854-467-1	R	5910	1.11	160	3.53	–	–	23.430
TYC5048-313-1	R	4320	26.8	120	80.94	–	–	1.983
TYC3063-2031-1	R	9790	2.38	220	11.01	–	–	1.223
TYC 1531-383-1	R	5340	0.70	340	0.41	–	–	1.629
TYC5636-577-1	R	5920	2.02	200	4.13	–	–	3.660
HD 149735	R	6090	2.04	170	6.11	–	–	1.976
HD 149790	R	6360	1.53	300	1.60	–	–	0.820
TYC8333-1549-1	R	6290	1.25	180	3.57	–	–	1.459
HD 149914	R	6750	4.47	180	14.65	35	387.57	105.245
TYC3499-1179-1	R	6130	0.97	300	0.95	–	–	10.773
TYC7358-263-1	P	5560	1.68	200	3.04	–	–	7.543
HD 151044	P	6160	1.18	60	29.11	–	–	0.927
TYC5632-973-1	R	7330	1.83	140	11.68	–	–	0.689
TYC7879-1506-1	R	8180	1.95	200	7.62	–	–	1.808
HD 150697	P	6170	2.15	140	9.74	–	–	2.306
TYC1520-925-1	R	5910	1.55	250	2.03	–	–	5.693
TYC387-634-1	R	7720	1.73	140	12.28	–	–	1.282
TYC7346-1504-1	R	6110	1.30	120	7.86	–	–	17.250
TYC6817-2179-1	R	8890	1.61	150	13.23	–	–	1.222
TYC7875-196-1	R	4070	12.6	180	15.08	–	–	4.287
HD 151109	R	9930	2.76	190	17.58	115	47.98	2.545
TYC8717-2184-1	R	6110	1.70	325	1.41	–	–	6.371

Continued on Next Page...

Table A.1 – Continued

Name	Catalog	$T_{*,SED}$ (K)	$R_{*,SED}$ ($R_\odot$)	T_{dust} (K)	R_{disk} (au)	T_{dust2} (K)	R_{disk2} (au)	$\frac{L_{IR}}{L_{star}}$ ($\times 10^{-4}$)
TYC8330-2024-1	R	7000	2.27	120	18.05	–	–	2.075
HD 151376	P	6330	1.32	300	1.37	120	8.59	5.071
TYC8713-933-1	R	6360	1.97	160	7.27	–	–	1.294
TYC7359-2091-1	R	6130	1.34	190	3.26	–	–	6.100
HD 151721	R	8400	1.74	150	12.75	–	–	0.761
TYC5054-1711-1	R	7290	2.65	160	12.81	–	–	0.631
TYC8331-632-1	R	6120	1.10	240	1.67	–	–	3.845
TYC7868-172-1	R	7460	1.49	130	11.43	–	–	3.268
TYC8327-548-1	R	6500	1.31	150	5.72	–	–	35.331
TYC8335-1185-1	R	6080	1.23	160	4.15	–	–	1.823
TYC6223-328-1	R	4120	13.5	220	11.04	–	–	4.942
TYC7372-990-1	R	6520	1.57	185	4.54	–	–	3.251
TYC988-1468-1	R	6130	1.53	155	5.59	–	–	10.214
TYC8726-806-1	R	6560	2.41	210	5.49	–	–	4.704
TYC410-586-1	R	2970	102.	450	10.40	–	–	52.028
TYC7881-561-1	R	4640	4.20	180	6.50	–	–	4.909
HD 154145	R	7680	2.33	58	95.12	–	–	4.222
TYC8328-461-1	R	4010	0.53	200	0.50	–	–	3.410
TYC8328-113-1	R	4950	1.80	160	4.02	–	–	23.849
HD 154577	P	5070	0.63	85	5.24	–	–	0.200
TYC6236-1042-1	R	4810	2.85	360	1.18	–	–	7.502
TYC5065-592-1	R	5700	0.85	280	0.82	–	–	3.981
TYC7370-237-1	R	8060	1.62	165	9.00	–	–	16.429
TYC9056-548-1	R	5430	0.99	200	1.71	–	–	8.801
TYC7370-626-1	R	5920	1.70	230	2.63	–	–	9.086
TYC7874-596-1	R	4290	6.80	120	20.23	–	–	4.638
TYC400-774-1	R	3950	7.64	145	13.20	–	–	7.187
TYC2078-810-1	R	4280	0.81	400	0.22	–	–	4.498
HD 155915	R	5390	0.84	120	3.96	–	–	0.890
TYC7874-747-1	R	5280	0.79	245	0.86	–	–	12.798
TYC7362-633-1	R	8180	1.70	120	18.44	–	–	0.777
TYC7362-255-1	R	5460	1.38	170	3.32	–	–	23.480
TYC9280-1438-1	R	5650	1.04	230	1.47	–	–	18.247
TYC2592-1266-1	R	4790	0.68	400	0.23	–	–	8.003
73 Her	P	7590	1.58	200	5.32	90	26.26	4.662
TYC5658-453-1	R	6400	1.92	180	5.67	–	–	1.747
HD 157587	P	6370	1.45	80	21.41	–	–	35.376
HD 158633	P	5420	0.75	300	0.57	55	17.08	1.082
TYC7891-223-1	R	4190	7.30	190	8.26	–	–	6.874
HD 323410	P	5920	1.02	215	1.82	–	–	4.709
TYC7887-1692-1	R	4850	0.74	195	1.07	–	–	13.660
TYC6837-736-1	R	6410	1.34	120	8.92	–	–	3.311
HR 6511	P	8860	3.00	110	45.42	–	–	0.123
TYC6838-418-1	R	8560	1.79	140	15.62	–	–	1.871
TYC7883-505-1	R	6290	1.83	180	5.21	–	–	1.303
TYC7888-1250-1	R	5100	0.67	220	0.84	–	–	4.360
TYC6247-13-1	R	5910	1.50	170	4.22	–	–	6.701
HR 6532	P	8950	2.63	170	17.02	35	401.47	14.828
TYC7380-335-1	R	8360	1.60	100	26.14	–	–	15.908
TYC7892-4279-1	R	9000	1.82	210	7.81	–	–	1.293
TYC7893-1217-1	R	6320	1.09	170	3.52	–	–	8.257
TYC7889-407-1	P	6720	1.71	195	4.73	–	–	9.008
TYC424-1952-1	R	4630	2.79	500	0.56	–	–	12.175
HD 161734	R	7940	4.27	330	5.76	–	–	6.423
HD 161733	R	8820	3.92	120	49.30	–	–	0.189
TYC2620-505-1	R	6520	1.58	170	5.41	–	–	3.869
TYC3089-170-1	R	3350	0.29	400	0.05	–	–	20.593
HD 164330	P	5900	2.09	40	106.23	–	–	10.098

Continued on Next Page...

Table A.1 – Continued

Name	Catalog	$T_{*,SED}$ (K)	$R_{*,SED}$ ($R_\odot$)	T_{dust} (K)	R_{disk} (au)	T_{dust2} (K)	R_{disk2} (au)	$\frac{L_{IR}}{L_{star}}$ ($\times 10^{-4}$)
TYC7386-1606-1	R	7170	2.78	140	17.00	–	–	0.829
TYC5095-523-1	R	7370	1.57	190	5.52	–	–	1.062
TYC9054-701-1	R	6600	2.78	190	7.82	–	–	5.576
HD 164029	R	4300	0.60	625	0.07	–	–	180.213
TYC8361-1861-1	R	9690	1.88	145	19.57	–	–	0.761
HD 164249	P	6450	1.41	85	18.96	–	–	7.932
TYC6264-707-1	R	5920	1.28	200	2.61	–	–	3.294
TYC4574-482-1	R	5940	1.49	205	2.91	–	–	14.866
TYC1022-431-1	R	11120	4.55	120	90.89	–	–	2.687
HD 169666	P	6540	1.63	180	5.02	–	–	2.116
TYC6277-1594-1	R	5920	1.17	220	1.98	–	–	3.128
TYC5681-1571-1	R	3940	11.0	135	21.91	–	–	7.058
TYC5685-2670-1	R	5680	1.05	45	38.97	–	–	32.035
HD 168746	P	5690	1.04	450	0.39	80	12.30	7.637
TYC4214-1171-1	R	6300	0.90	155	3.47	–	–	11.360
TYC5099-369-1	R	3790	11.2	180	11.61	–	–	3.584
TYC6266-3014-1	R	5670	2.09	240	2.72	–	–	6.379
TYC6266-2341-1	R	4530	4.02	180	5.94	–	–	11.645
TYC7910-57-1	R	7870	1.73	170	8.63	–	–	0.820
TYC9291-1885-1	R	6490	1.96	180	5.93	–	–	5.177
TYC7402-1806-1	R	5530	1.20	500	0.34	–	–	4.847
HR 6948	P	6590	1.40	45	70.00	–	–	4.399
TYC9081-1908-1	R	7230	1.50	145	8.68	–	–	1.770
TYC3531-1441-1	P	5230	0.73	270	0.64	–	–	8.358
TYC450-619-1	R	5620	1.09	230	1.52	–	–	13.204
TYC3531-1261-1	R	8140	1.72	120	18.46	–	–	1.181
TYC5692-1657-1	R	5070	2.43	220	3.01	–	–	5.100
TYC5692-233-1	R	4500	9.64	300	5.05	–	–	7.116
TYC5125-1912-1	R	3930	0.51	170	0.64	–	–	9.496
TYC452-385-1	R	5130	3.20	220	4.05	–	–	4.889
TYC5122-824-1	R	6360	1.69	200	4.00	–	–	2.113
TYC8758-70-1	R	6150	0.92	205	1.94	–	–	16.532
TYC452-465-1	R	4590	0.71	180	1.07	–	–	15.851
TYC3930-1649-1	R	6420	2.15	220	4.27	–	–	4.237
TYC7928-1234-1	R	6230	1.13	210	2.32	–	–	14.533
TYC2646-1742-1	R	6130	1.18	200	2.59	–	–	10.969
TYC5118-469-1	R	7110	2.64	140	15.84	–	–	0.823
TYC5118-18-1	R	6190	2.47	180	6.80	–	–	2.470
TYC3926-1315-1	R	4550	0.85	400	0.26	–	–	8.159
TYC8377-2703-1	R	8170	1.89	220	6.08	–	–	0.871
TYC6281-975-1	R	5890	1.47	205	2.83	–	–	8.194
TYC8377-2702-1	R	8950	2.17	160	15.84	–	–	0.512
TYC8381-2315-1	R	8160	5.41	140	42.82	–	–	0.766
TYC461-727-1	R	4540	2.24	190	2.98	–	–	8.769
TYC5119-79-1	R	4750	0.68	200	0.90	–	–	5.309
TYC5119-275-1	R	5470	3.10	200	5.41	–	–	4.340
TYC1039-551-1	R	5910	1.08	210	1.99	–	–	3.852
TYC1043-170-1	R	6150	2.07	175	5.96	–	–	4.341
TYC461-155-1	R	6130	1.98	290	2.07	–	–	3.873
TYC449-518-1	R	5930	1.12	195	2.43	–	–	7.478
TYC1040-160-1	R	7030	2.41	180	8.55	–	–	3.337
TYC7421-1061-1	R	6620	1.38	270	1.94	–	–	8.303
TYC7421-1163-1	R	7880	1.69	155	10.21	–	–	15.838
TYC1590-1044-1	R	5750	0.91	400	0.44	–	–	6.606
TYC4229-229-1	R	9140	2.17	200	10.59	–	–	0.722
TYC6882-255-1	R	6640	4.26	290	5.20	–	–	3.935
TYC471-1564-1	R	3860	0.52	200	0.45	–	–	3.828
TYC1599-138-1	R	5910	1.98	210	3.67	–	–	5.112

Continued on Next Page...

Table A.1 – Continued

Name	Catalog	$T_{*,SED}$ (K)	$R_{*,SED}$ ($R_\odot$)	T_{dust} (K)	R_{disk} (au)	T_{dust2} (K)	R_{disk2} (au)	$\frac{L_{IR}}{L_{star}}$ ($\times 10^{-4}$)
TYC1041-1127-1	R	5680	1.59	175	3.91	–	–	43.910
TYC467-681-1	R	5620	1.66	225	2.42	–	–	35.603
TYC2127-723-1	R	5250	2.61	190	4.64	–	–	5.406
TYC7427-63-1	R	4580	0.65	180	0.98	–	–	7.138
TYC6296-1814-1	R	8720	3.02	190	14.84	–	–	1.567
TYC1599-1737-1	R	4440	0.84	215	0.83	–	–	7.616
TYC1604-975-1	R	4330	5.30	190	6.40	–	–	5.036
TYC2654-591-1	R	5370	1.04	195	1.84	–	–	19.764
HD 181327	P	6430	1.35	80	20.35	–	–	32.029
TYC2129-720-1	R	4180	17.4	240	12.35	–	–	5.449
TYC1609-4-1	R	3320	31.2	120	55.66	–	–	10.447
TYC2663-22-1	R	6140	1.07	150	4.19	–	–	1.583
TYC6880-1781-1	R	3070	0.19	450	0.02	–	–	54.913
TYC7425-2426-1	R	7710	1.49	140	10.58	–	–	0.703
TYC5736-2110-1	R	8900	1.88	180	10.71	–	–	0.438
TYC479-1738-1	R	6110	2.01	250	2.80	–	–	2.760
TYC8390-1158-1	R	7610	1.90	205	6.11	–	–	6.189
TYC9097-721-1	R	3790	0.48	400	0.10	–	–	16.550
TYC2143-558-1	R	5630	2.31	200	4.26	–	–	15.854
TYC8787-1146-1	R	3310	0.27	400	0.04	–	–	11.391
TYC3136-728-1	R	6290	1.64	200	3.79	–	–	7.061
TYC484-1444-1	R	6140	1.30	120	7.96	–	–	7.148
TYC5725-63-1	R	4570	5.33	450	1.28	–	–	9.599
TYC2677-1018-1	R	2500	0.14	220	0.04	–	–	30.537
HD 187897	P	5940	1.07	200	2.21	55	29.17	1.299
TYC2669-2267-1	R	4750	10.6	250	8.92	–	–	4.063
TYC5725-3091-1	R	11530	3.09	220	19.78	–	–	0.223
TYC5750-1884-1	R	6110	1.45	160	4.93	–	–	3.676
TYC2674-851-1	R	4770	12.1	280	8.22	–	–	4.302
TYC2674-926-1	R	4900	0.70	200	0.99	–	–	17.178
TYC2674-2101-1	R	5300	2.71	230	3.35	–	–	10.210
HD 190228	P	5590	2.24	350	1.33	50	65.16	4.685
HD 190470	R	5210	0.75	100	4.78	–	–	0.519
TYC2678-2088-1	P	5440	2.60	195	4.71	–	–	10.950
TYC2153-1758-1	R	5460	2.28	255	2.43	–	–	5.292
TYC3158-832-1	R	6140	1.55	175	4.45	–	–	11.034
TYC2679-1864-1	P	4270	0.69	200	0.74	–	–	37.598
TYC8784-1182-1	R	5090	0.72	400	0.27	–	–	8.177
TYC8404-354-1	R	4290	0.61	200	0.66	–	–	1.289
TYC2679-798-1	R	5220	0.72	260	0.68	–	–	11.501
TYC2679-2863-1	R	6110	0.99	170	3.00	–	–	3.095
TYC3559-479-1	P	6280	4.04	200	9.28	–	–	4.219
TYC3158-1310-1	R	5080	8.79	350	4.31	–	–	8.624
HD 191089	P	6440	1.33	100	12.85	–	–	16.603
TYC3155-1649-1	R	6120	1.16	190	2.82	–	–	1.813
TYC2675-513-1	R	5890	0.86	210	1.57	–	–	5.737
TYC2679-1264-1	R	5160	4.28	240	4.61	–	–	9.006
TYC2671-118-1	R	7470	1.50	190	5.41	–	–	5.176
TYC3163-836-1	R	6140	1.12	170	3.41	–	–	7.938
HD 192263	P	5210	0.72	70	9.39	–	–	0.443
TYC2671-1250-1	R	6310	1.50	180	4.29	–	–	1.870
TYC3159-622-1	R	4470	0.63	200	0.74	–	–	7.880
TYC3155-807-1	P	6130	1.80	300	1.75	–	–	5.405
TYC3576-213-1	P	5070	0.78	235	0.85	–	–	9.456
TYC3159-584-1	R	5180	5.27	170	11.38	–	–	10.492
TYC8777-2025-1	R	6620	2.74	150	12.45	–	–	1.167
HD 192758	P	7050	1.57	170	6.29	55	60.11	7.939
TYC504-468-1	R	6870	1.56	100	17.18	–	–	5.123

Continued on Next Page...

Table A.1 – Continued

Name	Catalog	$T_{*,SED}$ (K)	$R_{*,SED}$ ($R_\odot$)	T_{dust} (K)	R_{disk} (au)	T_{dust2} (K)	R_{disk2} (au)	$\frac{L_{IR}}{L_{star}}$ ($\times 10^{-4}$)
TYC2163-1542-1	R	4580	9.65	200	11.78	–	–	5.379
TYC1643-70-1	R	5500	1.20	200	2.12	–	–	9.763
TYC2680-1143-1	R	8720	1.85	160	12.85	–	–	0.682
TYC1082-1928-1	R	3360	63.4	170	57.68	–	–	4.478
TYC2684-55-1	R	6110	1.05	180	2.83	–	–	2.313
TYC3576-852-1	R	5920	1.52	170	4.29	–	–	10.291
TYC2697-734-1	R	6130	2.64	120	16.06	–	–	2.183
TYC3156-709-1	R	4290	15.0	140	32.85	–	–	10.115
TYC2168-109-1	R	6120	1.40	200	3.06	–	–	6.327
TYC3156-1027-1	R	4670	11.4	260	8.57	–	–	8.198
TYC3156-1235-1	R	6120	1.22	110	8.81	–	–	13.293
TYC3160-85-1	R	5890	0.80	205	1.55	–	–	28.789
TYC8414-872-1	R	5220	1.93	200	3.06	–	–	11.105
TYC3573-2231-1	R	4590	0.73	160	1.41	–	–	10.343
TYC8418-179-1	R	4780	0.68	250	0.58	–	–	9.003
TYC9316-99-1	R	8960	1.58	140	15.06	–	–	1.038
TYC2690-1017-1	R	6170	1.46	160	5.06	–	–	19.538
TYC7468-1114-1	R	5160	0.75	320	0.46	–	–	7.265
TYC7950-1215-1	R	3700	0.45	300	0.16	–	–	44.080
TYC3165-787-1	R	6610	1.70	160	6.78	–	–	1.451
TYC3581-1077-1	R	6150	1.47	145	6.19	–	–	13.271
TYC7950-1387-1	R	5750	1.48	125	7.31	–	–	14.165
TYC2698-1078-1	P	5910	1.06	190	2.41	–	–	15.974
TYC3153-726-1	R	5620	0.87	125	4.12	–	–	14.064
TYC2698-310-1	R	3390	0.31	300	0.09	–	–	9.360
TYC3161-329-1	R	4460	7.96	110	30.46	–	–	21.221
TYC3166-1587-1	R	6120	1.36	230	2.24	–	–	10.985
TYC515-1701-1	R	4620	0.65	150	1.45	–	–	4.933
TYC3178-1159-1	R	5890	1.15	215	2.02	–	–	21.436
AU Mic	P	3520	0.86	65	5.87	–	–	6.709
TYC3578-983-1	R	5380	1.97	165	4.89	–	–	8.461
TYC3174-755-1	R	4730	9.60	200	12.50	–	–	7.086
TYC8803-1199-1	R	8440	3.23	190	14.86	–	–	6.110
TYC3178-28-1	R	6380	1.81	195	4.53	–	–	5.445
TYC8791-1056-1	R	6410	1.31	120	8.75	–	–	1.360
TYC3175-878-1	R	4820	12.8	270	9.54	–	–	3.995
TYC3175-325-1	R	5920	1.09	180	2.77	–	–	21.641
TYC3587-448-1	R	5730	0.95	180	2.26	–	–	7.999
TYC3175-519-1	P	5850	1.86	235	2.69	–	–	10.180
TYC4259-1185-1	P	5000	10.2	75	105.79	–	–	19.895
TYC2184-820-1	R	5600	1.01	200	1.84	–	–	16.530
TYC3592-4476-1	R	6090	1.27	200	2.75	–	–	9.059
HR 8019	R	8200	1.97	50	123.36	–	–	2.493
TYC3592-6130-1	R	8510	2.07	170	12.08	–	–	0.584
HD 200565	P	5900	1.12	30	101.05	–	–	9.449
TYC9101-1055-1	R	4550	0.64	250	0.50	–	–	7.241
TYC1112-317-1	P	5210	0.59	245	0.63	–	–	10.880
HD 201219	P	5760	0.89	300	0.76	50	27.50	2.952
TYC3957-1600-1	R	5780	2.30	205	4.26	–	–	34.068
TYC3953-1359-1	R	8960	2.13	150	17.70	–	–	0.592
TYC3961-501-1	R	3940	11.7	150	18.81	–	–	5.054
TYC1113-1057-1	P	5180	1.62	250	1.63	–	–	8.397
HD 202206	P	5850	0.98	210	1.78	50	31.44	2.252
TYC3181-116-1	R	4900	5.49	200	7.67	–	–	4.769
HD 202406	R	6680	5.87	230	11.53	–	–	42.727
TYC3597-664-1	R	4780	0.82	280	0.56	–	–	6.190
TYC3601-449-1	R	6550	1.63	170	5.65	–	–	4.668
TYC3601-1010-1	R	5940	1.15	205	2.25	–	–	14.026

Continued on Next Page...

Table A.1 – Continued

Name	Catalog	$T_{*,SED}$ (K)	$R_{*,SED}$ ($R_\odot$)	T_{dust} (K)	R_{disk} (au)	T_{dust2} (K)	R_{disk2} (au)	$\frac{L_{IR}}{L_{star}}$ ($\times 10^{-4}$)
TYC9461-74-1	R	9020	1.88	120	24.81	–	–	0.494
TYC4469-533-1	R	6170	4.31	160	14.93	30	424.70	238.816
HD 202917	P	5710	0.85	280	0.83	75	11.54	6.820
HD 202947	R	5140	1.60	320	0.96	–	–	2.737
TYC3194-690-1	R	6680	1.39	195	3.81	–	–	14.995
TYC2199-312-1	R	4740	11.8	280	7.88	–	–	5.361
TYC529-289-1	R	3750	0.46	200	0.38	–	–	9.998
TYC3598-1594-1	R	4350	0.82	400	0.23	–	–	12.598
HD 204041	R	7800	1.80	150	11.33	–	–	0.199
TYC3966-288-1	R	6110	1.38	190	3.32	–	–	3.733
TYC2708-2168-1	R	5620	1.85	220	2.81	–	–	8.638
TYC3190-1094-1	R	7220	3.63	200	11.03	–	–	0.734
HD 205674	P	6620	1.37	190	3.88	50	56.07	5.084
3 Peg	P	8970	1.82	140	17.43	–	–	0.211
TYC6948-271-1	R	5450	2.66	120	12.76	–	–	3.838
HD 205536	P	5560	0.87	75	11.19	–	–	3.089
TYC3603-226-1	R	5960	1.07	180	2.73	–	–	17.445
TYC5213-327-1	R	5660	0.76	220	1.18	–	–	3.397
TYC2725-107-1	R	6090	1.67	290	1.72	–	–	15.466
HD 206893	P	6490	1.31	50	51.37	–	–	2.906
TYC2726-266-1	R	5000	0.69	290	0.48	–	–	22.625
TYC6375-730-1	R	4210	19.8	120	56.87	–	–	2.680
TYC3972-2737-1	R	10010	2.74	180	19.77	45	316.28	62.795
HD 207575	R	6340	1.23	220	2.39	–	–	0.432
TYC5210-221-1	R	4220	0.58	400	0.15	–	–	12.865
TYC7994-894-1	R	6330	2.19	220	4.23	–	–	16.711
HD 207889	R	6480	1.31	140	6.58	–	–	0.248
HD 208038	R	5130	0.69	85	5.88	–	–	1.919
TYC3980-394-1	R	7110	2.40	170	9.79	–	–	1.714
TYC3977-1919-1	R	6280	1.52	170	4.85	–	–	4.167
TYC4275-1813-1	R	8020	7.25	100	108.54	–	–	1.833
TYC4463-1484-1	R	6120	0.96	155	3.48	–	–	6.455
TYC5224-99-1	R	4790	5.07	225	5.35	–	–	5.672
TYC6377-1108-1	R	5890	1.12	120	6.32	–	–	8.899
HD 210277	P	5580	1.06	20	192.21	–	–	0.043
TYC3977-493-1	R	7660	1.81	200	6.18	–	–	1.467
TYC3203-1131-1	R	4190	0.43	400	0.11	–	–	10.764
TYC4271-788-1	R	5600	2.72	320	1.94	–	–	4.906
TYC4267-186-1	R	4480	12.0	220	11.65	–	–	6.208
TYC3994-592-1	R	4720	4.78	300	2.76	–	–	5.402
TYC6384-1362-1	R	5870	1.60	270	1.77	–	–	5.943
HD 212265	R	6150	1.50	500	0.53	–	–	1.142
TYC3212-2836-1	R	5910	0.81	340	0.57	–	–	11.277
TYC4276-296-1	R	6460	1.91	200	4.65	–	–	2.554
TYC3208-881-1	R	4820	5.13	240	4.82	–	–	3.925
TYC3990-439-1	R	3110	0.20	400	0.03	–	–	43.757
TYC2738-2150-1	R	5870	2.13	240	2.97	–	–	5.980
TYC3995-102-1	R	5650	0.73	190	1.52	–	–	5.305
TYC9343-163-1	R	3340	0.28	300	0.08	–	–	16.003
39 Peg	P	6910	1.67	55	61.45	–	–	1.211
HD 213941	R	5680	0.93	300	0.78	–	–	4.700
TYC9337-518-1	R	6100	0.75	165	2.40	–	–	17.362
TYC6964-765-1	R	6440	1.43	190	3.84	–	–	7.500
TYC3226-1310-1	R	4380	3.05	550	0.45	–	–	18.210
HD 215152	R	5030	0.76	80	7.08	–	–	0.635
TYC1697-927-1	R	4600	7.76	250	6.12	–	–	6.160
TYC3222-1324-1	R	5730	0.90	320	0.68	–	–	5.195
TYC5812-1232-1	R	6450	1.66	175	5.26	–	–	5.100

Continued on Next Page...

Table A.1 – Continued

Name	Catalog	$T_{*,SED}$ (K)	$R_{*,SED}$ ($R_\odot$)	T_{dust} (K)	R_{disk} (au)	T_{dust2} (K)	R_{disk2} (au)	$\frac{L_{IR}}{L_{star}}$ ($\times 10^{-4}$)
TYC4273-189-1	R	5680	2.21	200	4.16	–	–	4.186
TYC4265-276-1	R	5510	2.27	250	2.57	–	–	6.144
TYC8830-410-1	P	4900	0.89	425	0.28	–	–	190.361
TYC4278-373-1	R	5690	1.53	210	2.63	–	–	22.513
TYC2758-1624-1	R	4570	3.86	500	0.75	–	–	17.606
TYC4278-339-1	R	5640	1.54	185	3.34	–	–	7.374
HR 8799	P	7180	1.47	220	3.65	45	87.25	3.339
TYC4291-1206-1	R	9000	3.07	140	29.55	–	–	0.358
HD 218860	R	5690	0.85	200	1.60	–	–	0.407
TYC4010-200-1	R	6560	1.52	130	9.02	–	–	2.558
TYC2244-1797-1	R	9110	1.86	140	18.38	–	–	0.469
HD 219498	R	5800	0.83	200	1.64	60	18.21	3.335
TYC4006-81-1	R	3780	9.81	140	16.64	–	–	3.513
TYC4283-1221-1	R	4580	12.4	235	10.96	–	–	5.809
TYC4011-164-1	R	4850	3.37	200	4.62	–	–	3.256
TYC4007-582-1	R	5600	1.91	205	3.33	–	–	10.998
TYC3230-381-1	R	9130	2.27	190	12.20	45	217.45	16.852
TYC2256-1759-1	R	4550	9.71	120	32.50	–	–	1.283
HD 221853	P	6650	1.40	85	20.03	–	–	9.280
TYC6987-349-1	R	6120	1.41	200	3.08	–	–	13.212
TYC4602-1115-1	R	7060	2.19	190	7.06	–	–	3.427
TYC6981-32-1	R	7260	5.40	350	5.41	–	–	1.615
TYC4487-569-1	R	6140	4.39	420	2.19	–	–	5.152
TYC1176-827-1	R	6520	2.38	300	2.62	–	–	3.270
TYC9477-353-1	R	6120	1.05	165	3.37	–	–	12.598
CD-30 19671	R	5230	8.89	500	2.26	–	–	3.940
TYC2254-26-1	R	5740	1.17	230	1.70	–	–	21.173
TYC2775-1057-1	R	8600	1.95	110	27.81	–	–	1.973
TYC4285-1240-1	R	7460	1.59	190	5.72	–	–	1.654
TYC2767-750-1	R	7550	1.71	220	4.71	–	–	2.847
TYC4009-2149-1	R	5070	1.97	215	2.56	–	–	10.905
TYC4479-3-1	R	5920	0.87	410	0.43	–	–	120.747
BD+28 4660	R	4150	0.59	80	3.73	–	–	1.952
TYC6408-96-1	R	6120	1.42	265	1.76	–	–	19.746
HD 224228	R	5040	0.68	120	2.80	–	–	1.967
TYC8021-480-1	R	6130	1.04	160	3.56	–	–	5.711
TYC4650-2790-1	R	8680	1.79	190	8.71	–	–	1.158
TYC5834-909-1	R	6520	1.26	200	3.13	–	–	8.262

Appendix B

Prime Catalog of Nearby IR Excess Stars

Table B.1: Prime IR Excess Stars from the Literature and Tycho-2 cross-correlation with AllWISE

Name	R.A. and Decl.	Spectral Type	$T_{*,SED}$ (K)	$R_{*,SED}$ ($R_\odot$)	T_{dust} (K)	R_{disk} (au)	T_{dust2} (K)	R_{disk2} (au)	$\frac{L_{IR}}{L_{star}}$ ($\times 10^{-4}$)	Dist. (pc)	Num Excess	λ_{start} (μm)	Has IRS?	Known Reference
HR 9102	00:04:20.33 -29:16:07.7	A0V	8820	2.580	200	11.60	70	95.53	1.370	124.840	2	22	N	Su et al. 2006
HD 105	00:05:52.64 -41:45:11.7	G0V	6070	1.010	390	0.50	50	34.66	4.530	39.380	3	22	Y	Zuckerman et al. 2004
HD 166	00:06:37.13 +29:01:15.4	K0V	5700	0.780	300	0.60	70	12.10	3.560	13.670	4	22	Y	Bryden et al. 2006
HD 203	00:06:50.17 -23:06:27.4	F3V	6710	1.480	160	6.00	–	–	1.690	39.380	3	22	Y	Rebull et al. 2008
HD 377[b]	00:08:25.80 +06:37:00.5	G2V	5910	1.030	200	2.10	60	23.44	5.310	39.070	3	22	Y	Moor et al. 2006
sig And	00:18:19.60 +36:47:06.4	A2V	8780	2.000	155	14.90	–	–	0.190	41.320	3	22	Y	Morales et al. 2009
HD 1466	00:18:26.27 -63:28:39.6	F8V	6140	1.060	140	4.70	–	–	1.680	41.540	2	22	Y	Smith et al. 2006
HD 1461	00:18:42.17 -08:03:12.4	G3V	5880	1.070	65	20.50	–	–	0.500	23.240	1	22	Y	Lawler et al. 2009
9 Cet	00:22:51.79 -12:12:33.9	G3V	5920	0.950	40	48.50	–	–	0.090	20.860	2	60	Y	Chen et al. 2014
kap Phe	00:26:12.32 -43:40:46.7	A5IV	8010	1.760	170	9.00	–	–	0.180	23.800	3	22	Y	Rieke et al. 2005
HD 2834	00:31:24.98 -48:48:12.6	A1V	8950	2.240	95	46.30	–	–	0.170	52.960	1	22	Y	Chen et al. 2014
HD 2772	00:31:46.36 +54:31:20.2	B8V	12230	3.500	400	7.60	35	995.02	2.290	115.740	4	11	N	Chen et al. 2005
bet03 Tuc	00:32:44.03 -63:01:53.8	A0V	9050	1.630	300	3.40	150	13.85	2.730	45.550	5	11	Y	Song et al. 2001
HD 3126	00:34:27.12 -06:30:14.9	F4V	6380	1.230	200	2.90	45	57.84	1.910	40.910	1	22	Y	Trilling et al. 2008
HD 3296	00:36:02.03 -05:34:15.6	:F5	6450	1.460	60	39.20	–	–	0.230	45.040	1	22	Y	Trilling et al. 2008
HD 3670	00:38:56.78 -52:32:03.6	F5V	6440	1.350	290	1.50	55	43.12	6.470	83.120[a]	1	22	Y	Moor et al. 2011
64 Psc	00:48:58.71 +16:56:26.3	F8V	6570	1.520	300	1.70	–	–	1.380	23.450	2	60	N	Koerner et al. 2010
HD 5133	00:53:01.13 -30:21:24.9	K2.5V	5170	0.660	30	45.70	–	–	0.110	14.170	3	60	N	Lawler et al. 2009
66 Psc	00:54:35.23 +19:11:18.0	A1Vn	9340	2.700	250	8.70	35	447.82	2.200	108.100	2	22	Y	Rhee et al. 2007
TYC2278-834-1	01:04:25.30 +31:18:27.7	:K0	5310	0.780	260	0.70	–	–	6.190	62.890[a]	2	11	N	–
V443 And	01:10:41.91 +42:55:54.5	G7V	5660	0.780	200	1.40	50	23.32	1.960	27.070	1	22	Y	Kim et al. 2005
HR 333	01:12:17.23 +79:40:26.3	A3V	8920	2.410	80	69.70	–	–	1.880	82.840	2	22	N	Jura et al. 2004
HD 7570	01:15:11.12 -45:31:54.0	F9VFe	6170	1.190	85	14.50	–	–	0.080	15.110	2	22	Y	Beichman et al. 2006
HD 7590	01:16:29.15 +42:56:21.5	G0-V	6090	0.900	200	1.90	40	48.87	3.130	23.190	1	22	Y	Plavchan et al. 2009
2MASS J01203226-1128035	01:20:32.35 -11:28:05.2	G9V	5500	0.750	300	0.50	–	–	1.960	34.390	1	22	Y	Carpenter et al. 2009
HD 8907	01:28:34.42 +42:16:02.8	:F7	6250	1.230	50	45.00	–	–	2.850	34.770	1	22	Y	Zuckerman et al. 2004
EO Psc	01:29:04.90 +21:43:23.4	K2.5V	4930	0.960	70	11.10	–	–	0.440	23.730	1	22	Y	Ballering et al. 2013
49 Cet	01:34:37.84 -15:40:34.9	A1V	8670	1.770	180	9.60	65	73.64	11.140	59.380	8	22	Y	Oudmaijer et al. 1992
EX Cet	01:37:35.58 -06:45:38.5	G5V	5440	0.750	200	1.30	60	14.53	1.950	23.950	2	22	Y	Plavchan et al. 2009
HD 10472	01:40:24.15 -60:59:56.7	F2IV/V	6610	1.340	200	3.40	60	37.93	5.470	67.240	2	22	Y	Zuckerman et al. 2004
HD 10647[b]	01:42:29.53 -53:44:27.9	F9V	6280	1.010	300	1.00	55	30.90	5.800	17.430	7	22	Y	Zuckerman et al. 2004
tau Cet	01:44:04.08 -15:56:14.9	G8.5V	5750	0.680	500	0.20	70	10.69	6.450	3.650[a]	2	60	N	Greaves et al. 2004
HD 10638	01:44:22.86 +32:30:56.5	:A6	7470	1.620	65	49.80	–	–	4.580	69.300	2	22	Y	Moor et al. 2006
HD 10939	01:46:06.40 -53:31:18.7	A1V	8960	2.300	200	10.70	55	142.07	1.460	62.030[a]	6	22	Y	Rhee et al. 2007
TYC8850-1468-1	01:54:07.70 -60:54:23.9	:K2	5040	0.730	185	1.20	–	–	15.280	92.950	2	11	N	–
BD+20 307	01:54:50.37 +21:18:22.2	:F9	6110	1.280	410	0.66	–	–	115.802	96.150	3	11	N	Song et al. 2005
DK Cet	01:57:49.05 -21:54:05.8	G4V	5800	0.910	350	0.50	35	58.59	3.130	40.890	3	22	Y	Hines et al. 2006
eps Tri	02:02:57.96 +33:17:02.7	A2V	8630	3.830	200	16.60	40	415.15	2.050	120.040	2	22	Y	Rhee et al. 2007
HD 13246	02:07:26.25 -59:40:46.2	F7V	6160	1.100	165	3.50	–	–	1.980	44.160	2	22	Y	Moor et al. 2009
HD 12467	02:09:25.21 +81:17:45.7	A1.5V	8140	1.920	200	7.40	50	118.81	1.660	70.570	1	22	Y	Rhee et al. 2007

Continued on Next Page...

Table B.1 – Continued

Name	R.A. and Decl.	Sp. Type	$T_{*,SED}$	$R_{*,SED}$	T_{dust}	R_{disk}	T_{dust2}	R_{disk2}	$\frac{L_{IR}}{L_{star}}$	Dist.	Num	λ_{start}	IRS?	Known?
TYC3698-2277-1	02:15:32.18 +59:14:24.4	:F0	6940	1.450	200	4.00	–	–	3.510	113.100[a]	2	11	N	–
gam Tri	02:17:18.92 +33:50:49.6	A1V	8970	2.050	85	53.20	–	–	0.970	34.430	8	22	N	Zuckerman et al. 2004
HD 14082B	02:17:24.79 +28:44:29.8	G2V	5910	0.670	220	1.10	55	18.18	5.740	27.330	4	22	N	Rebull et al. 2008
HD 15115[b]	02:26:16.33 +06:17:32.8	:F3	6660	1.300	320	1.30	60	37.52	6.210	45.220	4	22	Y	Zuckerman et al. 2004
AG Tri	02:27:29.32 +30:58:23.9	K7V	4330	0.820	205	0.80	55	11.82	16.550	39.950	4	22	N	Rebull et al. 2008
phi For	02:28:01.70 -33:48:39.7	A2.5V	8630	1.740	100	30.20	–	–	0.450	46.590	2	22	Y	Ballering et al. 2013
HD 15407	02:30:50.76 +55:32:53.3	F5V	6380	1.610	525	0.50	–	–	85.080	54.700	2	11	Y	Oudmaijer et al. 1992
HD 15745[b]	02:32:55.85 +37:20:00.6	:F2	6730	1.310	120	9.50	65	32.68	40.240	63.490	2	22	Y	Zuckerman et al. 2004
HD 16743	02:39:07.65 -52:56:04.7	F1III/IV	6850	1.600	200	4.30	50	70.18	7.170	58.850	3	22	Y	Moor et al. 2006
33 Ari	02:40:41.12 +27:03:39.1	A2/3V	8450	2.560	95	47.10	–	–	0.170	70.970	1	22	Y	Trilling et al. 2007
HR 826	02:46:45.15 -21:38:22.0	F3IV/V	6760	1.550	50	66.10	–	–	2.350	48.030	1	22	Y	Zuckerman et al. 2004
HD 17848	02:49:01.64 -62:48:23.2	A2V	8420	1.850	220	6.30	55	100.99	0.960	50.450	6	22	Y	Rhee et al. 2007
41 Ari	02:49:59.12 +27:15:36.9	B8V	11840	2.730	265	12.60	–	–	0.240	50.780	1	22	Y	Rieke et al. 2005
HR 857	02:52:32.39 -12:46:12.9	K1V	5510	0.700	350	0.40	45	24.57	4.600	10.350	4	11	N	Trilling et al. 2008
HD 19257	03:06:51.94 +30:31:36.8	:A8	7110	1.760	235	3.70	–	–	9.590	79.170	2	11	N	–
IS Eri	03:09:42.35 -09:34:47.6	G0V	5590	0.750	180	1.70	–	–	1.130	37.410	1	22	Y	Meyer et al. 2008
94 Cet	03:12:46.58 -01:11:46.4	F8.5V	6140	1.720	40	94.60	–	–	0.040	22.570	3	60	N	Trilling et al. 2008
zet Eri	03:15:50.04 -08:49:10.1	A9V	7490	1.900	70	50.70	–	–	0.410	33.640	3	22	Y	Rhee et al. 2007
zet02 Ret	03:18:12.82 -62:30:22.9	G0V	6100	0.860	220	1.50	50	30.00	0.560	12.030	2	22	Y	Laureijs et al. 2002
TYC3706-340-1	03:18:49.94 +55:20:15.0	:G6	5590	0.850	185	1.80	–	–	7.870	97.400[a]	2	11	N	–
HD 278507	03:19:42.87 +36:41:01.2	:G6	5570	0.850	195	1.60	–	–	10.140	96.760[a]	2	11	N	–
BD+47 837	03:29:26.24 +48:12:11.6	F9V	5920	0.970	220	1.60	–	–	1.760	109.640[a]	1	22	Y	Chen et al. 2014
HD 21997	03:31:53.69 -25:36:51.1	A3IV/V	8220	1.640	65	61.20	–	–	5.410	71.940	9	22	N	Zuckerman et al. 2004
eps Eri	03:32:55.84 -09:27:29.7	K2V	5440	0.620	300	0.40	60	12.03	7.120	3.210	3	22	N	Greaves et al. 2005
HD 22179	03:35:29.94 +31:13:36.9	G5IV	5920	1.010	70	16.80	–	–	2.880	68.000[a]	2	22	Y	Hillenbrand et al. 2008
10 Tau	03:36:52.38 +00:24:05.9	F9IV-V	6150	1.560	105	12.30	–	–	0.150	13.960	2	60	Y	Decin et al. 2000
TYC2359-1127-1	03:40:25.96 +33:42:28.1	:K6	4350	0.620	75	4.80	60	22.89	46.630	16.940[a]	2	22	N	–
HD 23281	03:43:33.83 -10:29:08.3	A5III-IV	7660	1.590	160	8.40	–	–	0.540	42.420	4	22	N	Gaspar et al. 2013
TYC1799-73-1	03:43:43.26 +24:22:28.0	A7V	7250	1.480	205	4.30	–	–	5.180	119.090[a]	2	11	N	–
HD 23356	03:43:55.58 -19:06:37.3	K2V	5210	0.700	45	22.00	–	–	0.080	13.940	3	60	N	Lawler et al. 2009
HD 23484	03:44:09.36 -38:16:51.4	K2V	5400	0.760	60	14.40	–	–	1.030	16.020	5	60	Y	Koerner et al. 2010
TYC1803-808-1	03:44:56.41 +24:25:56.8	:G2	5910	0.750	420	0.30	100	6.10	6.330	100.000[a]	2	11	Y	Chen et al. 2014
HD 23361	03:45:26.12 +24:02:06.5	A3V	7480	1.500	230	3.70	100	19.59	21.530	117.760[a]	2	11	Y	Gorlova et al. 2006
HD 23267	03:45:31.08 +42:00:24.6	:A0	9490	2.080	140	22.20	–	–	0.940	140.840	1	22	Y	Rieke et al. 2005
HD 23430	03:45:59.15 +25:23:54.4	:A5	7680	1.530	220	4.30	105	19.12	4.330	125.000	2	11	Y	Gorlova et al. 2006
HD 282954	03:46:38.79 +24:57:34.2	G0V	5920	0.420	100	3.40	–	–	2.190	54.090[a]	1	22	Y	Chen et al. 2014
V1210 Tau	03:47:04.23 +23:59:42.3	F0V	7150	1.210	300	1.60	85	20.00	1.190	100.000[a]	1	22	Y	Gorlova et al. 2006
HD 23632	03:47:20.98 +23:48:11.6	A1V	8800	1.730	120	21.70	65	74.16	0.900	112.360	1	22	Y	Gorlova et al. 2006
V1229 Tau	03:47:29.47 +24:17:17.5	A0V	8510	1.890	80	49.80	–	–	0.190	106.150	1	22	Y	Rieke et al. 2005
HD 24636	03:48:11.63 -74:41:38.5	F3IV/V	6630	1.340	120	9.50	–	–	1.360	54.050	2	22	Y	Zuckerman et al. 2011
HD 23863	03:49:12.20 +23:53:12.0	A7V	7610	1.200	170	5.60	–	–	0.310	100.000[a]	1	22	Y	Gorlova et al. 2006
HD 24141	03:53:43.42 +57:58:29.6	:A4	7830	1.650	150	10.50	–	–	0.340	50.500	1	22	Y	Morales et al. 2009

Continued on Next Page...

Table B.1 – Continued

Name	R.A. and Decl.	Sp. Type	$T_{*,SED}$	$R_{*,SED}$	T_{dust}	R_{disk}	T_{dust2}	R_{disk2}	$\frac{L_{IR}}{L_{star}}$	Dist.	Num	λ_{start}	IRS?	Known?
HD 24966	03:56:29.40 -38:57:43.7	A0V	9140	1.620	170	10.90	80	49.44	6.070	105.810	3	11	Y	Moor et al. 2006
HD 24817	03:57:01.74 +06:02:23.2	A0V	8690	1.690	250	4.70	–	–	0.480	70.220	1	22	Y	Morales et al. 2009
HD 25457	04:02:36.87 -00:16:10.8	F6V	6430	1.120	180	3.30	60	30.16	2.320	18.830	2	22	Y	Moor et al. 2006
HR 1254	04:03:56.60 +08:11:50.1	F2V	6780	1.790	200	4.80	50	76.98	0.890	34.850	1	22	Y	Rhee et al. 2007
V1299 Tau	04:05:40.58 +22:48:12.0	G3V	5890	0.960	250	1.20	–	–	1.430	79.460[a]	1	22	Y	Chen et al. 2014
50 Per	04:08:36.77 +38:02:21.0	F7V	6360	1.200	270	1.50	40	70.69	1.150	20.990	2	22	Y	Beichman et al. 2006
HD 281683	04:12:12.16 +30:25:00.2	:G5	5670	0.880	220	1.30	–	–	4.520	63.500[a]	2	11	N	–
gam Dor	04:16:01.72 -51:29:09.8	F1V	7000	1.700	65	46.00	–	–	0.220	20.460	5	22	Y	Mannings et al. 1998
HD 27045	04:17:15.66 +20:34:42.9	:A4	7770	1.420	110	16.50	–	–	0.180	28.940	1	22	Y	Su et al. 2006
HD 27026	04:18:08.14 +42:08:27.7	B9V	10570	2.210	65	136.30	–	–	3.510	121.350	2	22	N	–
chi Tau	04:22:35.53 +25:38:03.3	B9V	6130	1.610	200	3.50	35	114.99	4.290	89.280	1	22	Y	Chen et al. 2014
b Tau	04:28:50.26 +13:02:51.0	F0V	7810	2.290	200	8.10	70	66.38	0.950	48.850	2	22	Y	Rieke et al. 2005
HD 28447	04:30:20.06 +28:07:54.8	:G4	5740	1.830	300	1.50	30	156.00	15.570	38.560	1	22	Y	Chen et al. 2014
HD 283759	04:36:49.13 +24:12:58.8	:G7	5560	0.840	70	12.40	–	–	99.360	150.000[a]	3	22	N	–
51 Eri	04:37:36.13 -02:28:24.7	F0IV	7400	1.400	300	1.90	45	88.35	0.650	29.420	2	60	N	Riviere-Marichalar et al. 2014
CPD-35 525	04:41:15.76 -35:13:58.1	:G7	5550	0.830	250	0.90	–	–	7.450	80.460[a]	2	11	N	–
HD 30051	04:43:17.24 -23:37:42.0	F2/3IV/V	6500	1.680	55	54.70	–	–	0.320	63.570	2	60	N	Zuckerman et al. 2011
EX Eri	04:46:25.74 -28:05:14.5	A3V	7760	1.570	200	5.50	65	52.36	0.890	56.170	2	22	Y	Rieke et al. 2005
HD 30447[b]	04:46:49.55 -26:18:08.8	F3V	6670	1.410	300	1.60	70	29.86	11.130	80.250	2	22	Y	Moor et al. 2006
58 Eri	04:47:36.40 -16:56:02.0	G1.5V	5920	0.910	90	9.20	–	–	0.510	13.270	2	22	Y	Trilling et al. 2008
HD 32195	04:48:05.37 -80:46:44.8	F7V	6180	1.120	300	1.10	65	23.56	2.160	61.010	2	22	Y	Zuckerman et al. 2011
TYC88-1288-1	04:50:13.22 +03:41:00.3	:A6	7470	1.500	170	6.70	30	216.95	21.120	93.150[a]	3	22	N	–
HD 31392	04:54:04.21 -35:24:16.2	G9V	5560	0.770	300	0.60	40	34.96	4.110	25.160	1	22	Y	Hillenbrand et al. 2008
HD 31295	04:54:53.77 +10:09:01.6	A3V	8630	1.660	200	7.20	60	80.08	1.390	35.660	2	22	Y	Jura et al. 2004
HD 32297[b]	05:02:27.44 +07:27:39.4	A0V	7610	1.330	130	10.60	70	36.80	98.710	112.360	5	11	Y	Moor et al. 2006
TYC4079-687-1	05:02:44.34 +60:43:01.5	:K4	4910	0.700	260	0.50	–	–	7.190	53.930[a]	2	11	N	–
iot Tau	05:03:05.75 +21:35:23.8	A7V	7960	2.890	160	16.60	–	–	0.300	52.960	1	22	Y	Chen et al. 2014
TYC5323-272-1	05:04:51.51 -08:17:42.4	:F7	6300	1.180	220	2.20	50	43.62	53.830	86.470[a]	2	22	N	–
zet Dor	05:05:30.63 -57:28:20.4	F9V	6170	1.050	130	5.50	–	–	0.150	11.640	2	22	Y	Bryden et al. 2006
HD 33081	05:07:08.67 -17:18:01.2	F7V	6330	1.460	250	2.10	45	67.29	0.920	50.600	1	22	Y	Moor et al. 2011
l Tau	05:07:48.36 +20:25:05.7	A5IV	8370	2.120	140	17.70	–	–	0.300	58.100	1	22	Y	Morales et al. 2009
HD 33636	05:11:46.54 +04:24:10.9	G0V	5940	0.950	250	1.20	55	25.94	0.970	28.360	1	22	Y	Beichman et al. 2005
HD 34324	05:15:43.89 -22:53:39.6	A3V	8040	1.480	190	6.10	55	73.85	3.330	74.570	2	22	Y	Rhee et al. 2007
AS Col	05:20:38.08 -39:45:17.6	F6V	6250	1.220	110	9.20	–	–	0.650	48.300	2	22	Y	Zuckerman et al. 2011
16 Cam	05:23:27.87 +57:32:39.2	A0Vne	9460	3.160	500	2.60	50	263.14	2.550	103.090	3	11	Y	Rhee et al. 2007
TYC9162-586-1	05:23:43.35 -68:10:16.5	:K4	4850	0.690	230	0.70	–	–	7.770	76.880[a]	2	11	N	–
HD 35841[b]	05:26:36.60 -22:29:23.8	F3V	6470	1.220	70	24.30	–	–	17.070	104.000[a]	2	22	Y	Moor et al. 2006
AF Lep	05:27:04.77 -11:54:03.8	F8V	6130	1.180	300	1.10	75	18.45	1.500	27.040	3	22	Y	Zuckerman et al. 2004
HD 290609	05:33:05.58 -01:43:15.5	:A0	9550	0.160	400	0.20	115	2.72	7.740	23.850	2	11	Y	Hernandez et al. 2006
HD 36968	05:33:24.06 -39:27:04.4	F2V	6880	1.440	200	3.90	55	52.63	17.770	145.920[a]	2	22	Y	Moor et al. 2011
TYC1852-1694-1	05:33:30.76 +24:37:43.2	:A1	8730	1.810	220	6.60	120	22.35	89.010	113.890	3	11	N	–
HR 1915	05:36:10.31 -28:42:28.8	A2III-IV	7980	1.350	200	5.00	–	–	1.200	52.790	1	22	Y	Zuckerman et al. 2011

Continued on Next Page...

Table B.1 – Continued

Name	R.A. and Decl.	Sp. Type	$T_{*,SED}$	$R_{*,SED}$	T_{dust}	R_{disk}	T_{dust2}	R_{disk2}	$\frac{L_{IR}}{L_{star}}$	Dist.	Num	λ_{start}	IRS?	Known?
HD 37306	05:37:08.77 -11:46:31.8	A1V	8750	1.480	400	1.60	100	26.53	1.850	62.890	2	22	Y	Ballering et al. 2013
HD 37484	05:37:39.65 -28:37:34.7	F4V	6610	1.340	190	3.70	75	24.33	6.080	56.780	2	22	Y	Rhee et al. 2007
HD 37564	05:39:15.06 -02:31:37.6	A8V	7300	1.480	600	0.50	130	10.93	19.350	133.350[a]	2	11	Y	Hernandez et al. 2007
HD 38207	05:43:20.97 -20:11:21.5	F2V	6760	1.350	200	3.60	55	47.72	14.780	103.000[a]	2	22	Y	Moor et al. 2006
HR 1975	05:43:21.69 -18:33:27.0	A0V	9800	1.820	230	7.60	70	83.07	2.940	75.070	3	11	Y	Mannings et al. 1998
HD 38529	05:46:34.88 +01:10:04.0	G4V	5670	2.410	300	2.00	60	50.22	2.020	39.270	1	22	Y	Moro-Martin et al. 2007a
zet Lep	05:46:57.33 -14:49:18.5	A2IV-V	8400	1.750	215	6.20	–	–	1.290	21.600	5	11	Y	Rieke et al. 2005
bet Pic[b]	05:47:17.11 -51:03:58.4	A6V	8070	1.460	210	5.00	95	24.63	45.230	19.440	9	11	N	Aumann et al. 1984
HD 38858	05:48:35.01 -04:05:43.0	G2V	6100	0.770	65	15.00	–	–	0.910	15.170	2	22	Y	Beichman et al. 2006
HD 40307	05:54:04.19 -60:01:24.9	K2.5V	5100	0.630	85	5.30	–	–	0.210	12.990	3	60	N	Bryden et al. 2009
HD 39415	05:54:41.53 +44:30:07.4	F5V	6170	1.080	240	1.60	–	–	57.540	66.200[a]	2	11	N	Oudmaijer et al. 1992
eta Lep	05:56:24.29 -14:10:03.7	F2V	6950	1.610	125	11.60	–	–	0.090	14.870	3	22	Y	Beichman et al. 2006
HD 40540	05:57:52.61 -34:28:34.1	A8IV	7240	1.380	80	26.30	–	–	6.470	80.970	2	22	Y	Rhee et al. 2007
HD 40979	06:04:30.05 +44:15:36.0	:F9	6160	1.160	80	16.10	–	–	0.140	33.110	1	22	Y	Trilling et al. 2008
HD 43162	06:13:45.27 -23:51:42.1	G6.5V	5840	0.810	240	1.10	–	–	0.800	16.720	2	60	N	Kospal et al. 2009
HD 43319	06:15:29.67 -04:54:52.9	A3V	8590	1.660	200	7.10	–	–	0.170	65.060	1	22	Y	Chen et al. 2014
V1358 Ori	06:19:08.06 -03:26:20.8	F9V	6110	1.030	140	4.50	–	–	0.600	49.230	1	22	Y	Carpenter et al. 2009
AB Pic	06:19:12.94 -58:03:15.0	K1Ve	5330	0.840	30	62.00	–	–	0.360	46.060	2	60	N	Zuckerman et al. 2011
HD 45184	06:24:43.79 -28:46:49.6	G1.5V	5920	1.010	280	1.00	60	22.89	1.980	21.880	1	22	Y	Lawler et al. 2009
HD 46190	06:27:48.64 -62:08:59.2	A0V	8400	1.670	120	19.10	–	–	0.160	83.890	1	22	Y	Rieke et al. 2005
HD 53842	06:46:13.60 -83:59:28.7	F5V	6400	1.300	170	4.30	–	–	1.070	56.020	2	22	Y	Moor et al. 2006
56 Aur	06:46:44.36 +43:34:40.6	F9V	6230	1.130	80	15.90	–	–	1.070	16.710	5	60	N	Chen et al. 2006
HR 2562	06:50:01.04 -60:14:55.8	F5V	6480	1.400	50	55.00	–	–	1.100	33.620	5	22	Y	Moor et al. 2006
HD 50554	06:54:42.81 +24:14:43.0	F8V	6110	1.020	60	24.80	–	–	0.480	29.910	1	22	Y	Beichman et al. 2005
pi. CMa	06:55:37.55 -20:08:07.6	F1.5V	6950	2.020	50	91.00	–	–	0.030	29.580	1	60	Y	Trilling et al. 2007
HD 53143[b]	06:59:59.41 -61:20:07.5	G9V	5620	0.840	250	0.90	60	17.25	3.400	18.320	2	22	N	Mannings et al. 1998
HD 52265	07:00:17.95 -05:22:00.7	G0V	6150	1.260	55	36.70	–	–	0.220	28.960	1	22	Y	Beichman et al. 2005
HD 54341	07:06:20.94 -43:36:38.5	A0V	9090	1.880	70	74.00	–	–	2.450	102.350	2	22	Y	Moor et al. 2006
HD 57703	07:23:04.58 +18:16:23.8	:F5	6480	1.280	55	41.40	–	–	0.400	41.370	1	22	Y	Trilling et al. 2008
bet CMi	07:27:09.00 +08:17:21.4	B8Ve	10810	4.060	260	16.30	–	–	1.569	49.570	3	11	N	–
HD 59967	07:30:42.44 -37:20:21.2	G3V	5900	0.890	400	0.40	80	11.31	2.440	21.810	1	22	Y	Plavchan et al. 2009
HD 61005[b]	07:35:47.42 -32:12:13.3	G8V	5700	0.780	500	0.20	60	16.44	33.640	35.340	3	11	Y	Rhee et al. 2007
TYC9385-93-1	07:56:34.41 -78:34:00.1	:K1	5170	0.760	255	0.70	–	–	6.440	88.350[a]	2	11	N	–
HD 69830	08:18:23.95 -12:37:55.8	G8V	5750	0.790	300	0.60	–	–	3.890	12.600[a]	2	11	N	Mannings et al. 1998
HD 70298	08:21:16.10 +01:03:48.1	:F4	6500	1.740	35	139.80	–	–	6.480	67.470	1	22	Y	Rhee et al. 2007
HD 71043	08:22:55.15 -52:07:25.2	A0V	9130	1.700	200	8.20	50	132.54	1.080	70.020	2	22	Y	Su et al. 2006
HD 70313	08:23:48.47 +53:13:10.0	A3V	8240	1.700	120	18.70	50	108.00	1.380	50.420	4	22	Y	Rhee et al. 2007
30 Mon	08:25:39.59 -03:54:23.2	A0V	10360	1.970	350	4.00	100	49.23	1.140	37.500	5	11	Y	Rieke et al. 2005
HD 71722	08:26:25.18 -52:48:27.0	A0V	8630	1.720	160	11.60	70	60.91	1.760	69.440	4	22	Y	Morales et al. 2009
HD 72687	08:33:15.35 -29:57:23.6	G5V	5890	0.890	220	1.50	–	–	1.220	45.060	1	22	Y	Meyer et al. 2008
HR 3383	08:34:01.61 -02:09:05.3	A1V	9290	2.270	40	284.90	–	–	1.020	90.330	1	22	Y	Rhee et al. 2007
HD 73526	08:37:16.42 -41:19:07.1	G6V	5760	1.490	85	16.00	–	–	4.800	100.700	2	22	N	Bryden et al. 2009

Continued on Next Page...

Table B.1 – Continued

Name	R.A. and Decl.	Sp. Type	$T_{*,SED}$	$R_{*,SED}$	T_{dust}	R_{disk}	T_{dust2}	R_{disk2}	$\frac{L_{IR}}{L_{star}}$	Dist.	Num	λ_{start}	IRS?	Known?
V401 Hya	08:37:50.08 -06:48:24.2	G5V	5900	0.950	150	3.40	40	48.56	1.930	23.970	1	22	Y	Plavchan et al. 2009
pi.01 UMa	08:39:11.69 +65:01:16.0	G1.5V	6080	0.880	400	0.40	70	15.45	2.030	14.350	2	22	N	Bryden et al. 2006
eta Cha	08:41:19.43 -78:57:47.8	B8V	11850	2.170	350	5.70	–	–	1.470	94.960	3	11	Y	Rieke et al. 2005
EK Cha	08:42:26.98 -78:57:47.6	:M0	2390	1.240	140	0.80	–	–	876.100	97.000[a]	2	11	N	Lyo et al. 2003
50 Cnc	08:46:55.98 +12:06:35.3	A1V	8160	1.570	210	5.50	–	–	1.100	53.960	1	22	Y	Morales et al. 2009
HD 75616	08:53:06.05 +52:23:25.2	:F8	6230	1.120	50	40.50	–	–	0.480	35.420	1	22	Y	Trilling et al. 2008
HD 76151	08:54:17.64 -05:26:03.8	G3V	5870	0.980	120	5.50	–	–	0.250	17.380	2	60	Y	Beichman et al. 2006
HD 76748	08:54:51.20 -63:42:06.9	K0V	5320	0.710	190	1.20	–	–	1.250	47.030	1	22	Y	Chen et al. 2014
HR 3570	08:55:11.82 -54:57:57.9	F6V	6540	1.190	150	5.20	–	–	0.440	24.150	2	22	Y	Lawler et al. 2009
TYC8160-1896-1	08:56:10.74 -49:29:26.4	:G2	5910	0.950	210	1.70	–	–	7.240	123.040[a]	2	11	N	–
omi02 Cnc	08:57:35.24 +15:34:52.8	F0IV	7610	1.690	120	15.80	40	142.42	3.720	46.120	2	22	Y	Zuckerman et al. 2004
HR 3638	09:09:04.18 -18:19:42.6	A0/A1V	9020	2.240	120	29.50	35	347.29	3.300	83.680	3	22	Y	Zuckerman et al. 2004
HR 3651	09:12:12.84 +03:52:01.0	A0V	9270	2.130	190	11.80	70	86.93	1.170	99.300	2	22	Y	Rieke et al. 2005
HR 3721	09:17:27.45 -74:44:04.0	A0V	9440	1.940	165	14.80	–	–	2.730	81.960	3	11	Y	Rieke et al. 2005
HD 82443	09:32:43.65 +26:59:16.1	G9V	5570	0.720	350	0.40	45	25.74	3.880	17.790	1	22	Y	Smith et al. 2006
HD 82943	09:34:50.82 -12:07:49.6	F9V	6120	1.110	50	38.60	–	–	1.700	27.470	1	22	Y	Beichman et al. 2005
HD 84075	09:36:17.58 -78:20:41.0	G2V	6120	1.050	300	1.00	55	30.46	4.060	67.980	2	22	Y	Zuckerman et al. 2011
HD 84870	09:49:02.82 +34:05:06.9	:A6	7500	1.640	170	7.40	45	106.55	7.640	88.020	2	22	Y	Moor et al. 2006
HD 85301	09:52:16.55 +49:11:26.1	:G5	5660	0.890	220	1.30	70	13.67	3.160	32.790	2	22	Y	Meyer et al. 2008
HD 85672	09:53:59.12 +27:41:43.6	:A4	7850	1.530	80	34.40	–	–	6.400	107.060	2	22	N	Moor et al. 2006
HR 3927	09:54:51.19 -50:14:38.2	A0V	9380	2.380	170	16.80	60	135.39	4.950	92.850	2	22	N	Jura et al. 2004
TYC8946-1580-1	09:58:57.86 -62:18:59.9	A3V	7220	1.480	350	1.40	65	42.51	29.430	86.600[a]	3	11	N	–
21 LMi	10:07:25.80 +35:14:41.0	A7V	7810	1.700	300	2.60	–	–	0.700	28.240	4	22	Y	Lawler et al. 2009
HD 88215	10:10:05.82 -12:48:58.4	F3V	6860	1.490	220	3.30	–	–	0.320	27.730	1	22	Y	Trilling et al. 2007
LW Vel	10:13:22.84 -51:13:58.6	A7V	7400	2.390	150	13.50	–	–	0.360	51.890	1	22	Y	Chen et al. 2014
TYC6623-942-1	10:24:55.66 -25:38:46.9	:G2	5830	0.940	240	1.20	–	–	5.110	104.080[a]	2	11	N	–
HD 90874	10:27:25.28 -65:42:16.7	A2V	8460	1.770	350	2.40	90	36.43	0.830	68.440	1	22	Y	Ballering et al. 2013
HR 4084	10:31:04.62 +82:33:31.5	F4V	6640	1.270	30	144.70	–	–	0.090	21.500	3	60	N	Beichman et al. 2006
HR 4132	10:33:13.89 +40:25:32.0	A7IV	7490	2.040	35	218.10	–	–	1.280	34.620	2	60	Y	Rhee et al. 2007
HD 92536	10:39:22.82 -64:06:42.3	B8V	10710	2.480	250	10.60	–	–	0.800	146.190	2	11	Y	Rieke et al. 2005
TWA 7A	10:42:30.00 -33:40:16.3	M2Ve	3420	1.610	220	0.90	65	10.37	24.740	53.000[a]	4	22	N	–
V419 Hya[b]	10:43:28.10 -29:03:52.1	K1V	5210	0.740	200	1.10	45	23.10	6.600	21.390	3	22	Y	Zuckerman et al. 2004
HD 93738	10:47:53.51 -64:15:46.1	B9.5V	8980	2.810	200	13.20	–	–	0.200	145.340	1	22	Y	Rieke et al. 2005
TYC8203-154-1	10:56:29.46 -48:19:55.2	F0V	7110	1.430	135	9.20	–	–	10.620	96.990	2	11	N	–
TYC8962-532-1	10:56:42.15 -62:17:40.8	:K7	4250	0.590	260	0.30	–	–	12.460	46.010[a]	2	11	N	–
TYC9410-532-1	11:01:25.83 -76:45:07.1	A9V	6120	1.050	170	3.10	–	–	10.610	117.800[a]	2	11	N	–
bet UMa	11:01:50.59 +56:22:57.1	A1IV	8770	3.210	120	39.80	–	–	0.120	24.440	6	22	Y	Rieke et al. 2005
HD 95698	11:02:24.51 -26:49:54.8	F1V	6990	1.920	200	5.40	50	87.42	1.360	56.080	1	22	Y	Trilling et al. 2007
tet Leo	11:14:14.40 +15:25:46.4	A2IV	8940	4.190	160	30.40	–	–	0.090	50.600	1	22	Y	Wyatt et al. 2007
HD 308379	11:17:30.42 -64:02:34.4	:G0	5920	0.970	185	2.30	–	–	7.610	85.630[a]	2	11	N	–
HD 98363	11:17:58.09 -64:02:33.3	A2V	7890	1.540	350	1.80	130	13.26	20.160	123.600	3	11	Y	Patten et al. 1991
HR 4388	11:21:49.21 +57:04:29.7	A7V	7850	1.980	220	5.80	75	50.53	1.210	80.840	2	22	Y	Morales et al. 2009

Continued on Next Page...

Table B.1 – Continued

Name	R.A. and Decl.	Sp. Type	$T_{*,SED}$	$R_{*,SED}$	T_{dust}	R_{disk}	T_{dust2}	R_{disk2}	$\frac{L_{IR}}{L_{star}}$	Dist.	Num	λ_{start}	IRS?	Known?
HD 98800	11:22:05.22 -24:46:39.4	K5V(e)	4200	1.930	210	1.70	115	6.00	1537.100	44.900	5	11	N	Walker and Wolstencroft 1988
TWA 30A	11:32:18.24 -30:19:52.1	M5V	2980	0.820	240	0.30	–	–	214.970	53.000[a]	5	–	N	Schneider et al. 2012
HD 101088	11:37:14.56 -69:40:27.2	F5IV	6170	3.460	200	7.68	40	192.01	1.536	93.800	1	22	Y	Bitner et al. 2010
HD 102458	11:47:24.55 -49:53:03.0	G4V	5900	1.280	200	2.50	45	51.35	3.540	91.650	1	22	Y	Ballering et al. 2013
bet Leo	11:49:03.58 +14:34:19.4	A3V	8200	1.770	125	17.80	–	–	0.270	10.990	4	22	Y	Laureijs et al. 2002
HD 102902	11:50:42.01 -33:08:28.4	G4IV-V	5580	2.850	400	1.20	30	229.98	15.420	82.440	1	22	Y	Chen et al. 2014
HD 103234	11:53:07.95 -56:43:38.3	F2IV/V	6640	1.460	200	3.70	–	–	1.500	98.130	1	22	Y	Chen et al. 2005
HD 103266	11:53:26.81 -35:03:59.9	A1V	8550	1.740	190	8.20	–	–	0.380	74.120	1	22	Y	Ballering et al. 2013
TYC8981-4034-1	11:56:06.95 -64:19:45.5	:K5	4560	0.640	230	0.50	–	–	35.810	49.680[a]	2	11	N	–
HD 103703	11:56:26.51 -58:49:16.8	F3V	6510	1.390	240	2.30	–	–	4.650	98.910	2	11	Y	Chen et al. 2005
HD 104231	12:00:09.36 -57:07:02.2	F5V	6470	1.530	260	2.20	–	–	3.330	110.490	2	11	Y	Chen et al. 2005
HR 4597	12:02:37.61 -69:11:32.3	B9V	10940	2.130	230	11.20	105	53.86	2.100	105.700	3	11	Y	Chen et al. 2012
HD 104860	12:04:33.63 +66:20:12.3	:F9	6100	0.970	300	0.90	45	41.71	6.280	45.470	5	22	Y	Carpenter et al. 2009
eta Cru	12:06:52.96 -64:36:49.5	F2V	6800	1.850	55	65.90	–	–	0.420	19.750	1	22	Y	Beichman et al. 2006
EF Cha	12:07:05.39 -78:44:28.3	A9III/IV	7050	1.990	295	2.60	–	–	12.689	102.980	3	11	N	–
TYC8241-2652-1	12:09:02.22 -51:20:41.0	:K4	4770	0.740	200	0.90	–	–	10.890	81.810[a]	2	11	N	Melis et al. 2012
HD 105613	12:09:38.74 -58:20:58.8	A3V	7940	1.600	200	5.90	–	–	1.080	104.160	2	11	Y	Chen et al. 2012
3 Crv	12:11:03.84 -23:36:08.7	A1V	8720	1.870	150	14.70	–	–	0.370	58.820	2	22	Y	Ballering et al. 2013
HD 105857	12:11:05.82 -56:24:04.9	A2V	8180	1.690	190	7.30	–	–	1.840	112.990	2	11	Y	Chen et al. 2012
HD 105912	12:11:21.73 -03:46:44.7	F5V	6540	1.380	110	11.40	–	–	0.900	49.670	2	22	Y	Trilling et al. 2008
HD 106036	12:12:10.21 -63:27:14.9	A2V	8420	1.680	200	6.90	–	–	4.110	100.700	2	11	Y	Chen et al. 2012
CD-54 4621	12:12:35.72 -55:20:27.4	K0Ve	5010	1.390	170	2.80	–	–	4.240	125.000[a]	1	22	Y	Chen et al. 2011
HD 106252	12:13:29.53 +10:02:27.0	:G0	6070	1.020	120	6.10	–	–	0.370	37.700	1	22	Y	Moro-Martin et al. 2007
HD 106389	12:14:28.61 -47:36:46.2	F6IV	6140	1.290	280	1.40	–	–	3.910	136.980	2	22	Y	Chen et al. 2011
HR 4669	12:17:06.25 -65:41:34.6	A0V	9010	2.210	200	10.40	–	–	4.440	95.960	2	11	Y	Fujiwara et al. 2009
HD 106906[b]	12:17:53.14 -55:58:31.9	F5V	6450	1.790	120	12.00	55	57.55	35.740	92.080	3	22	Y	Chen et al. 2005
HD 107146	12:19:06.38 +16:32:52.0	G2V	5910	0.940	200	1.90	50	30.71	11.400	27.450	5	22	Y	Hillenbrand et al. 2008
HR 4692	12:20:28.15 -65:50:33.7	B9V	9880	1.830	240	7.20	115	31.43	2.710	93.890	3	11	Y	Chen et al. 2012
HD 107649	12:22:24.82 -51:01:34.5	F5V	6450	1.160	190	3.10	–	–	1.910	93.720	2	11	Y	Chen et al. 2011
CD-52 5008	12:22:33.20 -53:33:49.0	G2IV	5880	1.490	145	5.70	–	–	2.190	124.000[a]	1	22	Y	Hillenbrand et al. 2008
HD 107947	12:24:51.82 -72:36:14.1	A0V	9320	1.560	350	2.50	130	18.68	2.510	91.070	3	11	Y	Chen et al. 2012
16 Com	12:26:59.31 +26:49:32.3	A4V	8280	3.710	180	18.20	–	–	0.230	85.170	2	22	N	Su et al. 2006
HD 108874	12:30:26.98 +22:52:46.4	G9V	5710	1.050	300	0.80	50	32.10	2.700	62.610	1	22	Y	Bryden et al. 2009
HD 108857	12:30:46.22 -58:11:16.9	F7V	6110	1.550	225	2.60	100	5.34	11.610	96.990	2	11	Y	Chen et al. 2011
eta Crv	12:32:04.23 -16:11:45.6	F2V	6720	1.640	180	5.30	40	108.05	1.680	18.280	6	22	N	Mannings et al. 1998
HR 4796A[b]	12:36:00.97 -39:52:10.9	A0V	9000	1.910	140	18.30	90	44.49	84.640	72.780	7	11	Y	Jura et al. 1991
f Vir	12:36:47.35 -05:49:54.8	A3V	8660	1.830	160	12.50	–	–	0.420	69.010	1	22	Y	Ballering et al. 2013
HD 109832	12:38:42.78 -68:45:49.1	A9V	6830	1.680	170	6.30	80	28.61	9.530	111.850	3	11	Y	Chen et al. 2012
HD 110058[b]	12:39:46.17 -49:11:55.6	A0V	7940	1.260	575	0.50	100	18.61	41.810	107.410	3	11	N	Mannings et al. 1998
rho Vir	12:41:53.13 +10:14:07.2	A3V	8740	1.500	200	6.60	75	47.57	1.180	36.270	7	22	Y	Su et al. 2006
TYC8992-106-1	12:42:15.98 -63:01:04.6	:G3	5860	0.950	190	2.10	–	–	8.680	82.510[a]	2	11	N	–
HD 110634	12:44:01.90 -53:30:20.6	F2V	6730	1.410	150	6.60	–	–	0.540	115.600	1	22	Y	Chen et al. 2011

Continued on Next Page...

Table B.1 – Continued

Name	R.A. and Decl.	Sp. Type	$T_{*,SED}$	$R_{*,SED}$	T_{dust}	R_{disk}	T_{dust2}	R_{disk2}	$\frac{L_{IR}}{L_{star}}$	Dist.	Num	λ_{start}	IRS?	Known?
10 CVn	12:44:59.41 +39:16:44.1	F9V	6130	0.890	65	18.40	–	–	0.280	17.370	2	22	Y	Trilling et al. 2008
HD 111103	12:47:38.71 -58:24:56.6	:F5	6410	1.440	110	11.40	–	–	3.250	142.650	1	22	Y	Chen et al. 2011
HD 111347	12:48:22.02 +30:46:01.8	F7V	6380	1.240	140	5.90	–	–	0.670	67.930	1	22	Y	Chen et al. 2014
HD 111520	12:50:19.68 -49:51:49.1	F5/F6V	6360	1.330	160	4.90	70	25.61	33.590	108.570	3	11	Y	Chen et al. 2011
8 Dra	12:55:28.55 +65:26:18.4	F1V	7180	1.480	100	17.70	–	–	0.260	29.290	1	22	Y	Chen et al. 2005
HD 112383	12:57:26.11 -67:57:38.6	A2IV/V	8720	1.910	240	5.80	–	–	1.800	110.740	2	11	Y	Chen et al. 2012
TYC8648-2098-1	12:58:10.01 -54:11:08.7	:A2	8560	1.610	140	14.00	–	–	8.440	117.640[a]	2	11	N	–
HD 112810	12:59:59.86 -50:23:22.5	F4IV/V	6560	1.480	180	4.50	55	49.03	12.620	143.260	3	11	Y	Chen et al. 2011
HD 113337	13:01:46.64 +63:36:37.0	F6V	6600	1.560	60	44.00	–	–	0.920	36.880	1	22	Y	Rhee et al. 2007
CPD-52 6110	13:01:50.66 -53:04:58.2	K3V(e)	5200	1.010	140	3.20	–	–	3.000	125.000[a]	1	22	Y	Meyer et al. 2008
HD 113524	13:04:59.44 -47:23:48.5	:F5	6440	1.240	200	2.90	–	–	1.460	107.410	1	22	Y	Chen et al. 2011
HD 113457	13:05:02.00 -64:26:29.8	A0V	9310	1.680	220	7.00	–	–	2.710	99.400	2	11	Y	Chen et al. 2012
TYC8656-483-1	13:05:17.73 -57:58:15.7	:F9	6100	1.030	250	1.40	–	–	4.090	116.470[a]	2	11	N	–
HD 113556	13:05:32.56 -58:32:08.1	F2V	6770	1.600	180	5.20	60	47.65	9.530	106.720	2	22	Y	Chen et al. 2005
BD+21 2486	13:06:15.35 +20:43:46.0	K4V	4140	0.620	350	0.20	50	9.92	9.710	18.800	2	22	Y	Smith et al. 2006
HD 113766	13:06:35.76 -46:02:02.1	F3/5V	5910	2.770	500	0.90	260	3.33	690.370	122.540	3	11	N	Oudmaijer et al. 1992
HR 4951	13:07:38.28 -53:27:35.1	B8V	9830	2.470	230	10.50	–	–	0.540	100.090	3	11	Y	Chen et al. 2012
TYC8653-1256-1	13:07:52.53 -54:46:57.0	:K5	4770	0.700	280	0.40	–	–	13.770	64.920[a]	2	11	N	–
HD 114082	13:09:16.14 -60:18:30.2	F3V	6520	1.340	110	10.90	–	–	35.840	85.470	3	11	Y	Chen et al. 2005
HR 4978	13:11:39.15 -26:33:06.2	A5V	7670	2.740	65	88.80	–	–	3.630	110.610	2	22	N	Rhee et al. 2007
HD 115361	13:17:55.42 -61:00:38.8	F5V	6470	1.780	150	7.70	–	–	3.020	125.000	2	11	Y	Chen et al. 2011
61 Vir	13:18:24.31 -18:18:40.3	G7V	5720	0.920	200	1.70	45	34.83	0.870	8.550	3	22	Y	Bryden et al. 2006
HD 115600[b]	13:19:19.50 -59:28:20.6	F2IV/V	6800	1.580	120	11.80	90	21.07	37.260	110.490	3	11	Y	Chen et al. 2005
HD 115820	13:20:26.81 -49:13:25.2	A7/A8V	7370	1.320	160	6.50	–	–	1.410	96.520	1	22	Y	Chen et al. 2012
iot Cen	13:20:35.53 -36:42:44.8	A3V	8580	2.040	195	9.20	–	–	0.120	18.020	1	22	Y	Rieke et al. 2005
TYC8252-1917-1	13:25:44.64 -47:49:08.6	A0V	8200	1.570	170	8.50	–	–	1.930	119.040[a]	2	11	N	–
HD 116956	13:25:45.53 +56:58:13.7	G9V	5530	0.780	70	11.40	–	–	0.190	21.590	1	22	Y	Chen et al. 2014
TYC8995-2386-1	13:25:48.42 -62:04:06.4	:K5	4630	0.660	240	0.50	–	–	9.500	39.630[a]	2	11	N	–
HD 117043	13:25:59.86 +63:15:40.5	G6V	5700	1.010	140	3.90	–	–	0.330	21.160	1	22	Y	Bryden et al. 2006
70 Vir	13:28:25.81 +13:46:43.6	G4V	5660	1.800	100	13.40	–	–	0.180	17.980	1	22	Y	Beichman et al. 2005
HD 117376	13:28:27.09 +59:56:44.8	A1V	9260	2.110	65	99.60	–	–	0.510	71.370	1	22	Y	Ballering et al. 2013
HD 117214	13:30:08.95 -58:29:04.3	F6V	6340	1.970	130	10.90	85	25.57	50.640	110.250	3	11	Y	Chen et al. 2005
HD 117484	13:31:30.97 -46:44:06.8	B9V	9150	1.670	165	11.90	80	50.95	5.540	147.270	3	11	Y	Chen et al. 2012
TYC8991-3324-1	13:31:50.78 -60:10:41.0	:K6	4350	0.610	205	0.60	–	–	15.730	53.480[a]	2	11	N	–
HD 117716	13:32:35.90 -28:41:33.9	A2V	8880	1.990	180	11.20	–	–	0.140	71.580	1	22	Y	Chen et al. 2014
HD 117665	13:32:39.21 -44:27:01.0	A1/A2V	8660	2.120	190	10.20	–	–	2.020	147.920	3	11	Y	Chen et al. 2012
BH CVn	13:34:47.91 +37:10:56.7	:F8	6190	3.770	600	0.90	–	–	7.380	45.660	1	22	Y	Trilling et al. 2007
CD-40 8031	13:37:57.26 -41:34:42.1	K0IV	5270	1.490	180	2.90	–	–	3.700	125.000[a]	1	22	Y	Meyer et al. 2008
HD 118588	13:38:42.85 -44:30:58.8	A1V	8510	1.610	160	10.60	–	–	2.480	126.420	2	11	Y	Chen et al. 2012
HD 119124	13:40:23.16 +50:31:09.5	F7.7V	6130	1.100	200	2.40	50	38.69	1.020	25.320	1	22	Y	Chen et al. 2005
HD 118972	13:41:04.36 -34:27:52.7	K0V	5510	0.670	300	0.50	–	–	3.840	15.650	1	22	Y	Trilling et al. 2008
TYC5549-1004-1	13:44:25.71 -11:28:01.3	:K6	4420	0.620	240	0.40	–	–	11.750	45.540[a]	2	11	N	–

Continued on Next Page...

Table B.1 – Continued

Name	R.A. and Decl.	Sp. Type	$T_{*,SED}$	$R_{*,SED}$	T_{dust}	R_{disk}	T_{dust2}	R_{disk2}	$\frac{L_{IR}}{L_{star}}$	Dist.	Num	λ_{start}	IRS?	Known?
HD 119511	13:44:43.92 -49:17:57.9	F3V	6640	1.240	270	1.70	–	–	0.760	91.570	1	22	Y	Chen et al. 2005
HD 119718	13:46:35.36 -62:04:10.0	F5V	6380	2.380	140	11.50	–	–	3.380	131.750	1	22	Y	Chen et al. 2011
HD 120326	13:49:54.47 -50:14:24.0	F0V	6840	1.410	160	6.00	85	21.29	30.690	107.410	3	11	Y	Chen et al. 2011
HD 120534	13:50:40.18 -31:12:23.4	A5V	7140	1.510	90	22.10	–	–	4.560	67.000[a]	2	22	Y	Moor et al. 2006
HD 120160	13:53:30.76 -80:16:22.2	F0IV/V	6750	2.580	60	76.20	–	–	1.210	138.310	1	22	Y	Moor et al. 2011
HD 121189	13:55:09.97 -50:44:43.1	F3V	6660	1.460	150	6.70	–	–	4.880	118.760	2	11	Y	Chen et al. 2011
HIP 68080	13:56:19.97 -54:07:56.7	A1V	8110	3.430	160	20.50	–	–	0.650	139.860	2	22	Y	Chen et al. 2014
HD 121812	13:57:15.88 +23:21:42.8	:G7	5500	0.850	55	19.80	–	–	15.900	37.570	2	60	N	Moor et al. 2006
HD 121617	13:57:41.10 -47:00:34.4	A1V	8710	1.630	140	14.70	85	39.99	93.360	119.440[a]	3	11	N	Sylvester et al. 2001
HD 122652	14:02:31.56 +31:39:39.1	:F9	6160	1.140	50	40.40	–	–	1.740	39.290	1	22	Y	Zuckerman et al. 2004
HD 122705	14:04:42.12 -50:04:17.2	A2V	8290	1.430	230	4.30	–	–	0.860	112.860	1	22	Y	Chen et al. 2012
HD 123889	14:10:59.61 -36:16:01.7	F2V	6710	1.620	120	11.80	–	–	0.440	132.270	1	22	Y	Chen et al. 2014
HD 124718	14:15:49.85 -27:20:55.1	G5V	5810	0.970	65	18.10	–	–	18.040	63.170	2	22	N	Zuckerman et al. 2004
HD 124619	14:16:16.97 -53:49:02.1	F0V	6720	1.500	190	4.30	–	–	1.180	133.330	2	11	Y	Chen et al. 2011
lam Boo	14:16:22.79 +46:05:19.8	A3V	8550	1.790	200	7.60	80	47.73	1.110	30.350	6	22	N	Rieke et al. 2005
18 Boo	14:19:16.28 +13:00:15.4	F5IV	6720	1.400	65	34.90	–	–	0.220	26.090	1	22	Y	Ballering et al. 2013
HD 125283	14:19:23.88 -37:00:10.4	A2V	8510	1.960	200	8.20	–	–	0.280	73.470	2	11	Y	Morales et al. 2009
psi Cen	14:20:33.39 -37:53:06.9	A0IV	9650	4.260	200	23.10	45	456.23	0.300	79.360	1	22	Y	Rhee et al. 2007
HD 125541	14:21:11.54 -41:42:24.9	A9V	7170	1.090	130	7.70	–	–	2.750	113.250	2	11	Y	Chen et al. 2012
HD 126062	14:24:37.00 -47:10:39.8	A1V	8770	1.390	150	11.00	55	82.44	4.910	110.370	2	22	Y	Chen et al. 2012
CD-46 9327	14:27:05.53 -47:14:21.9	G9V	5320	1.180	400	0.40	–	–	6.330	132.000[a]	1	22	Y	Meyer et al. 2008
HD 127821	14:30:45.86 +63:11:11.8	F4IV	5210	1.160	200	1.80	30	82.07	10.470	31.780	2	22	Y	Moor et al. 2006
gam Boo	14:32:04.67 +38:18:29.7	A7IV	7530	3.380	60	124.10	–	–	0.130	26.600	1	22	Y	Rhee et al. 2007
HD 128165	14:33:28.65 +52:54:34.3	K3V	5000	0.710	200	1.00	–	–	0.900	13.210	2	60	N	Lawler et al. 2009
sig Boo	14:34:40.98 +29:44:43.9	F4V	6740	1.310	220	2.80	20	347.42	0.410	15.830	3	60	N	Zuckerman et al. 2004
HD 128311	14:36:00.72 +09:44:44.6	K3V	5050	0.730	75	7.80	–	–	0.330	16.500	1	22	Y	Beichman et al. 2005
HR 5449	14:36:44.11 -40:12:41.8	B8V	12050	2.910	250	15.70	–	–	0.080	147.490	1	22	Y	Rieke et al. 2005
TYC8683-242-1	14:37:50.21 -54:57:41.4	K1V(e)	5210	0.760	240	0.80	–	–	14.810	79.280[a]	2	11	N	–
HD 129590	14:44:30.96 -39:59:20.6	G3V	5930	1.610	100	13.10	60	36.62	123.680	132.620	2	22	Y	Chen et al. 2011
TYC9011-3733-1	14:50:09.71 -62:32:23.2	:G4	5780	0.920	225	1.40	–	–	6.180	81.150[a]	2	11	N	–
HD 130693	14:50:18.54 -24:25:39.7	G8IV	5660	0.760	65	13.50	–	–	6.220	33.000[a]	2	60	N	Moor et al. 2006
HD 131496	14:53:23.05 +18:14:07.3	:K3	4940	4.350	70	50.40	–	–	0.160	110.010	2	100	N	Bonsor et al. 2014
DE Boo	14:53:23.77 +19:09:10.0	K0V	5520	0.740	300	0.50	–	–	3.640	11.510	3	22	Y	Koerner et al. 2010
HD 131625	14:55:44.73 -33:51:20.7	A0V	8700	2.670	220	9.70	35	384.06	1.540	77.820	1	22	Y	Rhee et al. 2007
TYC7824-2717-1	14:55:53.23 -39:43:44.5	F5/F6V	6260	1.150	215	2.20	–	–	5.760	113.080[a]	2	11	N	–
HD 132254	14:56:23.16 +49:37:40.0	F8-V	6270	1.420	140	6.60	–	–	0.170	25.100	2	60	N	Lawler et al. 2009
HD 131835[b]	14:56:54.45 -35:41:43.8	A2IV	7980	1.470	180	6.70	70	44.71	49.250	122.690	4	11	Y	Moor et al. 2006
del Lib	15:00:58.30 -08:31:08.1	A0V	8370	3.960	40	403.30	–	–	0.460	90.000	1	22	Y	Rhee et al. 2007
HD 132950	15:01:30.05 +15:52:05.5	K3V	4810	0.700	500	0.10	40	23.83	20.770	30.310	1	22	Y	Rhee et al. 2007
HD 133075	15:03:31.91 -31:22:34.6	F3IV	6150	3.100	120	18.90	–	–	0.650	151.510	1	22	Y	Chen et al. 2005
HD 133803	15:07:14.94 -29:30:16.1	A9V	6920	1.780	170	6.80	–	–	4.510	124.840	2	11	Y	Chen et al. 2012
HD 134888	15:13:27.94 -33:08:50.4	F4V	6480	1.120	200	2.70	75	19.60	14.950	89.920	2	11	Y	Chen et al. 2011

Continued on Next Page...

Table B.1 – Continued

Name	R.A. and Decl.	Sp. Type	$T_{*,SED}$	$R_{*,SED}$	T_{dust}	R_{disk}	T_{dust2}	R_{disk2}	$\frac{L_{IR}}{L_{star}}$	Dist.	Num	λ_{start}	IRS?	Known?
TYC7826-2474-1	15:13:50.37 -40:25:02.1	G0V	6190	1.100	115	7.40	–	–	62.480	112.700[a]	2	11	N	–
HD 135599	15:15:59.30 +00:47:45.5	K0V	5510	0.730	200	1.20	50	20.86	1.920	15.840	1	22	Y	Plavchan et al. 2009
bet Cir	15:17:30.80 -58:48:05.9	A3V	8470	1.920	220	6.60	–	–	0.560	30.550	1	22	Y	Morales et al. 2009
HD 135953	15:19:05.40 -36:21:44.4	F5V	6310	1.340	65	29.40	–	–	8.650	133.150	2	22	Y	Chen et al. 2011
GJ 581	15:19:26.82 -07:43:20.2	M5.0V	3250	0.330	120	0.50	25	13.30	1.810	6.210	3	60	N	Lestrade et al. 2012
HD 136246	15:20:31.39 -28:17:13.8	A1V	8470	1.990	240	5.70	55	109.96	1.010	131.570	1	22	Y	Rieke et al. 2005
HD 136482	15:22:11.24 -37:38:08.4	B8/B9V	10700	2.000	195	14.00	–	–	0.820	136.240	1	22	Y	Rieke et al. 2005
HD 137119	15:25:30.17 -36:11:57.9	A2V	8300	1.350	230	4.00	–	–	1.760	107.180	2	11	Y	Chen et al. 2012
HD 138296	15:32:20.13 -31:08:33.8	F2V	6490	1.900	120	12.90	–	–	0.220	142.650	1	22	Y	Chen et al. 2014
tet CrB	15:32:55.77 +31:21:32.8	B6V	12550	3.780	115	104.90	–	–	0.151	115.070	2	22	N	–
TYC9022-1316-1	15:34:14.44 -60:48:28.9	B9.2/A0V	8770	1.520	150	12.10	–	–	3.540	105.480	2	11	N	–
alf CrB	15:34:41.35 +26:42:51.9	A1IV	8770	3.090	120	38.40	–	–	0.340	23.000	4	22	Y	Rieke et al. 2005
HD 138813	15:35:16.09 -25:44:03.3	A0V	8660	2.070	170	12.50	85	50.17	22.670	150.830	5	11	Y	Carpenter et al. 2006
HD 139323	15:35:56.16 +39:49:52.2	K3V	5210	0.820	300	0.50	30	57.78	11.230	22.370	2	22	Y	Rhee et al. 2007
HR 5790	15:36:11.35 -33:05:34.3	B8V	11000	1.790	275	6.60	–	–	1.170	106.490	2	11	Y	Rieke et al. 2005
HR 5792	15:40:11.47 -70:13:41.0	A1V	8630	1.610	200	7.00	65	66.33	7.340	78.490	3	11	Y	Rhee et al. 2007
g Lup[b]	15:41:11.24 -44:39:43.3	F5V	6730	1.270	350	1.10	45	66.43	4.090	17.430	3	11	N	Beichman et al. 2006
HR 5859	15:45:23.49 +05:26:50.3	A0V	8750	3.420	180	18.80	35	498.44	2.920	113.370	3	22	Y	Rhee et al. 2007
HD 140817	15:47:04.44 -35:30:37.4	A0V	8770	2.490	180	13.70	–	–	1.750	147.270	3	11	Y	Chen et al. 2012
HD 140840	15:47:06.17 -35:31:04.9	B9.5V	9380	1.530	200	7.80	80	49.18	3.600	125.780	2	22	Y	Chen et al. 2012
TYC7340-321-1	15:48:07.81 -36:01:45.2	:F8	6170	1.080	240	1.60	–	–	3.980	120.970[a]	2	11	N	–
HD 141011	15:48:24.76 -42:37:05.3	F5V	6530	1.090	200	2.70	–	–	1.980	96.330	1	22	Y	Chen et al. 2012
HD 141227	15:48:50.77 -23:41:09.3	F5V	5900	0.960	180	2.40	–	–	16.400	60.220[a]	2	11	N	–
HD 141378	15:48:56.77 -03:49:06.5	A5IV-V	8240	1.810	190	7.90	60	79.77	1.440	54.020	2	22	Y	Morales et al. 2009
HD 141569	15:49:57.68 -03:55:15.6	A0Ve	8240	1.940	300	3.40	90	37.87	162.450	116.140	7	11	N	Weinberger et al. 1999
TYC7332-2514-1	15:50:44.36 -33:39:49.1	F3V	6630	1.380	250	2.20	–	–	3.230	106.990[a]	2	11	N	–
kap CrB	15:51:13.93 +35:39:23.0	K0III-IV	4990	5.090	90	36.40	–	–	0.690	30.490	3	60	N	Bonsor et al. 2013
HD 141943[b]	15:53:27.27 -42:16:01.3	:G2	5910	1.570	300	1.40	65	30.37	4.240	67.000[a]	2	22	Y	Hillenbrand et al. 2008
V1040 Sco	15:53:55.86 -23:58:41.4	B2V	9300	3.940	500	3.10	–	–	3.801	130.880	2	11	N	–
lam CrB	15:55:47.62 +37:56:49.9	F0IV	6990	2.020	320	2.20	40	144.07	0.840	41.560	1	22	Y	Trilling et al. 2007
HD 142446	15:56:05.61 -36:53:34.5	F3V	6670	1.570	70	33.20	–	–	7.610	144.300	2	22	Y	Chen et al. 2011
HD 142139	15:56:05.86 -60:28:58.3	A1IV/V	8670	1.840	160	12.50	–	–	0.350	66.000	1	22	Y	Morales et al. 2009
2MASS J15570641-2206060	15:57:06.40 -22:06:06.2	:M	2020	0.290	240	0.05	–	–	398.508	31.550[a]	2	11	N	–
2MASS J15584772-1757595	15:58:47.71 -17:57:59.8	:K8	3860	1.650	450	0.20	–	–	10.630	125.000[a]	1	22	N	Carpenter et al. 2006
44 Ser	16:02:17.71 +22:48:16.4	A3V	8840	2.290	200	10.40	50	166.70	0.600	54.880	1	22	Y	Rhee et al. 2007
HD 143538	16:02:18.53 -35:16:11.7	F0V	6880	1.240	240	2.30	–	–	0.580	106.260	1	22	Y	Chen et al. 2014
HD 143675	16:03:13.54 -35:17:14.9	A5IV/V	7750	1.330	190	5.10	110	15.39	10.900	113.370	3	11	Y	Chen et al. 2012
LM Lup	16:04:44.49 -39:26:04.7	:B8	10850	1.810	160	19.30	–	–	0.210	144.710	1	22	Y	Chen et al. 2012
TYC6212-349-1	16:04:55.45 -20:54:00.2	A3IV/V	6960	1.450	185	4.70	–	–	4.550	98.570[a]	2	11	N	–
HD 144587	16:07:29.92 -23:57:02.6	A9V	6540	1.890	205	4.40	–	–	5.110	108.450	3	11	Y	Carpenter et al. 2006
HD 144729	16:08:10.50 -23:51:02.6	F0V	6280	1.610	300	1.60	–	–	1.920	138.880	1	22	Y	Chen et al. 2011
TYC7851-810-1	16:08:30.70 -38:28:27.1	:K6	4590	0.650	90	3.90	–	–	1308.110	57.630[a]	4	11	N	–

Continued on Next Page...

Table B.1 – Continued

Name	R.A. and Decl.	Sp. Type	$T_{*,SED}$	$R_{*,SED}$	T_{dust}	R_{disk}	T_{dust2}	R_{disk2}	$\frac{L_{IR}}{L_{star}}$	Dist.	Num	λ_{start}	IRS?	Known?
TYC7338-1156-1	16:08:31.34 -35:09:49.9	A9V	7270	1.480	130	10.80	–	–	16.700	124.440[a]	2	11	N	–
HD 145229	16:09:26.56 +11:34:28.6	:G1	5940	0.960	200	1.90	50	31.66	1.880	34.500	1	22	Y	Kim et al. 2005
TYC6213-12-1	16:09:58.05 -22:24:35.1	A3IV/V	6970	1.450	160	6.40	–	–	10.110	83.550[a]	2	11	N	–
TYC6213-1122-1	16:10:12.67 -21:04:44.8	:K6	4360	0.610	120	1.80	70	5.54	3458.420	60.450[a]	3	11	N	–
HD 145357	16:12:16.75 -42:22:30.1	A5V	7240	1.890	190	6.30	–	–	1.210	146.840	1	22	Y	Chen et al. 2012
HD 145554	16:12:21.83 -19:34:44.8	B9V	7530	2.150	400	1.70	150	12.61	8.770	140.440	3	11	Y	Carpenter et al. 2006
HD 145631	16:12:44.10 -19:30:10.6	B9V	7430	2.130	200	6.80	–	–	1.180	131.750	2	11	Y	Carpenter et al. 2006
HD 145560	16:13:34.32 -45:49:03.8	F5V	6460	1.580	400	0.90	80	24.05	38.210	133.690	3	22	Y	Chen et al. 2011
HD 145880	16:14:57.77 -39:37:40.1	B9.5V	8090	2.160	200	8.20	75	58.61	13.100	127.870	3	11	Y	Chen et al. 2012
2MASS J16145918-2750230	16:14:59.17 -27:50:23.1	K0IV(e)	5070	1.110	230	1.20	–	–	4.560	125.000[a]	2	–	N	Carpenter et al. 2006
HD 145972	16:16:03.84 -49:04:29.3	F0V	6910	1.610	200	4.40	–	–	1.970	127.380	1	22	Y	Ballering et al. 2013
HD 146181	16:16:28.35 -38:44:12.6	F6V	6450	1.530	350	1.20	80	23.26	29.730	146.190	2	22	Y	Chen et al. 2011
HD 145689	16:17:05.33 -67:56:29.3	A4IV-V	8150	1.460	250	3.60	50	90.67	0.790	52.210	2	22	Y	Zuckerman et al. 2011
TYC8315-123-1	16:17:37.13 -47:16:03.7	:K0	5250	0.770	220	1.00	–	–	18.400	99.900[a]	2	11	N	–
HD 146606	16:18:16.15 -28:02:30.4	A0V	9300	1.800	190	10.00	–	–	1.100	129.360	2	11	Y	Carpenter et al. 2006
d Sco	16:18:17.89 -28:36:51.5	A1Va	9460	1.600	280	4.20	–	–	0.210	41.280	2	22	Y	Kennedy et al. 2010
HD 146897[b]	16:19:29.23 -21:24:13.4	F2/F3V	6280	1.460	130	7.90	75	23.82	142.140	122.690	3	11	N	Chen et al. 2006
HD 147137	16:20:50.22 -22:35:38.8	A9V	6390	1.660	170	5.40	50	63.14	12.630	139.080	4	11	Y	Carpenter et al. 2006
HD 147196	16:21:19.18 -23:42:28.9	B6/B7V	7260	3.280	210	9.10	–	–	9.362	150.600	2	11	N	–
HD 147594	16:23:53.85 -29:46:40.3	G3IV	5910	1.850	240	2.60	–	–	1.940	142.040	1	22	Y	Chen et al. 2011
TYC8316-4073-1	16:24:58.32 -48:36:05.3	F0V	6950	1.450	180	5.00	–	–	4.930	108.220[a]	2	11	N	–
V2505 Oph	16:29:48.69 -21:52:12.1	K2IVe	3920	2.170	70	15.80	–	–	5.830	125.000[a]	1	22	Y	Spangler et al. 2001
HD 150706	16:31:18.02 +79:47:22.4	G3V	5940	0.960	350	0.60	55	26.12	1.470	28.220	1	22	Y	Moro-Martin et al. 2007
37 Her	16:40:38.69 +04:13:10.9	A1V	9290	2.280	190	12.70	50	183.62	1.820	90.000	2	22	Y	Rhee et al. 2007
39 Her	16:41:36.72 +26:55:00.4	F3V	6580	1.940	55	64.80	–	–	0.110	43.740	1	22	Y	Trilling et al. 2007
TYC7358-263-1	16:42:19.22 -36:39:20.4	:G7	5560	0.840	200	1.50	–	–	7.540	95.990[a]	2	11	N	–
HD 151044	16:42:27.97 +49:56:10.1	F8V	6160	1.170	60	28.90	–	–	1.830	29.330	1	22	Y	Rhee et al. 2007
HD 150697	16:43:18.69 -14:02:05.5	F3V	6170	2.580	140	11.60	–	–	2.300	133.510	1	22	Y	Chen et al. 2014
HD 151376	16:47:47.33 -19:52:32.1	F2/F3V	6330	1.600	300	1.60	120	10.39	5.070	135.680	1	22	Y	Chen et al. 2011
53 Her	16:52:57.98 +31:42:06.1	F0V	6990	1.490	180	5.20	–	–	0.420	29.180	1	22	Y	Moor et al. 2009
h Dra	16:56:01.69 +65:08:05.2	F8V	6340	1.180	240	1.90	35	90.17	0.590	15.250	2	60	N	Gaspar et al. 2013
HD 153053	17:00:06.28 -54:35:50.5	A5IV-V	7820	1.820	160	10.10	50	104.10	1.310	51.810	2	22	Y	Wyatt et al. 2007
TYC8327-1661-1	17:00:16.14 -46:24:41.1	:K5	4650	0.660	190	0.90	–	–	18.290	56.890[a]	2	11	N	–
HD 154577	17:10:10.35 -60:43:43.5	K2.5V	5070	0.620	85	5.10	–	–	0.200	13.620	1	22	Y	Lawler et al. 2009
TYC8341-414-1	17:20:50.60 -45:25:15.4	A0V	8390	1.730	190	7.80	90	35.17	78.450	118.340	3	11	N	–
73 Her	17:24:06.56 +22:57:36.7	A7V	7590	1.550	200	5.10	90	25.67	4.660	42.690	2	22	Y	Zuckerman et al. 2004
HD 157587	17:24:52.23 -18:51:33.5	F5V	6370	1.580	80	23.40	–	–	35.370	107.410	2	22	N	–
HD 158633	17:25:00.10 +67:18:24.1	K0V	5420	0.750	300	0.50	55	17.13	1.080	12.800	3	22	Y	Beichman et al. 2006
HD 323410	17:25:15.33 -40:32:01.1	:G2	5920	0.970	215	1.70	–	–	4.700	98.400[a]	2	11	N	–
HR 6511	17:25:41.33 +60:02:54.5	A1V	8860	2.800	110	42.30	–	–	0.120	96.890	1	22	Y	Su et al. 2006
HD 158352	17:28:49.61 +00:19:50.3	A8V	7400	2.600	60	92.20	–	–	0.950	59.630	2	22	Y	Moor et al. 2006
78 Her	17:31:49.58 +28:24:27.0	A1V	9280	2.190	75	78.20	30	489.02	6.140	82.030	3	22	N	Chen et al. 2014

Continued on Next Page...

Table B.1 – Continued

Name	R.A. and Decl.	Sp. Type	$T_{*,SED}$	$R_{*,SED}$	T_{dust}	R_{disk}	T_{dust2}	R_{disk2}	$\frac{L_{IR}}{L_{star}}$	Dist.	Num	λ_{start}	IRS?	Known?
HR 6532	17:32:14.88 +11:55:48.1	B9.5V	8950	2.700	170	17.40	35	410.85	14.820	135.310	2	22	N	Chen et al. 2014
HD 159170	17:33:29.81 -05:44:42.3	A4III-IV	7840	1.720	160	9.60	–	–	0.430	48.090	1	22	Y	Morales et al. 2009
HD 159492	17:38:05.47 -54:30:03.1	A5IV/V	7830	1.880	170	9.20	90	33.16	2.340	44.560	4	22	Y	Zuckerman et al. 2004
lam Ara	17:40:23.93 -49:24:58.2	F4V	6570	1.610	50	64.90	–	–	0.040	21.450	2	60	N	Beichman et al. 2006
V2384 Oph	17:42:30.35 -28:44:56.0	G5V	5760	1.220	125	6.00	–	–	18.850	78.000	2	11	N	–
TYC7889-407-1	17:44:45.31 -39:50:54.5	F0V	6720	1.420	195	3.90	–	–	9.000	114.540	2	11	N	–
gam Oph	17:47:53.55 +02:42:25.3	A1V	8920	2.130	85	54.60	–	–	1.020	31.510	8	22	Y	Oudmaijer et al. 1992
HD 162917	17:53:14.10 +06:06:05.7	F4IV-V	6620	1.440	150	6.50	50	58.97	2.960	31.120	2	22	N	Chen et al. 2006
HD 164330	17:56:20.01 +62:36:37.2	:G2	5900	1.930	40	98.00	–	–	10.090	76.560	2	60	N	Zuckerman et al. 2004
HD 165459	18:02:30.72 +58:37:38.4	A1V	8200	1.620	95	28.20	–	–	0.600	88.800	2	22	Y	Rieke et al. 2005
HD 164249	18:03:03.56 -51:38:57.0	F6V	6450	1.350	85	18.10	–	–	7.930	48.140	3	22	Y	Zuckerman et al. 2004
b Her	18:07:01.52 +30:33:44.4	F7V	6100	1.250	50	43.40	–	–	0.150	15.640	5	60	N	Koerner et al. 2010
V4046 Sgr	18:14:10.46 -32:47:34.5	:K6	4310	0.590	200	0.60	80	4.04	1649.960	30.670[a]	4	–	N	Kastner et al. 2008
HD 168161	18:18:53.36 -11:00:37.4	:G5	5710	0.890	275	1.00	–	–	0.070	58.310[a]	2	11	N	–
HD 169666	18:19:08.04 +71:31:04.2	F2V	6540	1.680	180	5.10	–	–	2.110	53.210	2	22	Y	Moor et al. 2006
HD 168746	18:21:49.78 -11:55:21.6	:G5	5690	1.060	450	0.40	80	12.51	7.630	42.730	1	22	Y	Chen et al. 2014
TYC5103-27-1	18:29:30.49 -02:02:15.6	:G6	5570	0.850	195	9.90	–	–	0.560	94.960[a]	2	11	N	–
HR 6948	18:33:01.00 -39:53:32.1	F5V	6590	1.420	45	70.90	–	–	4.390	36.980	7	22	Y	Zuckerman et al. 2004
TYC3531-1441-1	18:36:37.54 +48:26:10.1	:K1	5230	0.770	270	0.60	–	–	8.350	120.120[a]	2	11	N	–
Vega	18:36:56.52 +38:47:04.4	A0V	9040	2.840	95	59.90	–	–	0.310	7.670	7	60	N	Aumann et al. 1984
HD 172555	18:45:26.94 -64:52:18.1	A7V	7670	1.560	285	2.60	–	–	7.720	28.540	6	11	N	Mannings et al. 1998
PZ Tel	18:53:05.89 -50:10:50.8	G9IV	5270	1.270	300	0.90	40	51.37	3.210	51.490	1	22	Y	Rebull et al. 2008
zet CrA	19:03:06.94 -42:05:42.9	B9.5V	9630	2.320	115	37.90	–	–	1.020	59.200	2	22	N	Mannings et al. 1998
rho Tel	19:06:19.99 -52:20:28.3	F7V	6290	3.890	170	12.40	–	–	0.360	56.720	2	22	Y	Smith et al. 2006
alf CrA	19:09:28.42 -37:54:17.4	A2V	8870	2.210	160	15.80	–	–	0.430	38.430	2	22	Y	Rieke et al. 2005
HR 7297	19:18:09.82 -53:23:14.4	F7V	6300	1.800	85	23.10	–	–	0.110	45.060	1	22	Y	Smith et al. 2006
eta Tel	19:22:51.22 -54:25:26.9	A0V	9350	1.690	450	1.70	120	23.90	5.620	48.210	5	11	N	Zuckerman et al. 2004
HD 181327[b]	19:22:58.97 -54:32:17.9	F6V	6430	1.440	80	21.60	–	–	32.020	51.810	5	22	Y	Mannings et al. 1998
5 Vul	19:26:13.24 +20:05:51.4	A0V	9360	1.970	150	17.80	–	–	0.260	72.880	1	22	Y	Morales et al. 2009
HD 182681	19:26:56.50 -29:44:36.1	B8.5V	9430	1.840	90	47.00	–	–	2.560	69.930	8	22	N	Moor et al. 2006
c Aql	19:29:00.98 +01:57:01.3	A0IV	8460	1.760	300	3.20	80	45.90	0.520	61.190	1	22	Y	Rieke et al. 2005
HD 183216	19:29:40.58 -30:47:54.6	G2V	6110	1.030	140	4.50	–	–	0.370	34.340	1	22	Y	Carpenter et al. 2009
HD 187897	19:52:09.39 +07:27:36.1	:G1	5940	1.120	200	2.30	55	30.63	1.290	35.090	1	22	Y	Hillenbrand et al. 2008
eps Pav	20:00:35.75 -72:54:39.1	A0V	9010	1.980	90	46.20	–	–	0.050	32.210	4	60	Y	Su et al. 2006
HD 190228	20:03:00.88 +28:18:24.6	G5IV	5590	2.170	350	1.20	50	63.33	4.680	61.610[a]	2	22	Y	Bryden et al. 2009
TYC2678-2088-1	20:04:34.44 +34:22:07.8	K0V	5440	0.810	195	8.30	–	–	0.520	96.530[a]	2	11	N	–
TYC2679-1864-1	20:06:15.80 +34:14:27.2	:K6	4270	0.590	200	4.90	–	–	2.950	59.590[a]	2	11	N	–
TYC3559-479-1	20:08:11.94 +46:47:07.3	:F7	6280	1.160	200	2.60	–	–	4.210	117.170[a]	2	11	N	–
HD 191089[b]	20:09:05.24 -26:13:27.2	F5V	6440	1.360	100	13.10	–	–	16.600	52.210	4	22	N	Mannings et al. 1998
HD 192263	20:13:59.82 -00:51:58.0	K2.5V	5210	0.660	70	9.20	–	–	0.440	19.310	1	22	Y	Saffe et al. 2004
rho Aql	20:14:16.67 +15:11:52.1	A1V	8600	1.890	130	19.30	45	161.15	0.860	45.970	2	22	Y	Morales et al. 2009
TYC3155-807-1	20:15:14.61 +40:05:51.1	:F9	6130	1.050	300	1.00	–	–	5.400	63.150[a]	2	11	N	–

Continued on Next Page...

Table B.1 – Continued

Name	R.A. and Decl.	Sp. Type	$T_{*,SED}$	$R_{*,SED}$	T_{dust}	R_{disk}	T_{dust2}	R_{disk2}	$\frac{L_{IR}}{L_{star}}$	Dist.	Num	λ_{start}	IRS?	Known?
TYC3576-213-1	20:15:44.98 +48:03:02.2	:K2	5070	0.740	235	1.80	–	–	0.250	64.930[a]	2	11	N	–
HD 192758	20:18:15.83 -42:51:36.9	F0V	7050	1.450	170	5.80	55	55.45	7.930	62.000[a]	2	22	Y	Moor et al. 2006
TYC3151-603-1	20:19:17.61 +38:58:45.4	:K6	4420	0.620	195	0.70	–	–	12.660	35.700[a]	2	11	N	–
kap01 Sgr	20:22:27.50 -42:02:58.3	A0V	9250	1.840	75	65.10	–	–	0.280	66.130	1	22	Y	Ballering et al. 2013
HR 7848	20:35:34.94 -60:34:56.3	F0V	7170	1.750	140	10.70	55	69.45	1.510	27.790	7	22	Y	Zuckerman et al. 2004
TYC2698-1078-1	20:36:07.61 +35:47:47.3	:G2	5910	0.960	190	2.10	–	–	15.970	118.730[a]	2	11	N	–
iot Del	20:37:49.13 +11:22:39.7	A1IV	8850	1.830	200	8.30	65	78.93	0.920	57.930	2	22	Y	Rhee et al. 2007
AU Mic[b]	20:45:09.76 -31:20:31.0	M1Ve	3520	0.870	65	5.90	–	–	6.700	9.900	5	160	N	Song et al. 2002
HR 8013	20:56:47.39 -26:17:47.5	F6V	6420	1.120	300	1.20	70	22.01	0.940	21.960	2	22	Y	Beichman et al. 2006
TYC3175-519-1	20:58:45.45 +42:42:17.6	G0V	5850	0.940	235	1.30	–	–	10.180	96.270[a]	2	11	N	–
TYC4259-1185-1	20:59:58.95 +66:25:04.9	:K3	5000	0.720	75	7.50	–	–	19.890	23.590[a]	2	22	N	–
HD 200565	21:04:05.69 +03:58:50.4	:G2	5900	1.220	30	110.30	–	–	9.440	65.740	1	22	Y	Chen et al. 2014
alf Oct	21:04:43.17 -77:01:29.9	:G2	5910	3.690	450	1.40	40	187.77	2.950	43.530	1	22	Y	Trilling et al. 2007
TYC1112-317-1	21:06:23.95 +12:51:45.5	:G9	5210	0.760	245	0.80	–	–	10.880	93.210[a]	2	11	N	–
HD 201219	21:07:56.52 +07:25:58.5	:G4	5760	0.890	300	0.70	50	27.50	2.950	38.120	1	22	Y	Hillenbrand et al. 2008
TYC3593-4938-1	21:11:19.02 +48:26:51.3	:K6	4350	0.610	190	0.70	–	–	12.210	56.380[a]	2	11	N	–
TYC1113-1057-1	21:13:03.33 +13:01:08.4	:K2	5180	0.760	250	0.70	–	–	8.390	94.460[a]	2	11	N	–
HD 202206	21:14:57.74 -20:47:22.4	G6V	5850	0.980	210	1.70	50	31.27	2.250	45.330	1	22	Y	Kospal et al. 2009
TYC3181-1403-1	21:15:23.95 +44:37:42.2	:K4	4870	0.700	250	0.60	–	–	6.860	70.010[a]	2	11	N	–
HD 202628	21:18:27.48 -43:20:04.3	G5V	5910	0.940	70	15.60	–	–	1.300	24.420	1	60	N	Koerner et al. 2010
HD 202917[b]	21:20:49.99 -53:02:04.2	G7V	5710	0.770	280	0.70	75	10.41	6.810	42.970	4	22	Y	Spangler et al. 2001
HD 205674	21:37:21.15 -18:26:29.3	F3/F5IV	6620	1.260	190	3.50	50	51.77	5.080	51.810	2	22	Y	Moor et al. 2006
3 Peg	21:37:43.65 +06:37:06.2	A2V	8970	1.920	140	18.30	–	–	0.210	87.640	1	22	Y	Ballering et al. 2013
HD 205536	21:40:29.41 -74:04:25.3	G9V	5560	0.860	75	11.00	–	–	3.080	22.020	1	60	N	Zuckerman et al. 2004
HN Peg	21:44:31.49 +14:46:17.8	G0V	6110	0.930	350	0.60	80	12.65	0.980	17.880	2	22	Y	Bryden et al. 2006
HD 206893	21:45:21.98 -12:46:59.9	F5V	6490	1.230	50	48.40	–	–	2.900	38.340	1	22	Y	Zuckerman et al. 2004
HD 207129[b]	21:48:15.91 -47:18:16.2	G2V	6140	0.990	350	0.70	50	34.78	2.640	15.990	7	22	Y	Jourdain et al. 1999
HD 209253	22:02:32.95 -32:08:01.2	F6.5V	6250	1.080	250	1.50	60	27.43	1.510	30.130	1	22	Y	Zuckerman et al. 2004
HD 210277	22:09:29.94 -07:32:59.9	G8V	5580	1.070	20	194.50	–	–	0.040	21.560	2	100	N	Bryden et al. 2006
HD 212695	22:26:14.42 -02:47:21.2	:F5	6450	1.340	40	81.50	–	–	0.480	46.490	1	22	Y	Trilling et al. 2008
bet PsA	22:31:30.33 -32:20:45.8	A1V	9150	2.220	135	23.70	–	–	0.180	43.780	2	60	N	Gaspar et al. 2013
39 Peg	22:32:35.58 +20:13:48.5	F1V	6910	1.590	55	58.40	–	–	1.210	50.250	1	22	Y	Rhee et al. 2007
69 Aqr	22:47:42.76 -14:03:23.1	B9V	9720	2.440	150	23.80	–	–	0.350	97.370	1	22	Y	Morales et al. 2009
tau01 Gru	22:53:38.18 -48:35:54.8	G0V	6100	1.620	220	2.90	55	46.55	0.800	32.610	1	22	Y	Kospal et al. 2009
Fomalhaut[b]	22:57:39.31 -29:37:21.7	A4V	8240	1.950	70	62.90	–	–	0.720	7.700	8	60	N	Aumann et al. 1984
TYC8830-410-1	23:01:12.67 -58:58:22.0	:K3	4900	0.700	425	0.20	–	–	190.360	120.160[a]	2	11	N	–
HD 217792	23:03:29.81 -34:44:57.8	F1V	7190	1.550	90	23.00	–	–	0.110	29.420	1	22	Y	Chen et al. 2014
TYC6972-692-1	23:06:25.60 -23:10:02.4	G5V	5820	0.930	210	1.60	–	–	5.950	102.300[a]	2	11	N	–
HR 8799	23:07:28.80 +21:08:02.7	F0V	7180	1.430	220	3.50	45	85.12	3.330	39.400	8	22	Y	Sadakane et al. 1986
HD 218340	23:08:12.53 -63:37:42.0	G3V	6100	0.950	400	0.50	40	51.93	3.550	56.590	1	22	Y	Smith et al. 2006
HD 219623	23:16:42.44 +53:12:46.1	F7V	6300	1.170	110	8.90	–	–	0.420	20.500	1	22	Y	Beichman et al. 2006
HD 219482	23:16:57.93 -62:00:04.5	F6V	6450	1.070	350	0.80	75	18.49	1.750	20.530	2	22	Y	Beichman et al. 2006

Continued on Next Page...

Table B.1 – Continued

Name	R.A. and Decl.	Sp. Type	$T_{*,SED}$	$R_{*,SED}$	T_{dust}	R_{disk}	T_{dust2}	R_{disk2}	$\frac{L_{IR}}{L_{star}}$	Dist.	Num	λ_{start}	IRS?	Known?
kap Psc	23:26:56.02 +01:15:19.3	A2V	9290	1.670	240	5.80	–	–	0.650	47.050	1	22	Y	Morales et al. 2009
HD 221853	23:35:36.20 +08:22:56.9	:F3	6650	1.530	85	21.70	–	–	9.280	68.440	2	22	Y	Zuckerman et al. 2004
del Scl	23:48:55.62 -28:07:50.4	A0V	9320	1.820	210	8.30	–	–	0.450	42.140	3	22	Y	Morales et al. 2009

Notes: The spectral types are taken from SIMBAD unless designated by a ':'. The Num_Excess parameter describes the number of passbands that demonstrate IR excess. The λ_{start} column offers an approximate starting wavelength for the IR excess. The IRS column designates whether this study was able to acquire IRS spectra from the Enhanced Products Archive, which in many cases supplements the IR excess we report.

[a] : This flag indicates that the disk has been resolved through scattered light and plotted in Figure 2.17.

[b] : This flag indicates that the distance shown is from the SED, as described in detail in the text (Section 2.3.2)

Appendix C

Measurements and Methods of Age-Dating for Prime and Reserved Catalog Stars

Table C.1: Measurements and Methods of Age-Dating for Prime and Reserved Catalog Stars

Name	Catalog	Obs. MJD	Instrument	Hα (mÅ)	Li6708 (mÅ)	$v \sin(i)$ (kms^{-1})	RV (kms^{-1})	[Fe/H] (dex)	log (g)	log ($\frac{L_X}{L_{bol}}$)	log (R'_{HK})	Multiple Ref.	Age (Myr)	Age-Dating Method	Refs	Notes
HR 9102	P	–	–	–	–	341.00	18.40±1	–	–	–	–	–	485^{+110}_{-60}	CMD	62,13,-,-	–
HD 105	P	54249.40950	VUA	1196	146	15.84	2.29±0.60	-0.12±0.01	4.46±0.02	-4.41	-4.60	–	30^{+345}_{-0}	Tuc-Hor (X-ray)	1,1,1,10/30	–
HD 166	P	53253.12860	OEA	1040	76	5.40	1.88±1.32	0.15±0.02	–	-4.39	–	WDS	375^{+0}_{-0}	Li	1,1,29,-	X-ray agreement
HD 203	P	57323.49316 57320.46287	SEO SWO	3238	0	96.75	-0.28±11.15	-0.87±0.02	3.65±0.18	–	–	–	15^{+610}_{-0}	β Pic (Li)	1,1,1,30	–
HD 377	P	56561.92090	OSA	1116	145	15.96	1.62±21.75	-0.06±0.02	4.34±0.04	-4.20	-4.54	–	125^{+250}_{-0}	Li (X-ray)	1,1,1,-	–
sig And	P	–	–	–	–	123.00	-8.20±1	–	–	–	–	WDS,10	665^{+65}_{-120}	CMD	61,13,-,-	–
HD 1466	P	53311.16184	EHA	1381	134	20.60	7.06±2.84	-0.13±0.04	4.44±0.09	-4.18	-4.60	WDS	30^{+345}_{-0}	Tuc-Hor (X-ray)	1,1,1,10/30	Li agreement
HD 1461	P	51150.78318	OEA	1132	11	3.09	-8.32±1.31	0.16±0.03	–	–	–	–	0^{+0}_{-625}	Li	1,1,29,-	–
9 Cet	P	53624.24352	EHA	1233	82	7.88	-2.36±0.44	0.19±0.01	4.58±0.03	-4.64	-4.69	WDS	625^{+0}_{-0}	Li	1,1,1,-	X-ray agreement
kap Phe	P	–	–	–	–	213.00	11.30±3	±-0.04	–	–	–	–	940^{+30}_{-140}	CMD	21,13,4,-	–
HD 2834	P	–	–	–	–	111.00	-2.00±4	–	–	–	–	WDS	520^{+55}_{-120}	CMD	12,13,-,-	–
HD 2772	P	–	–	–	–	253.00	-12.20±1	–	–	–	–	WDS	195^{+30}_{-40}	CMD	61,13-,-,-	–
bet03 Tuc	P	53278.33238	EHA	4505	0	82.45	7.70±1	–	–	–	–	CCDM	30^{+170}_{-0}	Tuc-Hor (CMD)	1,13,-,10/30	–
HD 3126	P	53358.03861	EHA	1599	58	24.15	12.25±3.86	0.09±0.08	4.08±0.14	-4.53	-4.68	–	625^{+0}_{-0}	Li	1,1,1,-	X-ray agreement
HD 3296	P	57293.62442 57358.44166	SWO SEO	1986	18	22.49	6.69±3.65	0.07±0.02	4.10±0.04	-5.10	–	–	625^{+0}_{-0}	Li	1,1,1,-	X-ray agreement
HD 3670	P	57293.59045 57358.45082	SWO SEO	2142	90	29.30	5.26±5.08	0.10±0.02	4.15±0.05	-4.46	–	–	125^{+250}_{-0}	Li (X-ray)	1,1,1,-	–
64 Psc	P	56138.43972	EHA	1665	59	2.97	3.76±0	-0.20±0.02	4.25±0.07	-6.41	–	CCDM	625^{+4000}_{-0}	Li (X-ray)	1,13,1,-	spec. binary
HD 5133	P	53359.03329	EHA	934	0	4.94	-13.05±0.22	0.11±0.02	4.60±0.03	-5.29	-4.80	–	100^{+50}_{-50}	CMD	1,1,1,-	–
66 Psc	P	–	–	–	–	144.00	8.50±3	–	–	–	–	CCDM	375^{+95}_{-60}	CMD	62,13,-,-	–
V443 And	P	57272.42065	DMO	1121	0	12.24	-34.10±1	-0.15±0.03	–	-5.23	–	WDS	0^{+2000}_{-0}	X-ray	1,13,49,-	–
HR 333	P	–	–	–	–	207.00	10.00±4	–	–	–	–	–	595^{+90}_{-50}	CMD	62,13,-,-	–
HD 7570	P	52236.01297	VUA	1343	74	5.30	11.08±0.21	0.09±0.01	4.22±0.02	-6.42	-5.14	–	625^{+4000}_{-0}	Li (X-ray)	1,1,1,-	–
HD 7590	P	53255.11679	OEA	1290	91	8.00	-11.52±2.12	-0.13±0.01	4.40±0.03	-4.73	–	–	375^{+250}_{-0}	Li (X-ray)	1,1,1,-	–
2MASS J01203226-1128035	P	55391.41051	VUA	851	151	8.47	10.65±0.20	-0.07±0.01	4.63±0.01	-4.37	–	–	110^{+15}_{-0}	AB Dor (Li)	1,1,1,10/30	CMD agreement
HD 8907	P	55096.10068	OSA	1325	65	13.97	8.77±21.22	-0.13±0.02	4.17±0.03	-4.40	-4.59	–	625^{+0}_{-250}	Li (X-ray)	1,1,1,-	–
EO Psc	P	57287.37616	DMO	888	0	13.35	–	–	–	-4.70	–	WDS	21^{+600}_{-0}	CMD (X-ray)	1,-,-,-	–
49 Cet	P	53986.35559	EHA	6407	0	140.43	10.30±1	–	–	–	–	–	470^{+115}_{-145}	CMD	1,13,-,-	–
EX Cet	P	51563.74172	OEA	960	97	5.83	14.72±1.27	0.06±0.02	4.44±0.03	-4.47	–	WDS	8^{+370}_{-0}	TWA (Li)	1,1,1,10	–
HD 10472	P	55094.26260	EHA	2603	131	66.75	–	-0.41±0.03	3.64±0.22	–	–	–	15^{+1330}_{-0}	Li (CMD)	1,-,1,-	–
HD 10647	P	55430.17214	VUA	1445	63	6.05	25.86±0.76	0.01±0.01	4.52±0.04	–	-4.94	–	110^{+515}_{-0}	AB Dor (Li)	1,1,1,1	–
tau Cet	P	55413.50457	EHA	1071	3	1.62	-16.57±0.29	-0.25±0.01	4.58±0.01	-6.92	-5.14	WDS	625^{+4000}_{-0}	Li (X-ray)	1,1,1,-	–

Continued on Next Page...

Table C.1 – Continued

Name	Catalog	Obs. MJD	Instrument	Hα (mÅ)	Li6708 (mÅ)	$v \sin(i)$ (kms^{-1})	RV (kms^{-1})	[Fe/H] (dex)	log (g)	log ($\frac{L_X}{L_{bol}}$)	log (R'_{HK})	Multiple Ref.	Age (Myr)	Age-Dating Method	Refs	Notes
HD 10638	P	–	–	–	–	–	-0.40±3	–	–	–	–	–	470^{+225}_{-220}	CMD	-,13,-,-	–
HD 10939	P	–	–	–	–	72.80	9.50±3	–	–	–	–	–	605^{+80}_{-50}	CMD	21,13,-,-	–
TYC8850-1468-1	P	57358.48478 57320.54567	SEO SWO	1295	0	23.83	24.70±2.13	0.86±0.05	1.25±0.22	–	–	–	*****	–	1,1,1,-	giant:Gaia
DK Cet	P	54281.37285	VUA	1072	178	17.39	7.50±0.60	-0.21±0.01	4.41±0.02	-4.02	-4.48	WDS,5	30^{+95}_{-0}	Tuc-Hor (X-ray)	1,1,1,10/30	Li agreement
eps Tri	P	–	–	–	–	107.00	0.00±1	–	–	–	–	WDS	525^{+300}_{-25}	CMD	62,13,-,-	–
HD 13246	P	54755.14922	VUA	1536	138	33.21	9.32±2.16	0.08±0.03	4.18±0.05	-4.01	–	WDS	30^{+95}_{-0}	Tuc-Hor (X-ray)	1,1,1,10/30	unreliable [Fe/H]
HD 12467	P	–	–	–	–	120.00	-9.00±3	–	–	–	–	–	855^{+40}_{-75}	CMD	21,13,-,-	–
TYC3698-2277-1	P	57272.46885	DMO	3306	12	58.57	–	–	–	–	–	–	0^{+625}_{-0}	Li	1,-,-,-	–
gam Tri	P	53609.03973	OEA	7303	0	118.46	9.90±3	-1.20±0.15	–	–	–	WDS	450^{+75}_{-115}	CMD	1,13,20,-	–
HD 14082B	P	54805.15230	VUA	1181	164	10.96	3.88±0.30	-0.09±0.01	4.33±0.02	-3.91	–	WDS, 44	15^{+110}_{-0}	β Pic (Li)	1,1,1,30	X-ray agreement
HD 15115	P	56168.10397	OSA	2585	74	55.88	4.14±10.17	-0.40±0.03	3.63±0.19	–	–	WDS	15^{+1295}_{-0}	β Pic (CMD)	1,1,1,10/30	–
AG Tri	P	–	–	–	–	–	–	0.00±0.09	–	-3.10	–	WDS, 44	15^{+125}_{-0}	β Pic(X-ray)	-,-,49,30	CMD agreement
phi For	P	–	–	–	–	141.00	–	–	–	–	–	WDS	580^{+105}_{-115}	CMD	12,-,-,-	–
HD 15407	P	57272.44664	DMO	808	236	5.28	-12.70±1	0.15±0.08	–	-5.10	–	WDS	8^{+615}_{-0}	Li (X-ray)	1,13,4,-	–
HD 15745	P	56168.09036	OSA	2524	0	51.19	-0.61±32.61	-0.14±0.02	3.74±0.18	–	–	WDS	630^{+615}_{-555}	CMD	1,1,1,-	–
HD 16743	P	57323.61659 57320.58478	SEO SWO	3289	0	79.28	16.60±10.67	-0.44±0.02	2.88±0.21	–	–	–	625^{+545}_{-0}	Li (CMD)	1,1,1,-	–
33 Ari	P	–	–	–	–	107.00	18.30±3	–	–	–	–	WDS	750^{+15}_{-40}	CMD	61,13,-,-	–
HR 826	P	57323.71523 57320.60493	SEO SWO	2857	2	57.42	8.08±8.41	0.53±0.02	3.90±0.08	–	–	–	30^{+595}_{-0}	Tuc-Hor (X-ray)	1,1,1,1	–
HD 17848	P	53601.40964	EHA	5567	0	109.49	±30.90	–	–	–	–	–	760^{+55}_{-120}	CMD	1,13,-,-	–
41 Ari	P	53609.07431	OEA	5076	0	105.42	±4.00	–	–	–	–	CCDM	180^{+55}_{-20}	CMD	1,13,-,-	–
HR 857	P	53923.39339	VUA	881	205	10.02	19.41±0.50	0.25±0.02	4.89±0.05	-4.19	–	WDS	30^{+120}_{-0}	Li (CMD)	1,1,1,-	X-ray agreement
HD 19257	P	53344.96034	OEA	4131	0	83.83	±7.40	–	–	–	–	–	995^{+270}_{-295}	CMD	1,13,-,-	–
IS Eri	P	56574.60966	OSA	889	185	7.25	14.89±4.65	-0.05±0.01	4.52±0.02	–	-4.62	WDS	110^{+15}_{-0}	AB Dor (X-ray)	1,1,1,10/30	–
94 Cet	P	52141.34856	VUA	1372	6	9.02	18.46±0.30	0.04±0.01	3.94±0.02	–	-5.05	WDS	0^{+0}_{-625}	Li	1,1,1,-	–
zet Eri	P	–	–	–	–	72.30	-5.80±4	–	–	–	–	WDS, 44	920^{+115}_{-5}	CMD	21,13,-,-	–
zet02 Ret	P	54736.22201	EHA	1223	8	2.58	12.00±0.37	-0.15±0.01	4.57±0.02	–	-5.08	WDS	0^{+0}_{-625}	Li	1,1,1,-	–
TYC3706-340-1	P	56679.31672	LHO	1351	0	15.08	-5.78±4.52	-0.35±0.02	2.71±0.06	–	–	–	12^{+0}_{-0}	CMD	1,1,1,-	–
HD 278507	P	56257.34263	LHO	1440	16	9.86	60.41±36.77	-0.68±0.01	2.13±0.05	–	–	–	*****	–	1,1,1,-	giant:Gaia
HD 21997	P	–	–	–	–	70.00	–	–	–	–	–	WDS	500^{+190}_{-100}	CMD	62,-,-,-	–
eps Eri	P	52237.20024	VUA	896	6	6.31	12.58±0.15	-0.03±0.01	4.15±0.02	-4.83	-4.79	WDS	625^{+0}_{-575}	Li (CMD)	1,1,1,-	X-ray agreement
HD 22179	P	52605.98308	OEA	1147	195	26.27	7.58±8.22	0.05±0.03	4.26±0.06	-3.55	–	WDS	30^{+95}_{-0}	Li (X-ray)	1,1,1,-	–
10 Tau	P	56969.08194	OSA	1355	43	4.00	28.16±6.36	-0.08±0.01	4.09±0.01	–	-4.76	–	110^{+515}_{-0}	AB Dor (X-ray)	1,1,1,1	–
HD 23281	P	–	–	–	–	78.60	–	–	–	–	–	–	450^{+190}_{-185}	CMD	17,-,-,-	–
TYC1799-73-1	P	–	–	–	–	40.70	–	–	–	–	–	–	125^{+0}_{-0}	Pleiades	21,-,-,50	–
HD 23356	P	52940.23779	EHA	930	8	5.84	25.34±0.22	0.09±0.01	4.62±0.01	-5.11	-4.88	–	375^{+0}_{-225}	Li (CMD)	1,1,1,-	X-ray agreement

Continued on Next Page...

Table C.1 – Continued

Name	Catalog	Obs. MJD	Instrument	Hα (mÅ)	Li6708 (mÅ)	$v \sin(i)$ (kms^{-1})	RV (kms^{-1})	[Fe/H] (dex)	log (g)	log ($\frac{L_X}{L_{bol}}$)	log (R'_{HK})	Multiple Ref.	Age (Myr)	Age-Dating Method	Refs	Notes
HD 23484	P	57294.71851 57418.43657	SWO SEO	1101	13	11.13	26.53±1.87	0.15±0.02	4.90±0.03	-5.10	–	–	625^{+0}_{-575}	Li (CMD)	1,1,1,-	X-ray agreement
TYC 1803-808-1	P	–	–	–	–	16.80	5.21±0	–	–	–	–	–	125^{+0}_{-0}	Pleiades	21,33,-,50	–
HD 23361	P	–	–	–	–	184.00	11.90±3	–	–	–	–	WDS	125^{+0}_{-0}	Pleiades	21,24,-,50	–
HD 23267	P	–	–	–	–	–	–	–	–	–	–	–	385^{+85}_{-115}	CMD	-,-,-,-	–
HD 23430	P	–	–	–	–	81.30	6.50±2	–	–	–	–	–	650^{+195}_{-185}	CMD	21,13,-,-	–
HD 282954	P	–	–	–	–	20.00	5.70±0	-0.02±0.16	–	–	–	WDS	125^{+0}_{-0}	Pleiades	21,33,26,50	–
V1210 Tau	P	–	–	–	–	85.60	4.30±1	–	–	–	–	–	125^{+670}_{-0}	Pleiades (CMD)	21,24,-,50	–
HD 23632	P	–	–	–	–	193.00	4.90±1	0.05±0.28	–	–	–	WDS	125^{+365}_{-0}	Pleiades (CMD)	21,13,49,50	–
V1229 Tau	P	53038.90598	OEA	2107	0	23.79	±5.40	–	–	–	–	WDS	525^{+65}_{-145}	CMD	1,19,-,-	eclipsing binary
HD 24636	P	56122.42264	VUA	2012	56	25.12	15.50±1	0.21±0.03	4.11±0.06	–	–	–	30^{+1540}_{-0}	Tuc-Hor (CMD)	1,30,1,10/30	Li agreement
HD 23863	P	–	–	–	–	137.00	3.30±2	0.03±0.11	–	–	–	–	125^{+0}_{-0}	Pleiades	21,24,49,50	–
HD 24141	P	–	–	–	–	54.80	-0.20±1	–	–	–	–	WDS	690^{+335}_{-175}	CMD	21,13,-,-	–
HD 24966	P	–	–	–	–	–	–	–	–	–	–	–	125^{+75}_{-45}	CMD	-,-,-,-	–
HD 24817	P	–	–	–	–	285.00	12.00±5	–	–	–	–	–	415^{+85}_{-165}	CMD	61,13,-,-	–
HD 25457	P	55391.41991	VUA	1528	109	18.64	17.42±0.91	0.04±0.02	4.51±0.02	-4.22	–	–	125^{+0}_{-0}	Li (X-ray)	1,1,1,-	Li agreement
HR 1254	P	57358.59295	SEO	1871	0	34.36	38.20±1	0.66±0.04	3.89±0.13	–	–	–	1630^{+80}_{-390}	CMD	1,13,1,-	–
V1299 Tau	P	–	–	–	–	72.23	12.75±1	–	–	-3.12	–	WDS	0^{+125}_{-0}	X-ray	57,57,-,-	–
50 Per	P	52884.08181	OEA	1618	82	18.65	28.02±4.68	-0.11±0.10	–	-4.46	–	–	125^{+250}_{-0}	Li (X-ray)	1,1,49,-	–
HD 281683	P	56257.35024	LHO	1347	0	15.12	-28.18±100.34	-0.65±0.02	2.91±0.05	–	–	–	*****	–	1,1,1,-	–
gam Dor	P	52537.41512	VUA	2959	0	57.78	25.20±0	–	–	–	–	–	1235^{+150}_{-225}	CMD	-,13,-,-	–
HD 27045	P	–	–	–	–	70.10	15.00±1	–	–	–	–	WDS	795^{+190}_{-210}	CMD	21,13,-,-	–
HD 27026	P	54829.06755	OSA	5716	0	9.73	±6.50	–	–	–	–	–	250^{+35}_{-50}	CMD	-,13,-,-	–
chi Tau	P	57287.31855	DMO	1358	44	12.33	13.99±0	–	–	–	–	WDS	355^{+30}_{-50}	CMD	-,13,-,-	–
b Tau	P	53658.98896	OEA	3524	0	56.82	±27.10	0.20±0.15	–	–	–	–	*****	–	1,20,20,-	–
HD 28447	P	57287.32682	DMO	1197	25	11.17	24.80±1	-0.12±0.01	–	–	–	–	625^{+0}_{-0}	Li	1,13,27,-	–
51 Eri	P	50830.85620	OEA	2881	0	63.65	12.60±0	0.00±0.01	–	–	–	CCDM	15^{+55}_{-0}	β Pic (CMD)	1,13,41,30	–
CPD-35 525	P	57293.74192	SWO	1090	172	23.23	22.90±2.14	–	–	–	–	–	30^{+95}_{-0}	Columba (Li)	1,1,-,1	CMD agreement
HD 30051	P	56138.34789	VUA	2232	56	23.19	21.15±1.31	0.05±0.04	4.02±0.06	–	–	–	30^{+95}_{-0}	Tuc-Hor (X-ray)	1,1,1,30	–
EX Eri	P	–	–	–	–	128.00	–	–	–	–	–	–	365^{+155}_{-165}	CMD	61,-,-,-	–
HD 30447	P	56988.16957	EHA	2800	57	67.98	21.30±2	-0.15±0.04	3.57±0.24	–	–	WDS	30^{+1075}_{-0}	Columba (CMD)	1,30,1,10/30	–
58 Eri	P	53956.35177	VUA	1238	56	8.00	23.67±0.61	0.09±0.02	4.53±0.05	-4.78	-4.75	–	40^{+585}_{-0}	Argus (Li)	1,1,1,1	–
HD 32195	P	56138.34703	VUA	1649	150	48.06	11.43±3.52	0.19±0.03	4.00±0.08	-3.91	–	–	30^{+95}_{-0}	Tuc-Hor (X-ray)	1,1,1,10/30	Li agreement
HD 31392	P	57418.49913	SEO	989	9	10.38	6.04±60.25	0.91±0.01	3.44±0.03	–	–	–	625^{+0}_{-0}	Li	1,1,1,-	–
HD 31295	P	53323.99845	OEA	4898	0	105.11	11.10±1	±-0.89	–	–	–	WDS	495^{+120}_{-180}	CMD	1,13,8,-	–
HD 32297	P	56168.12635	OSA	2774	0	32.98	±23.00	-0.44±0.15	–	–	–	–	240^{+240}_{-230}	CMD	1,13,20,-	–

Continued on Next Page...

Table C.1 – Continued

Name	Catalog	Obs. MJD	Instrument	Hα (mÅ)	Li6708 (mÅ)	$v \sin(i)$ (kms^{-1})	RV (kms^{-1})	[Fe/H] (dex)	log (g)	log ($\frac{L_X}{L_{bol}}$)	log (R'_{HK})	Multiple Ref.	Age (Myr)	Age-Dating Method	Refs	Notes
iot Tau	P	53657.15013	OEA	4526	0	83.00	38.30±1	±0.15	–	–	–	WDS	625^{+370}_{-0}	Hyades (CMD)	1,13,4,38	–
zet Dor	P	–	–	–	–	15.40	-1.30±0	-0.17±0.08	–	-5.08	–	WDS	15^{+610}_{-0}	β Pic (X-ray)	3,13,43,1	–
HD 33081	P	55824.41520	EHA	1479	0	7.68	-11.46±0.74	-0.11±0.03	3.88±0.09	–	-5.03	–	*****	–	1,1,1,-	–
l Tau	P	53609.14984	OEA	4210	0	86.53	-1.70±4	–	–	–	–	–	840^{+35}_{-70}	CMD	1,13,-,-	–
HD 33636	P	53361.10825	VUA	1232	52	4.66	4.18±0.21	-0.21±0.01	4.28±0.01	–	-4.62	–	625^{+0}_{-0}	Li	1,1,1,-	–
HD 34324	P	–	–	–	–	–	–	–	–	–	–	–	640^{+60}_{-325}	CMD	-,-,-,-	–
AS Col	P	57358.65984	SEO	1254	60	21.00	37.92±10.10	-0.23±0.02	3.73±0.08	-3.86	–	–	625^{+0}_{-250}	Li (X-ray)	34,1,1,-	–
16 Cam	P	53323.10340	OEA	923	0	136.41	12.00±4	–	–	–	–	WDS	455^{+55}_{-45}	CMD	1,13,-,-	–
TYC9162-586-1	P	57321.73690	SWO	998	0	–	-6.34±1.88	–	–	–	–	–	22^{+8}_{-7}	CMD	-,1,-,-	–
HD 35841	P	57432.43146	SEO	1264	111	34.21	–	-0.05±0.02	4.27±0.04	–	–	–	30^{+0}_{-0}	Li	1,-,1,-	–
AF Lep	P	53332.23537	EHA	1578	126	54.69	17.36±2.17	0.17±0.03	3.81±0.17	-3.53	-4.53	44	15^{+110}_{-0}	β Pic (Li)	1,1,1,10/30	X-ray agreement
HD 36968	P	57432.44604	SEO	1769	0	40.02	15.00±2	-0.11±0.02	4.10±0.07	–	–	–	1105^{+370}_{-935}	CMD	1,35,1,-	–
TYC1852-1694-1	P	57081.16487	DMO	1963	0	5.93	±20.40	–	–	–	–	–	610^{+5}_{-140}	CMD	1,13,-,-	–
HR 1915	P	–	–	–	–	66.40	22.40±1	–	–	–	–	WDS	50^{+50}_{-0}	Tuc-Hor (CMD)	21,30,-,10/30	assumed ZAMS
HD 37306	P	53774.10292	EHA	5316	0	104.68	±23.00	–	–	–	–	–	320^{+140}_{-320}	CMD	1,13,-,-	–
HD 37484	P	57418.51274	SEO	1449	67	46.05	23.50±0	-0.18±0.02	2.10±0.11	-5.03	–	–	30^{+595}_{-0}	Columba (X-ray)	1,30,1,30	Li agreement
HD 38207	P	–	–	–	–	69.88	24.77±1	–	–	–	–	–	1930^{+645}_{-380}	CMD	57,57,-,-	–
HR 1975	P	56049.96698	EHA	2335	0	37.72	25.30±0	±0.06	–	–	–	–	30^{+20}_{-0}	Columba (CMD)	1,13,49,10/30	–
HD 38529	P	55910.25780	VUA	1224	18	5.46	24.48±0.16	0.26±0.01	3.81±0.02	-5.46	–	WDS	625^{+0}_{-0}	Li	1,1,1,-	–
zet Lep	P	–	–	–	–	229.00	–	–	–	–	–	–	705^{+65}_{-95}	CMD	62,-,-,-	–
bet Pic	P	52942.25597	EHA	4817	0	102.01	20.00±1	±0.05	–	–	–	WDS	15^{+205}_{-0}	β Pic (CMD)	1,13,23,1	–
HD 38858	P	50835.91659	OEA	1150	9	3.39	29.21±1.62	-0.25±0.01	–	-6.11	–	–	110^{+515}_{-0}	AB Dor (Li)	1,1,29,1	X-ray no agreement
HD 40307	P	55910.25231	EHA	934	5	4.61	31.29±0.19	-0.11±0.01	4.55±0.01	-6.35	-5.00	–	40^{+335}_{-0}	IC 2391 (X-ray)	1,1,1,63;1	CMD agreement
HD 39415	P	57081.21046	DMO	2139	24	180.39	–	–	–	–	–	–	0^{+0}_{-625}	Li	1,-,-,-	–
eta Lep	P	55172.24296	EHA	2596	24	16.07	-2.14±0	-0.38±0.02	2.90±0.09	–	–	–	30^{+1425}_{-0}	Li (CMD)	1,13,1,-	–
HD 40540	P	–	–	–	–	–	–	–	–	–	–	–	705^{+315}_{-345}	CMD	-,-,-,-	–
HD 40979	P	54400.10457	OSA	1317	81	8.03	32.65±8.50	0.10±0.01	4.16±0.02	–	-4.79	WDS	625^{+0}_{-0}	Li	1,1,1,-	–
HD 43162	P	57418.53234	SEO	1009	63	11.61	-3.45±38.59	0.75±0.01	3.90±0.02	-4.34	–	WDS	625^{+0}_{-250}	Li (X-ray)	1,1,1,-	–
HD 43319	P	–	–	–	–	76.00	–	–	–	–	–	WDS	560^{+95}_{-135}	CMD	61,-,-,-	–
V1358 Ori	P	–	–	–	–	45.55	19.10±2	–	–	-3.67	–	–	30^{+95}_{-0}	Columba (X-ray)	57,30,-,10/30	–
AB Pic	P	54226.99146	VUA	489	288	12.62	24.08±0.32	-0.10±0.01	4.31±0.02	-3.32	-4.90	WDS	30^{+95}_{-5}	Carina (X-ray,CMD)	1,1,1,30	Li agreement
HD 45184	P	57358.70120	SEO	1084	41	9.92	-5.46±16.60	0.11±0.02	4.35±0.03	–	–	–	625^{+0}_{-0}	Li	1,1,1,-	–
HD 46190	P	–	–	–	–	–	–	–	–	–	–	–	315^{+95}_{-190}	CMD	-,-,-,-	–
HD 53842	P	54167.12406	MFA	1776	93	29.50	15.35±13.00	-0.12±0.02	4.18±0.03	-4.45	-4.79	–	30^{+95}_{-0}	Tuc-Hor (X-ray)	1,1,1,10/30	Li agreement

Continued on Next Page...

Table C.1 – Continued

Name	Catalog	Obs. MJD	Instrument	Hα (mÅ)	Li6708 (mÅ)	$v \sin(i)$ (kms^{-1})	RV (kms^{-1})	[Fe/H] (dex)	log (g)	log ($\frac{L_X}{L_{bol}}$)	log (R'_{HK})	Multiple Ref.	Age (Myr)	Age-Dating Method	Refs	Notes
56 Aur	P	53075.86284	OEA	1303	60	5.67	-22.86±1.73	0.09±0.02	–	-5.83	–	WDS	15^{+610}_{-0}	β Pic (Li)	1,1,29,1	X-ray no agreement
HR 2562	P	57418.54037	SEO	1454	25	44.35	22.10±1	0.07±0.01	4.90±0.00	-5.28	–	–	30^{+595}_{-0}	Carina (Li)	1,13,1,1	X-ray agreement
HD 50554	P	52717.81867	OEA	1315	47	3.67	-2.36±1.72	-0.08±0.01	4.23±0.03	–	–	–	625^{+0}_{-0}	Li	1,1,1,-	–
pi. CMa	P	–	–	–	–	92.30	-37.90±6	±-0.13	–	–	–	WDS	1820^{+135}_{-585}	CMD	21,13,4,-	–
HD 53143	P	54167.21422	MFA	1004	22	7.27	22.38±1.46	0.09±0.01	4.73±0.02	-4.72	-4.69	WDS	625^{+0}_{-585}	Li (CMD)	1,1,1,-	X-ray agreement
HD 52265	P	53784.84102	OEA	1309	71	3.60	56.06±1.69	0.14±0.01	4.10±0.03	–	–	–	625^{+0}_{-0}	Li	1,1,1,-	–
HD 54341	P	–	–	–	–	–	–	–	–	–	–	–	250^{+85}_{-130}	CMD	-,-,-,-	–
bet CMi	P	52361.83882	OEA	-3925	0	105.05	22.00±2	–	–	–	–	WDS	255^{+50}_{-20}	CMD	1,13,-,-	–
HD 59967	P	56283.22537	MFA	1153	94	5.18	9.76±37.37	-0.11±0.01	4.51±0.01	-4.51	-4.72	–	375^{+0}_{-0}	Li	1,1,1,-	X-ray agreement
HD 61005	P	56179.37546	VUA	975	171	10.70	24.40±0.29	-0.23±0.01	4.90±0.00	–	-4.52	WDS	40^{+95}_{-0}	Argus (Li)	1,1,1,30	–
HD 69830	P	55915.29380	VUA	1076	12	3.56	28.33±0.16	-0.06±0.01	3.93±0.02	-5.95	-5.08	–	625^{+4000}_{-0}	Li (X-ray)	1,1,1,-	–
HD 70298	P	51896.06093	OEA	1632	2	11.58	-10.70±4.23	-0.36±0.08	–	–	–	–	0^{+0}_{-625}	Li	1,1,4,-	–
HD 71043	P	57358.72694	SEO	2395	0	70.91	22.50±1	–	–	–	–	WDS	30^{+55}_{-0}	Carina (CMD)	1,13,-,1	–
HD 70313	P	53847.86281	OEA	4578	0	74.10	21.30±3	-0.30±0.15	–	–	–	–	695^{+90}_{-75}	CMD	1,13,20,-	–
30 Mon	P	50408.14580	OEA	5353	0	89.61	10.00±2	-0.40±0.01	–	–	–	WDS	395^{+5}_{-145}	CMD	1,13,41,-	–
HD 71722	P	–	–	–	–	146.00	30.20±1	–	–	–	–	–	200^{+175}_{-200}	CMD	12,13,-,-	–
HD 72687	P	57358.75539	SEO	957	127	11.36	20.60±18.00	0.03±0.02	4.55±0.03	-4.25	–	–	125^{+95}_{-0}	Li (X-ray)	1,1,1,-	–
HR 3383	P	53007.05406	OEA	1688	0	1.69	±2.80	-0.20±0.15	–	–	–	–	415^{+30}_{-60}	CMD	1,13,42,-	–
HD 73526	P	53452.03638	VUA	1149	15	4.26	24.13±0.15	0.20±0.01	4.19±0.01	–	–	–	625^{+0}_{-0}	Li	1,1,1,-	–
V401 Hya	P	56298.28360	EHA	1197	42	4.48	35.46±0.34	0.09±0.01	4.49±0.02	-4.83	-4.72	WDS	625^{+0}_{-0}	Li	1,1,1,-	X-ray agreement
pi.01 UMa	P	51534.04544	OEA	1159	100	9.28	-12.23±2.28	-0.10±0.01	4.60±0.02	-4.51	–	–	40^{+585}_{-0}	Argus (Li)	1,1,1,1	X-ray agreement
eta Cha	P	57432.67936	SEO	1418	0	68.12	14.00±7	–	–	–	–	WDS	6^{+25}_{-0}	η Cha (CMD)	1,13,-,31	–
EK Cha	P	–	–	–	–	–	–	–	–	–	–	–	6^{+0}_{-0}	η Cha	-,-,-,31	–
50 Cnc	P	56049.07272	EHA	4812	0	76.61	23.30±3	–	–	–	–	–	20^{+135}_{-15}	CMD	1,13,-,-	–
HD 75616	P	55579.05265	OSA	1319	64	11.16	-6.23±15.03	-0.33±0.01	4.15±0.03	-4.61	-4.65	–	625^{+0}_{-250}	Li (X-ray)	1,1,1,-	–
HD 76151	P	52946.36529	EHA	1167	18	2.83	32.06±0.29	0.11±0.01	4.52±0.01	-5.30	-4.98	–	625^{+2000}_{-0}	Li (X-ray)	1,1,1,-	–
HD 76748	P	57434.64188	SWO	1154	17	1.80	41.35±2.28	-0.07±0.08	–	–	–	WDS	625^{+0}_{-575}	Li (CMD)	21,1,4,-	–
HR 3570	P	53881.00094	EHA	1591	45	12.04	-5.90±0	-0.05±0.01	4.31±0.04	-4.69	–	–	625^{+0}_{-250}	Li (X-ray)	1,13,1,-	–
omi02 Cnc	P	54081.13728	OSA	3097	0	73.11	-4.00±4	–	–	–	–	–	755^{+25}_{-150}	CMD	1,13,-,-	–
HR 3638	P	–	–	–	–	222.00	16.90±2	–	–	–	–	WDS	420^{+85}_{-105}	CMD	62,13,-,-	–
HR 3651	P	–	–	–	–	172.00	22.60±2	–	–	–	–	–	380^{+105}_{-100}	CMD	62,13,-,-	–
HR 3721	P	–	–	–	–	40.00	±11.20	–	–	–	–	–	290^{+65}_{-80}	CMD	62,13,-,-	–
HD 82443	P	53078.91704	OEA	888	182	11.82	7.87±1.58	-0.07±0.01	4.65±0.02	-3.97	–	WDS	125^{+0}_{-0}	Li	1,1,1,-	X-ray agreement
HD 82943	P	51973.10323	VUA	1259	46	4.47	4.24±0.17	0.25±0.01	4.46±0.01	–	-5.07	–	625^{+0}_{-0}	Li	1,1,1,-	–

Continued on Next Page. . .

Table C.1 – Continued

Name	Catalog	Obs. MJD	Instrument	Hα (mÅ)	Li6708 (mÅ)	$v \sin(i)$ (kms^{-1})	RV (kms^{-1})	[Fe/H] (dex)	$\log(g)$	$\log(\frac{L_X}{L_{bol}})$	$\log(R'_{HK})$	Multiple Ref.	Age (Myr)	Age-Dating Method	Refs	Notes
HD 84075	P	54898.18329	VUA	1332	162	18.02	4.12±0.80	-0.04±0.02	4.59±0.02	-4.37	-4.58	–	40^{+335}_{-0}	Argus (X-ray)	1,1,1,10/30	Li agreement
HD 84870	P	57081.31046	DMO	2756	0	55.73	–	–	–	–	–	WDS	620^{+205}_{-400}	CMD	1,-,-,-	–
HD 85301	P	53093.87130	OEA	1112	51	15.31	15.06±1.55	-0.01±0.01	4.37±0.03	-5.12	–	–	625^{+0}_{-0}	Li	1,1,1,-	X-ray agreement
HD 85672	P	53828.88185	OEA	2131	0	22.02	-5.20±7	–	–	–	–	–	245^{+195}_{-205}	CMD	1,13,-,-	–
HR 3927	P	57434.65389	SWO	3704	0	149.00	13.90±2	–	–	–	–	–	485^{+100}_{-50}	CMD	12,13,-,-	–
21 LMi	P	50501.06050	OEA	4376	0	74.69	-11.40±1	–	–	–	–	–	805^{+175}_{-65}	CMD	1,13,-,-	–
HD 88215	P	56713.35576	LHO	2624	0	71.44	23.60±0	-0.45±0.02	3.81±0.16	–	–	WDS	1360^{+275}_{-240}	CMD	1,13,1,-	–
LW Vel	P	–	–	–	–	201.00	48.10±3	–	–	–	–	–	1275^{+60}_{-25}	CMD	21,13,-,-	–
HD 90874	P	–	–	–	–	64.00	–	–	–	–	–	–	670^{+105}_{-170}	CMD	61,-,-,-	–
HR 4084	P	53038.06476	OEA	2354	14	47.46	-2.93±21.90	-0.19±0.10	–	–	–	–	625^{+0}_{-620}	Li (CMD)	1,1,53,-	–
HR 4132	P	–	–	–	–	128.00	9.00±4	–	–	–	–	WDS	1080^{+115}_{-100}	CMD	61,13,-,-	–
HD 92536	P	–	–	–	–	171.00	±10.00	–	–	–	–	–	185^{+70}_{-65}	CMD	21,13,-,-	–
TWA 7A	P	53402.37176	EHA	-4610	490	9.90	12.05±0.54	-0.23±0.03	4.37±0.08	-2.97	–	WDS	8^{+118}_{-0}	TWA	1,1,1,1	–
V419 Hya	P	53411.26514	EHA	831	154	7.35	22.94±0.31	-0.04±0.01	4.55±0.02	-4.53	-4.81	WDS	125^{+25}_{-75}	Li (CMD)	1,1,1,-	–
HD 93738	P	–	–	–	–	201.00	±4.00	–	–	–	–	WDS	465^{+45}_{-75}	CMD	21,13,-,-	–
TYC8203-154-1	P	–	–	–	–	–	–	–	–	–	–	–	500^{+345}_{-445}	CMD	-,-,-,-	–
TYC8962-532-1	P	57431.68839	SWO	-152	30	–	36.29±2.49	–	–	-4.47	–	–	*****	–	-,1,-,-	giant:Gaia
bet UMa	P	53074.00191	OEA	2815	0	44.15	-13.10±0	±0.78	–	–	–	–	400^{+5}_{-5}	CMD	1,13,49,-	–
HD 95698	P	56713.35841	LHO	2252	0	36.61	0.70±2	0.10±0.04	4.45±0.09	–	–	WDS	1315^{+170}_{-80}	CMD	1,13,1,-	–
tet Leo	P	–	–	–	–	23.00	7.30±0	-0.16±0.13	–	–	–	–	420^{+70}_{-30}	CMD	61,13,42,-	–
HD 308379	P	57088.58188	SWO	2439	70	24.41	-2.23±8.33	–	–	–	–	–	625^{+0}_{-0}	Li	1,1,-,-	–
HD 98363	P	–	–	–	–	–	9.60±1	–	–	–	–	–	10^{+740}_{-0}	LCC (CMD)	-,13,-,15	–
HR 4388	P	57081.34193	DMO	3792	0	116.28	-10.00±4	–	–	–	–	–	1020^{+95}_{-75}	CMD	1,13,-,-	–
HD 98800	P	50842.12615	OEA	234	329	18.90	20.54±1.28	–	–	-3.31	–	CCDM	15^{+110}_{-0}	Li (X-ray,CMD)	1,1,-,-	–
TWA 30A	P	–	–	–	–	–	–	–	–	-2.89	–	–	8^{+118}_{-0}	TWA (X-ray)	-,-,-,48	–
HD 101088	P	–	–	–	–	152.00	±17.80	0.08±0.08	–	-4.12	–	WDS	10^{+115}_{-0}	LCC (X-ray)	9,13,4,15	–
HD 102458	P	56706.31190	EHA	1147	212	29.68	14.40±0	0.05±0.06	4.07±0.09	-3.21	-4.38	WDS	10^{+115}_{-0}	LCC (X-ray)	1,30,1,36	–
bet Leo	P	56389.00145	OSA	2793	0	98.41	-0.20±0	±0.07	–	–	–	WDS, 44	485^{+20}_{-45}	CMD	1,13,4,-	–
HD 103234	P	–	–	–	–	57.00	8.00±1	–	–	–	–	–	10^{+2100}_{-0}	LCC (CMD)	9,13,-,15	–
HD 103266	P	–	–	–	–	146.00	–	–	–	–	–	–	635^{+115}_{-105}	CMD	12,-,-,-	–
TYC8981-4034-1	P	57431.69910	SWO	1198	24	–	-15.98±1.85	–	–	–	–	–	*****	–	-,1,-,-	giant:Gaia
HD 103703	P	54870.23109	MFA	2183	88	46.84	8.00±1	-0.33±0.01	4.12±0.05	–	–	WDS	10^{+115}_{-0}	LCC (Li)	1,13,1,15	–
HD 104231	P	–	–	–	–	–	7.70±1	–	–	-4.65	–	WDS	10^{+365}_{-0}	LCC (X-ray)	-,13,-,15	–
HR 4597	P	–	–	–	–	214.00	7.60±4	–	–	–	–	–	10^{+20}_{-0}	LCC (CMD)	61,13,-,15	–
HD 104860	P	57081.35381	DMO	1251	11	8.79	-11.73±0	-0.22±0.08	–	-4.41	–	WDS	0^{+0}_{-375}	X-ray	1,13,4,-	–

Continued on Next Page. . .

Table C.1 – Continued

Name	Catalog	Obs. MJD	Instrument	Hα (mÅ)	Li6708 (mÅ)	$v \sin(i)$ (kms^{-1})	RV (kms^{-1})	[Fe/H] (dex)	log (g)	log ($\frac{L_X}{L_{bol}}$)	log (R'_{HK})	Multiple Ref.	Age (Myr)	Age-Dating Method	Refs	Notes
eta Cru	P	52080.94919	VUA	2799	36	49.61	±10.40	-0.05±0.03	3.85±0.11	–	–	WDS	30^{+1430}_{-0}	Li (CMD)	1,13,1,-	–
EF Cha	P	–	–	–	–	–	–	–	–	–	–	–	1165^{+275}_{-95}	CMD	-,-,-,-	–
TYC 8241-2652-1	P	57431.70834	SWO	-17	421	–	14.35±1.89	–	–	-3.01	–	–	8^{+115}_{-0}	Li (X-ray)	-,1,-,-	–
HD 105613	P	–	–	–	–	–	7.40±1	–	–	–	–	–	10^{+40}_{-0}	LCC (CMD)	-,13,-,15	–
3 Crv	P	–	–	–	–	135.00	–	–	–	–	–	–	505^{+125}_{-110}	CMD	61,-,-,-	–
HD 105857	P	–	–	–	–	–	7.20±1	–	–	–	–	–	10^{+560}_{-0}	LCC (CMD)	-,13,-,15	–
HD 105912	P	57081.37708	DMO	1485	30	42.30	-5.30±1	-0.08±0.08	–	-5.22	–	–	625^{+0}_{-0}	Li	40,13,4,-	X-ray agreement
HD 106036	P	–	–	–	–	–	7.70±1	–	–	–	–	WDS	10^{+305}_{-0}	LCC (CMD)	-,13,-,15	–
CD-54 4621	P	57431.71939	SWO	384	376	–	16.95±2.31	–	–	-3.23	–	WDS	10^{+115}_{-0}	LCC (X-ray,CMD)	-,1,-,36	–
HD 106252	P	53485.93216	OEA	1228	18	3.89	16.91±1.61	-0.04±0.01	4.28±0.03	–	–	–	0^{+0}_{-625}	Li	1,1,1,-	–
HD 106389	P	–	–	–	–	–	6.20±1	–	–	–	–	WDS	10^{+0}_{-0}	LCC	-,13,-,15	–
HR 4669	P	–	–	–	–	172.00	–	–	–	–	–	WDS	10^{+380}_{-0}	LCC (CMD)	61,-,-,15	–
HD 106906	P	56794.07387	EHA	2270	49	29.77	10.20±2	-0.17±0.03	3.77±0.19	–	–	–	10^{+610}_{-0}	LCC (Li)	1,13,1,15	–
HD 107146	P	53068.04950	OEA	1183	119	7.09	2.49±1.70	-0.14±0.01	4.35±0.03	-4.38	–	WDS	125^{+0}_{-0}	Li	1,1,1,-	–
HR 4692	P	–	–	–	–	209.00	-8.30±3	–	–	–	–	–	10^{+80}_{-0}	LCC (CMD)	61,13,-,15	–
HD 107649	P	–	–	–	–	–	6.10±1	–	–	-4.28	–	WDS	10^{+365}_{-0}	LCC (X-ray)	-,13,-,15	–
CD-52 5008	P	–	–	–	–	–	–	–	–	–	–	–	10^{+0}_{-0}	LCC	-,-,-,36	–
HD 107947	P	–	–	–	–	149.00	7.90±1	–	–	–	–	–	10^{+55}_{-0}	LCC (CMD)	12,13,-,15	–
16 Com	P	53102.90051	OEA	3466	0	65.46	0.40±1	-0.14±0.15	–	–	–	–	700^{+165}_{-10}	CMD	1,13,20,-	–
HD 108874	P	54569.93615	OSA	953	13	2.98	-29.91±3.50	0.39±0.02	4.13±0.04	–	-5.32	–	625^{+0}_{-0}	Li	1,1,1,-	–
HD 108857	P	–	–	–	–	–	6.50±1	–	–	–	–	–	10^{+0}_{-0}	LCC	-,13,-,15	–
eta Crv	P	53016.35074	VUA	2457	81	54.29	-2.80±2	-0.16±0.01	3.77±0.10	–	–	WDS	30^{+1100}_{-0}	Li (CMD)	1,13,1,-	–
HR 4796A	P	–	–	–	–	–	–	–	–	–	–	–	375^{+120}_{-125}	CMD	-,-,-,-	–
f Vir	P	–	–	–	–	154.00	–	–	–	–	–	–	560^{+80}_{-130}	CMD	61,-,-,-	–
HD 109832	P	–	–	–	–	–	7.20±1	–	–	–	–	–	10^{+1000}_{-0}	LCC (CMD)	-,13,-,15	–
HD 110058	P	–	–	–	–	–	5.00±1	–	–	–	–	–	10^{+975}_{-0}	LCC (CMD)	-,13,-,15	–
rho Vir	P	53093.99689	OEA	5872	0	180.12	-0.70±2	±-0.64	–	–	–	WDS	115^{+135}_{-50}	CMD	1,13,49,-	–
HD 110634	P	–	–	–	–	140.00	5.40±1	-0.31±0.15	–	–	–	–	10^{+1475}_{-0}	LCC (CMD)	9,13,4,15	–
HD 111103	P	–	–	–	–	–	5.80±1	–	–	-3.62	–	WDS	10^{+115}_{-0}	LCC (X-ray)	-,13,-,15	–
HD 111347	P	57121.17716	DMO	1938	0	40.87	-3.60±1	-0.10±0.05	–	-4.70	–	–	625^{+0}_{-0}	X-ray	1,13,4,-	–
HD 111520	P	–	–	–	–	–	4.60±1	–	–	-4.34	–	WDS, 18	10^{+365}_{-0}	LCC (X-ray)	-,13,-,15	–
8 Dra	P	52038.86698	OEA	3759	0	81.65	9.00±3	–	–	–	–	–	*****	–	1,13,-,-	–
HD 112383	P	–	–	–	–	–	6.60±1	–	–	–	–	WDS	10^{+305}_{-0}	LCC (CMD)	-,13,-,15	–

Continued on Next Page...

Table C.1 – Continued

Name	Catalog	Obs. MJD	Instrument	Hα (mÅ)	Li6708 (mÅ)	$v \sin(i)$ (kms^{-1})	RV (kms^{-1})	[Fe/H] (dex)	log (g)	log ($\frac{L_X}{L_{bol}}$)	log (R'_{HK})	Multiple Ref.	Age (Myr)	Age-Dating Method	Refs	Notes
HD 112810	P	–	–	–	–	82.00	4.20±1	–	–	–	–	–	10^{+305}_{-0}	LCC (CMD)	9,13,-,15	–
HD 113337	P	54126.21590	OSA	1424	3	8.15	-15.60±12.63	0.29±0.02	3.84±0.06	-5.07	–	WDS, 44	0^{+0}_{-625}	Li	1,1,1,-	X-ray agreement
CPD-52 6110	P	–	–	–	–	–	–	–	–	-3.27	–	–	10^{+115}_{-0}	LCC (X-ray)	-,-,-,36	CMD agreement
HD 113524	P	–	–	–	–	–	3.50±1	–	–	–	–	WDS	10^{+0}_{-0}	LCC	-,13,-,15	–
HD 113457	P	–	–	–	–	149.00	15.00±7	–	–	–	–	WDS	10^{+30}_{-0}	LCC (CMD)	12,13,-,15	–
TYC8656-483-1	P	–	–	–	–	–	–	–	–	-3.44	–	–	125^{+0}_{-0}	X-ray	-,-,-,-	–
HD 113556	P	–	–	–	–	49.00	5.10±1	-0.02±0.08	–	–	–	WDS	10^{+1445}_{-0}	LCC (CMD)	9,13,4,15	–
BD+21 2486	P	51564.19031	OEA	272	34	6.96	-0.22±1.66	–	–	-4.05	–	WDS	30^{+595}_{-0}	Li (X-ray)	1,1,-,-	CMD agreement
HD 113766	P	–	–	–	–	44.90	-1.00±3	-0.01±0.08	–	–	–	WDS	10^{+1955}_{-0}	LCC (CMD)	21,13,4,15	–
HR 4951	P	–	–	–	–	281.00	22.00±4	–	–	–	–	–	10^{+90}_{-0}	LCC (CMD)	21,13,-,15	–
TYC8653-1256-1	P	57092.75544	SWO	1254	6	25.68	-33.36±6.48	–	–	–	–	–	*****	–	1,1,-,-	giant:Gaia
HD 114082	P	–	–	–	–	43.00	5.20±1	–	–	–	–	WDS	10^{+0}_{-0}	LCC	9,13,-,15	–
HR 4978	P	-	–	–	–	201.00	–	–	–	–	–	WDS	1030^{+30}_{-115}	CMD	61,-,-,-	–
HD 115361	P	–	–	–	–	–	5.00±1	–	–	–	–	WDS	10^{+0}_{-0}	LCC	-,13,-,15	–
61 Vir	P	54680.99942	EHA	1120	9	3.29	-7.79±0.28	-0.03±0.01	4.52±0.01	–	-5.19	WDS	625^{+0}_{-0}	Li	1,1,1,-	–
HD 115600	P	–	–	–	–	61.00	4.70±1	–	–	–	–	WDS	10^{+1750}_{-0}	LCC (CMD)	9,13,-,15	–
HD 115820	P	–	–	–	–	–	3.00±1	–	–	–	–	–	10^{+340}_{-0}	LCC (CMD)	-,13,-,15	–
iot Cen	P	–	–	–	–	79.00	–	–	–	–	–	–	605^{+10}_{-0}	CMD	12,-,-,-	–
TYC8252-1917-1	P	–	–	–	–	–	–	–	–	–	–	–	630^{+150}_{-100}	CMD	-,-,-,-	–
HD 116956	P	55380.87529	OSA	979	29	6.41	-12.01±6.52	0.05±0.01	4.61±0.01	-4.40	-4.58	WDS	625^{+0}_{-475}	Li (CMD)	1,1,1,-	–
HD 117043	P	56442.81552	OSA	1026	12	3.35	-30.85±3.79	0.16±0.01	4.34±0.02	–	-4.91	–	625^{+0}_{-0}	Li	1,1,1,-	–
70 Vir	P	51535.21005	OEA	1122	30	2.85	8.61±1.35	-0.14±0.01	3.90±0.02	–	–	WDS	*****	–	1,1,1,-	giant:Gaia
HD 117376	P	54145.05332	OSA	4289	0	80.56	-11.10±1	–	–	–	–	WDS	385^{+70}_{-125}	CMD	1,13,-,-	–
HD 117214	P	–	–	–	–	35.90	7.10±1	-0.07±0.08	–	–	–	–	10^{+0}_{-0}	LCC	21,13,4,15	–
HD 117484	P	–	–	–	–	–	2.00±1	–	–	–	–	WDS	10^{+90}_{-0}	LCC (CMD)	-,13,-,15	–
HD 117716	P	–	–	–	–	196.00	-22.40±3	–	–	–	–	–	505^{+115}_{-110}	CMD	61,13,-,-	–
HD 117665	P	–	–	–	–	–	1.50±1	–	–	–	–	–	10^{+640}_{-0}	LCC (CMD)	-,13,-,15	–
BH CVn	P	51334.90403	OEA	1101	11	14.24	11.62±4.46	-0.67±0.01	2.49±0.04	-4.14	–	55	0^{+0}_{-625}	Li	1,1,1,-	X-ray no agreement
CD-40 8031	P	54309.11451	MFA	367	323	14.86	6.41±1.78	-0.24±0.01	4.10±0.02	-3.19	-4.88	–	15^{+105}_{-0}	Li (X-ray)	1,1,1,-	CMD agreement
HD 118588	P	–	–	–	–	–	1.20±1	–	–	–	–	–	10^{+100}_{-0}	LCC (CMD)	-,13,-,15	–
HD 119124	P	56713.37696	LHO	550	0	7.49	-16.11±16.22	-0.29±0.02	4.21±0.06	-4.49	–	WDS, 44	0^{+625}_{-0}	Li	1,1,1,-	–
HD 118972	P	56699.39735	MFA	917	21	7.52	-6.69±1.44	-0.03±0.01	4.89±0.02	-4.70	-4.63	–	625^{+0}_{-575}	Li (CMD)	1,1,1,-	X-ray agreement
TYC5549-1004-1	P	56713.47669	LHO	1226	30	4.60	-50.54±10.93	-0.53±0.01	1.73±0.05	–	–	–	375^{+0}_{-0}	Li	1,1,1,-	–
HD 119511	P	–	–	–	–	124.00	1.80±1	–	–	–	–	–	10^{+0}_{-0}	LCC	9,13,-,15	–

Continued on Next Page...

Table C.1 – Continued

Name	Catalog	Obs. MJD	Instrument	Hα (mÅ)	Li6708 (mÅ)	$v \sin(i)$ (kms^{-1})	RV (kms^{-1})	[Fe/H] (dex)	log (g)	log ($\frac{L_X}{L_{bol}}$)	log (R'_{HK})	Multiple Ref.	Age (Myr)	Age-Dating Method	Refs	Notes
HD 119718	P	–	–	–	–	–	4.10±1	–	–	–	–	WDS	10^{+0}_{-0}	LCC	-,13,-,15	–
HD 120326	P	–	–	–	–	70.00	7.30±1	–	–	–	–	–	10^{+580}_{-0}	UCL (CMD)	9,13,-,15	–
HD 120160	P	–	–	–	–	–	–	0.10±0.15	–	–	–	WDS	1540^{+560}_{-35}	CMD	-,-,4,-	–
HD 121189	P	–	–	–	–	50.00	7.20±1	–	–	–	–	WDS	10^{+0}_{-0}	UCL	9,13,-,15	–
HIP 68080	P	–	–	–	–	–	12.80±2	–	–	–	–	WDS	10^{+105}_{-0}	UCL (CMD)	-,13,-,15	–
HD 121812	P	55398.86809	OSA	889	16	6.34	-15.11±3.46	0.11±0.02	4.68±0.03	–	-4.78	–	625^{+275}_{-525}	Li (CMD)	1,1,1,-	–
HD 121617	P	–	–	–	–	–	–	–	–	–	–	–	585^{+95}_{-115}	CMD	-,-,-,-	–
HD 122652	P	53783.13053	OEA	1383	70	4.49	4.09±1.88	-0.01±0.01	4.13±0.03	-5.48	–	–	625^{+2000}_{-0}	Li (X-ray)	1,1,1,-	–
HD 122705	P	–	–	–	–	–	6.60±1	–	–	–	–	–	10^{+225}_{-0}	UCL (CMD)	-,13,-,15	–
HD 123889	P	–	–	–	–	71.00	3.20±1	-0.04±0.08	–	–	–	WDS	10^{+615}_{-0}	UCL (CMD)	9,13,4,15	–
HD 124718	P	56713.50633	LHO	1137	23	4.93	-33.73±4.52	0.14±0.02	4.39±0.03	–	–	–	625^{+0}_{-0}	Li	1,1,1,-	–
HD 124619	P	–	–	–	–	115.00	6.90±1	–	–	–	–	WDS	10^{+1065}_{-0}	UCL (CMD)	9,13,-,15	–
lam Boo	P	49769.11726	OEA	4753	0	95.82	-7.90±2	–	–	–	–	WDS	630^{+85}_{-120}	CMD	1,13,-,-	–
18 Boo	P	–	–	–	–	41.00	-0.40±1	0.01±0.05	–	–	–	WDS	1895^{+380}_{-520}	CMD	21,13,42,-	–
HD 125283	P	–	–	–	–	230.00	–	–	–	–	–	WDS	600^{+95}_{-110}	CMD	61,-,-,-	–
psi Cen	P	–	–	–	–	124.00	1.80±1	–	–	–	–	WDS, 44	300^{+70}_{-10}	CMD	62,13,-,-	–
HD 125541	P	–	–	–	–	–	3.90±1	–	–	–	–	WDS	10^{+795}_{-0}	UCL (CMD)	-,13,-,15	–
HD 126062	P	–	–	–	–	–	5.10±1	–	–	–	–	–	10^{+510}_{-0}	UCL (CMD)	-,13,-,15	–
CD-46 9327	P	–	–	–	–	–	–	–	–	-3.23	–	–	10^{+105}_{-0}	UCL (X-ray)	-,-,-,36	CMD agreement
HD 127821	P	57081.44135	DMO	2141	0	44.23	-11.80±2	-0.19±0.08	–	-5.10	–	–	625^{+0}_{-0}	X-ray	1,13,4,-	–
gam Boo	P	–	–	–	–	117.00	-32.40±1	±-0.20	–	–	–	WDS, 44	970^{+15}_{-35}	CMD	21,13,49,-	–
HD 128165	P	50858.16922	OEA	875	11	12.37	12.96±1.13	-0.04±0.05	–	-5.53	–	–	375^{+0}_{-315}	Li (CMD)	1,1,29,-	X-ray no agreement
sig Boo	P	53904.91248	OEA	1807	0	6.61	0.06±4.16	-0.40±0.04	–	–	–	WDS	40^{+25}_{-5}	Argus (CMD)	1,1,43,1	–
HD 128311	P	53511.03721	VUA	860	10	7.80	-13.95±0.14	0.06±0.01	4.65±0.01	-4.61	–	WDS	375^{+250}_{-0}	Li (X-ray)	1,1,1,-	–
HR 5449	P	–	–	–	–	–	2.00±4	–	–	–	–	–	10^{+115}_{-0}	CMD	-,13,-,-	–
TYC8683-242-1	P	54928.14387	VUA	0	0	–	–	–	–	-2.92	–	–	10^{+115}_{-0}	UCL (X-ray)	-,-,-,36	–
HD 129590	P	–	–	–	–	–	2.30±1	–	–	–	–	–	10^{+0}_{-0}	UCL	-,13,-,15	–
HD 130693	P	–	–	–	–	–	–	–	–	-3.63	–	–	125^{+0}_{-0}	X-ray	-,-,-,-	–
HD 131496	P	57082.50294	DMO	1063	16	12.14	–	0.12±0.03	–	–	–	–	*****	–	1,-,49,-	giant:Gaia
DE Boo	P	–	–	–	–	6.35	–	0.14±0.03	–	-4.83	–	45	40^{+585}_{-0}	Argus (X-ray)	32,-,29,1	CMD agreement
HD 131625	P	–	–	–	–	191.00	0.00±4	–	–	–	–	WDS	660^{+55}_{-50}	CMD	21,13,-,-	–
TYC7824-2717-1	P	–	–	–	–	–	–	–	–	-4.17	–	–	125^{+0}_{-0}	X-ray	-,-,-,-	–
HD 132254	P	53904.89197	OEA	1456	36	9.95	-16.06±2.29	0.05±0.03	–	-5.90	–	–	625^{+4000}_{-0}	Li (X-ray)	1,1,29,-	–
HD 131835	P	–	–	–	–	–	0.50±1	–	–	–	–	–	10^{+0}_{-0}	UCL	-,13,-,15	–

Continued on Next Page. . .

Table C.1 – Continued

Name	Catalog	Obs. MJD	Instrument	Hα (mÅ)	Li6708 (mÅ)	$v \sin(i)$ (kms^{-1})	RV (kms^{-1})	[Fe/H] (dex)	log (g)	log ($\frac{L_X}{L_{bol}}$)	log (R'_{HK})	Multiple Ref.	Age (Myr)	Age-Dating Method	Refs	Notes
del Lib	P	57082.52552	DMO	4061	0	68.78	-40.00±4	–	–	–	–	WDS	460^{+20}_{-85}	CMD	1,13,-,-	–
HD 132950	P	50893.02366	OEA	822	17	6.89	1.04±2.81	–	–	–	–	–	375^{+0}_{-325}	Li (CMD)	1,1,-,-	–
HD 133075	P	–	–	–	–	–	-78.30±4	-0.28±0.15	–	–	–	–	10^{+0}_{-0}	UCL	-,13,4,15	–
HD 133803	P	56713.53395	LHO	2700	0	70.13	-1.70±1	0.07±0.15	–	–	–	WDS	10^{+1160}_{-0}	UCL (CMD)	1,13,4,15	–
HD 134888	P	56713.53794	LHO	1772	122	29.25	-1.00±1	0.28±0.05	3.90±0.14	–	–	–	10^{+20}_{-0}	UCL (Li)	1,13,1,15	–
HD 135599	P	56713.51348	LHO	944	16	6.97	-4.14±33.73	-0.01±0.01	4.83±0.02	-5.16	–	–	625^{+0}_{-575}	Li (CMD)	1,1,1,-	X-ray no agreement
bet Cir	P	–	–	–	–	60.70	–	–	–	–	–	WDS	800^{+125}_{-40}	CMD	21,-,-,-	–
HD 135953	P	–	–	–	–	–	-0.40±1	–	–	–	–	WDS	10^{+0}_{-0}	UCL	-,13,-,15	–
GJ 581	P	55646.34181	EHA	299	0	7.49	-9.72±0.38	-0.20±0.04	4.23±0.08	–	–	–	70^{+9}_{-8}	CMD	1,1,1,-	–
HD 136246	P	–	–	–	–	–	-2.70±1	–	–	–	–	–	10^{+515}_{-0}	CMD	-,13,-,-	–
HD 136482	P	–	–	–	–	–	-0.20±1	–	–	–	–	–	10^{+85}_{-0}	CMD	-,13,-,-	–
HD 137119	P	–	–	–	–	–	-0.70±1	–	–	–	–	–	10^{+250}_{-0}	UCL (CMD)	-,13,-,15	–
HD 138296	P	–	–	–	–	–	-2.50±1	-0.11±0.15	–	-4.55	–	–	10^{+365}_{-0}	UCL (X-ray)	-,13,4,15	–
tet CrB	P	51570.17947	OEA	4370	0	155.49	-25.70±0	0.00±0.01	–	–	–	WDS, 44	120^{+35}_{-20}	CMD	1,13,41,-	–
TYC9022-1316-1	P	–	–	–	–	–	–	–	–	–	–	–	500^{+110}_{-100}	CMD	-,-,-,-	–
alf CrB	P	50294.89338	OEA	5032	0	89.49	1.40±2	0.20±0.15	–	–	–	44,45	400^{+10}_{-5}	CMD	1,13,20,-	–
HD 138813	P	–	–	–	–	–	–	–	–	–	–	WDS	5^{+460}_{-0}	UpperSco (CMD)	-,-,-,15	–
HD 139323	P	54245.98457	OSA	886	15	6.24	-67.02±2.83	0.40±0.02	4.31±0.03	–	-4.94	WDS	375^{+0}_{-275}	Li (CMD)	1,1,1,-	–
HR 5790	P	–	–	–	–	271.00	-3.60±4	–	–	–	–	WDS	10^{+50}_{-0}	CMD	61,13,-,-	assumed ZAMS
HR 5792	P	–	–	–	–	146.00	–	–	–	–	–	–	380^{+130}_{-180}	CMD	12,-,-,-	–
g Lup	P	53091.26784	VUA	2482	0	61.67	-5.40±3	-0.35±0.02	4.19±0.08	-5.05	–	WDS	625^{+0}_{-0}	X-ray	1,13,1,-	–
HR 5859	P	53050.13241	OEA	3235	0	63.02	-8.00±1	–	–	–	–	–	500^{+35}_{-340}	CMD	1,13,-,-	–
HD 140817	P	–	–	–	–	–	–	–	–	–	–	CCDM	10^{+150}_{-0}	UCL (CMD)	-,-,-,15	–
HD 140840	P	–	–	–	–	–	–	–	–	–	–	TDSC	10^{+240}_{-0}	UCL (CMD)	-,-,-,15	–
HD 141011	P	–	–	–	–	–	0.20±1	–	–	–	–	WDS	10^{+0}_{-0}	UCL	-,13,-,15	–
HD 141227	P	56402.42471	LHO	1602	120	19.94	-11.78±8.08	-0.11±0.03	3.11±0.07	–	–	–	125^{+0}_{-0}	Li	1,1,1,-	–
HD 141378	P	–	–	–	–	107.00	-16.40±3	–	–	–	–	–	810^{+55}_{-60}	CMD	61,13,-,-	–
HD 141569	P	50632.88863	OEA	-2625	0	92.82	-6.40±2	0.03±0.15	–	–	–	WDS, 58, 37	495^{+120}_{-180}	CMD	1,13,49,-	–
TYC7332-2514-1	P	–	–	–	–	–	–	–	–	-4.67	–	–	375^{+0}_{-0}	X-ray	-,-,-,-	–
kap CrB	P	51709.89711	OEA	1055	23	5.02	-27.14±1.06	0.13±0.03	–	–	–	WDS	375^{+0}_{-0}	Li	1,1,46,-	–
HD 141943	P	54945.12587	EHA	873	224	35.09	2.13±2.65	0.09±0.05	4.14±0.08	-3.45	-4.36	WDS	10^{+115}_{-0}	UCL (X-ray)	1,1,1,36	–
V1040 Sco	P	55299.14568	VUA	0	0	300.00	±-9.20	–	–	–	–	–	5^{+200}_{-0}	UpperSco (CMD)	-,13,-,15	–
lam CrB	P	53136.01743	OEA	3010	20	61.55	-10.34±26.25	-0.01±0.02	3.82±0.15	–	–	WDS	30^{+1650}_{-0}	Li (CMD)	1,1,1,-	–
HD 142446	P	–	–	–	–	–	-1.90±1	–	–	–	–	–	10^{+0}_{-0}	UCL	-,13,-,15	–
HD 142139	P	55346.27777	EHA	3993	0	79.98	±-16.70	–	–	–	–	–	630^{+15}_{-90}	CMD	1,13,-,-	–

Continued on Next Page. . .

Table C.1 – Continued

Name	Catalog	Obs. MJD	Instrument	Hα (mÅ)	Li6708 (mÅ)	$v \sin(i)$ (kms^{-1})	RV (kms^{-1})	[Fe/H] (dex)	log (g)	log ($\frac{L_X}{L_{bol}}$)	log (R'_{HK})	Multiple Ref.	Age (Myr)	Age-Dating Method	Refs	Notes
2MASS J15570641-2206060	P	–	–	–	–	–	–	–	–	–	–	–	5^{+0}_{-0}	UpperSco	-,-,-,25	–
2MASS J15584772-1757595	P	–	–	–	–	14.86	–	–	–	-2.79	–	WDS	5^{+120}_{-0}	UpperSco (X-ray,CMD)	57,-,-,36	–
44 Ser	P	53144.02819	OEA	5230	0	106.28	-28.20±4	±0.38	–	–	–	–	770^{+95}_{-25}	CMD	1,13,4,-	–
HD 143538	P	–	–	–	–	73.00	-2.60±1	–	–	–	–	WDS	10^{+830}_{-0}	UCL (CMD)	9,13,-,15	–
HD 143675	P	–	–	–	–	–	-2.70±1	–	–	–	–	–	10^{+240}_{-0}	UCL (CMD)	-,13,-,15	–
LM Lup	P	–	–	–	–	–	1.60±7	–	–	–	–	WDS	10^{+40}_{-0}	UCL (CMD)	-,13,-,15	–
TYC6212-349-1	P	–	–	–	–	–	–	–	–	–	–	–	1290^{+600}_{-355}	CMD	-,-,-,-	–
HD 144587	P	–	–	–	–	–	0.00±2	–	–	–	–	–	5^{+0}_{-0}	UpperSco	-,13,-,15	–
HD 144729	P	–	–	–	–	–	-0.10±2	–	–	-4.21	–	WDS	5^{+120}_{-0}	UpperSco (X-ray)	-,13,-,15	–
TYC7851-810-1	P	57087.75339	SWO	262	425	28.39	4.90±4.50	–	–	–	–	–	8^{+0}_{-0}	Li	1,1,-,-	–
TYC7338-1156-1	P	–	–	–	–	–	–	–	–	–	–	–	1030^{+245}_{-260}	CMD	-,-,-,-	–
HD 145229	P	52111.84068	OEA	1262	64	5.91	-34.37±1.83	-0.27±0.01	4.25±0.03	-4.66	–	–	625^{+0}_{-0}	Li	1,1,1,-	X-ray agreement
TYC6213-1122-1	P	56402.43890	LHO	57	404	17.22	-5.16±13.08	0.11±0.04	2.47±0.07	-4.04	–	–	8^{+0}_{-3}	Li (CMD)	1,1,1,-	–
HD 145357	P	–	–	–	–	–	-0.80±1	–	–	–	–	CCDM	10^{+480}_{-0}	UCL (CMD)	-,13,-,15	–
HD 145554	P	–	–	–	–	154.00	–	–	–	–	–	WDS	5^{+745}_{-0}	UpperSco (CMD)	21,-,-,15	–
HD 145631	P	–	–	–	–	154.00	–	–	–	–	–	–	5^{+740}_{-0}	UpperSco (CMD)	21,-,-,15	–
HD 145560	P	–	–	–	–	–	0.30±1	–	–	-4.12	–	WDS	10^{+110}_{-0}	UCL (X-ray)	-,13,-,15	–
HD 145880	P	–	–	–	–	–	-1.80±1	–	–	–	–	WDS	10^{+70}_{-0}	UCL (CMD)	-,13,-,15	–
2MASS J16145918-2750230	P	–	–	–	–	22.77	–	–	–	-3.41	–	WDS	5^{+120}_{-0}	UpperSco (X-ray)	57,-,-,36	CMD agreement
HD 145972	P	–	–	–	–	61.00	1.20±1	–	–	–	–	WDS	10^{+1315}_{-0}	UCL (CMD)	9,13,-,15	–
HD 146181	P	–	–	–	–	–	-2.10±1	–	–	–	–	WDS	10^{+0}_{-0}	UCL	-,13,-,15	–
HD 145689	P	–	–	–	–	85.60	–	–	–	–	–	–	660^{+100}_{-345}	CMD	21,-,-,-	–
HD 146606	P	–	–	–	–	137.00	±0.80	–	–	–	–	–	5^{+100}_{-0}	UpperSco (CMD)	11,13,-,15	–
d Sco	P	–	–	–	–	39.00	-13.00±1	-0.27±0.12	–	–	–	–	280^{+120}_{-120}	CMD	61,13,42,-	–
HD 146897	P	–	–	–	–	–	-1.10±2	–	–	–	–	–	5^{+0}_{-0}	UpperSco	-,13,-,15	–
HD 147137	P	–	–	–	–	79.10	–	–	–	–	–	–	5^{+1965}_{-0}	UpperSco (CMD)	11,-,-,15	–
HD 147196	P	–	–	–	–	320.00	-3.00±6	–	–	–	–	–	5^{+875}_{-0}	UpperSco (CMD)	21,13,-,15	–
HD 147594	P	–	–	–	–	–	1.10±2	–	–	-3.65	–	–	5^{+120}_{-0}	UpperSco (X-ray)	-,13,-,36	–
TYC8316-4073-1	P	–	–	–	–	–	–	–	–	–	–	–	1430^{+225}_{-155}	CMD	-,-,-,-	–
V2505 Oph	P	–	–	–	–	83.53	–	–	–	-3.23	–	WDS	5^{+120}_{-0}	UpperSco (X-ray)	57,-,-,36	–

Continued on Next Page...

Table C.1 – Continued

Name	Catalog	Obs. MJD	Instrument	Hα (mÅ)	Li6708 (mÅ)	$v \sin(i)$ (kms^{-1})	RV (kms^{-1})	[Fe/H] (dex)	log (g)	log ($\frac{L_X}{L_{bol}}$)	log (R'_{HK})	Multiple Ref.	Age (Myr)	Age-Dating Method	Refs	Notes
HD 150706	P	52112.90824	OEA	1232	63	6.14	-15.42±1.68	-0.16±0.01	4.31±0.02	-4.73	–	–	625^{+0}_{-0}	Li	1,1,1,-	X-ray agreement
37 Her	P	57081.49698	DMO	3052	0	76.12	-28.00±4	–	–	–	–	WDS, 44	385^{+80}_{-135}	CMD	1,13,-,-	–
39 Her	P	57081.50934	DMO	0	0	23.30	-13.60±1	-0.14±0.08	–	–	–	WDS	2175^{+95}_{-1230}	CMD	21,13,4,-	–
HD 151044	P	53150.07837	OEA	1310	69	4.00	-14.06±1.89	-0.03±0.01	–	–	–	–	625^{+0}_{-0}	Li	1,1,29,-	–
HD 151376	P	–	–	–	–	–	-2.30±2	–	–	–	–	–	5^{+0}_{-0}	UpperSco	-,13,-,15	–
53 Her	P	53902.95213	OEA	3006	28	53.17	-20.49±15.36	-0.22±0.02	3.38±0.19	–	–	WDS	30^{+80}_{-0}	Li (CMD)	1,1,1,-	–
iot Oph	P	57081.53051	DMO	2797	0	82.75	±-19.00	0.09±0.04	–	–	–	–	175^{+50}_{-45}	CMD	1,13,4,-	–
h Dra	P	57272.20737	DMO	1563	74	4.89	-21.00±1	-0.07±0.03	–	-5.12	–	45	110^{+515}_{-0}	AB Dor (X-ray)	1,13,29,1	Li agreement
HD 153053	P	55385.21860	EHA	4157	0	84.10	±-20.20	–	–	–	–	WDS	*****	–	1,13,-,-	–
TYC8327-1661-1	P	57294.38986	SWO	1134	14	23.39	-30.17±2.30	–	–	–	–	–	15^{+0}_{-0}	Li	1,1,-,-	–
HD 154577	P	55341.25188	EHA	917	3	3.29	6.50±0.25	-0.48±0.01	4.53±0.01	–	-5.00	–	625^{+0}_{-575}	Li (CMD)	1,1,1,-	–
TYC8341-414-1	P	–	–	–	–	–	–	–	–	–	–	–	580^{+90}_{-265}	CMD	-,-,-,-	–
73 Her	P	–	–	–	–	92.00	-19.70±3	–	–	–	–	–	470^{+180}_{-195}	CMD	62,13,-,-	–
HD 157587	P	56165.15209	LHO	1744	102	38.75	-27.29±84.90	-0.02±0.03	3.81±0.08	-4.71	–	–	125^{+250}_{-0}	Li (X-ray)	1,1,1,-	–
HD 158633	P	52114.91392	OEA	1034	17	5.75	-36.98±1.41	-0.44±0.01	4.56±0.02	–	–	–	625^{+0}_{-0}	Li	1,1,1,-	–
HD 323410	P	57294.39513	SWO	1442	102	17.75	-10.44±3.19	–	–	-4.22	–	WDS	375^{+0}_{-0}	Li	1,1,-,-	X-ray agreement
HR 6511	P	–	–	–	–	296.00	7.00±4	–	–	–	–	–	560^{+60}_{-70}	CMD	62,13,-,-	–
HD 158352	P	54937.31888	VUA	5031	0	101.41	-36.10±3	-0.06±0.04	–	–	–	WDS	1230^{+275}_{-35}	CMD	1,13,4,-	–
78 Her	P	–	–	–	–	223.00	-25.70±3	-0.55±0.04	–	–	–	–	380^{+80}_{-90}	CMD	12,13,4,-	–
HR 6532	P	–	–	–	–	22.00	-13.70±4	–	–	–	–	WDS	390^{+90}_{-15}	CMD	61,13,-,-	–
HD 159170	P	52499.82821	OEA	6467	0	87.18	-26.00±4	–	–	–	–	WDS	855^{+115}_{-115}	CMD	1,13,-,-	–
HD 159492	P	53156.24723	EHA	3027	0	54.74	±-3.30	±0.13	–	–	–	–	*****	–	1,13,4,-	–
lam Ara	P	54928.40779	EHA	1689	0	14.16	3.70±0	-0.49±0.02	3.74±0.07	–	–	–	2155^{+195}_{-385}	CMD	1,14,1,-	–
V2384 Oph	P	57294.39969	SWO	1017	250	24.61	-4.47±2.60	±-0.14	–	-3.67	–	–	30^{+95}_{-0}	Li (X-ray)	1,1,4,-	–
TYC7889-407-1	P	57294.40418	SWO	2687	45	–	-20.01±9.92	-0.03±0.15	–	–	–	–	125^{+905}_{-0}	Li (CMD)	-,1,4,-	–
gam Oph	P	53622.00632	EHA	7007	0	139.76	-7.60±0	-0.21±0.15	–	–	–	WDS	615^{+0}_{-125}	CMD	1,13,49,-	–
HD 162917	P	54902.12792	OSA	1645	0	29.69	-26.64±37.98	0.16±0.04	4.07±0.08	-5.40	–	WDS	0^{+0}_{-625}	Li	1,1,1,-	X-ray agreement
HD 164330	P	57201.25461	DMO	1268	43	12.06	-13.05±0	0.20±0.07	–	–	–	WDS	625^{+0}_{-0}	Li	1,13,4,-	–
HD 165459	P	–	–	–	–	142.00	-24.10±4	–	–	–	–	–	515^{+150}_{-135}	CMD	12,13,-,-	–
HD 164249	P	54209.40160	VUA	1670	93	19.80	0.18±1.13	-0.11±0.01	4.09±0.03	-4.53	–	WDS	15^{+15}_{-0}	β Pic (Li)	1,1,1,10/30	X-ray agreement
b Her	P	50562.13927	OEA	1206	40	3.17	3.60±2.34	-0.56±0.01	4.11±0.03	-6.75	–	WDS,65	625^{+4000}_{-0}	Li (X-ray)	1,1,1,-	–
V4046 Sgr	P	52381.36096	VUA	0	0	–	–	–	–	–	–	WDS	*****	–	-,-,-,-	no age info.
HD 168161	P	57294.43293	SWO	1727	33	13.83	–	–	–	–	–	WDS	0^{+0}_{-625}	Li	1,-,-,-	–
HD 169666	P	57200.33020	DMO	2012	0	18.35	-44.30±0	0.00±0.08	–	-5.70	–	–	0^{+2000}_{-0}	X-ray	1,7,4,-	–
HD 168746	P	56009.37350	VUA	1110	7	2.52	-25.97±0.17	-0.13±0.00	4.28±0.01	–	-5.19	WDS	625^{+0}_{-0}	Li	1,1,1,-	–
TYC5103-27-1	P	57294.43839	SWO	2392	6	45.55	24.75±7.89	–	–	–	–	–	625^{+0}_{-0}	Li	1,1,-,-	–

Continued on Next Page...

Table C.1 – Continued

Name	Catalog	Obs. MJD	Instrument	Hα (mÅ)	Li6708 (mÅ)	$v \sin(i)$ (kms^{-1})	RV (kms^{-1})	[Fe/H] (dex)	log (g)	log ($\frac{L_X}{L_{bol}}$)	log (R'_{HK})	Multiple Ref.	Age (Myr)	Age-Dating Method	Refs	Notes
HR 6948	P	54939.39590	MFA	2261	46	48.45	-25.20±1	0.05±0.02	4.19±0.03	-4.99	–	–	125^{+500}_{-0}	Li (X-ray)	1,13,1,-	–
Vega	P	53792.13439	OEA	2157	0	21.54	-20.60±0	-0.50±0.01	–	–	–	WDS	405^{+390}_{-390}	CMD	1,13,41,-	–
HD 172555	P	53156.25656	EHA	4734	0	99.38	±2.00	±0.07	–	–	–	WDS, 44,59	15^{+175}_{-0}	β Pic (CMD)	1,13,49,10/30	–
PZ Tel	P	54942.26187	EHA	560	308	67.84	8.70±2.54	-0.35±0.03	3.08±0.08	-3.24	-5.22	WDS, 44	15^{+110}_{-2}	Li (X-ray,CMD)	1,1,1,-	–
zet CrA	P	53880.37521	EHA	7291	0	135.14	-13.00±4	–	–	–	–	–	340^{+80}_{-90}	CMD	1,13,-,-	–
rho Tel	P	56798.22169	EHA	2232	0	40.27	55.40±2.84	-0.31±0.03	3.49±0.15	-4.10	-4.74	–	125^{+0}_{-0}	X-ray	1,1,1,-	–
alf CrA	P	–	–	–	–	195.00	–	–	–	–	–	–	700^{+75}_{-95}	CMD	60,-,-,-	–
HR 7297	P	53500.29358	EHA	1371	0	5.52	-22.40±0.59	-0.16±0.02	3.83±0.07	–	-5.09	–	0^{+0}_{-625}	Li	1,1,1,-	–
eta Tel	P	53156.34028	EHA	7571	0	136.01	13.00±2	–	–	–	–	WDS, 44	250^{+110}_{-125}	CMD	1,30,-,-	–
HD 181327	P	54942.25007	EHA	1676	118	17.15	0.11±1.78	-0.02±0.02	4.39±0.06	–	–	WDS	15^{+15}_{-0}	β Pic (Li)	1,1,1,10/30	–
5 Vul	P	–	–	–	–	154.00	-20.90±3	–	–	–	–	–	315^{+95}_{-110}	CMD	61,13,-,-	–
HD 182681	P	–	–	–	–	304.00	1.40±7	–	–	–	–	–	210^{+105}_{-210}	CMD	12,13,-,-	–
c Aql	P	55708.34068	VUA	3917	0	72.76	12.00±4	±-1.24	–	–	–	WDS	595^{+65}_{-100}	CMD	1,13,42,-	–
HD 183216	P	57294.47183	SWO	1646	77	20.25	-43.07±2.67	0.09±0.08	–	-4.96	–	–	625^{+0}_{-0}	Li	1,1,4,-	X-ray agreement
HD 187897	P	56115.00000	OSA	1221	61	5.11	-37.38±7.24	0.04±0.01	4.29±0.02	-5.07	-4.69	–	625^{+0}_{-0}	Li	1,1,1,-	X-ray agreement
eps Pav	P	53270.15918	EHA	3956	0	77.13	-6.70±1	–	–	–	–	–	40^{+60}_{-0}	Argus (CMD)	1,13,-,30	–
HD 190228	P	53165.05520	OEA	1097	8	4.44	-47.84±1.52	-0.22±0.01	3.99±0.02	–	–	–	*****	–	1,1,1,-	giant:Gaia
TYC2679-1864-1	P	–	–	–	–	–	–	–	–	–	–	–	50^{+10}_{-13}	CMD	-,-,-,-	–
HD 191089	P	55843.10125	VUA	1804	86	37.34	-8.88±3.83	0.05±0.04	4.13±0.08	-4.90	–	WDS	15^{+610}_{-0}	β Pic (X-ray)	1,1,1,10/30	Li agreement
HD 192263	P	53238.87499	OEA	888	17	7.29	-9.59±1.18	0.00±0.01	4.70±0.02	-5.14	–	WDS	375^{+0}_{-325}	Li (CMD)	1,1,1,-	–
rho Aql	P	53608.90453	OEA	5821	0	121.85	-23.00±3	-0.48±0.04	–	–	–	–	550^{+85}_{-130}	CMD	1,13,4,-	–
TYC3576-213-1	P	–	–	–	–	–	–	–	–	–	–	–	37^{+3}_{-0}	CMD	-,-,-,-	–
HD 192758	P	–	–	–	–	–	–	–	–	–	–	–	1190^{+285}_{-325}	CMD	-,-,-,-	–
kap01 Sgr	P	–	–	–	–	79.00	-3.40±1	–	–	–	–	WDS	305^{+100}_{-105}	CMD	61,13,-,-	–
HR 7848	P	–	–	–	–	114.00	-20.00±4	±-0.11	–	–	–	–	1285^{+225}_{-90}	CMD	21,13,49,-	–
TYC2698-1078-1	P	56519.23060	LHO	1173	26	3.52	-0.19±29.07	-0.16±0.01	4.12±0.03	–	–	–	0^{+0}_{-625}	Li	1,1,1,-	–
iot Del	P	–	–	–	–	41.00	-4.90±3	-0.12±0.10	–	–	–	44	515^{+115}_{-110}	CMD	61,13,42,-	–
AU Mic	P	55844.09559	VUA	-2436	36	13.59	-6.25±0.45	-0.68±0.03	1.15±0.09	-2.77	–	WDS	15^{+110}_{-12}	Li (X-ray,CMD)	1,1,1,-	–
HR 8013	P	53156.41910	EHA	1448	82	14.26	-15.88±1.42	-0.18±0.02	4.51±0.03	-4.73	–	–	40^{+85}_{-0}	Castor (Li)	1,1,1,10	–
TYC4259-1185-1	P	57201.27028	DMO	1296	14	11.48	–	–	–	–	–	–	*****	–	1,-,-,-	giant:Gaia
HD 200565	P	56165.18488	EHA	1185	15	5.35	-1.53±0.39	-0.02±0.01	4.48±0.02	–	-5.02	WDS	0^{+0}_{-625}	Li	1,1,1,-	–
alf Oct	P	55031.24057	MFA	2028	0	41.71	85.94±21.81	0.03±0.01	2.53±0.04	-4.45	-4.78	55	375^{+0}_{-0}	X-ray	1,1,1,-	–
TYC1112-317-1	P	–	–	–	–	–	–	–	–	–	–	–	50^{+50}_{0}	CMD	-,-,-,-	assumed ZAMS
HD 201219	P	57287.16949	DMO	1196	6	12.64	4.50±0	0.11±0.04	–	-5.02	–	–	625^{+0}_{-0}	Li	1,7,4,-	X-ray agreement
TYC1113-1057-1	P	–	–	–	–	–	–	–	–	–	–	–	8^{+4}_{-0}	CMD	-,-,-,-	–
HD 202206	P	53263.19792	EHA	1167	13	4.71	14.77±0.28	0.28±0.01	4.54±0.01	–	-4.90	–	625^{+0}_{-0}	Li	1,1,1,-	–

Continued on Next Page...

Table C.1 – Continued

Name	Catalog	Obs. MJD	Instrument	Hα (mÅ)	Li6708 (mÅ)	$v \sin(i)$ (kms^{-1})	RV (kms^{-1})	[Fe/H] (dex)	log (g)	log ($\frac{L_X}{L_{bol}}$)	log (R'_{HK})	Multiple Ref.	Age (Myr)	Age-Dating Method	Refs	Notes
TYC3181-1403-1	P	–	–	–	–	–	–	–	–	-3.36	–	–	125^{+0}_{-0}	X-ray	-,-,-,-	–
HD 202628	P	55074.07208	VUA	1178	41	4.42	10.24±0.18	-0.04±0.01	4.49±0.01	-5.21	-4.89	–	625^{+1375}_{-0}	Li (X-ray)	1,1,1,-	–
HD 202917	P	54226.34418	VUA	553	218	16.01	-1.78±0.52	-0.06±0.04	4.52±0.07	-3.37	-4.59	WDS	30^{+95}_{-0}	Tuc-Hor (X-ray)	1,1,1,10/30	Li agreement
HD 205674	P	56582.17235	EHA	2085	43	26.93	–	0.04±0.06	4.25±0.13	-5.14	–	–	625^{+0}_{-0}	Li	1,-,1,-	X-ray agreement
3 Peg	P	–	–	–	–	102.00	–	–	–	–	–	WDS	440^{+95}_{-125}	CMD	61,-,-,-	–
HD 205536	P	55102.05924	EHA	1086	10	2.68	34.43±0.26	0.03±0.01	4.39±0.02	–	-5.09	–	625^{+0}_{-0}	Li	1,1,1,-	–
HN Peg	P	51000.07352	OEA	1344	97	12.34	-18.72±2.33	-0.14±0.01	4.51±0.02	-4.46	–	WDS	125^{+0}_{-0}	Li	1,1,1,-	X-ray no agreement
HD 206893	P	54783.03560	MFA	1858	17	33.85	-16.73±14.49	-0.15±0.02	4.29±0.03	-4.87	–	–	0^{+0}_{-625}	Li	1,1,1,-	X-ray agreement
HD 207129	P	53505.30817	VUA	1200	30	6.01	-7.44±0.21	0.02±0.01	4.54±0.01	-5.67	-5.09	WDS, 44	625^{+4000}_{-0}	Li (X-ray)	1,1,1,-	–
HD 209253	P	–	–	–	–	16.00	16.30±1	-0.09±0.03	–	-4.55	–	–	0^{+0}_{-375}	X-ray	34,13,49,-	–
HD 210277	P	53263.21553	EHA	1078	6	2.89	-20.83±0.26	0.15±0.01	4.30±0.02	–	-5.17	WDS	*****	–	1,1,1,-	giant:Gaia
HD 212695	P	57323.47801 57320.41870	SEO SWO	1728	13	20.97	23.52±4.44	-0.05±0.01	2.75±0.10	-4.81	–	–	0^{+0}_{-375}	X-ray	1,1,1,-	Li agreement
bet PsA	P	–	–	–	–	30.00	5.50±0	±0.01	–	–	–	WDS	480^{+5}_{-20}	CMD	61,13,4,-	–
39 Peg	P	57201.34152	DMO	3485	0	52.37	-18.90±3	-0.01±0.15	–	–	–	WDS	1205^{+35}_{-385}	CMD	1,13,4,-	–
69 Aqr	P	–	–	–	–	68.50	15.00±4	–	–	–	–	WDS	305^{+90}_{-25}	CMD	21,13,-,-	–
tau01 Gru	P	53297.03006	EHA	1276	76	5.30	-0.98±0.41	0.18±0.01	4.12±0.02	–	-5.14	–	625^{+0}_{-0}	Li	1,1,1,-	–
Fomalhaut	P	53278.20523	EHA	4064	0	84.64	±6.50	–	–	–	–	WDS, 52, 44	605^{+605}_{-515}	CMD	1,13,-,-	–
TYC8830-410-1	P	57293.52946	SWO	1270	32	–	8.97±2.42	–	–	–	–	–	375^{+0}_{-345}	Li (CMD)	-,1,-,-	–
HD 217792	P	–	–	–	–	27.70	-6.00±4	±0.18	–	–	–	55	830^{+165}_{-405}	CMD	21,13,49,-	–
TYC6972-692-1	P	57293.54240	SWO	1301	185	–	-0.84±2.31	–	–	–	–	WDS	30^{+0}_{-0}	Li	-,1,-,-	–
HR 8799	P	52850.98199	OEA	2621	0	42.27	-12.60±1	-0.47±0.15	–	–	–	WDS	30^{+5}_{-0}	Columba (CMD)	1,13,20,30	–
HD 218340	P	56468.36083	EHA	1217	17	3.83	3.65±0.33	0.24±0.02	4.56±0.04	–	-4.97	–	0^{+0}_{-625}	Li	1,1,1,-	–
HD 219623	P	52532.93012	OEA	1355	61	5.30	-25.83±1.92	0.04±0.05	–	–	–	WDS	625^{+0}_{-0}	Li	1,1,43,-	–
HD 219482	P	53602.30455	EHA	1408	76	7.68	0.66±0.73	-0.03±0.01	4.50±0.02	–	–	WDS	15^{+610}_{-0}	Castor (Li)	1,1,1,10	–
kap Psc	P	52241.77078	OEA	2966	0	41.67	-4.40±1	0.78±0.14	–	–	–	WDS	110^{+260}_{-0}	AB Dor (CMD)	1,30,42,10/30	–
HD 221853	P	57323.53387 57321.52949	SEO SWO	2195	0	36.80	-7.54±5.71	-0.20±0.03	3.05±0.16	–	–	WDS	375^{+0}_{-0}	Li	1,1,1,-	–
del Scl	P	53986.29537	EHA	7874	0	120.75	8.70±2	-0.11±0.08	–	–	–	WDS	110^{+40}_{-0}	AB Dor (CMD)	1,30,4,10/30	–
TYC2789-507-1	R	–	–	–	–	–	-9.10±2	–	–	–	–	–	610^{+75}_{-50}	CMD	-,13,-,-	–
TYC4294-584-1	R	9130	–	–	–	–	–	-5.40±1	–	–	–	–	–	475^{+50}_{-100}	CMD	-,13,-,- –
HD 870	R	54079.09029	EHA	1079	8	3.56	1.26±0.26	-0.02±0.01	4.59±0.01	–	-4.88	–	625^{+0}_{-0}	Li	1,1,1,-	–
HD 987	R	54245.41706	VUA	780	205	9.60	9.51±0.26	-0.10±0.01	4.52±0.01	-3.40	-4.60	WDS	30^{+95}_{-0}	Tuc-Hor (X-ray)	1,1,1,30	Li agreement
HD 1237	R	–	–	–	–	3.60	-2.10±0	0.06±0.03	–	-4.43	–	WDS	0^{+0}_{-375}	X-ray	21,13,56,-	–
TYC2272-1059-1	R	–	–	–	–	–	2.00±1	–	–	–	–	WDS	510^{+120}_{-110}	CMD	-,13,-,-	–
39 Psc	R	–	–	–	–	13.00	8.10±0	-0.15±0.08	–	-5.14	–	WDS	625^{+0}_{-0}	X-ray	34,13,4,-	–
26 And	R	–	–	–	–	18.00	1.00±6	–	–	–	–	WDS	205^{+80}_{-10}	CMD	61,13,-,-	–

Continued on Next Page...

Table C.1 – Continued

Name	Catalog	Obs. MJD	Instrument	Hα (mÅ)	Li6708 (mÅ)	$v \sin(i)$ (kms^{-1})	RV (kms^{-1})	[Fe/H] (dex)	log (g)	log ($\frac{L_X}{L_{bol}}$)	log (R'_{HK})	Multiple Ref.	Age (Myr)	Age-Dating Method	Refs	Notes
HD 1562	R	53278.99681	OEA	1165	19	4.31	15.46±1.64	-0.25±0.01	4.39±0.03	–	–	WDS	0^{+0}_{-625}	Li	1,1,1,-	–
TYC8846-897-1	R	–	–	–	–	–	–	–	–	–	–	–	415^{+95}_{-95}	CMD	-,-,-,-	–
TYC1186-730-1	R	–	–	–	–	–	–	–	–	–	–	–	590^{+410}_{-500}	CMD	-,-,-,-	–
TYC9135-268-1	R	57293.58130	SWO	224	0	–	47.54±18.50	–	–	–	–	–	1025^{+25}_{-275}	CMD	-,1,-,-	–
eta Phe	R	–	–	–	–	124.00	7.70±1	–	–	–	–	WDS	705^{+45}_{-130}	CMD	61,13,-,-	–
HR 189	R	–	–	–	–	164.00	-66.00±1	–	–	–	–	–	135^{+25}_{-40}	CMD	21,13,-,-	–
TYC8034-360-1	R	57320.46854	SWO	1519	0	–	7.82±3.61	–	–	–	–	–	*****	–	-,1,-,-	–
TYC4017-1710-1	R	–	–	–	–	–	-4.00±7	–	–	–	–	–	735^{+65}_{-355}	CMD	-,13,-,-	–
HD 5349	R	56912.30590	EHA	1008	35	5.75	-21.07±0.21	0.46±0.01	4.04±0.02	–	-5.18	–	*****	–	1,1,1,-	giant:Gaia
TYC2802-1387-1	R	–	–	–	–	–	6.00±2	–	–	–	–	–	680^{+95}_{-205}	CMD	-,13,-,-	–
TYC25-152-1	R	56679.14448	LHO	1262	0	5.23	-30.24±11.32	0.39±0.02	3.92±0.04	–	–	–	7943^{+7920}_{-7929}	CMD	1,1,1,-	–
TYC8479-1036-1	R	57320.47953	SWO	1552	26	–	71.03±4.74	–	–	–	–	–	625^{+0}_{-0}	Li	-,1,-,-	–
HD 7193	R	55096.06819	OSA	1394	74	7.70	-1.10±11.40	-0.32±0.01	4.08±0.03	-4.77	-4.60	–	375^{+250}_{-0}	Li (X-ray)	1,1,1,-	–
CPD-64 120	R	–	–	–	–	32.00	–	–	–	-3.02	–	–	100^{+25}_{-50}	CMD (X-ray)	21,-,-,-	–
TYC3272-1224-1	R	–	–	–	–	–	±-1.00	–	–	–	–	–	395^{+60}_{-80}	CMD	-,13,-,-	–
TYC2813-111-1	R	–	–	–	–	–	–	–	–	–	–	WDS	60^{+18}_{-16}	CMD	-,-,-,-	–
HD 8558	R	–	–	–	–	13.50	8.30±0	-0.24±0.08	–	-3.43	–	WDS	30^{+95}_{-0}	Tuc-Hor (X-ray)	21,30,4,30	–
TYC3265-2401-1	R	–	–	–	–	57.10	12.40±1	0.07±0.04	–	-5.30	–	WDS	625^{+0}_{-0}	X-ray	47,13,4,-	–
TYC3678-166-1	R	–	–	–	–	–	–	–	–	-4.17	–	–	0^{+0}_{-375}	X-ray	-,-,-,-	–
TYC4305-1804-1	R	–	–	–	–	–	–	-0.19±0.08	–	-4.89	–	–	625^{+0}_{-0}	X-ray	-,-,4,-	–
TYC2302-1580-1	R	–	–	–	–	48.00	-1.90±3	–	–	–	–	–	125^{+125}_{-45}	CMD	61,13,-,-	–
TYC4310-903-1	R	–	–	–	–	14.00	5.10±3	–	–	–	–	–	290^{+20}_{-40}	CMD	61,13,-,-	–
BD Phe	R	–	–	–	–	139.00	3.00±1	±-1.50	–	–	–	–	1030^{+45}_{-65}	CMD	61,13,49,-	–
TYC2824-15-1	R	–	–	–	–	–	–	–	–	–	–	–	1235^{+375}_{-225}	CMD	-,-,-,-	–
TYC7543-602-1	R	57293.59572	SWO	-923	15	–	-19.98±3.01	–	–	-3.04	–	–	375^{+0}_{-300}	Li (CMD)	-,1,-,-	Young? Hα emission
TYC9360-1318-1	R	–	–	–	–	11.70	6.80±0	-0.06±0.08	–	–	–	–	2370^{+30}_{-250}	CMD	21,13,4,-	–
TYC8485-568-1	R	57320.55252	SWO	1206	0	–	1.22±7.82	–	–	–	–	–	*****	–	-,1,-,-	–
TYC7553-86-1	R	57320.56190	SWO	1437	19	–	68.05±4.05	–	–	–	–	–	625^{+0}_{-0}	Li	-,1,-,-	–
TYC1757-1096-1	R	–	–	–	–	–	–	–	–	–	–	–	50^{+50}_{-50}	CMD	-,-,-,-	ZAMS
50 Cas	R	53669.03505	OEA	4017	0	58.78	-18.20±1	0.00±0.01	–	–	–	–	500^{+100}_{-5}	CMD	1,13,41,-	–
TYC4689-810-1	R	56257.23927	LHO	1339	0	5.18	–	–	–	–	–	–	*****	–	1,-,-,-	–
TYC2321-561-1	R	56165.41409	LHO	974	17	21.89	-76.19±44.65	-0.24±0.03	3.33±0.05	–	–	–	*****	–	1,1,1,-	giant:Gaia
TYC2838-2293-1	R	–	–	–	–	–	–	–	–	–	–	–	1390^{+150}_{-460}	CMD	-,-,-,-	–
TYC3294-2222-1	R	–	–	–	–	–	–	–	–	-3.44	–	–	125^{+0}_{-0}	X-ray	-,-,-,-	–
kap For	R	51893.83683	OEA	1244	48	5.18	18.00±1.64	-0.11±0.01	3.69±0.03	-4.56	–	WDS	625^{+0}_{-0}	Li	1,1,1,-	X-ray agreement
HD 15060	R	57418.42810	SEO	1252	0	9.47	-15.91±13.84	-0.43±0.01	4.20±0.04	–	–	–	*****	–	1,1,1,-	–
HD 14907	R	–	–	–	–	25.10	22.20±1	-0.14±0.05	–	-4.36	–	–	0^{+375}_{-0}	X-ray	21,13,4,-	–
TYC2335-45-1	R	–	–	–	–	43.00	5.70±4	–	–	–	–	WDS	390^{+105}_{-140}	CMD	61,13,-,-	–
TYC4046-1651-1	R	–	–	–	–	–	-6.00±8	–	–	–	–	–	525^{+105}_{-80}	CMD	-,13,-,-	–
TYC1774-769-1	R	56679.23066	LHO	1125	0	3.24	68.01±9.10	0.03±0.02	4.37±0.04	–	–	–	*****	–	1,1,1,-	no age info.
TYC638-129-1	R	–	–	–	–	–	–	–	–	–	–	–	1510^{+240}_{-75}	CMD	-,-,-,-	–

Continued on Next Page...

Table C.1 – Continued

Name	Catalog	Obs. MJD	Instrument	Hα (mÅ)	Li6708 (mÅ)	$v \sin(i)$ (kms^{-1})	RV (kms^{-1})	[Fe/H] (dex)	log (g)	log ($\frac{L_X}{L_{bol}}$)	log (R'_{HK})	Multiple Ref.	Age (Myr)	Age-Dating Method	Refs	Notes
TYC2327-1909-1	R	–	–	–	–	–	–	–	–	–	–	–	565^{+180}_{-185}	CMD	-,-,-,-	–
TYC2832-2209-1	R	–	–	–	–	–	–	–	–	–	–	–	950^{+155}_{-90}	CMD	-,-,-,-	–
TYC2335-1086-1	R	–	–	–	–	–	–	–	–	–	–	–	780^{+30}_{-235}	CMD	-,-,-,-	–
TYC4051-785-1	R	–	–	–	–	–	1.70±2	–	–	–	–	WDS	315^{+75}_{-85}	CMD	-,13,-,-	–
TYC4051-1211-1	R	–	–	–	–	–	–	–	–	–	–	WDS	590^{+90}_{-190}	CMD	-,-,-,-	–
12 Per	R	52211.02403	OEA	1364	32	14.24	-22.91±2.92	±0.21	–	-6.27	–	WDS	625^{+4000}_{-0}	Li (X-ray)	1,1,28,-	–
TYC1776-36-1	R	–	–	–	–	–	3.90±2	–	–	–	–	–	810^{+70}_{-175}	CMD	-,13,-,-	–
TYC5289-743-1	R	57320.59407	SWO	1328	6	–	35.57±1.97	–	–	–	–	–	625^{+0}_{-0}	Li	-,1,-,-	–
HR 820	R	57287.41375	DMO	2056	8	35.10	-3.50±3	-0.13±0.08	–	–	–	WDS	625^{+325}_{-0}	Li (CMD)	1,13,4,-	–
BD+14 466	R	56641.81418	OSA	1010	18	4.19	-5.95±3.07	0.20±0.01	4.06±0.01	–	-4.92	–	*****	–	1,1,1,-	giant:Gaia
TYC3704-1028-1	R	53343.90507	OEA	6411	0	69.33	7.70±7	–	–	–	–	–	710^{+75}_{-85}	CMD	1,13,-,-	–
TYC3701-937-1	R	–	–	–	–	–	0.10±2	–	–	–	–	–	885^{+35}_{-350}	CMD	-,13,-,-	–
TYC3709-994-1	R	–	–	–	–	–	–	–	–	–	–	–	875^{+205}_{-530}	CMD	-,-,-,-	–
TYC7015-583-1	R	57320.60971	SWO	1123	4	–	29.23±2.17	–	–	–	–	–	375^{+0}_{-325}	Li (CMD)	-,1,-,-	–
TYC4060-490-1	R	–	–	–	–	–	–	–	–	–	–	–	50^{+50}_{0}	CMD	-,-,-,-	assumed ZAMS
bet Per	R	50469.79398	OEA	2730	0	45.52	3.70±4	–	–	–	–	WDS	385^{+290}_{-185}	CMD	1,13,-,-	–
TYC2847-544-1	R	–	–	–	–	–	–	–	–	–	–	–	55^{+0}_{-50}	CMD	-,-,-,-	assumed ZAMS
BD+21 418	R	54365.13325	OSA	995	149	10.27	5.31±58.48	0.06±0.03	4.34±0.06	-3.99	-4.48	WDS	125^{+0}_{-0}	Li	1,1,1,-	X-ray agreement
HD 19624	R	–	–	–	–	280.00	1.40±2	–	–	–	–	–	500^{+100}_{-80}	CMD	21,13,-,-	–
TYC4049-426-1	R	–	–	–	–	–	–	–	–	–	–	–	2310^{+445}_{-2020}	CMD	-,-,-,-	–
HD 19893	R	–	–	–	–	270.00	0.00±4	–	–	–	–	–	600^{+50}_{-125}	CMD	21,13,-,-	–
TYC7023-69-1	R	57320.62200	SWO	1479	3	–	95.24±4.07	–	–	–	–	WDS	0^{+0}_{-625}	Li	-,1,-,-	–
HD 20631	R	57358.54913 57320.63365	SEO SWO	1706	0	40.53	15.20±7.20	0.78±0.03	4.00±0.09	–	–	WDS	1180^{+335}_{-335}	CMD	1,1,1,-	–
TYC8860-1359-1	R	57320.64030	SWO	1585	0	–	8.29±3.96	–	–	–	–	–	*****	–	-,1,-,-	no age info.
HD 20759	R	57293.71911 57358.55709	SWO SEO	1829	0	19.53	22.78±5.67	0.33±0.03	3.44±0.09	–	–	–	0^{+0}_{-625}	Li	1,1,1,-	–
e Eri	R	–	–	–	–	2.00	87.40±1	-0.38±0.02	–	-6.75	–	–	4000^{+0}_{-0}	X-ray	3,13,29,-	–
V459 Per	R	–	–	–	–	72.30	±-11.00	0.21±0.13	–	–	–	–	380^{+755}_{-375}	CMD	21,24,49,-	–
TYC3715-724-1	R	–	–	–	–	–	–	–	–	–	–	WDS	795^{+210}_{-790}	CMD	-,-,-,-	–
TYC1809-78-1	R	–	–	–	–	–	6.40±3	–	–	–	–	–	765^{+60}_{-120}	CMD	-,13,-,-	–
TYC7027-1218-1	R	–	–	–	–	136.00	19.00±0	–	–	–	–	WDS	785^{+110}_{-15}	CMD	61,13,-,-	–
HD 21091	R	–	–	–	–	321.00	1.80±1	–	–	–	–	–	540^{+55}_{-130}	CMD	21,13,-,-	–
HD 21122	R	–	–	–	–	–	4.50±2	–	–	–	–	–	1000^{+135}_{-120}	CMD	-,13,-,-	–
TYC3316-489-1	R	–	–	–	–	–	4.50±2	–	–	–	–	–	1000^{+135}_{-120}	CMD	-,13,-,-	–
HD 21117	R	–	–	–	–	–	3.10±2	–	–	–	–	–	810^{+105}_{-35}	CMD	-,13,-,-	–
HD 21375	R	–	–	–	–	260.00	1.50±1	–	–	–	–	–	865^{+90}_{-75}	CMD	21,13,-,-	–
TYC3320-399-1	R	–	–	–	–	260.00	1.50±1	–	–	–	–	–	865^{+90}_{-75}	CMD	21,13,-,-	–
TYC3316-2311-1	R	–	–	–	–	136.00	1.60±1	–	–	–	–	WDS	725^{+95}_{-70}	CMD	61,13,-,-	–
HD 21480	R	–	–	–	–	48.20	–	–	–	–	–	–	1530^{+140}_{-345}	CMD	21,-,-,-	–
TYC4326-1934-1	R	–	–	–	–	88.00	–	–	–	–	–	–	500^{+75}_{-50}	CMD	61,-,-,-	–

Continued on Next Page. . .

Table C.1 – Continued

Name	Catalog	Obs. MJD	Instrument	Hα (mÅ)	Li6708 (mÅ)	$v \sin(i)$ (kms^{-1})	RV (kms^{-1})	[Fe/H] (dex)	log (g)	log ($\frac{L_X}{L_{bol}}$)	log (R'_{HK})	Multiple Ref.	Age (Myr)	Age-Dating Method	Refs	Notes
CD-46 1064	R	–	–	–	–	–	–	–	–	-3.61	–	–	36^{+90}_{-2}	CMD (X-ray)	-,-,-,-	–
TYC1806-170-1	R	–	–	–	–	85.60	8.00±4	–	–	–	–	WDS	400^{+145}_{-140}	CMD	21,13,-,-	–
HR 1056	R	–	–	–	–	217.00	-21.40±2	–	–	–	–	–	720^{+90}_{-75}	CMD	61,13,-,-	–
HD 21641	R	–	–	–	–	202.00	3.30±1	–	–	–	–	WDS	405^{+85}_{-50}	CMD	21,13,-,-	–
TYC8870-626-1	R	57320.65161	SWO	1906	10	–	5.32±3.74	–	–	–	–	–	0^{+0}_{-625}	Li	-,1,-,-	–
HD 22705	R	–	–	–	–	17.10	14.40±1	-0.17±0.08	–	-4.16	–	WDS, 54	30^{+345}_{-0}	Tuc-Hor (X-ray)	21,30,4,30	–
TYC2874-69-1	R	–	–	–	–	–	12.00±7	–	–	–	–	WDS	765^{+35}_{-130}	CMD	-,13,-,-	–
TYC1803-410-1	R	–	–	–	–	25.70	3.00±3	–	–	–	–	WDS	290^{+110}_{-190}	CMD	21,13,-,-	–
TYC4723-932-1	R	–	–	–	–	–	–	–	–	–	–	–	250^{+245}_{-250}	CMD	-,-,-,-	–
TYC5880-75-1	R	54282.41660	VUA	563	260	12.11	19.36±0.34	-0.18±0.01	4.24±0.02	–	–	–	30^{+0}_{-0}	Li	1,1,1,-	–
TYC7031-220-1	R	–	–	–	–	–	–	–	–	–	–	–	1985^{+565}_{-520}	CMD	-,-,-,-	–
TYC1799-1062-1	R	57272.39810	DMO	2402	0	41.08	-46.90±2	0.12±0.07	–	–	–	WDS	125^{+725}_{-0}	Pleiades (CMD)	1,13,49,50	–
TYC1803-486-1	R	–	–	–	–	30.40	2.60±2	0.20±0.10	–	–	–	–	125^{+35}_{-0}	Pleiades (CMD)	21,24,49,50	–
TYC 1803-818-1	R	–	–	–	–	13.32	4.95±0	-0.15±0.47	–	–	–	–	125^{+0}_{-0}	Pleiades	57,33,26,50	–
TYC1799-1440-1	R	–	–	–	–	212.00	5.50±1	–	–	–	–	WDS	125^{+495}_{-0}	Pleiades (CMD)	61,13,-,50	–
TYC 1803-1061-1	R	–	–	–	–	16.83	5.14±0	0.06±0.31	–	–	–	–	125^{+0}_{-0}	Pleiades	57,33,26,50	–
TYC1799-306-1	R	–	–	–	–	68.10	8.20±1	0.34±0.10	–	–	–	–	125^{+1040}_{-0}	Pleiades (CMD)	21,24,49,50	–
TYC1803-1583-1	R	–	–	–	–	212.00	4.80±1	–	–	–	–	WDS	125^{+35}_{-0}	Pleiades (CMD)	61,13,-,50	–
TYC9156-2237-1	R	–	–	–	–	30.00	6.60±1	–	–	–	–	–	80^{+70}_{-50}	CMD	21,13,-,-	–
V1045 Tau	R	–	–	–	–	10.60	6.43±0	0.04±0.17	–	–	–	WDS	125^{+0}_{-0}	Pleiades	21,33,26,50	–
TYC1800-1908-1	R	–	–	–	–	85.60	6.40±1	-0.02±0.22	–	–	–	WDS	125^{+575}_{-0}	Pleiades (CMD)	21,24,49,50	–
TYC1804-2081-1	R	–	–	–	–	214.00	9.10±1	–	–	–	–	WDS	125^{+215}_{-0}	Pleiades (CMD)	21,13,-,50	–
TYC2875-1341-1	R	–	–	–	–	–	7.30±2	–	–	–	–	–	320^{+80}_{-160}	CMD	-,22,-,-	–
TYC1800-2201-1	R	–	–	–	–	133.00	7.70±2	-0.08±0.16	–	–	–	CCDM	125^{+385}_{-0}	Pleiades (CMD)	21,24,49,50	–
BD+23 551	R	–	–	–	–	18.40	–	-0.07±0.17	–	–	–	–	125^{+0}_{-0}	Pleiades	21,-,26,50	–
HD 23763	R	–	–	–	–	85.60	7.00±1	–	–	–	–	WDS	125^{+660}_{-0}	Pleiades (CMD)	21,13,-,50	–
TYC1804-2047-1	R	–	–	–	–	94.20	7.20±1	–	–	–	–	CCDM	125^{+195}_{-0}	Pleiades (CMD)	21,13,-,50	–
TYC5884-1513-1	R	57294.72375 57432.46328	SWO SEO	3099	70	55.01	17.78±13.30	-0.21±0.02	4.08±0.07	–	–	–	125^{+0}_{-0}	Li	1,1,1,-	–
TYC3725-758-1	R	–	–	–	–	–	13.30±2	–	–	–	–	WDS	795^{+20}_{-315}	CMD	-,13,-,-	–
HR 1183	R	54146.78176	OSA	4793	0	142.99	9.50±0	–	–	–	–	WDS	125^{+70}_{-0}	Pleiades (CMD)	1,13,-,50	–
TYC2360-286-1	R	–	–	–	–	–	–	–	–	–	–	–	1995^{+250}_{-890}	CMD	-,-,-,-	–
TYC1804-1545-1	R	–	–	–	–	72.80	8.30±3	–	–	–	–	–	725^{+40}_{-475}	CMD	21,24,-,-	–
HD 24649	R	57294.75506 57418.44530	SWO SEO	1788	83	36.43	14.30±4.26	0.95±0.00	4.35±0.05	-4.37	–	–	125^{+250}_{-0}	Li (X-ray)	1,1,1,-	–
TYC1813-734-1	R	–	–	–	–	34.20	13.00±5	–	–	–	–	–	1070^{+220}_{-255}	CMD	21,13,-,-	–
TYC2876-1915-1	R	–	–	–	–	–	3.40±2	–	–	–	–	–	410^{+90}_{-160}	CMD	-,13,-,-	–

Continued on Next Page. . .

Table C.1 – Continued

Name	Catalog	Obs. MJD	Instrument	Hα (mÅ)	Li6708 (mÅ)	$v \sin(i)$ (kms^{-1})	RV (kms^{-1})	[Fe/H] (dex)	log (g)	log ($\frac{L_X}{L_{bol}}$)	log (R'_{HK})	Multiple Ref.	Age (Myr)	Age-Dating Method	Refs	Notes
TYC2868-941-1	R	–	–	–	–	–	–	–	–	–	–	–	50^{+350}_{-10}	CMD	-,-,-,-	–
TYC2881-432-1	R	56679.26005	LHO	1662	0	22.54	26.31±31.26	0.17±0.05	2.56±0.11	–	–	–	*****	–	1,1,1,-	no age info.
TYC1822-2314-1	R	–	–	–	–	21.70	2.30±4	±0.03	–	–	–	–	130^{+55}_{-30}	CMD	21,13,49,-	–
TYC2877-249-1	R	56679.28354	LHO	2488	0	31.73	–	–	–	–	–	–	2045^{+270}_{-445}	CMD	1,-,-,-	–
TYC5312-2218-1	R	57293.73609 57432.48713	SWO SEO	2007	8	12.90	43.63±4.33	-0.25±0.01	3.65±0.06	–	–	–	0^{+0}_{-625}	Li	1,1,1,-	–
TYC4072-576-1	R	56679.33958	LHO	1816	0	13.60	–	-0.13±0.03	3.43±0.08	–	–	–	*****	–	1,-,1,-	–
HD 27346	R	57418.45766	SEO	1526	36	63.13	–	0.34±0.01	4.90±0.00	–	–	–	1300^{+45}_{-640}	CMD	1,-,1,-	–
HD 26784	R	50737.94696	OEA	1669	80	17.74	38.70±4.10	0.14±0.04	–	-4.65	–	–	625^{+0}_{-250}	Hyades (Li)	1,1,53,38	X-ray agreement
V819 Tau	R	–	–	–	–	–	–	–	–	-3.50	–	WDS	625^{+0}_{-0}	X-ray	-,-,-,-	–
HD 27934	R	–	–	–	–	94.00	37.30±1	±0.05	–	–	–	–	625^{+270}_{-0}	Hyades (CMD)	61,13,4,38	–
V776 Tau	R	57082.11002	DMO	1363	0	2.94	39.00±0	±0.13	–	–	–	WDS	625^{+0}_{-100}	Hyades (CMD)	1,13,42,38	–
HD 28069	R	57418.46624	SEO	1243	110	26.80	1.45±44.39	0.78±0.01	3.66±0.04	-4.46	–	–	375^{+0}_{-250}	X-ray (Li)	1,1,1,-	–
TYC7578-425-1	R	–	–	–	–	–	–	–	–	-2.75	–	–	20^{+0}_{-0}	CMD	-,-,-,-	X-ray agreement
TYC6463-1240-1	R	–	–	–	–	5.40	–	-0.31±0.08	–	-4.42	–	–	50^{+325}_{50}	CMD (X-ray)	21,-,4,-	assumed ZAMS
HR 1427	R	53321.01767	OEA	3204	0	63.26	38.10±1	±0.13	–	–	–	WDS	*****	–	1,13,4,-	–
TYC1269-469-1	R	–	–	–	–	–	–	–	–	-3.15	–	WDS	125^{+0}_{-0}	X-ray	-,-,-,-	–
TYC2888-369-1	R	57082.21400	DMO	2266	0	57.45	2.20±2	–	–	–	–	CCDM	200^{+195}_{-195}	CMD	1,13,-,-	–
HU Tau	R	57082.15169	DMO	1218	0	53.98	-2.30±4	–	–	–	–	–	420^{+70}_{-95}	CMD	1,13,-,-	–
TYC3346-806-1	R	–	–	–	–	–	–	–	–	–	–	–	795^{+695}_{-790}	CMD	-,-,-,-	–
TYC1835-1066-1	R	–	–	–	–	–	–	–	–	–	–	WDS	1615^{+30}_{-405}	CMD	-,-,-,-	–
TYC5322-663-1	R	57434.47914	SWO	-125	7	–	29.69±4.14	–	–	-3.21	–	–	*****	–	-,1,-,-	giant:Gaia
HD 282630	R	49711.81730	OEA	-560	459	24.50	11.11±4.85	–	–	-3.01	–	WDS	8^{+125}_{-0}	Li	1,1,-,-	–
TYC7587-734-1	R	57321.70264	SWO	1916	51	–	56.50±4.64	–	–	–	–	–	125^{+0}_{-0}	Li	-,1,-,-	–
TYC4342-270-1	R	–	–	–	–	187.00	1.00±5	–	–	–	–	–	570^{+5}_{-70}	CMD	61,13,-,-	–
TYC2906-2792-1	R	–	–	–	–	–	–	–	–	-2.76	–	–	0^{+125}_{-0}	X-ray	-,-,-,-	–
TYC2396-810-1	R	–	–	–	–	–	8.00±3	–	–	–	–	–	2110^{+585}_{-125}	CMD	-,13,-,-	–
ome Aur	R	50472.89770	OEA	4876	0	79.63	7.70±2	±-0.12	–	–	–	WDS	390^{+100}_{-100}	CMD	1,13,49,-	–
TYC1853-1069-1	R	–	–	–	–	–	–	–	–	–	–	–	1035^{+60}_{-80}	CMD	-,-,-,-	–
TYC7050-818-1	R	–	–	–	–	–	–	–	–	–	–	–	970^{+1470}_{-945}	CMD	-,-,-,-	–
TYC4511-575-1	R	–	–	–	–	–	–	–	–	–	–	–	1010^{+30}_{-90}	CMD	-,-,-,-	–
h Ori	R	53405.81204	OEA	1857	0	11.32	44.44±0	0.45±0.12	–	–	–	WDS	625^{+495}_{-0}	Hyades (CMD)	1,13,49,38	–
TYC9161-718-1	R	57321.70731	SWO	1080	8	–	-0.59±1.93	–	–	–	–	–	125^{+25}_{-75}	Li (CMD)	-,1,-,-	–
TYC8097-337-1	R	57321.71705	SWO	1419	94	–	62.15±2.62	–	–	–	–	WDS	125^{+0}_{-0}	Li	-,1,-,-	–
TYC3747-1379-1	R	56258.49646	LHO	3986	0	108.23	–	-0.68±0.03	3.61±0.17	–	–	–	*****	–	1,-,1,-	–
TYC2896-391-1	R	–	–	–	–	–	–	–	–	-4.53	–	–	0^{+0}_{-375}	X-ray	-,-,-,-	–
TYC8085-246-1	R	–	–	–	–	–	–	–	–	-4.93	–	–	625^{+0}_{-0}	X-ray	-,-,-,-	–
TYC5331-856-1	R	57321.74862	SWO	1134	11	–	39.26±1.85	–	–	–	–	–	625^{+0}_{-25}	Li (CMD)	-,1,-,-	–

Continued on Next Page...

Table C.1 – Continued

Name	Catalog	Obs. MJD	Instrument	Hα (mÅ)	Li6708 (mÅ)	$v \sin(i)$ (kms^{-1})	RV (kms^{-1})	[Fe/H] (dex)	log (g)	log ($\frac{L_X}{L_{bol}}$)	log (R'_{HK})	Multiple Ref.	Age (Myr)	Age-Dating Method	Refs	Notes
HD 35150	R	–	–	–	–	–	–	–	–	–	–	–	500^{+295}_{-260}	CMD	-,-,-,-	–
HD 287787	R	–	–	–	–	–	–	–	–	–	–	WDS	695^{+35}_{-695}	CMD	-,-,-,-	–
HD 35416	R	–	–	–	–	11.70	-10.50±1	-0.40±0.08	–	–	–	WDS	175^{+890}_{-140}	CMD	21,13,4,-	–
HD 35351	R	–	–	–	–	–	–	–	–	–	–	–	495^{+115}_{-125}	CMD	-,-,-,-	–
HD 35367	R	–	–	–	–	–	–	–	–	–	–	–	250^{+405}_{-250}	CMD	-,-,-,-	–
HD 35650	R	54784.24615	VUA	427	9	6.46	29.36±0.19	-0.14±0.01	4.17±0.03	-3.64	–	–	110^{+15}_{-50}	AB Dor (X-ray,CMD)	1,1,1,30	–
TYC1847-1200-1	R	56679.42301	LHO	1285	178	6.58	16.85±11.56	0.13±0.02	3.87±0.05	–	–	–	30^{+0}_{-0}	Li	1,1,1,-	–
HD 287861	R	–	–	–	–	–	–	–	–	–	–	–	0^{+480}_{-0}	CMD	-,-,-,-	assumed ZAMS
HD 287850	R	–	–	–	–	–	–	–	–	–	–	–	440^{+565}_{-435}	CMD	-,-,-,-	–
TYC8089-513-1	R	57434.49697	SWO	1166	6	–	54.62±1.93	–	–	–	–	–	*****	–	-,1,-,-	giant:Gaia
HD 287854	R	–	–	–	–	–	–	–	–	–	–	–	775^{+770}_{-390}	CMD	-,-,-,-	–
HD 35625	R	–	–	–	–	–	–	–	–	–	–	–	160^{+225}_{-160}	CMD	-,-,-,-	–
TYC113-534-1	R	57082.23322	DMO	3807	0	61.19	13.10±4	–	–	–	–	WDS	125^{+135}_{-125}	CMD	1,13,-,-	–
VZ Col	R	56382.02399	EHA	524	20	6.27	-3.81±0.27	-0.21±0.02	3.18±0.06	-5.25	–	–	30^{+33}_{-0}	Li (CMD)	1,1,1,-	X-ray no agreement
HR 1832	R	57082.16704	DMO	3215	0	114.74	-16.00±4	–	–	–	–	–	830^{+65}_{-75}	CMD	1,13,-,-	–
TYC126-1078-1	R	–	–	–	–	–	–	–	–	-4.53	–	–	0^{+375}_{-0}	X-ray	-,-,-,-	–
HD 290540	R	–	–	–	–	–	–	–	–	–	–	–	50^{+50}_{-50}	CMD	-,-,-,-	–
HD 36444	R	–	–	–	–	–	–	–	–	–	–	–	415^{+85}_{-100}	CMD	-,-,-,-	–
HD 290598	R	–	–	–	–	–	–	–	–	–	–	–	255^{+255}_{-245}	CMD	-,-,-,-	–
TYC8090-477-1	R	–	–	–	–	–	–	–	–	–	–	WDS	990^{+35}_{-80}	CMD	-,-,-,-	–
TYC1860-185-1	R	–	–	–	–	–	25.40±10	–	–	–	–	–	50^{+96}_{0}	CMD	-,13,-,-	assumed ZAMS
TYC705-940-1	R	–	–	–	–	24.20	–	–	–	-2.68	–	–	0^{+125}_{-0}	X-ray	21,-,-,-	–
TYC4089-1079-1	R	–	–	–	–	–	9.10±3	–	–	–	–	–	755^{+40}_{-445}	CMD	-,13,-,-	–
TYC709-241-1	R	–	–	–	–	–	–	–	–	–	–	–	50^{+50}_{0}	CMD	-,-,-,-	assumed ZAMS
TYC4081-2201-1	R	–	–	–	–	–	-7.00±4	–	–	–	–	–	435^{+190}_{-390}	CMD	-,13,-,-	–
TYC2918-2067-1	R	–	–	–	–	–	–	–	–	–	–	–	1220^{+310}_{-80}	CMD	-,-,-,-	–
TYC4779-587-1	R	57081.18750	DMO	1538	91	19.03	–	–	–	-4.87	–	–	125^{+500}_{-0}	Li (X-ray)	1,-,-,-	–
TYC722-21-1	R	57082.24851	DMO	2982	0	8.18	-5.00±9	-0.04±0.08	–	–	–	–	1540^{+310}_{-375}	CMD	1,13,4,-	–
HR 1966	R	–	–	–	–	195.00	28.10±2	–	–	–	–	–	265^{+75}_{-95}	CMD	61,13,-,-	–
TYC1873-26-1	R	–	–	–	–	–	–	–	–	–	–	–	1040^{+440}_{-170}	CMD	-,-,-,-	–
TYC4779-179-1	R	57082.11867	DMO	1682	110	39.48	–	–	–	-4.48	–	–	125^{+250}_{-0}	Li (X-ray)	1,-,-,-	–
TYC8891-115-1	R	57434.56902	SWO	1610	24	–	9.96±4.44	–	–	–	–	–	375^{+0}_{-0}	Li	-,1,-,-	–
TYC4775-384-1	R	–	–	–	–	–	–	-0.14±0.08	–	-5.22	–	WDS	625^{+0}_{-0}	X-ray	-,-,4,-	–
gam Lep	R	57358.69561	SEO	1130	64	12.28	-9.29±0	-0.05±0.01	4.25±0.03	–	–	WDS	625^{+0}_{-0}	Li	1,13,1,-	–
TYC2405-551-1	R	–	–	–	–	–	–	–	–	–	–	–	500^{+115}_{-115}	CMD	-,-,-,-	–
HD 38949	R	57418.52234	SEO	1128	104	11.43	-24.52±47.21	0.32±0.01	4.47±0.04	-4.77	–	–	125^{+500}_{-0}	Li (X-ray)	1,1,1,-	–
TYC2912-46-1	R	–	–	–	–	–	–	-0.17±0.23	–	–	–	–	50^{+50}_{0}	CMD	-,-,26,-	assumed ZAMS
TYC8529-1004-1	R	–	–	–	–	–	–	–	–	-4.35	–	–	0^{+0}_{-375}	X-ray	-,-,-,-	–
TYC3382-1505-1	R	–	–	–	–	18.00	25.40±4	–	–	–	–	–	310^{+45}_{-120}	CMD	61,13,-,-	–

Continued on Next Page. . .

Table C.1 – Continued

Name	Catalog	Obs. MJD	Instrument	Hα (mÅ)	Li6708 (mÅ)	$v \sin(i)$ (kms^{-1})	RV (kms^{-1})	[Fe/H] (dex)	log (g)	log ($\frac{L_X}{L_{bol}}$)	log (R'_{HK})	Multiple Ref.	Age (Myr)	Age-Dating Method	Refs	Notes
TYC1313-1482-1	R	–	–	–	–	–	–	–	–	-3.10	–	–	39^{+5}_{-6}	CMD	-,-,-,-	X-ray agreement
TYC4790-1831-1	R	–	–	–	–	–	–	-0.76±0.50	–	–	–	WDS	435^{+190}_{-325}	CMD	-,-,26,-	–
alf Men	R	–	–	–	–	2.30	37.10±1	0.13±0.02	–	-6.77	–	WDS	110^{+0}_{-0}	AB Dor	21,13,29,1	–
TYC8110-320-1	R	57321.76213	SWO	1592	57	–	27.46±2.91	–	–	–	–	–	625^{+0}_{-0}	Li	-,1,-,-	–
TYC5371-1216-1	R	–	–	–	–	–	–	–	–	–	–	–	1475^{+150}_{-305}	CMD	-,-,-,-	–
TYC8110-1373-1	R	–	–	–	–	–	–	–	–	–	–	–	2040^{+530}_{-870}	CMD	-,-,-,-	–
TYC1878-756-1	R	–	–	–	–	–	–	–	–	–	–	–	1195^{+305}_{-345}	CMD	-,-,-,-	–
TYC8107-500-1	R	–	–	–	–	–	–	–	–	-3.21	–	–	0^{+125}_{-0}	X-ray	-,-,-,-	–
HD 46375	R	56273.17204	EHA	1028	8	5.75	-0.93±0.23	0.28±0.02	3.57±0.03	–	-4.83	WDS	625^{+0}_{-600}	Li (CMD)	1,1,1,-	–
TYC7622-1681-1	R	57434.58153	SWO	1570	26	–	-5.95±2.80	–	–	–	–	–	625^{+0}_{-0}	Li	-,1,-,-	–
HD 46317	R	57287.36362	DMO	1472	47	12.02	6.10±0	-0.24±0.10	–	–	–	–	625^{+0}_{-0}	Li	1,13,49,-	–
HD 49855	R	–	–	–	–	10.80	20.70±0	-0.14±0.08	–	-3.87	–	WDS	125^{+0}_{-0}	X-ray	21,30,4,-	–
TYC9493-1937-1	R	57432.50744	SEO	1439	26	15.18	0.12±9.51	-0.41±0.02	3.15±0.07	–	–	–	0^{+0}_{-625}	Li	1,1,1,-	–
TYC5385-1444-1	R	57434.59596	SWO	825	6	–	-31.06±2.14	–	–	–	–	–	125^{+0}_{-42}	Li (CMD)	-,1,-,-	–
TYC7633-97-1	R	7434.62881	SWO	1203	14	–	87.79±1.97	–	–	–	–	–	625^{+0}_{-0}	Li	-,1,-,-	–
TYC8554-1604-1	R	57434.51377	SWO	1075	15	–	47.88±1.73	–	–	–	–	–	*****	–	-,1,-,-	giant:Gaia
48 Gem	R	57082.18252	DMO	2521	0	69.33	14.23±6	0.13±0.21	–	–	–	–	*****	–	1,16,49,-	CMD giant branch
TYC8559-1994-1	R	–	–	–	–	–	–	–	–	–	–	WDS	30^{+170}_{-30}	CMD	-,-,-,-	assumed ZAMS
TYC8137-2204-1	R	–	–	–	–	–	–	–	–	–	–	–	615^{+2415}_{-575}	CMD	-,-,-,-	–
TYC2958-831-1	R	57082.32014	DMO	4843	0	62.77	7.00±4	–	–	–	–	–	400^{+130}_{-275}	CMD	1,13,-,-	–
TYC6543-1535-1	R	–	–	–	–	–	–	–	–	–	–	–	21^{+4}_{-2}	CMD	-,-,-,-	–
HD 60491	R	57358.71153	SEO	753	26	11.69	-15.03±15.33	0.04±0.02	4.71±0.03	-4.56	–	–	375^{+0}_{-275}	Li (CMD)	1,1,1,-	–
TYC7648-583-1	R	–	–	–	–	–	–	–	–	–	–	–	75^{+50}_{-50}	CMD	-,-,-,-	ZAMS
HD 60234	R	55129.16834	OSA	1280	3	8.48	-1.46±7.78	0.00±0.01	3.53±0.02	-5.02	-5.00	–	0^{+0}_{-625}	Li	1,1,1,-	X-ray agreement
HD 60856	R	–	–	–	–	42.80	31.20±2	–	–	–	–	–	310^{+45}_{-120}	CMD	21,13,-,-	–
2MASS J07372200-1424262	R	57434.52649	SWO	1228	0	–	151.63±2.32	–	–	–	–	WDS	*****	–	-,1,-,-	no age info.
HD 60737	R	57081.24934	DMO	1199	104	3.49	6.45±0	0.01±0.04	–	-4.31	–	WDS	125^{+0}_{-0}	Li	1,13,4,-	–
TYC7114-2140-1	R	57432.53311	SEO	1622	0	39.38	–	0.12±0.03	4.23±0.09	–	–	–	50^{+30}_{0}	CMD	1,-,1,-	assumed ZAMS
HD 62938	R	–	–	–	–	–	–	–	–	–	–	–	400^{+110}_{-150}	CMD	-,-,-,-	–
CD-37 3869	R	57434.55910	SWO	1665	53	–	-13.27±2.67	–	–	–	–	–	625^{+0}_{-0}	Li	-,1,-,-	–
2MASS J07454585-3753499	R	57433.57132	SWO	333	236	–	23.05±1.84	–	–	–	–	–	30^{+0}_{-0}	Li	-,1,-,-	–
CPD-37 1582	R	57433.58831	SWO	1602	90	–	-2.42±2.49	–	–	–	–	–	125^{+0}_{-0}	Li	-,1,-,-	–
2MASS J07465939-3822415	R	57433.60197	SWO	651	169	–	13.81±2.62	–	–	–	–	–	30^{+0}_{-0}	Li	-,1,-,-	–
TYC188-407-1	R	–	–	–	–	–	–	–	–	–	–	–	795^{+60}_{-5}	CMD	-,-,-,-	–
CD-60 1960	R	–	–	–	–	163.00	–	–	–	–	–	–	970^{+30}_{-220}	CMD	21,-,-,-	–
CD-60 2007	R	57434.60648	SWO	6355	0	–	5.13±14.66	–	–	–	–	–	1240^{+1740}_{-1215}	CMD	-,1,-,-	–
TYC206-1249-1	R	56257.54111	LHO	1332	29	8.63	-7.86±1.79	-0.35±0.02	3.76±0.05	–	–	WDS	625^{+0}_{-0}	Li	1,1,1,-	–

Continued on Next Page. . .

Table C.1 – Continued

Name	Catalog	Obs. MJD	Instrument	Hα (mÅ)	Li6708 (mÅ)	$v \sin(i)$ (kms^{-1})	RV (kms^{-1})	[Fe/H] (dex)	log (g)	log ($\frac{L_X}{L_{bol}}$)	log (R'_{HK})	Multiple Ref.	Age (Myr)	Age-Dating Method	Refs	Notes
HD 67985	R	–	–	–	–	–	–	–	–	–	–	–	170^{+70}_{-90}	CMD	-,-,-,-	–
TYC9402-936-1	R	57431.59633	SWO	1763	35	–	18.98±3.99	–	–	–	–	–	*****	–	-,1,-,-	no age info.
TYC8148-924-1	R	57431.60817	SWO	1058	39	–	42.02±2.41	–	–	–	–	–	625^{+0}_{-0}	Li	-,1,-,-	–
HD 68420	R	54189.13539	VUA	0	0	–	–	–	–	–	–	–	*****	–	-,-,-,-	no age info.
HD 68558	R	54229.04287	VUA	0	0	–	–	–	–	–	–	–	940^{+345}_{-140}	CMD	-,-,-,-	–
HD 68698	R	–	–	–	–	–	–	–	–	–	–	–	50^{+50}_{0}	CMD	-,-,-,-	assumed ZAMS
TYC8144-571-1	R	–	–	–	–	–	–	–	–	–	–	–	1320^{+345}_{-360}	CMD	-,-,-,-	–
TYC7130-1982-1	R	57432.55071	SEO	1396	0	22.41	20.52±7.01	-0.27±0.02	3.80±0.05	-4.95	–	–	625^{+0}_{-0}	X-ray	1,1,1,-	–
TYC9193-870-1	R	57431.61876	SWO	955	0	–	10.89±1.82	–	–	–	–	–	*****	–	-,1,-,-	–
V478 Hya	R	54520.18144	VUA	1102	153	14.90	17.47±0.53	-0.20±0.01	4.44±0.02	-4.15	–	WDS	125^{+250}_{-0}	Li (X-ray)	1,1,1,-	–
TYC8149-4422-1	R	–	–	–	–	–	–	–	–	–	–	–	490^{+100}_{-170}	CMD	-,-,-,-	–
TYC8572-94-1	R	–	–	–	–	–	–	–	–	–	–	–	515^{+125}_{-200}	CMD	-,-,-,-	–
TYC1387-1215-1	R	57082.34736	DMO	3065	0	58.33	–	–	–	–	–	–	680^{+290}_{-235}	CMD	1,-,-,-	–
CD-52 2472	R	–	–	–	–	–	14.33±0	–	–	–	–	–	40^{+0}_{-0}	IC2391	-,33,-,39	–
HD 74009	R	57432.56302	SEO	1466	0	71.27	–	-1.28±0.04	0.72±0.07	–	–	WDS	40^{+1650}_{-0}	IC2391 (CMD)	1,-,1,39	Close companion
HD 74340	R	57434.61644	SWO	2170	109	43.00	13.73±4.89	–	–	–	–	–	40^{+0}_{-10}	IC2391 (Li)	21,1,-,39	–
HD 73890	R	–	–	–	–	133.00	42.00±6	–	–	–	–	WDS	1230^{+50}_{-25}	CMD	21,24,-,-	–
HD 74374	R	57434.62236	SWO	2632	81	–	10.10±8.47	–	–	–	–	–	40^{+80}_{-0}	IC2391 (Li)	-,1,-,39	–
TYC8926-1954-1	R	–	–	–	–	60.00	41.60±1	–	–	–	–	–	190^{+50}_{-70}	CMD	21,13,-,-	–
TYC8930-2250-1	R	–	–	–	–	–	–	–	–	–	–	–	730^{+490}_{-155}	CMD	-,-,-,-	–
TYC216-386-1	R	–	–	–	–	12.61	10.80±0	0.05±0.04	–	-5.05	–	WDS	625^{+0}_{-0}	X-ray	57,13,43,-	–
TYC8938-1028-1	R	–	–	–	–	83.00	43.80±2	0.06±0.15	–	-5.98	–	WDS	2000^{+0}_{-0}	X-ray	3,13,4,-	–
GJ 322	R	51566.99916	OEA	539	7	12.22	-22.64±1.45	–	–	-4.33	–	–	30^{+55}_{-0}	Li (CMD)	1,1,-,-	X-ray no agreement
TYC8577-3016-1	R	–	–	–	–	236.00	23.90±2	–	–	–	–	WDS	315^{+90}_{-75}	CMD	61,13,-,-	–
TYC2488-933-1	R	–	–	–	–	–	11.00±9	–	–	–	–	–	810^{+30}_{-60}	CMD	-,13,-,-	–
TYC8160-1758-1	R	57431.62887	SWO	1204	8	–	94.09±2.36	–	–	–	–	–	*****	–	-,1,-,-	no age info.
TYC8586-143-1	R	–	–	–	–	–	–	–	–	–	–	–	460^{+120}_{-130}	CMD	-,-,-,-	–
TYC6022-1079-1	R	–	–	–	–	–	–	–	–	-2.83	–	–	31^{+1}_{-0}	CMD	-,-,-,-	X-ray agreement
TYC7681-2133-1	R	57434.67089	SWO	1299	6	–	25.58±2.33	–	–	–	–	–	0^{+0}_{-625}	Li	-,1,-,-	–
TYC8169-371-1	R	–	–	–	–	–	–	–	–	–	–	–	2355^{+900}_{-385}	CMD	-,-,-,-	–
TYC8169-1002-1	R	57431.64593	SWO	-1199	0	–	27.39±5.35	–	–	-3.18	–	–	25^{+100}_{-5}	CMD (X-ray)	-,1,-,-	Young? Hα emission
TYC6587-1091-1	R	–	–	–	–	–	–	–	–	–	–	–	810^{+65}_{-65}	CMD	-,-,-,-	–
TYC233-561-1	R	–	–	–	–	–	–	–	–	-3.48	–	–	125^{+0}_{-0}	X-ray	-,-,-,-	–
TYC8587-2400-1	R	–	–	–	–	–	–	–	–	–	–	–	375^{+150}_{-45}	CMD	-,-,-,-	–
TYC8170-855-1	R	57434.65731	SWO	1040	6	–	37.91±2.02	–	–	–	–	–	625^{+0}_{-0}	Li	-,1,-,-	–
128 Car	R	57432.68494	SEO	1485	0	14.70	33.60±5	-0.03±0.01	4.24±0.03	–	–	WDS	1995^{+30}_{-975}	CMD	1,13,1,-	–
TYC7678-3447-1	R	–	–	–	–	–	–	–	–	–	–	–	430^{+130}_{-180}	CMD	-,-,-,-	–
TYC8170-948-1	R	57433.68501	SWO	1289	60	–	103.17±2.36	–	–	–	–	–	*****	–	-,1,-,-	giant:Gaia

Continued on Next Page. . .

Table C.1 – Continued

Name	Catalog	Obs. MJD	Instrument	Hα (mÅ)	Li6708 (mÅ)	$v \sin(i)$ (kms^{-1})	RV (kms^{-1})	[Fe/H] (dex)	log (g)	log ($\frac{L_X}{L_{bol}}$)	log (R'_{HK})	Multiple Ref.	Age (Myr)	Age-Dating Method	Refs	Notes
HD 80425	R	57082.19806	DMO	3019	0	78.16	14.20±2	–	–	–	–	–	*****	–	1,13,-,-	no age info.
TYC7153-2033-1	R	–	–	–	–	97.00	22.40±4	–	–	–	–	WDS	400^{+85}_{-55}	CMD	61,13,-,-	–
TYC8948-1822-1	R	–	–	–	–	–	–	–	–	–	–	–	1405^{+985}_{-655}	CMD	-,-,-,-	–
TYC9408-1798-1	R	–	–	–	–	129.70	7.00±4	0.10±0.08	–	-6.30	–	–	4000^{+0}_{-0}	X-ray	3,13,4,-	–
TYC8588-2277-1	R	–	–	–	–	–	–	–	–	–	–	–	505^{+125}_{-380}	CMD	-,-,-,-	–
BD+40 2208	R	56712.40321	LHO	111	0	5.81	-66.66±32.12	-1.02±0.02	4.68±0.06	-4.00	–	WDS	24^{+600}_{-0}	CMD (X-ray)	1,1,1,-	–
TYC8588-463-1	R	57433.66808	SWO	1648	45	–	-1.37±2.96	–	–	–	–	–	0^{+0}_{-625}	Li	-,1,-,-	–
TYC9208-272-1	R	–	–	–	–	–	–	-0.15±0.08	–	–	–	–	1920^{+475}_{-270}	CMD	-,-,4,-	–
TYC3426-581-1	R	–	–	–	–	–	–	–	–	–	–	–	655^{+275}_{-275}	CMD	-,-,-,-	–
TYC7166-1923-1	R	57433.62823	SWO	2057	12	–	6.50±3.68	–	–	–	–	–	0^{+0}_{-625}	Li	-,1,-,-	–
TYC8949-1690-1	R	–	–	–	–	145.00	–	–	–	–	–	–	345^{+140}_{-220}	CMD	12,-,-,-	–
TYC6602-1274-1	R	57431.65968	SWO	1434	5	–	77.91±3.35	–	–	–	–	–	0^{+0}_{-625}	Li	-,1,-,-	–
TYC8953-1669-1	R	–	–	–	–	–	–	–	–	–	–	–	520^{+285}_{-270}	CMD	-,-,-,-	–
TYC6614-884-1	R	–	–	–	–	–	–	–	–	-3.39	–	–	20^{+2}_{-5}	CMD	-,-,-,-	X-ray agreement
TYC7701-1621-1	R	–	–	–	–	–	–	–	–	–	–	–	680^{+100}_{-180}	CMD	-,-,-,-	–
TYC8598-2166-1	R	–	–	–	–	–	±25.00	–	–	–	–	–	1285^{+285}_{-150}	CMD	-,13,-,-	–
TYC7698-2416-1	R	–	–	–	–	–	–	–	–	–	–	–	620^{+105}_{-115}	CMD	-,-,-,-	–
TYC9221-1576-1	R	–	–	–	–	–	–	–	–	–	–	–	775^{+45}_{-180}	CMD	-,-,-,-	–
TYC8606-82-1	R	57431.67416	SWO	1673	0	–	14.23±15.90	–	–	–	–	–	*****	–	-,1,-,-	–
TYC1964-883-1	R	56679.44125	LHO	1166	20	4.84	12.42±5.62	0.52±0.02	4.44±0.04	–	–	–	0^{+0}_{-625}	Li	1,1,1,-	–
TYC8602-649-1	R	–	–	–	–	–	–	–	–	–	–	–	1440^{+495}_{-515}	CMD	-,-,-,-	–
TYC7711-312-1	R	–	–	–	–	–	–	–	–	–	–	–	315^{+220}_{-40}	CMD	-,-,-,-	–
TYC6046-407-1	R	–	–	–	–	53.30	13.80±2	0.05±0.15	–	–	–	–	1105^{+730}_{-410}	CMD	21,13,4,-	–
HD 88230	R	49844.82689	OEA	650	7	5.88	-24.06±1.26	±-0.05	–	-5.09	–	WDS	375^{+1625}_{-25}	Li (X-ray,CMD)	1,1,42,-	–
TYC7178-160-1	R	–	–	–	–	–	–	–	–	–	–	–	2125^{+215}_{-60}	CMD	-,-,-,-	–
HD 89846	R	–	–	–	–	–	–	–	–	–	–	WDS	1460^{+190}_{-375}	CMD	-,-,-,-	–
TYC8612-556-1	R	–	–	–	–	–	–	–	–	–	–	–	2045^{+590}_{-255}	CMD	-,-,-,-	–
TYC8608-1868-1	R	–	–	–	–	–	–	–	–	–	–	WDS	250^{+245}_{-250}	CMD	-,-,-,-	–
HD 90905	R	57099.95628	OSA	1344	114	10.48	16.66±10.53	-0.09±0.01	4.27±0.03	-4.25	-4.51	WDS	125^{+250}_{-0}	Li (X-ray)	1,1,1,-	–
HR 4138	R	–	–	–	–	11.60	7.50±0	±0.06	–	–	–	–	435^{+35}_{-65}	CMD	21,13,49,-	–
36 UMa	R	56711.97252	OSA	1383	59	2.66	8.68±6.77	-0.09±0.01	4.38±0.02	-5.57	-4.82	WDS	40^{+585}_{-0}	Argus (Li)	1,1,1,1	–
TYC4912-802-1	R	56256.56479	LHO	1022	13	4.23	56.22±12.63	-0.04±0.02	3.70±0.03	–	–	–	*****	–	1,1,1,-	giant:Gaia
TYC841-503-1	R	–	–	–	–	–	21.10±3	–	–	–	–	–	1020^{+180}_{-35}	CMD	-,13,-,-	–
TYC6620-1350-1	R	–	–	–	–	–	–	–	–	–	–	–	410^{+65}_{-90}	CMD	-,-,-,-	–
TYC9215-3039-1	R	–	–	–	–	–	–	–	–	–	–	–	480^{+100}_{-125}	CMD	-,-,-,-	–
CCDM J10389-6430AB	R	–	–	–	–	94.20	±13.00	–	–	–	–	WDS	185^{+120}_{-115}	CMD	21,13,-,-	–
TYC8605-1553-1	R	–	–	–	–	–	–	–	–	–	–	–	575^{+20}_{-130}	CMD	-,-,-,-	–
TYC8969-738-1	R	–	–	–	–	–	–	–	–	–	–	–	1485^{+1630}_{-1450}	CMD	-,-,-,-	–
TYC8957-2919-1	R	–	–	–	–	–	8.00±2	–	–	–	–	WDS	620^{+35}_{-240}	CMD	-,13,-,-	–
TYC5505-824-1	R	–	–	–	–	–	–	–	–	–	–	–	570^{+195}_{-60}	CMD	-,-,-,-	–

Continued on Next Page. . .

Table C.1 – Continued

Name	Catalog	Obs. MJD	Instrument	Hα (mÅ)	Li6708 (mÅ)	$v \sin(i)$ (kms^{-1})	RV (kms^{-1})	[Fe/H] (dex)	$\log(g)$	$\log(\frac{L_X}{L_{bol}})$	$\log(R'_{HK})$	Multiple Ref.	Age (Myr)	Age-Dating Method	Refs	Notes
TYC1434-1074-1	R	56256.55068	LHO	1453	20	16.39	3.74±55.95	0.10±0.02	4.36±0.05	–	–	–	0^{+0}_{-625}	Li	1,1,1,-	–
CS Cha	R	–	–	–	–	14.50	–	–	–	-3.08	–	WDS	125^{+0}_{-0}	X-ray	21,-,-,-	–
TYC7734-537-1	R	–	–	–	–	–	–	–	–	-3.07	–	–	125^{+0}_{-0}	X-ray	-,-,-,-	–
TYC8628-1696-1	R	–	–	–	–	–	–	–	–	–	–	–	255^{+115}_{-95}	CMD	-,-,-,-	–
TYC8628-1491-1	R	–	–	–	–	–	–	–	–	–	–	–	500^{+300}_{-320}	CMD	-,-,-,-	–
TYC8624-403-1	R	–	–	–	–	–	–	–	–	–	–	–	50^{+50}_{-0}	CMD	-,-,-,-	assumed ZAMS
TYC9233-1852-1	R	–	–	–	–	–	–	–	–	–	–	–	510^{+30}_{-120}	CMD	-,-,-,-	–
TYC9415-2314-1	R	–	–	–	–	–	–	–	–	-2.93	–	–	19^{+1}_{-3}	CMD	-,-,-,-	X-ray agreement
TYC6091-2196-1	R	–	–	–	–	–	–	–	–	–	–	–	1030^{+115}_{-150}	CMD	-,-,-,-	–
TYC8625-1007-1	R	–	–	–	–	215.00	6.20±0	–	–	–	–	–	455^{+100}_{-100}	CMD	21,13,-,-	–
gam Crt	R	53480.93630	OEA	4272	0	73.27	1.00±4	±-0.11	–	–	–	WDS	955^{+85}_{-50}	CMD	1,13,49,-	–
TYC9225-4802-1	R	–	–	–	–	–	–	–	–	–	–	WDS	5^{+75}_{-5}	CMD	-,-,-,-	ZAMS
HD 99945	R	–	–	–	–	–	3.20±3	–	–	–	–	–	1160^{+120}_{-145}	CMD	-,13,-,-	–
TYC8630-2190-1	R	–	–	–	–	160.00	5.70±2	–	–	–	–	–	295^{+135}_{-100}	CMD	61,13,-,-	–
HD 101259	R	56713.36031	LHO	1177	26	3.75	91.48±5.80	-0.69±0.01	3.12±0.03	–	–	–	*****	–	1,1,1,-	giant:Gaia
TYC8634-844-1	R	–	–	–	–	–	–	–	–	–	–	–	475^{+470}_{-475}	CMD	-,-,-,-	–
TYC9419-30-1	R	–	–	–	–	–	–	–	–	–	–	–	715^{+125}_{-130}	CMD	-,-,-,-	–
TYC8634-1258-1	R	–	–	–	–	–	–	–	–	–	–	–	285^{+280}_{-215}	CMD	-,-,-,-	–
TYC9411-1067-1	R	–	–	–	–	–	–	–	–	–	–	–	720^{+65}_{-125}	CMD	-,-,-,-	–
TYC7754-1736-1	R	–	–	–	–	–	7.10±1	–	–	–	–	–	10^{+355}_{-0}	LCC (CMD)	-,13,-,15	–
HD 102981	R	–	–	–	–	–	7.10±1	–	–	–	–	–	10^{+355}_{-0}	LCC (CMD)	-,13,-,15	–
TYC1985-520-1	R	–	–	–	–	–	–	–	–	–	–	–	10^{+0}_{-0}	CMD	-,-,-,-	–
HD 104067	R	–	–	–	–	6.70	–	0.10±0.03	–	–	–	–	50^{+100}_{0}	CMD	51,-,29,-	assumed ZAMS
HD 104304	R	52695.31414	VUA	1109	17	4.22	1.09±0.15	0.28±0.01	4.67±0.01	–	–	WDS	625^{+0}_{-0}	Li	1,1,1,-	–
TYC8241-3236-1	R	–	–	–	–	290.00	±16.00	–	–	–	–	TDSC	100^{+60}_{-100}	CMD	61,24,-,-	–
TYC8644-340-1	R	–	–	–	–	–	–	–	–	-3.17	–	–	10^{+115}_{-0}	LCC (X-ray)	-,-,-,36	–
HD 105994	R	–	–	–	–	–	6.60±1	–	–	–	–	WDS	10^{+0}_{-0}	LCC	-,13,-,15	–
TYC7756-372-1	R	–	–	–	–	–	–	–	–	–	–	–	65^{+710}_{-65}	CMD	-,-,-,-	–
TYC6685-190-1	R	–	–	–	–	–	–	–	–	–	–	–	1660^{+1410}_{-160}	CMD	-,-,-,-	–
HD 108035	R	–	–	–	–	–	5.90±1	–	–	–	–	WDS	10^{+60}_{-0}	LCC (CMD)	-,13,-,15	–
HD 108257	R	–	–	–	–	269.00	5.00±4	–	–	–	–	WDS	10^{+75}_{-0}	LCC (CMD)	21,13,-,15	–
TYC6106-964-1	R	56711.41235	LHO	1608	0	8.92	–	-0.02±0.02	4.02±0.04	–	–	WDS	*****	–	1,-,1,-	no age info.
TYC8654-2750-1	R	–	–	–	–	–	–	–	–	–	–	–	5^{+45}_{-0}	CMD	-,-,-,-	–
TYC8231-2373-1	R	–	–	–	–	–	–	–	–	-4.27	–	–	0^{+375}_{-0}	X-ray	-,-,-,-	–
TYC8654-1778-1	R	–	–	–	–	–	–	–	–	–	–	–	635^{+100}_{-375}	CMD	-,-,-,-	–
TYC7255-1491-1	R	–	–	–	–	–	–	–	–	–	–	–	1410^{+125}_{-215}	CMD	-,-,-,-	–
TYC5534-583-1	R	–	–	–	–	–	–	–	–	–	–	–	630^{+30}_{-120}	CMD	-,-,-,-	–
TYC9228-2332-1	R	–	–	–	–	–	–	–	–	–	–	WDS	735^{+70}_{-105}	CMD	-,-,-,-	–

Continued on Next Page. . .

Table C.1 – Continued

Name	Catalog	Obs. MJD	Instrument	Hα (mÅ)	Li6708 (mÅ)	$v \sin(i)$ (kms^{-1})	RV (kms^{-1})	[Fe/H] (dex)	log (g)	log ($\frac{L_X}{L_{bol}}$)	log (R'_{HK})	Multiple Ref.	Age (Myr)	Age-Dating Method	Refs	Notes
V940 Cen	R	–	–	–	–	0.00	–	±-0.58	–	-3.37	–	–	10^{+115}_{-2}	LCC (X-ray,CMD)	47,-,4,36	–
TYC8997-604-1	R	–	–	–	–	–	–	–	–	–	–	–	15^{+25}_{-0}	CMD	-,-,-,-	assumed ZAMS
TYC8989-583-1	R	–	–	–	–	–	10.80±0	–	–	-2.88	–	WDS	0^{+125}_{-0}	X-ray	-,16,-,-	–
TYC9421-683-1	R	–	–	–	–	–	–	–	–	–	–	–	390^{+140}_{-140}	CMD	-,-,-,-	–
HD 113319	R	–	–	–	–	3.60	6.43±0	-0.05±0.02	–	-4.98	–	WDS	625^{+0}_{-0}	X-ray	21,13,4,-	–
TYC8660-689-1	R	–	–	–	–	–	–	–	–	–	–	–	730^{+165}_{-195}	CMD	-,-,-,-	–
TYC8997-1155-1	R	–	–	–	–	31.40	11.40±1	-0.30±0.08	–	–	–	–	10^{+0}_{-0}	LCC	21,13,4,36	–
HR 4979	R	–	–	–	–	2.70	-11.20±1	0.07±0.02	–	-5.89	–	–	4000^{+0}_{-0}	X-ray	21,13,29,-	–
HD 115116	R	–	–	–	–	166.00	-2.10±1	–	–	–	–	–	620^{+225}_{-215}	CMD	61,13,-,-	–
TYC9002-1148-1	R	–	–	–	–	–	–	–	–	–	–	–	540^{+160}_{-225}	CMD	-,-,-,-	–
TYC8260-287-1	R	–	–	–	–	–	–	–	–	–	–	–	1895^{+125}_{-305}	CMD	-,-,-,-	–
TYC8662-2197-1	R	–	–	–	–	–	–	–	–	–	–	–	520^{+90}_{-125}	CMD	-,-,-,-	–
HD 116402	R	–	–	–	–	33.20	12.30±0	-0.24±0.08	–	-3.50	–	WDS	10^{+115}_{-0}	LCC (X-ray)	21,13,4,36	–
TYC8674-2480-1	R	–	–	–	–	–	–	–	–	–	–	–	8^{+3}_{-0}	CMD	-,-,-,-	–
TYC7799-1047-1	R	–	–	–	–	–	–	–	–	–	–	–	1165^{+395}_{-240}	CMD	-,-,-,-	–
TYC9438-1004-1	R	–	–	–	–	–	–	–	–	–	–	–	25^{+240}_{-0}	CMD	-,-,-,-	–
HD 117384	R	57082.45606	DMO	2061	0	32.85	–	–	–	–	–	–	*****	–	1,-,-,-	–
TYC8663-800-1	R	–	–	–	–	–	–	–	–	–	–	–	525^{+275}_{-250}	CMD	-,-,-,-	–
TYC7788-806-1	R	–	–	–	–	–	–	–	–	–	–	–	50^{+100}_{-0}	CMD	-,-,-,-	assumed ZAMS
HD 118379	R	–	–	–	–	–	6.10±1	–	–	–	–	–	655^{+200}_{-230}	CMD	-,13,-,-	–
HD 118878	R	–	–	–	–	–	6.60±1	–	–	–	–	–	10^{+585}_{-0}	UCL (CMD)	-,13,-,15	–
HD 119332	R	53385.17078	OEA	994	12	5.33	-5.48±1.16	-0.09±0.01	4.59±0.02	–	–	–	625^{+0}_{-525}	Li (CMD)	1,1,1,-	–
TYC6130-223-1	R	–	–	–	–	–	–	-0.05±0.15	–	–	–	–	1010^{+615}_{-375}	CMD	-,-,4,-	–
TYC7801-1120-1	R	–	–	–	–	–	–	–	–	–	–	–	600^{+420}_{-570}	CMD	-,-,-,-	–
TYC2540-406-1	R	–	–	–	–	–	–	–	–	–	–	–	50^{+150}_{-0}	CMD	-,-,-,-	assumed ZAMS
TYC8262-2554-1	R	–	–	–	–	–	–	–	–	–	–	–	565^{+180}_{-275}	CMD	-,-,-,-	–
TYC8270-2110-1	R	–	–	–	–	–	–	–	–	-3.73	–	–	0^{+125}_{-0}	X-ray	-,-,-,-	–
TYC7274-1776-1	R	–	–	–	–	–	–	–	–	–	–	–	1055^{+355}_{-420}	CMD	-,-,-,-	–
TYC6719-514-1	R	–	–	–	–	–	–	–	–	–	–	–	50^{+100}_{-0}	CMD	-,-,-,-	assumed ZAMS
HD 120178	R	–	–	–	–	–	2.50±1	–	–	–	–	–	10^{+0}_{-0}	LCC	-,13,-,15	–
TYC8664-713-1	R	–	–	–	–	–	2.50±1	–	–	–	–	WDS	10^{+0}_{-0}	LCC	-,13,-,15	–
mu. Cen	R	–	–	–	–	139.00	9.20±3	–	–	–	–	CCDM	10^{+40}_{-0}	UCL (CMD)	21,13,-,36	–
TYC7802-1796-1	R	–	–	–	–	–	–	–	–	-4.03	–	–	125^{+0}_{-0}	X-ray	-,-,-,-	–
TYC8664-564-1	R	–	–	–	–	–	–	–	–	–	–	–	745^{+50}_{-130}	CMD	-,-,-,-	–
HD 121191	R	–	–	–	–	–	–	–	–	–	–	–	790^{+195}_{-175}	CMD	-,-,-,-	–
HD 121504	R	51973.37303	VUA	1307	52	4.95	16.65±0.19	0.10±0.01	4.40±0.02	–	-5.02	WDS	625^{+0}_{-0}	Li	1,1,1,-	–
HR 5258	R	57081.42855	DMO	1685	0	15.62	-6.60±2	0.16±0.05	–	–	–	WDS	*****	–	1,13,42,-	–
TYC6149-284-1	R	56713.50090	LHO	1894	149	27.70	–	0.18±0.04	4.09±0.07	–	–	–	30^{+0}_{-0}	Li	1,-,1,-	–

Continued on Next Page. . .

Table C.1 – Continued

Name	Catalog	Obs. MJD	Instrument	Hα (mÅ)	Li6708 (mÅ)	$v \sin(i)$ (kms^{-1})	RV (kms^{-1})	[Fe/H] (dex)	log (g)	log ($\frac{L_X}{L_{bol}}$)	log (R'_{HK})	Multiple Ref.	Age (Myr)	Age-Dating Method	Refs	Notes
TYC6137-378-1	R	–	–	–	–	–	–	–	–	–	–	–	495^{+55}_{-75}	CMD	-,-,-,-	–
TYC8268-3628-1	R	–	–	–	–	–	–	–	–	–	–	–	325^{+75}_{-105}	CMD	-,-,-,-	–
HD 124498	R	–	–	–	–	–	–	–	–	-3.39	–	CCDM	13^{+10}_{-5}	CMD	-,-,-,-	X-ray no agreement
HD 124469	R	–	–	–	–	–	3.50±1	–	–	–	–	WDS	10^{+25}_{-0}	UCL (CMD)	-,13,-,15	–
TYC8678-260-1	R	–	–	–	–	–	6.90±1	–	–	–	–	WDS	10^{+1065}_{-0}	UCL (CMD)	-,13,-,15	–
TYC6743-252-1	R	56711.51365	LHO	1043	0	10.99	-61.73±29.58	-1.25±0.01	1.54±0.03	–	–	–	*****	–	1,1,1,-	giant:Gaia
TYC5566-791-1	R	–	–	–	–	–	–	–	–	–	–	–	885^{+90}_{-115}	CMD	-,-,-,-	–
TYC7805-1871-1	R	–	–	–	–	–	–	–	–	–	–	–	50^{+100}_{-0}	CMD	-,-,-,-	assumed ZAMS
TYC8678-1032-1	R	–	–	–	–	–	–	–	–	–	–	–	3015^{+1505}_{-1115}	CMD	-,-,-,-	–
HD 126135	R	–	–	–	–	–	12.00±6	–	–	–	–	–	10^{+100}_{-0}	UCL (CMD)	-,13,-,15	–
TYC9006-192-1	R	–	–	–	–	–	–	–	–	–	–	–	790^{+315}_{-400}	CMD	-,-,-,-	–
HD 127236	R	–	–	–	–	38.00	4.20±1	–	–	–	–	WDS	10^{+1010}_{-0}	UCL (CMD)	9,13,-,15	–
HR 5433	R	57081.45367	DMO	3600	0	81.32	±-14.50	–	–	–	–	WDS	1215^{+25}_{-45}	CMD	1,13,-,-	–
HD 127750	R	–	–	–	–	–	4.40±1	–	–	–	–	–	10^{+565}_{-0}	UCL (CMD)	-,13,-,15	–
HD 128155	R	–	–	–	–	–	6.30±1	–	–	–	–	WDS	10^{+40}_{-0}	UCL (CMD)	-,13,-,15	–
TYC7308-2055-1	R	–	–	–	–	–	–	–	–	–	–	–	50^{+100}_{-0}	CMD	-,-,-,-	assumed ZAMS
HD 128788	R	–	–	–	–	–	2.80±1	–	–	–	–	WDS	10^{+890}_{-0}	UCL(CMD)	-,13,-,15	–
TYC9011-4622-1	R	–	–	–	–	–	–	–	–	–	–	–	750^{+195}_{-15}	CMD	-,-,-,-	–
TYC326-428-1	R	–	–	–	–	–	6.80±1	–	–	–	–	–	500^{+105}_{-110}	CMD	-,13,-,-	–
HD 129490	R	–	–	–	–	–	2.60±1	–	–	-3.76	–	–	10^{+115}_{-0}	UCL (X-ray)	-,13,-,15	–
HD 129683	R	–	–	–	–	–	–	–	–	–	–	WDS	10^{+0}_{-0}	UCL	-,-,-,15	–
HD 130322	R	51704.91648	OEA	1069	6	4.96	-14.23±1.21	0.03±0.01	4.69±0.02	–	–	WDS	625^{+0}_{-0}	Li	1,1,1,-	–
GJ 563.1	R	–	–	–	–	–	–	–	–	–	–	–	52^{+4}_{-6}	CMD	-,-,-,-	–
TYC8684-2799-1	R	–	–	–	–	–	–	–	–	–	–	–	880^{+65}_{-75}	CMD	-,-,-,-	–
TYC7297-1759-1	R	–	–	–	–	–	–	–	–	–	–	–	1020^{+240}_{-215}	CMD	-,-,-,-	–
HD 130656	R	–	–	–	–	–	0.70±1	–	–	–	–	WDS	10^{+445}_{-0}	UCL (CMD)	-,13,-,15	–
TYC6756-303-1	R	56402.40831	LHO	2311	0	50.94	–	-0.19±0.03	3.21±0.25	–	–	–	50^{+50}_{-50}	CMD	1,-,1,-	–
TYC6176-925-1	R	56712.54725	LHO	1932	91	39.33	–	0.01±0.04	4.05±0.09	–	–	–	125^{+0}_{-0}	Li	1,-,1,-	–
TYC5587-1033-1	R	–	–	–	–	–	–	–	–	–	–	–	500^{+160}_{-435}	CMD	-,-,-,-	–
HR 5579	R	–	–	–	–	234.00	15.00±7	–	–	–	–	–	10^{+130}_{-0}	UCL (CMD)	61,13,-,15	–
TYC922-865-1	R	56402.48365	LHO	1983	67	24.61	–	0.19±0.03	3.89±0.09	–	–	–	125^{+1265}_{-0}	Li (CMD)	1,-,1,-	–
TYC8293-3733-1	R	–	–	–	–	–	–	–	–	–	–	–	1275^{+635}_{-335}	CMD	-,-,-,-	–
TYC8681-1601-1	R	–	–	–	–	–	–	–	–	–	–	–	11^{+2}_{-0}	CMD	-,-,-,-	–
TYC8293-3258-1	R	–	–	–	–	–	–	–	–	–	–	–	725^{+545}_{-670}	CMD	-,-,-,-	–
TYC7821-299-1	R	–	–	–	–	–	–	–	–	–	–	–	540^{+190}_{-220}	CMD	-,-,-,-	–
TYC6773-427-1	R	–	–	–	–	5.40	-37.00±0	-0.10±0.08	–	-4.23	–	–	0^{+375}_{-0}	X-ray	21,13,4,-	–

Continued on Next Page. . .

Table C.1 – Continued

Name	Catalog	Obs. MJD	Instrument	Hα (mÅ)	Li6708 (mÅ)	$v \sin(i)$ (kms^{-1})	RV (kms^{-1})	[Fe/H] (dex)	$\log(g)$	$\log(\frac{L_X}{L_{bol}})$	$\log(R'_{HK})$	Multiple Ref.	Age (Myr)	Age-Dating Method	Refs	Notes
TYC923-1568-1	R	57122.39884	DMO	2984	0	66.72	-13.00±4	–	–	–	–	WDS	525^{+130}_{-90}	CMD	1,13,-,-	–
TYC9025-1409-1	R	–	–	–	–	19.80	-1.20±2	0.26±0.08	–	-5.01	–	–	625^{+0}_{-0}	X-ray	21,13,4,-	–
TYC3051-1266-1	R	57121.36437	DMO	4579	0	108.57	-24.00±3	–	–	–	–	–	*****	–	1,13,-,-	–
chi Boo	R	53179.92664	OEA	4457	0	70.36	-16.00±1	–	–	–	–	–	515^{+185}_{-120}	CMD	1,13,-,-	–
HD 135454	R	–	–	–	–	–	1.40±1	–	–	–	–	WDS	10^{+260}_{-0}	UCL (CMD)	-,13,-,15	–
TYC7834-2020-1	R	–	–	–	–	–	–	–	–	–	–	–	50^{+100}_{-0}	CMD	-,-,-,-	assumed ZAMS
TYC6766-1629-1	R	–	–	–	–	–	–	–	–	–	–	–	1005^{+35}_{-145}	CMD	-,-,-,-	–
TYC7830-604-1	R	–	–	–	–	–	–	–	–	–	–	–	660^{+110}_{-120}	CMD	-,-,-,-	–
TYC7313-615-1	R	–	–	–	–	–	–	–	–	-3.04	–	–	1^{+1}_{-0}	CMD	-,-,-,-	X-ray agreement
HR 5697	R	–	–	–	–	–	-3.00±6	–	–	–	–	WDS	10^{+50}_{-0}	UCL (CMD)	-,13,-,15	–
HR 5722	R	–	–	–	–	119.60	–	–	–	–	–	CCDM	10^{+675}_{-0}	UCL (CMD)	17,-,-,15	–
HD 137057	R	–	–	–	–	55.00	-0.20±1	–	–	–	–	–	10^{+1565}_{-0}	UCL (CMD)	9,13,-,15	–
TYC8303-30-1	R	–	–	–	–	–	–	–	–	–	–	–	590^{+160}_{-175}	CMD	-,-,-,-	–
HD 137499	R	–	–	–	–	–	-0.80±1	–	–	–	–	WDS	10^{+0}_{-0}	UCL	-,13,-,15	–
TYC7326-638-1	R	–	–	–	–	–	–	–	–	-3.63	–	–	12^{+610}_{-2}	CMD (X-ray)	-,-,-,-	–
TYC7836-1284-1	R	–	–	–	–	–	–	–	–	–	–	–	2090^{+660}_{-2090}	CMD	-,-,-,-	–
TYC2567-151-1	R	57121.34905	DMO	3885	0	–	-24.20±1	–	–	–	–	–	395^{+105}_{-140}	CMD	-,13,-,-	–
TYC6764-1501-1	R	56713.54287	LHO	1679	28	15.90	-35.28±6.79	-0.40±0.03	2.77±0.13	–	–	–	0^{+0}_{-625}	Li	1,1,1,-	–
TYC7836-1029-1	R	–	–	–	–	154.00	0.30±4	–	–	–	–	–	200^{+110}_{-105}	CMD	61,13,-,-	–
TYC8708-405-1	R	–	–	–	–	–	–	–	–	–	–	–	1015^{+35}_{-120}	CMD	-,-,-,-	–
TYC7335-550-1	R	–	–	–	–	–	–	–	–	–	–	–	3^{+2}_{-0}	CMD	-,-,-,-	–
TYC941-1023-1	R	–	–	–	–	–	-8.00±7	–	–	–	–	–	680^{+95}_{-70}	CMD	-,13,-,-	–
TYC7327-689-1	R	–	–	–	–	–	–	–	–	-3.06	–	–	125^{+0}_{-0}	X-ray	-,-,-,-	–
HD 139590	R	57081.53897	DMO	1202	68	11.29	-29.30±0	0.15±0.01	–	–	–	–	625^{+0}_{-0}	Li	1,13,2,-	–
TYC6777-1626-1	R	–	–	–	–	180.00	-9.00±2	–	–	–	–	–	485^{+20}_{-95}	CMD	61,13,-,-	–
TYC6781-652-1	R	56713.55119	LHO	2596	135	47.30	–	-0.37±0.03	3.57±0.17	–	–	–	1820^{+355}_{-540}	CMD	1,-,1,-	–
TYC8704-2004-1	R	–	–	–	–	–	–	–	–	–	–	–	1925^{+1005}_{-360}	CMD	-,-,-,-	–
zet UMi	R	57082.53890	DMO	6208	0	180.00	-13.10±4	–	–	–	–	–	*****	–	21,13,-,-	CMD giant branch
HD 140374	R	–	–	–	–	1.80	0.30±3	-0.30±0.08	–	–	–	–	10^{+0}_{-0}	UCL	21,13,4,15	–
TYC7327-365-1	R	–	–	–	–	–	–	–	–	–	–	–	500^{+630}_{-495}	CMD	-,-,-,-	–
HD 140475	R	–	–	–	–	–	-2.00±1	–	–	–	–	WDS, 45	10^{+390}_{-0}	UCL (CMD)	-,13,-,15	–
TYC2571-983-1	R	–	–	–	–	–	-38.60±2	–	–	–	–	–	335^{+135}_{-55}	CMD	-,13,-,-	–
TYC6782-1207-1	R	–	–	–	–	–	–	–	–	–	–	–	940^{+145}_{-75}	CMD	-,-,-,-	–
TYC6782-2146-1	R	–	–	–	–	–	–	–	–	–	–	WDS	920^{+110}_{-75}	CMD	-,-,-,-	–
TYC7332-414-1	R	–	–	–	–	–	–	–	–	–	–	–	2050^{+550}_{-260}	CMD	-,-,-,-	–
HD 141327	R	–	–	–	–	–	-5.10±2	–	–	–	–	–	10^{+455}_{-0}	UCL (CMD)	-,13,-,15	–
HD 141441	R	–	–	–	–	–	0.90±2	–	–	–	–	–	5^{+0}_{-0}	UpperSco	-,13,-,15	–

Continued on Next Page. . .

Table C.1 – Continued

Name	Catalog	Obs. MJD	Instrument	Hα (mÅ)	Li6708 (mÅ)	$v \sin(i)$ (kms^{-1})	RV (kms^{-1})	[Fe/H] (dex)	log (g)	log ($\frac{L_X}{L_{bol}}$)	log (R'_{HK})	Multiple Ref.	Age (Myr)	Age-Dating Method	Refs	Notes
HD 141521	R	–	–	–	–	8.20	4.30±3	-0.30±0.08	–	-3.74	–	–	10^{+115}_{-0}	UCL (X-ray)	47,13,4,36	–
TYC6790-638-1	R	–	–	–	–	–	–	–	–	–	–	–	920^{+320}_{-520}	CMD	-,-,-,-	–
HD 142315	R	–	–	–	–	235.00	-7.40±10	–	–	–	–	WDS	5^{+495}_{-0}	UpperSco (CMD)	21,13,-,15	–
TYC6199-673-1	R	–	–	–	–	–	–	–	–	–	–	–	1590^{+815}_{-70}	CMD	-,-,-,-	–
TYC6779-1929-1	R	56711.54383	LHO	2963	0	70.10	–	-0.70±0.03	2.61±0.27	–	–	–	1720^{+395}_{-275}	CMD	1,-,1,-	–
TYC6783-296-1	R	–	–	–	–	–	–	–	–	-4.25	–	–	125^{+0}_{-0}	X-ray	-,-,-,-	–
HD 142705	R	–	–	–	–	–	-6.50±3	–	–	–	–	–	5^{+0}_{-0}	UpperSco	-,13,-,15	–
TYC5031-413-1	R	–	–	–	–	–	–	–	–	–	–	–	815^{+350}_{-410}	CMD	-,-,-,-	–
TYC9260-134-1	R	–	–	–	–	–	–	–	–	–	–	–	785^{+190}_{-175}	CMD	-,-,-,-	–
TYC6191-19-1	R	–	–	–	–	–	–	–	–	-3.47	–	WDS	5^{+620}_{-0}	UpperSco (X-ray)	-,-,-,36	–
TYC8310-1272-1	R	–	–	–	–	–	–	–	–	–	–	–	1025^{+20}_{-55}	CMD	-,-,-,-	–
TYC7851-91-1	R	–	–	–	–	–	–	–	–	–	–	–	270^{+125}_{-170}	CMD	-,-,-,-	–
LL Lup	R	–	–	–	–	28.50	-1.90±1	–	–	–	–	WDS	10^{+360}_{-0}	UCL (CMD)	21,13,-,15	–
2MASS J16020287-2236139	R	–	–	–	–	–	–	–	–	–	–	WDS	5^{+0}_{-0}	UpperSco	-,-,-,25	–
TYC9285-1347-1	R	–	–	–	–	–	–	–	–	–	–	–	1335^{+495}_{-540}	CMD	-,-,-,-	–
NO Lup	R	–	–	–	–	–	–	–	–	-2.63	–	–	125^{+0}_{-0}	X-ray	-,-,-,-	–
HD 143811	R	–	–	–	–	–	1.80±2	–	–	–	–	WDS	5^{+0}_{-0}	UpperSco	-,13,-,15	–
HD 143956	R	–	–	–	–	–	-1.10±2	–	–	–	–	WDS	5^{+745}_{-0}	UpperSco (CMD)	-,13,-,15	–
TYC7855-650-1	R	–	–	–	–	–	–	–	–	–	–	–	580^{+100}_{-140}	CMD	-,-,-,-	–
TYC7855-1120-1	R	–	–	–	–	–	1.60±7	–	–	–	–	WDS	10^{+40}_{-0}	UCL (CMD)	-,13,-,15	–
2MASS J16052556-2035397	R	–	–	–	–	–	–	–	–	–	–	–	5^{+0}_{-0}	UpperSco	-,-,-,25	–
2MASS J16053215-1933159	R	–	–	–	–	10.61	–	–	–	–	–	–	5^{+0}_{-0}	UpperSco	11,-,-,25	–
2MASS J16060061-1957114	R	–	–	–	–	–	–	–	–	–	–	–	5^{+0}_{-0}	UpperSco	-,-,-,25-	–
2MASS J16062196-1928445	R	–	–	–	–	–	–	–	–	-2.50	–	WDS	5^{+120}_{-0}	UpperSco (X-ray)	-,-,-,36	–
TYC7851-1636-1	R	–	–	–	–	–	–	-0.55±0.09	–	–	–	–	305^{+170}_{-305}	CMD	-,-,49,-	–
2MASS J16064385-1908056	R	–	–	–	–	–	–	–	–	–	–	WDS	5^{+0}_{-0}	UpperSco	-,-,-,25	–
HD 144569	R	–	–	–	–	–	-2.00±2	–	–	–	–	WDS	5^{+600}_{-0}	UpperSco (CMD)	-,13,-,15	–
HD 144586	R	–	–	–	–	–	-1.70±2	–	–	–	–	WDS	5^{+440}_{-0}	UpperSco (CMD)	-,13,-,15	–
TYC7859-891-1	R	–	–	–	–	–	–	–	–	–	–	–	740^{+65}_{-535}	CMD	-,-,-,-	–
2MASS J16073939-1917472	R	–	–	–	–	–	–	–	–	–	–	–	5^{+0}_{-0}	UpperSco	-,-,-,25	–
TYC8311-1974-1	R	–	–	–	–	–	–	–	–	–	–	–	595^{+80}_{-120}	CMD	-,-,-,-	–
HD 144713	R	–	–	–	–	–	–	–	–	-3.25	–	WDS	125^{+0}_{-0}	X-ray	-,-,-,-	–
2MASS J16081566-2222199	R	–	–	–	–	–	–	–	–	-2.66	–	–	0^{+125}_{-0}	X-ray	-,-,-,-	–

Continued on Next Page. . .

Table C.1 – Continued

Name	Catalog	Obs. MJD	Instrument	Hα (mÅ)	Li6708 (mÅ)	$v \sin(i)$ (kms^{-1})	RV (kms^{-1})	[Fe/H] (dex)	log (g)	log ($\frac{L_X}{L_{bol}}$)	log (R'_{HK})	Multiple Ref.	Age (Myr)	Age-Dating Method	Refs	Notes
2MASS J16082751-1949047	R	–	–	–	–	–	–	–	–	–	–	–	5^{+0}_{-0}	UpperSco	-,-,-,25	–
HD 144981	R	–	–	–	–	155.20	-1.30±2	–	–	–	–	WDS	5^{+605}_{-0}	UpperSco (CMD)	11,13,-,15	–
2MASS J16093019-2059536	R	–	–	–	–	–	–	–	–	–	–	–	5^{+0}_{-0}	UpperSco	-,-,-,25	–
2MASS J16094098-2217594	R	–	–	–	–	–	–	–	–	-2.80	–	–	5^{+120}_{-0}	UpperSco (X-ray)	-,-,-,36	–
2MASS J16095852-2345186	R	–	–	–	–	–	–	–	–	–	–	WDS	5^{+0}_{-0}	UpperSco	-,-,-,25	–
2MASS J16100608-2127440	R	–	–	–	–	–	–	–	–	–	–	–	5^{+0}_{-0}	UpperSco	-,-,-,25	–
TYC6784-1422-1	R	–	–	–	–	–	–	–	–	–	–	–	420^{+80}_{-105}	CMD	-,-,-,-	–
HD 145189	R	–	–	–	–	–	-0.40±2	–	–	–	–	WDS	5^{+255}_{-0}	UpperSco (CMD)	-,13,-,15	–
HD 145263	R	–	–	–	–	–	0.30±2	–	–	–	–	–	5^{+0}_{-0}	UpperSco	-,13,-,15	–
TYC2573-363-1	R	–	–	–	–	–	-24.00±3	–	–	–	–	–	840^{+120}_{-95}	CMD	-,13,-,-	–
TYC8311-1761-1	R	–	–	–	–	–	–	–	–	-4.11	–	–	125^{+0}_{-0}	X-ray	-,-,-,-	–
HR 6051	R	–	–	–	–	306.00	-7.80±2	–	–	–	–	WDS	5^{+270}_{-0}	UpperSco (CMD)	61,13,-,15	–
TYC3880-518-1	R	–	–	–	–	–	–	-0.22±0.24	–	–	–	–	50^{+100}_{-0}	CMD	-,-,26,-	assumed ZAMS
HD 146069	R	–	–	–	–	–	–	–	–	–	–	WDS	5^{+0}_{-0}	UpperSco	-,-,-,15	–
TYC8315-1750-1	R	–	–	–	–	278.00	1.40±4	–	–	–	–	–	160^{+45}_{-5}	CMD	21,13,-,-	–
2MASS J16152023-3255051	R	–	–	–	–	–	–	–	–	-3.11	–	–	125^{+0}_{-0}	X-ray	-,-,-,-	–
HD 145984	R	–	–	–	–	113.00	-1.20±1	0.00±0.08	–	–	–	WDS	10^{+1070}_{-0}	UCL (CMD)	9,13,4,15	–
2MASS J16183317-2517504	R	–	–	–	–	–	–	–	–	–	–	WDS	5^{+0}_{-0}	UpperSco	-,-,-,25	–
HD 147009	R	–	–	–	–	150.00	-15.00±4	–	–	–	–	WDS	5^{+1215}_{-0}	UpperSco (CMD)	21,13,-,15	–
HD 147343	R	–	–	–	–	–	–	–	–	–	–	WDS	5^{+0}_{-0}	UpperSco	-,-,-,15	–
HD 147432	R	–	–	–	–	–	-0.70±2	–	–	–	–	WDS	5^{+705}_{-0}	UpperSco (CMD)	-,13,-,15	–
2MASS J16230783-2300596	R	–	–	–	–	–	–	–	–	-2.86	–	WDS	5^{+120}_{-0}	UpperSco (X-ray)	-,-,-,36	–
TYC6798-35-1	R	–	–	–	–	–	–	–	–	-2.62	–	–	5^{+120}_{-0}	UpperSco (X-ray)	-,-,-,36	–
TYC6802-1242-1	R	–	–	–	–	240.00	–	–	–	–	–	–	1000^{+0}_{-95}	CMD	21,-,-,-	–
TYC2043-1337-1	R	–	–	–	–	–	–	–	–	–	–	–	51^{+3}_{-8}	CMD	-,-,-,-	–
HD 148040	R	–	–	–	–	–	0.50±2	–	–	-3.56	–	–	5^{+120}_{-0}	UpperSco (X-ray)	-,13,-,36	–
HD 148055	R	–	–	–	–	–	-2.10±1	–	–	–	–	–	10^{+65}_{-0}	UCL (CMD)	-,13,-,15	–
TYC9274-4091-1	R	–	–	–	–	–	–	–	–	–	–	WDS	355^{+40}_{-45}	CMD	-,-,-,-	–
TYC9037-1879-1	R	–	–	–	–	–	–	–	–	–	–	–	745^{+310}_{-15}	CMD	-,-,-,-	–
HD 148562	R	–	–	–	–	–	-0.40±2	–	–	–	–	WDS	5^{+20}_{-0}	UpperSco (CMD)	-,13,-,15	–
TYC6799-933-1	R	–	–	–	–	159.00	-3.00±6	–	–	–	–	–	1265^{+5}_{-25}	CMD	21,13,-,-	–
HD 148657	R	–	–	–	–	–	-2.70±1	–	–	–	–	–	10^{+0}_{-0}	UCL	-,13,-,15	–

Continued on Next Page...

Table C.1 – Continued

Name	Catalog	Obs. MJD	Instrument	Hα (mÅ)	Li6708 (mÅ)	$v \sin(i)$ (kms^{-1})	RV (kms^{-1})	[Fe/H] (dex)	log (g)	log ($\frac{L_X}{L_{bol}}$)	log (R'_{HK})	Multiple Ref.	Age (Myr)	Age-Dating Method	Refs	Notes
HD 328333	R	57294.38112	SWO	3092	0	–	-20.92±13.54	–	–	–	–	–	10^{+0}_{-0}	UCL	-,1,-,15	–
TYC390-217-1	R	–	–	–	–	–	-13.90±3	–	–	–	–	WDS	1305^{+290}_{-180}	CMD	-,13,-,-	–
sig Her	R	–	–	–	–	294.00	-10.90±2	0.03±0.04	–	–	–	WDS	400^{+70}_{-135}	CMD	61,13,4,-	–
TYC3063-2031-1	R	–	–	–	–	–	–	–	–	–	–	–	345^{+85}_{-95}	CMD	-,-,-,-	–
TYC 1531-383-1	R	–	–	–	–	–	–	–	–	–	–	–	50^{+100}_{-0}	CMD	-,-,-,-	assumed ZAMS
TYC5636-577-1	R	56713.55789	LHO	2247	68	40.83	3.37±92.87	-0.26±0.04	2.81±0.16	-4.79	–	–	625^{+0}_{-0}	Li	1,1,1,-	X-ray agreement
HD 149735	R	57294.38573	SWO	1551	185	–	4.46±3.52	–	–	-4.33	–	–	10^{+365}_{-0}	UCL (X-ray)	-,1,-,36	–
HD 149790	R	–	–	–	–	–	0.70±2	–	–	-3.87	–	–	5^{+120}_{-0}	UpperSco (X-ray)	-,13,-,15	–
HD 149914	R	–	–	–	–	–	-2.50±2	–	–	–	–	–	5^{+610}_{-0}	UpperSco (CMD)	-,13,-,15	–
TYC5632-973-1	R	–	–	–	–	–	-12.70±2	–	–	–	–	–	915^{+150}_{-110}	CMD	-,13,-,-	–
TYC7879-1506-1	R	–	–	–	–	–	–	–	–	–	–	–	790^{+20}_{-180}	CMD	-,-,-,-	–
TYC387-634-1	R	–	–	–	–	–	-23.00±2	–	–	–	–	CCDM	840^{+55}_{-350}	CMD	-,13,-,-	–
HD 150742	R	–	–	–	–	180.00	11.80±3	–	–	–	–	CCDM	10^{+155}_{-0}	UCL (CMD)	21,13,-,15	–
HR 6237	R	57081.52153	DMO	2129	0	44.20	-2.00±7	-0.22±0.04	–	–	–	WDS	1690^{+95}_{-315}	CMD	1,13,4,-	–
TYC6817-2179-1	R	–	–	–	–	–	–	–	–	–	–	–	300^{+100}_{-175}	CMD	-,-,-,-	–
HD 151109	R	–	–	–	–	–	-2.90±1	–	–	–	–	WDS	10^{+240}_{-0}	UCL (CMD)	-,13,-,15	–
TYC8330-2024-1	R	–	–	–	–	–	–	–	–	–	–	–	2120^{+590}_{-390}	CMD	-,13,-,-	–
HD 151721	R	–	–	–	–	–	-0.40±2	–	–	–	–	WDS	5^{+625}_{-0}	UpperSco (CMD)	-,13,-,15	–
TYC7868-172-1	R	–	–	–	–	–	–	–	–	–	–	–	1450^{+520}_{-135}	CMD	-,-,-,-	–
TYC7372-990-1	R	–	–	–	–	–	-3.90±1	–	–	-4.33	–	WDS	10^{+115}_{-0}	UCL (X-ray)	-,13,-,15	–
TYC988-1952-1	R	51335.95286	OEA	2668	0	39.17	-31.70±4	±0.54	–	–	–	–	315^{+100}_{-115}	CMD	1,13,4,-	–
HD 154145	R	–	–	–	–	–	–	–	–	–	–	–	1005^{+25}_{-65}	CMD	-,-,-,-	–
TYC8726-458-1	R	–	–	–	–	–	–	–	–	–	–	–	570^{+420}_{-570}	CMD	-,-,-,-	–
TYC6237-37-1	R	–	–	–	–	–	–	–	–	–	–	–	525^{+130}_{-275}	CMD	-,-,-,-	–
TYC7370-237-1	R	–	–	–	–	–	–	–	–	–	–	–	685^{+110}_{-285}	CMD	-,-,-,-	–
TYC9056-548-1	R	–	–	–	–	–	–	–	–	–	–	–	26^{+6}_{-6}	CMD	-,-,-,-	–
TYC2078-810-1	R	–	–	–	–	–	–	–	–	-2.94	–	–	26^{+5}_{-2}	CMD	-,-,-,-	X-ray agreement
HD 155915	R	–	–	–	–	–	1.30±1	–	–	-3.41	–	WDS	125^{+0}_{-0}	X-ray	-,30,-,-	–
TYC7874-747-1	R	–	–	–	–	–	–	–	–	–	–	–	50^{+100}_{-0}	CMD	-,-,-,-	assumed ZAMS
TYC7362-633-1	R	–	–	–	–	–	–	–	–	–	–	–	690^{+95}_{-120}	CMD	-,-,-,-	–
TYC6833-20-1	R	–	–	–	–	–	–	–	–	–	–	WDS	630^{+115}_{-145}	CMD	-,-,-,-	–
TYC6830-20-1	R	–	–	–	–	128.00	-8.30±3	–	–	–	–	–	240^{+115}_{-10}	CMD	61,13,-,-	–
TYC6838-418-1	R	–	–	–	–	–	–	–	–	–	–	–	630^{+145}_{-90}	CMD	-,-,-,-	–
TYC7888-1250-1	R	–	–	–	–	–	–	-0.28±0.06	–	–	–	WDS	50^{+100}_{-0}	CMD	-,-,49,-	assumed ZAMS
TYC7380-335-1	R	–	–	–	–	–	–	–	–	–	–	–	480^{+150}_{-280}	CMD	-,-,-,-	–
TYC7892-4279-1	R	–	–	–	–	–	–	–	–	–	–	–	415^{+90}_{-135}	CMD	-,-,-,-	–

Continued on Next Page. . .

Table C.1 – Continued

Name	Catalog	Obs. MJD	Instrument	Hα (mÅ)	Li6708 (mÅ)	$v \sin(i)$ (kms^{-1})	RV (kms^{-1})	[Fe/H] (dex)	log (g)	log ($\frac{L_X}{L_{bol}}$)	log (R'_{HK})	Multiple Ref.	Age (Myr)	Age-Dating Method	Refs	Notes
HD 161734	R	–	–	–	–	193.00	-4.00±8	–	–	–	–	–	755^{+390}_{-150}	CMD	21,13,-,-	–
HD 161733	R	–	–	–	–	34.20	-12.50±1	–	–	–	–	WDS	545^{+5}_{-180}	CMD	21,24,-,-	–
TYC2620-505-1	R	–	–	–	–	–	–	–	–	–	–	–	1280^{+1210}_{-1230}	CMD	-,-,-,-	–
TYC9054-701-1	R	57294.40845	SWO	2478	0	–	10.21±10.91	–	–	–	–	–	1360^{+740}_{-130}	CMD	-,1,-,-	–
HD 164029	R	57294.41412	SWO	1604	9	25.68	2.93±2.05	–	–	–	–	–	*****	–	1,1,-,-	giant:Gaia
TYC8361-1861-1	R	–	–	–	–	–	–	–	–	–	–	–	245^{+120}_{-90}	CMD	-,-,-,-	–
68 Oph	R	–	–	–	–	201.00	–	–	–	–	–	WDS	460^{+65}_{-110}	CMD	61,-,-,-	–
TYC3915-1288-1	R	–	–	–	–	142.00	-24.10±4	–	–	–	–	–	515^{+150}_{-135}	CMD	12,13,-,-	–
TYC7400-645-1	R	57294.42010	SWO	1530	5	–	-74.61±2.98	–	–	–	–	–	625^{+0}_{-0}	Li	-,1,-,-	–
TYC6272-1522-1	R	–	–	–	–	–	–	–	–	-4.73	–	–	4000^{+0}_{-0}	X-ray	-,-,-,-	–
TYC1022-431-1	R	–	–	–	–	–	–	–	–	–	–	–	290^{+65}_{-80}	CMD	-,-,-,-	–
TYC8756-2474-1	R	–	–	–	–	22.00	–	–	–	–	–	–	145^{+25}_{-45}	CMD	6,-,-,-	–
TYC7910-57-1	R	–	–	–	–	–	–	–	–	–	–	–	1030^{+110}_{-150}	CMD	-,-,-,-	–
TYC9291-1885-1	R	57294.44524	SWO	2005	7	–	-12.75±4.06	–	–	–	–	–	0^{+0}_{-625}	Li	-,1,-,-	–
TYC7402-1806-1	R	57294.45312	SWO	1151	0	22.06	-47.63±2.08	–	–	–	–	–	*****	–	1,1,-,-	no age info.
TYC3109-1699-1	R	–	–	–	–	–	–	–	–	-4.14	–	–	625^{+0}_{-0}	X-ray	-,-,-,-	–
TYC9081-1908-1	R	–	–	–	–	–	–	–	–	–	–	–	425^{+480}_{-420}	CMD	-,-,-,-	–
TYC7902-495-1	R	57294.45843	SWO	3146	0	–	–	–	–	–	–	–	1260^{+1010}_{-325}	CMD	-,-,-,-	–
TYC450-619-1	R	–	–	–	–	–	–	–	–	–	–	–	50^{+100}_{-0}	CMD	-,-,-,-	assumed ZAMS
TYC3531-1261-1	R	–	–	–	–	–	–	–	–	–	–	–	670^{+110}_{-270}	CMD	-,-,-,-	–
TYC7419-3077-1	R	–	–	–	–	23.50	3.90±3	–	–	–	–	WDS	65^{+20}_{-35}	CMD	21,13,-,-	–
HIP 91926	R	57287.19909	DMO	3497	0	35.19	-24.40±2	–	–	–	–	55	1215^{+85}_{-45}	CMD	1,13,-,-	–
110 Her	R	53314.75539	OEA	1716	2	17.69	28.55±5.22	-0.21±0.05	–	-5.34	–	WDS	0^{+0}_{-625}	Li	1,1,29,-	X-ray agreement
TYC7915-252-1	R	–	–	–	–	–	–	–	–	–	–	–	250^{+65}_{-120}	CMD	-,-,-,-	–
TYC452-465-1	R	–	–	–	–	–	–	–	–	–	–	–	50^{+100}_{-0}	CMD	-,-,-,-	assumed ZAMS
TYC3926-1315-1	R	–	–	–	–	–	–	–	–	-2.78	–	–	0^{+125}_{-0}	X-ray	-,-,-,-	–
TYC8377-2703-1	R	–	–	–	–	–	-43.60±4	–	–	–	–	–	770^{+50}_{-115}	CMD	-,13,-,-	–
TYC8377-2702-1	R	–	–	–	–	–	–	–	–	–	–	WDS	630^{+75}_{-160}	CMD	-,-,-,-	–
TYC5119-79-1	R	–	–	–	–	–	–	–	–	–	–	–	50^{+100}_{-0}	CMD	-,-,-,-	assumed ZAMS
TYC1040-160-1	R	57200.34296	DMO	3010	0	–	–	–	–	–	–	–	1475^{+355}_{-165}	CMD	-,-,-,-	–
TYC7421-1061-1	R	57294.46176	SWO	2810	0	–	-21.58±19.62	–	–	–	–	–	5^{+135}_{-0}	CMD	-,1,-,-	–
TYC7421-1163-1	R	–	–	–	–	–	–	–	–	–	–	–	815^{+165}_{-340}	CMD	-,-,-,-	–
HD 177996	R	57294.46588 57323.43096	SWO SEO	814	16	12.41	-41.30±2.40	-0.22±0.08	–	-3.90	–	WDS	625^{+0}_{-605}	Li (CMD)	1,1,4,-	–
TYC4229-229-1	R	–	–	–	–	86.00	-23.60±2	–	–	–	–	–	480^{+5}_{-105}	CMD	61,13,-,-	–
TYC471-1564-1	R	–	–	–	–	–	–	–	–	–	–	–	50^{+100}_{-0}	CMD	-,-,-,-	assumed ZAMS
TYC467-681-1	R	–	–	–	–	–	–	–	–	–	–	–	14^{+2}_{-14}	CMD	-,-,-,-	–
TYC6882-240-1	R	57294.46895	SWO	3185	61	–	-27.31±10.68	-0.22±0.08	–	–	–	–	30^{+1180}_{-0}	Li (CMD)	-,1,4,-	–
TYC6296-1814-1	R	–	–	–	–	–	–	–	–	–	–	–	610^{+70}_{-25}	CMD	-,-,-,-	–
TYC8764-2333-1	R	–	–	–	–	–	151.00±4	–	–	–	–	WDS	80^{+20}_{-20}	CMD	-,13,-,-	–

Continued on Next Page. . .

Table C.1 – Continued

Name	Catalog	Obs. MJD	Instrument	Hα (mÅ)	Li6708 (mÅ)	$v \sin(i)$ (kms^{-1})	RV (kms^{-1})	[Fe/H] (dex)	log (g)	log ($\frac{L_X}{L_{bol}}$)	log (R'_{HK})	Multiple Ref.	Age (Myr)	Age-Dating Method	Refs	Notes
TYC1599-1737-1	R	–	–	–	–	–	–	–	–	–	–	–	38^{+4}_{-5}	CMD	-,-,-,-	–
TYC2654-591-1	R	–	–	–	–	–	–	–	–	–	–	–	75^{+50}_{-50}	CMD	-,-,-,-	assumed ZAMS
TYC2663-22-1	R	–	–	–	–	16.20	-13.40±0	-0.19±0.05	–	-4.33	–	WDS	0^{+375}_{-0}	X-ray	21,13,4,-	–
TYC7425-2426-1	R	–	–	–	–	–	–	–	–	–	–	–	455^{+200}_{-255}	CMD	-,-,-,-	–
TYC5736-2110-1	R	–	–	–	–	–	–	–	–	–	–	–	420^{+110}_{-170}	CMD	-,-,-,-	–
TYC5725-3091-1	R	–	–	–	–	271.00	-6.00±7	–	–	–	–	–	230^{+50}_{-45}	CMD	61,13,-,-	–
TYC5750-1884-1	R	57293.41368	SWO	2087	5	–	-27.51±3.68	–	–	–	–	–	0^{+0}_{-625}	Li	-,1,-,-	–
HD 190470	R	57287.26794	DMO	973	6	13.50	–	0.13±0.06	–	–	–	–	375^{+0}_{-275}	Li (CMD)	1,-,4,-	–
TYC8784-1182-1	R	–	–	–	–	–	–	–	–	–	–	WDS	55^{+337}_{-7}	CMD	-,-,-,-	–
TYC8404-354-1	R	–	–	–	–	–	–	–	–	-2.78	–	–	65^{+4}_{-3}	CMD	-,-,-,-	X-ray agreement
33 Cyg	R	–	–	–	–	243.00	-18.00±4	–	–	–	–	–	830^{+15}_{-40}	CMD	61,13,-,-	–
TYC504-468-1	R	57201.31206	DMO	2505	0	66.56	–	–	–	–	–	–	1575^{+400}_{-345}	CMD	1,-,-,-	–
TYC2680-1143-1	R	–	–	–	–	–	–	–	–	–	–	–	475^{+140}_{-90}	CMD	-,-,-,-	–
TYC5167-2066-1	R	–	–	–	–	–	–	–	–	-3.14	–	–	0^{+125}_{-0}	X-ray	-,-,-,-	–
TYC3156-1235-1	R	57272.22824	DMO	1265	49	12.54	3.00±0	–	–	–	–	–	625^{+0}_{-0}	Li	1,7,-,-	–
TYC3160-85-1	R	–	–	–	–	–	–	–	–	-4.65	–	–	625^{+0}_{-0}	X-ray	-,-,-,-	–
TYC8414-872-1	R	–	–	–	–	–	–	–	–	–	–	–	10^{+0}_{-0}	CMD	-,-,-,-	–
TYC3573-2231-1	R	–	–	–	–	–	–	–	–	–	–	–	50^{+155}_{-13}	CMD	-,-,-,-	–
TYC9316-99-1	R	–	–	–	–	–	–	–	–	–	–	–	230^{+85}_{-230}	CMD	-,-,-,-	–
TYC7950-1215-1	R	57293.46265	SWO	713	0	14.10	-69.04±9.82	–	–	–	–	–	*****	–	1,1,-,-	giant:Gaia
TYC3165-787-1	R	57287.20766	DMO	2151	52	27.07	-6.90±3	-0.14±0.08	–	–	–	–	30^{+965}_{-0}	Li (CMD)	1,13,4,-	–
TYC3153-726-1	R	–	–	–	–	–	–	–	–	–	–	–	50^{+100}_{-0}	CMD	-,-,-,-	assumed ZAMS
bet Del	R	51400.98228	OEA	2742	58	38.02	-19.68±22.69	±-0.01	–	-5.45	–	WDS	625^{+0}_{-0}	Li	1,1,4,-	X-ray agreement
BO Mic	R	–	–	–	–	–	–	±-1.49	–	-2.12	–	WDS	11^{+115}_{-3}	CMD (X-ray)	-,-28,-	–
TYC8803-1199-1	R	–	–	–	–	–	–	–	–	–	–	–	605^{+65}_{-40}	CMD	-,-,-,-	–
HR 8019	R	–	–	–	–	212.00	–	–	–	–	–	–	755^{+35}_{-130}	CMD	17,-,-,-	–
TYC3592-6130-1	R	–	–	–	–	–	-9.00±7	–	–	–	–	–	615^{+150}_{-60}	CMD	-,13,-,-	–
TYC9101-1055-1	R	57293.47529	SWO	1232	11	–	-35.27±2.05	–	–	–	–	–	*****	–	-,1,-,-	giant:Gaia
HD 201377	R	51010.07131	OEA	5888	0	89.50	16.00±1	-0.47±0.01	–	–	–	–	975^{+45}_{-220}	CMD	1,13,41,-	–
TYC3953-1359-1	R	–	–	–	–	–	8.10±1	–	–	–	–	–	495^{+20}_{-90}	CMD	-,13,-,-	–
HD 202406	R	57293.48794 57323.46375	SWO SEO	3158	0	95.04	-12.47±15.56	-0.69±0.04	2.44±0.21	–	–	–	625^{+15}_{-50}	Li (CMD)	1,1,1,-	–
TYC3597-664-1	R	–	–	–	–	–	–	–	–	–	–	–	32^{+0}_{-3}	CMD	-,-,-,-	–
TYC9110-1485-1	R	–	–	–	–	147.00	11.50±1	–	–	–	–	–	255^{+95}_{-75}	CMD	61,13,-,-	–
TYC9461-74-1	R	–	–	–	–	264.40	–	–	–	–	–	–	390^{+110}_{-130}	CMD	17,-,-,-	–
TYC4469-533-1	R	56258.13994	LHO	3540	0	95.60	6.59±124.83	-0.76±0.04	2.32±0.26	–	–	–	*****	–	1,1,1,-	no age info.
TYC3194-690-1	R	56519.29135	LHO	1423	0	31.41	–	-0.77±0.05	2.36±0.23	–	–	–	*****	–	1,-,1,-	CMD giant branch
TYC541-35-1	R	57320.44241	SWO	1825	62	–	18.76±5.49	–	–	–	–	–	625^{+0}_{-0}	Li	-,1,-,-	–
bet Equ	R	–	–	–	–	49.00	–	–	–	–	–	WDS	590^{+20}_{-30}	CMD	61,-,-,-	–

Continued on Next Page. . .

Table C.1 – Continued

Name	Catalog	Obs. MJD	Instrument	Hα (mÅ)	Li6708 (mÅ)	$v \sin(i)$ (kms^{-1})	RV (kms^{-1})	[Fe/H] (dex)	log (g)	log ($\frac{L_X}{L_{bol}}$)	log (R'_{HK})	Multiple Ref.	Age (Myr)	Age-Dating Method	Refs	Notes
TYC3598-1594-1	R	–	–	–	–	–	–	–	–	-2.92	–	–	23^{+2}_{-4}	CMD	-,-,-,-	X-ray agreement
HD 204041	R	–	–	–	–	67.00	-17.90±0	-0.44±0.12	–	–	–	–	720^{+60}_{-220}	CMD	61,13,42,-	–
TYC3603-226-1	R	–	–	–	–	–	–	–	–	–	–	–	34^{+48}_{-7}	CMD	-,-,-,-	–
TYC2726-266-1	R	–	–	–	–	–	–	–	–	–	–	–	50^{+100}_{-0}	CMD	-,-,-,-	assumed ZAMS
TYC5218-1399-1	R	–	–	–	–	–	–	–	–	–	–	–	315^{+185}_{-75}	CMD	-,-,-,-	–
TYC3196-1605-1	R	–	–	–	–	–	-6.00±4	–	–	–	–	–	795^{+130}_{-45}	CMD	-,13,-,-	–
TYC3972-2737-1	R	–	–	–	–	51.40	-5.80±2	–	–	–	–	WDS	415^{+60}_{-110}	CMD	21,13,-,-	–
HD 207575	R	–	–	–	–	26.90	1.40±1	-0.18±0.08	–	–	–	WDS	30^{+0}_{-0}	Tuc-Hor	21,30,4,30	–
TYC7994-894-1	R	57321.49420	SWO	1837	3	–	-26.24±3.22	–	–	–	–	–	0^{+0}_{-625}	Li	-,1,-,-	–
HD 207889	R	52943.06503	EHA	1407	0	8.08	14.80±0.89	-0.12±0.08	3.81±0.27	–	–	–	*****	–	1,1,1,-	no age info.
HD 208038	R	53250.92860	OEA	833	20	6.49	10.19±1.20	-0.08±0.04	–	-4.50	–	–	375^{+0}_{-275}	Li (CMD)	1,1,29,-	–
TYC7994-1023-1	R	57321.50394	SWO	919	14	–	-11.67±1.49	–	–	–	–	–	375^{+0}_{-0}	Li	-,1,-,-	–
HD 208585	R	57287.24551	DMO	1100	9	11.62	–	–	–	–	–	–	375^{+0}_{-0}	Li	1,-,-,-	–
TYC2211-1309-1	R	–	–	–	–	–	–	–	–	-3.12	–	–	125^{+0}_{-0}	X-ray	-,-,-,-	–
TYC3977-493-1	R	–	–	–	–	–	-19.00±7	–	–	–	–	WDS	1020^{+25}_{-110}	CMD	-,13,-,-	–
TYC3203-1131-1	R	–	–	–	–	–	–	–	–	–	–	–	100^{+51}_{-0}	CMD	-,-,-,-	assumed ZAMS
TYC4271-788-1	R	–	–	–	–	–	–	–	–	-4.90	–	–	625^{+0}_{-0}	X-ray	-,-,-,-	–
eps Cep	R	51403.02968	OEA	3194	0	71.76	-4.70±1	-0.10±0.01	–	–	–	CCDM	*****	–	1,13,41,-	no age info.
HD 212265	R	57287.29458	DMO	1415	26	11.97	-34.50±0	-0.14±0.08	–	–	–	–	0^{+0}_{-625}	Li	1,13,4,-	–
TYC5807-1695-1	R	–	–	–	–	–	–	–	–	–	–	–	900^{+100}_{-215}	CMD	-,-,-,-	–
HR 8581	R	–	–	–	–	5.10	-9.72±0	-0.02±0.08	–	–	–	WDS	15^{+0}_{-0}	β Pic	21,13,4,1	–
HD 213941	R	–	–	–	–	2.70	67.30±0	-0.46±0.01	–	-5.13	–	–	625^{+0}_{-0}	X-ray	21,13,49,-	–
TYC9337-518-1	R	57321.46793	SWO	1329	0	–	32.67±2.98	–	–	–	–	–	*****	–	-,1,-,-	no age info.
42 Peg	R	52244.74095	OEA	4431	0	109.71	6.10±0	0.06±0.04	–	–	–	WDS	245^{+45}_{-25}	CMD	1,13,4,-	–
TYC5237-1606-1	R	–	–	–	–	–	–	–	–	–	–	–	380^{+115}_{-140}	CMD	-,-,-,-	–
HD 215152	R	–	–	–	–	9.20	–	-0.08±0.02	–	–	–	–	50^{+100}_{-0}	CMD	51,-,49,-	assumed ZAMS
TYC6970-702-1	R	57321.48172	SWO	1524	30	–	24.95±3.33	–	–	–	–	–	125^{+0}_{-0}	Li	-,1,-,-	–
TYC5812-1232-1	R	57293.50654	SWO	2132	6	–	7.48±3.61	–	–	–	–	–	0^{+0}_{-625}	Li	-,1,-,-	–
TYC7511-854-1	R	57321.51615	SWO	1494	11	–	-10.31±2.69	–	–	–	–	–	0^{+0}_{-625}	Li	-,1,-,-	–
TYC576-702-1	R	–	–	–	–	–	–	–	–	-3.17	–	–	125^{+0}_{-0}	X-ray	-,-,-,-	–
TYC4291-1206-1	R	–	–	–	–	–	–	–	–	–	–	–	520^{+35}_{-40}	CMD	-,-,-,-	–
HD 218860	R	–	–	–	–	6.30	9.60±0	-0.02±0.08	–	-3.64	–	WDS	110^{+15}_{-0}	AB Dor (X-ray)	21,13,4,30	–
TYC4010-200-1	R	57272.35650	DMO	2235	0	41.17	–	–	–	–	–	–	1355^{+600}_{-605}	CMD	1,-,-,-	–
TYC2244-1797-1	R	–	–	–	–	–	2.40±3	–	–	–	–	–	400^{+100}_{-125}	CMD	-,13,-,-	–
HD 219498	R	–	–	–	–	10.00	-10.60±2	–	–	-4.50	–	WDS	0^{+0}_{-375}	X-ray	57,57,-,-	–
TYC584-396-1	R	–	–	–	–	–	5.10±3	–	–	–	–	–	125^{+65}_{-75}	CMD	-,13,-,-	–
TYC3230-381-1	R	–	–	–	–	–	-4.40±2	–	–	–	–	–	370^{+110}_{-95}	CMD	-,13,-,-	–
TYC8455-294-1	R	57320.45131	SWO	1785	34	–	-6.13±4.30	–	–	–	–	–	625^{+0}_{-0}	Li	-,1,-,-	–
TYC6987-349-1	R	57293.60916	SWO	1695	36	–	23.18±4.04	–	–	–	–	–	0^{+0}_{-625}	Li	-,1,-,-	–

Continued on Next Page. . .

Table C.1 – Continued

Name	Catalog	Obs. MJD	Instrument	Hα (mÅ)	Li6708 (mÅ)	$v \sin(i)$ (kms^{-1})	RV (kms^{-1})	[Fe/H] (dex)	$\log(g)$	$\log(\frac{L_X}{L_{bol}})$	$\log(R'_{HK})$	Multiple Ref.	Age (Myr)	Age-Dating Method	Refs	Notes
TYC4602-1115-1	R	57201.40420	DMO	0	0	–	–	–	–	–	–	–	1770^{+270}_{-465}	CMD	-,-,-,-	–
TYC1176-827-1	R	–	–	–	–	–	–	–	–	–	–	–	1820^{+580}_{-225}	CMD	-,-,-,-	–
CD-30 19671	R	57293.61618	SWO	1296	4	20.94	-27.52±2.44	–	–	–	–	–	*****	–	1,1,-,-	giant:Gaia
TYC2254-26-1	R	56517.25237	LHO	1134	17	3.66	-9.93±10.27	0.23±0.01	4.19±0.03	–	–	–	625^{+0}_{-600}	Li (CMD)	1,1,1,-	–
TYC2775-1057-1	R	–	–	–	–	–	-6.00±3	–	–	–	–	–	725^{+60}_{-130}	CMD	-,13,-,-	–
TYC4285-1240-1	R	57201.35391	DMO	3624	0	–	–	–	–	–	–	–	645^{+265}_{-255}	CMD	-,-,-,-	–
TYC2767-750-1	R	–	–	–	–	–	–	–	–	–	–	–	590^{+585}_{-230}	CMD	-,-,-,-	–
HD 223575	R	57293.57339	SWO	1463	81	20.77	2.17±2.94	–	–	–	–	WDS	625^{+0}_{-0}	Li	1,1,-,-	–
BD+28 4660	R	–	–	–	–	0.00	0.60±0	–	–	–	–	WDS	59^{+5}_{-9}	CMD	21,13,-,-	–
TYC6408-96-1	R	56257.15186	LHO	1214	13	2.91	-16.06±32.09	–	–	–	–	–	0^{+0}_{-625}	Li	1,1,-,-	–
HD 224228	R	–	–	–	–	–	–	±0.04	–	-4.41	–	–	100^{+275}_{-50}	CMD (X-ray)	-,-,64,-	–
TYC4650-2790-1	R	–	–	–	–	147.00	-12.90±3	–	–	–	–	–	495^{+105}_{-135}	CMD	12,13,-	–
TYC5834-909-1	R	57321.53282	SWO	1743	46	–	-9.37±4.31	–	–	–	–	WDS	125^{+0}_{-0}	Li	-,1,-,-	–
TYC4293-174-1	R	57272.32729	DMO	2508	0	42.07	–	–	–	–	–	–	*****	–	1,-,-,-	no age info.

Observation Keys: VUA: Very Large Telescope, UVES, Archival Data; OEA: OHP Telescope, ELODIE, Archival Data; OSA: OHP Telescope, SOPHIE, Archival Data; EHA: ESO La Silla Observatory, HARPS, Archival Data; MFA: MPI/ESO Telescope, FEROS, Archival Data; SWO: Siding Spring Observatory, WiFeS, Observed: S. Murphy; SEO: Siding Spring Observatory, Echelle, Observed: S. Murphy; DMO: Dominian Astrophysical Observatory, McKellar, Observed: T. Cotten; LHO: Lick Observatory, Hamilton, Observed: C. Melis, A. Schneider *Notes*: Measurements of Hα, Li 6708Å, R'_{HK}, and L_X/L_{bol} were calculated in this study. The age method included in () was used for the upper/lower limit. References column lists the reference for $v \sin i$, radial velocity, [Fe/H], and Cluster membership in this order if applicable. *References for Table C.1:*

1 This work.

2 Adibekyan et al. (2016)

3 Ammler-von Eiff & Reiners (2012)

4 Anderson & Francis (2012)

5 Biller et al. (2007)

6 Braganca et al. (2012)

7 Casagrande et al. (2011)

8 Cenarro et al. (2007)

9 Chen et al. (2011)

10 Chen et al. (2014)

11 Dahm et al. (2012)

12 David & Hillenbrand (2015)

13 de Bruijne & Eilers (2012)

14 de Medeiros et al. (2014)

15 de Zeeuw et al. (1999)

16 Desidera et al. (2015)

17 Diaz et al. (2011)

18 Draper et al. (2016)

19 Eker et al. (2014)

20 Gebran et al. (2016)

21 Glebocki & Gnacinski (2005)

22 Gontcharov (2006)

23 Gray & Brown (2006)

65 Kennedy et al. (2012)

24 Kharchendo et al. (2007)

25 Luhman & Mamajek (2012)

26 Luo et al. (2015)

27 Mahdi et al. (2016)

63 Maldonado et al. (2010)

28 Maldonado et al. (2012)

29 Maldonado et al. (2015)

30 Malo et al. (2013)

31 Mamajek et al. (1999)

32 Martínez-Arnáiz et al. (2010)

33 Mermilliod et al. (2009)

34 Mizusawa et al. (2012)

64 Mortier et al. (2013)

35 Murphy & Lawson (2015)

36 Pecaut & Mamajek (2016)

37 Perrot et al. (2016)

38 Perryman et al. (1998)

39 Platais et al. (2007)

40 Pribulla et al. (2014)

41 Prugniel et al. (2007)

42 Prugniel et al. (2011)

43 Ramírez et al. (2012)

44 Rodriguez & Zuckerman (2012)

45 Rodriguez et al. (2015)

62 Royer et al. (2007)

60 Royer et al. (2012)

46 Santos et al. (2013)

47 Schröder et al. (2009)

48 Song et al. (2003)

49 Soubiran et al. (2016)

50 Stauffer et al. (2007)

51 Strassmeier et al. (2000)

52 Su et al. (2013)

53 Taylor & Joner (2005)

54 Thalmann et al. (2014)

55 Trilling et al. (2007)

56 Tsantaki et al. (2013)

57 White et al. (2007)

58 White et al. (2016)

59 Wilson et al. (2016)

61 Zorec & Royer (2012)

Bibliography

Absil, O., di Folco, E., Merand, A. et al., 2008, A&A, 487, 1041.

Abt, H. A. & Morrell, N. I., 1995, ApJS, 99, 135.

Acke, B., Min, M., Dominik, C., 2012, A&A, 540, 125.

Adibekyan, V., Delgado-Mena, E., Figueira, P. et al., 2016, A&A, 592, 87.

Akeson, R. L., Ciardi, D. R., Millan-Gabet, R. et al., 2009, ApJ, 691, 1896.

Allard, F., Homeier, D. & Freytag, B., 2011, ASPC, 448, 91.

Ammler-von Eiff, M. & Reiners, A., 2012, A&A, 542, 116.

Anderson, E. & Francis, C., 2012, AstL, 38, 331.

Apai, D., Schneider, G., Grady, C. A. et al., 2015, ApJ, 800, 136.

Ardila, D. R., Van Dyk, S. D., Makowiecki, W. et al., 2010, ApJS, 191, 301.

Armstrong, D. J., Osborn, H. P., Brown, D. J. A. et al., 2014, MNRAS, 444, 1873.

Asplund, M., Grevesse, N., Sauval, A. et al., 2009, ARA&A, 47, 481.

Aumann, H. H., Beichman, C. A., Gillett, F. C. et al., 1984, ApJ, 278L, 23.

Avenhaus, H., Schmid, H. M., & Meyer, M. R., 2012, A&A, 548, 105.

Backman, D. E. & Paresce, F., 1993, *Protostars and Planets III*, ed. E. H. Levy, J. I. Lunine, Tucson, Univ. Ariz. Press, 1253.

Bailey, V., Meshkat, T., Reiter, M. et al., 2014, ApJ, 780, 4.

Ballering, N. P. , Rieke, G. H., Su, K. Y. L., & Montiel, E., 2013, ApJ, 775, 55.

Ballering, N. P., Rieke, G. H., & Gaspar, A., 2014, ApJ, 793, 57.

Balog, Z., Kiss, L. L., Vinko, J. et al., 2009, ApJ, 698, 1989.

Barber, S. D., Patterson, A. J., Kilic, M. et al., 2012, ApJ, 760, 26.

Baraffe, I., Homeier, D., Allard, F. et al., 2015, A&A, 577, 42.

Baranne, A., Queloz, D., Mayor, M. et al., 1993, A&AS, 119, 373.

Barnes, S. A., 2003, ApJ, 586, 464.

Barnes, S. A., 2007, ApJ, 669, 1167.

Beichman, C. A., Neugebauer, G., Habing, H. J. et al., 1988, *IRAS catalogs and atlases. Volume 1: Explanatory supplement.*

Beichman, C. A., Bryden, G., Rieke, G. H. et al., 2005, ApJ, 622, 1160.

Beichman, C. A., Bryden, G., Gautier, T. N. et al., 2005b, ApJ, 626, 1061.

Beichman, C. A., Tanner, A., Bryden, G. et al., 2006a, ApJ, 639, 1166.

Beichman, C. A., Bryden, G., Stapelfeldt, K. R. et al., 2006b, ApJ, 652, 1674.

Beuzit, J.-L., Feldt, M., Dohlen, K. et al., 2008, SPIE, 7014, 701418.

Bessell, M. S. & Brett, J. M., 1988, PASP, 100, 1134.

Bessell, M. S., 2000, PASP, 112, 961.

Biller, B. A, Close, L. M., Masciadri, E. et al., 2007, ApJS, 173, 143.

Bitner, M. A., Chen, C. H., Muzerolle, J. et al., 2010, ApJ, 714, 1542.

Blanco-Cuaresma, S., Soubiran, C., Heiter, U. et al., 2014, A&A, 569, 111.

Bodenheimer, P., 1995, ARA&A, 33, 199.

Bonsor, A. & Wyatt, M., 2010, MNRAS, 409, 1631.

Bonsor, A., Kennedy, G. M., Crepp, J. R. et al., 2013, MNRAS, 431, 3025.

Bonsor, A., Kennedy, G. M., Crepp, J. R. et al., 2014, MNRAS, 437, 3288.

Booth, M., Wyatt, M. C., Morbidelli, A. et al., 2009, MNRAS, 399, 385.

Booth, M., Kennedy, G., Sibthorpe, B. et al., 2013, MNRAS, 428, 1263.

Borucki, W. J., Koch, D., Basri, G. et al., 2010, *Science*, 327, 977.

Bouchy, F., Díaz, R. F., Hébrard, G. et al., 2013, A&A, 549, 49.

Bouvier, J., Forestini, M., & Allain, S., 1997, A&A, 326, 1023.

Bouvier, J., Matt, S. P., Mohanty, S. et al., 2014, *Protostars and Planets VI*, ed. H. Beuther, R. S. Klessen, C. P. Dullemond, T. Henning, Tucson, Univ. Ariz. Press, 433.

Braganca, G. A., Daflon, S., Cunha, K. et al., AJ, 144, 130.

Brandt, T. D. & Huang, C. X., 2015, ApJ, 807, 58.

Broekhoven-Fiene, H., Matthews, B. C., Kennedy, G. M. et al., 2013, ApJ, 762, 52.

Brown, J. M., Blake, G. A., Qi, C. et al., 2008, ApJ, 675, 109.

Brown, J. M., Blake, G. A., Qi, C. et al., 2009, ApJ, 704, 496.

Bryden, G., Beichman, C. A., Trilling, D. E. et al., 2006a, ApJ, 636, 1098.

Bryden, G., Beichman, C. A., Rieke, G. H. et al., 2006b, ApJ, 646, 1038.

Bryden, G., Beichman, C. A., Carpenter, J. M. et al., 2009, ApJ, 705, 1226.

Buenzli, E., Thalmann, C., Vigan, A. et al., 2010, A&A, 524, 1.

Bulger, J., Hufford, T., Schneider, A. et al., 2013, ApJ, 636, 1098.

Carpenter, J. M., Mamajek, E. E., Hillenbrand, L. A. et al., 2006, ApJ, 651, 49.

Carpenter, J. M., Mamajek, E. E., Hillenbrand, L. A. & Meyer, M. R., 2009, ApJ, 705, 1646.

Carpenter, J. M., Ricci, L. & Isella, A., 2014, ApJ, 787, 42.

Casagrande, L., Schönrich, R., Asplund, M. et al., 2011, A&A, 530, 138.

Castelli, F. & Kurucz, R. L., IAUS 210, arXiv:0405087.

Cenarro, A. J., Peletier, R. F., Sánchez-Blázquez, P. et al., 2007, MNRAS, 374, 664.

Chandrasekhar, S. & Münch, G., 1950, ApJ, 111, 142.

Chen, C. H., Jura, M., Gordon, K. D. et al., 2005a, ApJ, 623, 493.

Chen, C. H., Patten, B. M., Werner, M. W. et al., 2005b, ApJ, 634, 1372.

Chen, C. H., Sargent, B. A., Bohac, C. et al., 2006, ApJS, 166, 351.

Chen, C. H., Fitzgerald, M. P. & Smith, P. S., 2008, ApJ, 689, 539.

Chen, C. H., Mamajek, E. E., Bitner, M. A. et al., 2011, ApJ, 738, 122.

Chen, C. H., Pecaut, M., Mamajek, E. E. et al., 2012, ApJ, 756, 133.

Chen, C. H., Mittal, T., Kuchner, M. et al., 2014, ApJS, 211, 25.

Childress, M. J., Vogt, F. P. A., Nielsen, J. et al., 2014, Ap&SS, 349, 617.

Churcher, L. J., Wyatt, M. C. & Smith, R., 2011a, MNRAS, 410, 2.

Churcher, L. J., Wyatt, M. C., Duchene, G. et al., 2011b, MNRAS, 417, 1715.

Cieza, L., Padgett, D. L., Stapelfeldt, K. R. et al., 2007, ApJ, 667, 308.

Cieza, L., Cochran, W. D., & Augereau, J.-C., 2008, ApJ, 679, 720.

Cieza, L. A., Schreiber, M. R., Romero, G. A. et al., 2010, ApJ, 712, 925.

Cieza, L. A., Schreiber, M. R., Romero, G. A. et al., 2012, ApJ, 750, 157.

Cloutier, R., Currie, T., Rieke, G. H. et al., 2014, ApJ, 796, 127.

Cotten, T. H. & Song, I., 2016, ApJ, 225, 15.

Cruz-Saenz de Miera, F., Chavez, M., Bertone, E. et al., 2014, MNRAS, 437, 391.

Cutri, R. M., Wright, E. L., Conrow, T. et al., 2012, Explanatory Supplement to the WISE All-Sky Data Release Products, Tech rep.

Cutri ,R. M., Wright, E. L., Conrow, T. et al., 2013, Explanatory Supplement to the AllWISE Data Release Products, Tech rep.

Currie, T., Plavchan, P. & Kenyon, S. J., 2008, ApJ, 688, 597.

Currie, T., Lisse, C. M., Sicilia-Aguilar, A. et al., 2011, ApJ, 734, 115.

Cushing, M. C., Marley, M. S., Saumon, D. et al., 2008, ApJ, 678, 1372.

Dahm, S. E., Slesnick, C. L., & White, R. J., 2012, ApJ, 745, 56.

David, T. J. & Hillenbrand, L. A., 2015, ApJ, 804, 146.

de Bruijne, J. H. J. & Eilers, A. -C., 2012, A&A, 546, 61.

Decin, G., Dominik, C., Malfait, K. et al., 2000, A&A, 357, 533.

Dekker, H., D‘ Odorico, S., Kaufer, A. et al., 2000, Proc. SPIE, 4008, 534.

Dell’Omodarme, M., Valle, G., Degl’Innocenti, S. et al., 2012, A&A, 540, 26.

Delmotte, N., Dolensky, M., Padovani, P. et al., 2006, *ASP Conference Series*, 351, 690.

de Medeiros, J. R., Alves, S., Udry, S. et al., 2014, A&A, 561, 126.

Dent, W. R. F., Thi, W. F., Kamp, I. et al., 2013, PASP, 125, 477.

Desidera, S., Covino, E., Messina, S. et al., 2011, A&A, 529, 54.

Desidera, S., Covino, E., Messina, S. et al., 2015, A&A, 573, 126.

de Zeeuw, P. T., Hoogerwerf, R., de Bruijne, J. H. J. et al., 1999, AJ, 117, 354.

Diaz, C. G., González, J. F., Levato, H. et al., 2011, A&A, 531, 143.

Dominik, C. & Decin, G., 2003, ApJ, 598, 626.

Dommanget, J. & Nys, O., 2002, VizieR Online Data Catalog, 1274, 0.

Donaldson, J. K., Roberge, A., Chen, C. H. et al., 2012, ApJ, 753, 147.

Draper, Z. H., Duchêne, G., Millar-Blanchaer, M. A. et al., 2016, ApJ, 826, 147.

Duchêne, G., McCabe, C., Pinte, C. et al., 2010, ApJ, 712, 112.

Duchêne, G. & Kraus, A., 2013, ARA&A, 51, 269.

Duncan, D. K., Vaughan, A. H., Wilson, O. C. et al., 1991, ApJS, 76, 383.

Eiroa, C., Fedele, D., Maldonado, J. et al., 2010, A&A, 518, 131.

Eiroa, C., Marshall, J. P., Mora, A. et al., 2011, A&A, 536, 4.

Eiroa, C., Marshall, J. P., Mora, A. et al., 2013, A&A, 555, 11.

Eker, Z., Bilir, S., Soydugan, F. et al., 2014, PASA, 31, 24.

Ekstrøm, S., Georgy, C., Eggenberger, P. et al, 2012, A&A, 537, 146.

Ertel, S., Wolf, S., Marschall, J. P. et al., 2012, A&A, 541, 148.

Esplin, T. L., Luhman, K. L., & Mamajek, E. E., 2014, ApJ, 784, 126.

Fabricius, C., Makarov, V. V., Knude, J. et al., 2002, A&A, 386, 709.

Fekel, F. C., 1997, PASP, 109, 514.

Fischer, D. A. & Marcy, G. W., 1992, ApJ, 396, 178.

Fischer, D. A. & Valenti, J., 2005, ApJ, 622, 1102.

Fujiwara, H., Yamashita, T., Ishihara, D. et al., 2009a, ApJ, 695, 88.

Fujiwara, H., Ishihara, D., Kataza, H. et al., 2009b, ASP Conference Series, 418, 109.

Fujiwara, H., Ishihara, D., Onaka, T. et al., 2013, A&A, 550, 45.

Gaia Collaboration: Brown, A. G. A., Vallenari, A., Prusti, T. et al., 2016, A&A*special Gaia volume*.

Gagné, J., Lafrenière, D., Doyon, R. et al., 2014, ApJ, 783, 121.

Galeazzi, M., Chiao, M., Collier, M. R. et al., 2014, *Nature*, 512, 171.

Gardner, J. P., Mather, J. C, Clampin, M. et al., 2006, Space Sci. Rev., 123, 485.

Gáspár, A., Rieke, G. H., Su, K. Y. L. et al., 2009, ApJ, 697, 1578.

Gáspár, A., Rieke, G. H., & Balog, Z., 2013, ApJ, 768, 25.

Gáspár, A., Rieke, G. H., & Ballering, N., 2016, ApJ, 826, 171.

Gautier, T. N. III, Rieke, G. H., Stansberry, J. et al., 2007, ApJ, 667, 527.

Gautier, T. N. III, Rebull, L. M., Stapelfeldt, K. R. et al., 2008, ApJ, 683, 813.

Gebran, M., Farah, W., Paletou, F. et al., 2016, A&A, 589, 83.

Georgy, C., Ekstrøm, S., Granada, A. et al., 2013, A&A, 553, 24.

Gizis, J. E., 2010, arXiv:1008.4576.

Glebocki, R. & Gnacinski, P., 2005, VizieR Online Data Catalog, 3244, 0.

Golimowski, D. A., Krist, J. E., Stapelfeldt, K. R. et al., 2011, AJ, 142, 30.

Gontcharov, G. A., 2006, *Astronomical and Astrophysical Transactions*, 25, 145.

Gonzalez, G., 1997, MNRAS, 285, 403.

Gonzalez, G., 2014, MNRAS, 443, 393.

Gorlova, N., Padgett, D. L., Rieke, G. H. et al., 2004, ApJS, 154, 448.

Gorlova, N., Rieke, G. H., Muzerolle, J. et al., 2006, ApJ, 649, 1028.

Gorlova, N., Balog, Z., Rieke, G. H. et al., 2007, ApJ, 670, 516.

Goto, M., Usuda, T., Dullemond, C. P. et al., 2006, ApJ, 652, 758.

Gray, R. O. & Corbally, C. J., 1994, AJ, 107, 742.

Gray, D. F. & Brown, K. I. T., 2006, PASP, 118, 399.

Greaves, J. S., Wyatt, M. C., Holland, W. S., & Dent, W. R. F., 2004, MNRAS, 351, 54.

Greaves, J. S., Holland, W. S., Wyatt, M. C. et al., 2005, ApJ, 619, 187.

Greaves, J. S., Fischer, D. A. & Wyatt, M. C., 2006, MNRAS, 366, 283.

Greaves, J. S., Wyatt, M. C. & Bryden, G., 2009, MNRAS, 397, 757.

Greaves, J. S. & Wyatt, M. C., 2010, MNRAS, 404, 1944.

Greaves, J. S., Kennedy, G. M., Thureau, N. et al., 2014a, MNRAS, 438, 31.

Greaves, J. S., Sibthorpe, B., Acke, B. et al., 2014b, ApJ, 791, 11.

Griffin, M. J., Abergel, A., Abreu, A. et al., 2010, A&A, 518, 3.

Grinin, V. P., Potravnov, I. S. & Musaev, F. A., 2010, A&A, 524, 8.

Guieu, S., Pinte, C., Monin, J.-L. et al., 2007, A&A, 465, 855.

Gustafsson, B., Edvardsson, B., Eriksson, K. et al., 2008, A&A, 486, 951.

Gutermuth, R. A., Megeath, S. T., Myers, P. C. et al., 2009, ApJS, 184, 18.

Hauschildt, P. H., Allard, F., & Baron, E., 1999, ApJ, 512, 377.

Heng, K., 2011, MNRAS, 415, 3365.

Henry, T. J., Jao, W.-C., Subasavage, J. P. et al., 2006, AJ, 132, 2360.

Herbst, W., Eislöffel, J., Mundt, R. et al., 2007, *Protostars and Planets V*, ed. B. Reipurth, D. Jewitt, K. Keil, Tucson, Univ. Ariz. Press, 297.

Hernandez, J., Briceno, C., Calvet, N. et al., 2006, ApJ, 652, 472.

Hernandez, J., Hartmann, L., Megeath, T. et al., 2007, ApJ, 662, 1067.

Hernandez, J., Hartmann, L., Calvet, N. et al., 2008, ApJ, 686, 1195.

Hernandez, J., Calvet, N., Hartmann, L. et al., 2009, ApJ, 707, 705.

Herbig, G. H. & Simon, T., 2001, AJ, 121, 3138.

Herczeg, G. J. & Hillenbrand, L. A., 2015, ApJ, 808, 23.

Hillenbrand, L. A., Carpenter, J. M., Kim, J. S. et al., 2008, ApJ, 677, 630.

Hines, D. C., Backman, D. E, Bouwman, J. et al., 2006, ApJ, 638, 1070.

Horch, E. P., Howell, S. B., Everett, M. E. et al., 2014, ApJ, 795, 60.

Høg, E., Fabricius, C., Makarov, V. V. et al., 2000, A&A, 355, 19.

Holman, M. J. & Wiegert, P. A., 1999, AJ, 117, 621.

Hung, L.-W., Duchene, G., Arriaga, P. et al., 2015, ApJ, 815, 14.

Jang-Condell, H., Chen, C. H., Mittal, T. et al., 2015, ApJ, 808, 167.

Janson, M., Brandt, T. D., Moro-Martin, A. et al., 2013, ApJ, 773, 73.

Jarrett, T. H., Cohen, M., Masci, F. et al, 2011, ApJ, 735, 112.

Jourdain de Muizon, M., Laureijs, R. J., Dominik, C. et al., 1999, A&A, 350, 875.

Judge, P. G., Solomon, S. C, & Ayres, T. R., 2003, ApJ, 593, 534.

Jura, M., 1991, ApJ, 383, 79.

Jura, M., Chen, C. H., Furlan, E. et al., 2004, ApJS, 154, 453.

Kains, N., Wyatt, M. C., & Greaves, J. S., 2011, MNRAS, 414, 2486.

Kalas, P., Graham, J. R., Beckwith, S. V. W. et al., 2002, ApJ, 567, 999.

Kalas, P., Graham, J. R. & Clampin, M., 2005, *Nature*, 435, 1067.

Kalas, P., Graham, J. R., Clampin, M. C. et al., 2006, ApJ, 637, 57.

Kalas, P., Fitzgerald, M. P., & Graham, J. R., 2007a, ApJ, 661, 85.

Kalas, P., Duchene, G., Fitzgerald, M. P. et al., 2007b, ApJ, 671, 161.

Kalas, P., Graham, J. R., Chiang, E. et al., 2008, *Science*, 322, 1345.

Kalas, P., Graham, J. R., Fitzgerald, M. et al., 2013, ApJ, 775, 56.

Kharchenko, N. V., Scholz, R. -D., Piskunov, A. E. et al., 2007, *Astronomische Nachrichten*, 328, 889.

Kastner, J. H., Zuckerman, B., Hily-Blant, P. et al., 2008, A&A, 492, 469.

Kastner, J. H., Hily-Blant, P., Sacco, G. G. et al., 2010, ApJ, 723, 248.

Kennedy, G. M. & Wyatt, M. C., 2010, MNRAS, 405, 1253.

Kennedy, G. M. & Wyatt, M. C., 2011, MNRAS, 417, 2281.

Kennedy, G. M. & Wyatt, M. C., 2013, MNRAS, 433, 2334.

Kennedy, G. M., Wyatt, M. C., Sibthorpe, B. et al., 2012, MNRAS, 426, 2115.

Kennedy, G. M., Wyatt, M. C., Kalas, P. et al., 2014a, MNRAS, 438, 96.

Kennedy, G. M., Murphy, S. J., Lisse, C. M. et al., 2014b, MNRAS, 438, 3299.

Kenyon, S. J. & Bromley, B. C., 2004, ApJ, 602, 133.

Kenyon, S. J. & Bromley, B. C., 2008, ApJS, 179, 451.

Kim, J. S., Hines, D. C., Backman, D. E. et al., 2005, ApJ, 632, 659.

Koerner, D. W., Kim, S., Trilling, D. E. et al., 2010, ApJ, 710, 26.

Kospal, A., Ardila, D. R., Moor, A. et al., 2009, ApJ, 700, 73.

Kraus, A. L. & Hillenbrand, L. A., 2012, ApJ, 757, 141.

Krivov, A. V., 2010, Research in Astronomy and Astrophysics, 10, 383.

Krivov, A. V., Eiroa, C., Löhne, T. et al., 2013, ApJ, 772, 32.

Kundurthy, P., Meyer, M. R., Robberto, M. et al., 2006, AJ, 132, 2469.

Lafreniere, D., Doyon, R., Marois, C. et al., 2007, ApJ, 670, 1367.

Laureijs, R. J., Jourdain de Muizon, M., Leech, K. et al., 2002, A&A, 387, 285.

Lagrange, A.-M., Bronnefoy, M., Chauvin, G. et al., 2010, *Science*, 329, 57.

Lawler, S. M., Beichman, C. A., Bryden, G. et al., 2009, ApJ, 705, 89.

Lawler, S. M. & Gladman, B., 2012, ApJ, 752, 53.

Lebreton, J., Augereau, J.-C., Thi, W.-F. et al., 2012, A&A, 539, 17.

Lee, J. & Song, I., 2016, in prep.

Lenz, P. & Breger, M., 2005, *Communications in Astroseismology*, 146, 53.

Lestrade, J.-F., Wyatt, M. C., Bertoldi, F. et al., 2006, A&A, 460, 733.

Lestrade, J.-F., Wyatt, M. C., Bertoldi, F. et al., 2009, A&A, 506, 1455.

Lestrade, J.-F., Matthews, B. C., Sibthorpe, B. et al., 2012, A&A, 548, 86.

Lindegren, L., Lammers, U., Bastian, U. et al., 2016, arXiv:1609.04303.

Liseau, R., Eiroa, C., Fedele, D. et al., 2010, A&A, 518, 132.

Lisse, C. M., Beichman, C. A., Bryden, G. et al., 2007, ApJ, 658, 584.

Liu, M. C., Matthews, B. C., Williams, J. P. et al., 2004, ApJ, 608, 526.

Liu, Q., Wang, T. & Jiang, P., 2014, AJ, 148, 3.

Lovis, C., Mayor, M., Pepe, F. et al., 2006, *Nature*, 331, 305.

Low, F. J., Smith, P. S., Werner, M. et al., 2005, ApJ, 631, 1170.

Luhman, K. L., Adame, L., D'Allessio, P. et al., 2007, ApJ, 666, 1219.

Luhman, K. L. & Mamajek, E. E., 2012, ApJ, 758, 31.

Luo, A. -Li, Zhao, Y. -H., Deng, Li-C. et al., 2015, *Research in Astronomy and Astrophysics*, 15, 1095.

Lyo, A.-R., Lawson, W. A., Mamajek, E. E. et al., 2003, MNRAS, 338, 616.

Macintosh, B., Graham, J., Palmer, D. et al., 2006, SPIE, 6272, 62720L.

Mahdi, D., Soubiran, C., Blanco-Cuaresma, S. et al., 2016, A&A, 587, 131.

Maldonado, J., Martínez-Arnáiz, R. M., Eiroa, C. et al., 2010, A&A, 521, 12.

Maldonado, J., Eiroa, C., Villaver, E. et al., 2012, A&A, 541, 40.

Maldonado, J., Eiroa, C., Villaver, E. et al., 2015, A&A, 579, 20.

Malo, L., Doyon, R., Lafreniére, D. et al., 2013, ApJ, 762, 88.

Mamajek, E. E., Lawson, W. A., Feigelson, E. D., 1999, ApJ, 516, 77.

Mamajek, E. E. & Hillenbrand, L. A., 2008, ApJ, 687, 1264.

Maness, H. L., Kalas, P., Peek, K. M. G. et al., 2009, ApJ, 707, 1098.

Mannings, V. & Barlow, M. J., 1998, ApJ, 497, 330.

Marois, C., Macintosh, B., Barman, T. et al., 2008, *Science*, 322, 1348.

Marshall, J. P., Lohne, T., Montesinos, B. et al., 2011, A&A, 529, 117.

Marshall, J. P., Moro-Martin, A., Eiroa, C. et al., 2014, A&A, 565, 15.

Martínez-Arnáiz, R., Maldonado, J., Montes, D. et al., 2010, A&A, 520, 79.

Mason, B. D., Wycoff, G. L., Hartkopf, W. I. et al., 2001, AJ, 122, 3466.

Mathews, G. S., Pinte, C., Duchene, G. et al., 2013, A&A, 558, 66.

Matthews, B. C., Kalas, P. G. & Wyatt, M. C., 2007a, ApJ, 663, 1103.

Matthews, B. C., Greaves, J. S., Holland, W. S. et al., 2007b, PASP, 119, 842.

Matthews, B. C., Sibthorpe, B., Kennedy, G. et al., 2010, A&A, 518, 135.

Matthews, B. C., Krivov, A. V., Wyatt, M.C., Bryden, G., & Eiroa, C., 2014, *Protostars and Planets VI*, eds. H. Beuther, R. Klessen, C. Dullemond & T. Henning.

Melis, C., Zuckerman, B., Song, I., et al., 2009, ApJ, 696, 1964.

Melis, C., Zuckerman, B., Rhee, J. H. et al., 2010, ApJ, 717, L57.

Melis, C., Zuckerman, B., Rhee, J. H. et al., 2012, Nature, 487, 74.

Melis, C., Zuckerman, B., Rhee, J. H. et al., 2013, ApJ, 778, 12.

Meng, H. Y. A., Rieke, G. H., Su, K. Y. L. et al., 2012, ApJ, 751, 17.

Mennesson, B., Absil, O., Lebreton, J. et al., 2013, ApJ, 763, 119.

Merin, B., Jorgensen, J., Spezzi, L. et al., 2008, ApJS, 177, 551.

Mermilliod, J. -C., Mayor, M. & Udry, S., 2009, A&A, 498,949.

Metchev, S. A., Hillenbrand, L. A. & Meyer, M. R., 2004, ApJ, 600, 435.

Metchev, S. A., Marois, C. & Zuckerman, B., 2009, ApJ, 705, 204.

Meyer, M. R., Carpenter, J. M., Mamajek, E. E. et al., ApJ, 2008, 673, 181.

Millan-Gabet, R., Serabyn, E., Mennesson, G. et al., 2011, ApJ, 734, 67.

Millar-Blanchaer, M. A., Graham, J. R., Pueyo, L. et al., 2015, ApJ, 811, 18.

Mizusawa, T. F., Rebull, L. M., Stauffer, J. R. et al., 2012, AJ, 144, 135.

Moerchen, M. M., Telesco, C. M., Packham, C. et al., 2007a, ApJ, 655, 109.

Moerchen, M. M., Telesco, C. M., De Buizer, J. M. et al., 2007b, ApJ, 666, 109.

Moerchen, M. M., Telesco, C. M. & Packham, C., 2010, ApJ, 723, 1418.

Monin, J.-L., Guieu, S., Pinte, C. et al., 2010, A&A, 515, 91.

Moor, A., Abraham, P., Derekas, A. et al., 2006, ApJ, 644, 525.

Moor, A., Apai, D., Pascucci, I. et al., 2009, ApJ, 700, 25.

Moor, A., Pascucci, I., Kospal, A. et al., 2011, ApJS, 193, 4.

Moor, A., Juhasz, A., Kospal, A., 2013, ApJ, 777, 25.

Moor, A., Kospal, A., Abraham, P. et al., 2015, MNRAS, 447, 577.

Morales, F. Y., Werner, M. W., Bryden, G. et al., 2009, ApJ, 699, 1067.

Morales, Farisa Y., Rieke, G. H., Werner, M. W., 2011, ApJ, 730, L29.

Morales, Farisa Y., Padgett, D., Bryden, G. et al., 2012, ApJ, 757, 7.

Morales, F. Y., Bryden, G., Werner, M. W. et al., 2013, ApJ, 776, 111.

Moro-Martin, A., Carpenter, J. M., Meyer, M. R. et al., 2007, ApJ, 658, 1312.

Moro-Martin, A., Malhotra, R., Carpenter, J. M. et al., 2007a, ApJ, 668, 1165.

Moro-Martin, A., Wyatt, M. C., Malhotra, R., Trilling, D. E., 2008, In *The Solar System Beyond Neptune*, ed. A. Barucci et al., 465.

Moro-Martin, A., Malhotra, R., Bryden, G. et al., 2010, ApJ, 717, 1123.

Moro-Martin, A., 2013, In *Planets, Stars and Stellar Systems*, ed. Oswalt, T. et al., 431.

Mortier, A., Santos, N. C., Sousa, S. et al., 2013, A&A, 551, 112.

Moultaka, J., Ilovaisky, S. A., Prugniel, P. et al., 2004, PASP, 116, 693.

Murphy, S. J. & Lawson, W. A., 2015, MNRAS, 447, 1267.

Najita, J. & Williams, J. P., 2005, ApJ, 635, 625.

Nesvorný, D., Jenniskens, P., Levison, H. F. et al., 2010, ApJ, 713, 816.

Nilsson, R., Liseau, R., Brandeker, A. et al., 2009, A&A, 508, 1057.

Nilsson, R., Liseau, R., Brandeker, A. et al., 2010, A&A, 518, 40.

Noyes, R. W., Hartmann, L. W., Baliunas, S. L. et al., 1984, ApJ, 279, 763.

Olofsson, J., Henning, Th., Nielbock, M. et al., 2013, A&A, 551, 134.

Oudmaijer, R. D., van der Veen, W. E. C. J., Waters, L. B. F. M. et al., 1992, A&AS, 96, 625.

Panic, O., Holland, W. S, Wyatt, M. C. et al., 2013, MNRAS, 435, 1037.

Panic, O., Ratzka, Th., Mulders, G. D. et al., 2014, A&A, 562, 101.

Pascucci, I, Apai, D., Hardegree-Ullman, E. E. et al., 2008, ApJ, 673, 477.

Patel, Rahul I., Metchev, S. A., & Heinze, A., 2014, ApJS, 212, 10.

Patience, J., Bulger, J., King, R. et al., 2011, A&A, 531, 17.

Patten, B. M. & Willson, L. A., 1991, AJ, 102, 323.

Pawellek, N., Krivov, A. V., Marshall, J. P. et al., 2014, ApJ, 792, 65.

Pecaut, M. J., Mamajek, E. E. & Bubar, E. J., 2012, ApJ, 746, 154.

Pecaut, M. J. & Mamajek, E. E., 2016, MNRAS, 461, 794.

Perrot, C., Boccaletti, A., Pantin, E. et al., 2016, A&A, 590, 7.

Perrin, M. D., Duchéne, G., Millar-Blanchaer, M. et al., 2015, ApJ, 799, 182.

Perryman, M. A. C., Brown, A. G. A., Lebreton, Y., 1998, A&A, 331, 81.

Peterson, D. E., Caratti o Garatti, A., Bourke, T. L. et al., 2011, ApJS, 194, 43.

Pilbratt, G. L., Riedinger, J. R., Passvogel, T. et al., 2010, A&A, 518, L1.

Platais, I., Melo, C., Mermilliod, J. -C. et al., 2007, A&A, 461, 509.

Plavchan, P., Jura, M., Lipscy, S. J., 2005, ApJ, 631, 1161.

Plavchan, P., Werner, M. W., Chen, C. H. et al., 2009, ApJ, 698, 1068.

Poglitsch, A., Waelkens, C., Geis, N. et al., 2010, A&A, 518, 2.

Preibisch, T. & Zinnecker, H., 1999, AJ, 117, 2381.

Pribulla, T., Sebastian, D., Ammler-von Eiff, M. et al., 2014, MNRAS, 443, 2815.

Prugniel, P., Soubiran, C., Koleva, M. et al., 2007, VizieR Online Data Catalog, 3251, 0.

Prugniel, P., Vauglin, I. & Koleva, M., 2011, A&A, 531, 165.

Ramírez, R., Neuerburg, N., Fernández-Serra, M. -V. et al., 2012, ApJ, 756, 46.

Rebull, L. M., Stauffer, J. R., Megeath, S. T. et al., 2006, ApJ, 646, 297.

Rebull, L. M., Stapelfeldt, K. R., Werner, M. W. et al., 2008, ApJ, 681, 1484.

Rebull, L. M., Padgett, D. L., McCabe, C.-E. et al., 2010, ApJS, 186, 259.

Rhee, J. H., Song, I., Zuckerman, B., & McElwain, M., 2007, ApJ, 660, 1556.

Rhee, J. H., Song, I., & Zuckerman, B., 2007b, ApJ, 671, 616.

Rhee, J. H., Song, I., & Zuckerman, B., 2008, ApJ, 675, 777.

Riaz, B., Mullan, D. J. & Gizis, J. E., 2006, ApJ, 650, 1133.

Riaz, B. & Gizis, J. E., 2012, A&A, 548, 54.

Ricci, L., Testi, L., Natta, A. et al., 2014, ApJ, 791, 20.

Reid, I. N., Turner, E. L., Turnbull, M. C. et al., 2007, ApJ, 665, 767.

Rieke, G. H., Su, K. Y., Stansberry, J. A. et al., 2005, ApJ, 620, 1010.

Ritchey, A. M., Gonzalez, G., Stone, M. et al., 2014, IAUS 299, 356.

Riviere-Marichalar, P., Menard, F., Thi, W. F. et al., 2012a, A&A, 538, 3.

Riviere-Marichalar, P., Barrado, D., Augereau, J.-C. et al., 2012b, A&A, 546, 8.

Riviere-Marichalar, P., Pinte, C., Barrado, D. et al., 2013, A&A, 555, 67.

Riviere-Marichalar, P., Barrado, D., Montesinos, B. et al., 2014, A&A, 565, 68.

Rizzuto, A. C., Ireland, M. J., & Zucker, D. B., 2012, MNRAS, 421, 97.

Roberge, A. & Weinberger, A. J., 2008, ApJ, 676, 509.

Roberge, A., Chen, C. H., Millan-Gabet, R. et al., 2012, PASP, 124, 799.

Roccatagliata, V., Henning, Th., Wolf, S. et al., 2009, A&A, 497, 409.

Rodigas, T. J., Hinz, P. M., Leisenring, J. et al., 2012, ApJ, 752, 57.

Rodigas, T. J., Debes, J. H., Hinz, P. M. et al., 2014, ApJ, 783, 21.

Rodigas, T. J., Stark, C. C., Weinberger, A. et al., 2015, ApJ, 798, 96.

Rodriguez, D. R. & Zuckerman, B., 2012, ApJ, 745, 147.

Rodriguez, D. R., Duchêne, G., Tom, H. et al., 2015, MNRAS, 449, 3160.

Royer, F., Grenier, S., Baylac, M. -O. et al., 2002, A&A, 393, 897.

Royer, F., Zorec, J. & Gómez, A. E., 2007, A&A, 463, 671.

Royer, F., Jégouzo, I., Tajahmady, F. et al., 2012, *ASP Conference Series*, eds. P. Ballester, D. Egret, N. P. F. Lorente, San Francisco, ASP, 431.

Sadakane, K. & Nishida, M., 1986, PASP, 98, 685.

Saffe, C. & Gomez, M., 2004, A&A, 423, 221.

Santos, N. C., Sousa, S. G., Mortier, A. et al., 2013, A&A, 556, 150.

Schatzman, E., 1962, *Annales d'Astrophysique*, 25, 18.

Schneider, G., Weinberger, A. J., Becklin, E. E. et al., 2009, AJ, 137, 53.

Schneider, A., Song, I., Melis, C. et al., 2012, ApJ, 757, 163.

Schneider, A., Song, I., Melis, C. et al., 2013, ApJ, 777, 78.

Schröder, C., Reiners, A. & Schmitt, J. H. M. M., 2009, A&A, 493, 1099.

Shu, F., Najita, J., Ostriker, E. et al., 1994, ApJ, 429, 781.

Sicilia-Aguilar, A., Bouwman, J., Juhasz, A. et al., 2009, ApJ, 701, 1188.

Siegler, N., Close, L. M, Burgasser, A. J. et al., 2007, AJ, 133, 2320.

Sierchio, J. M., Rieke, G. H., Su, K. Y. L. et al., 2010, ApJ, 712, 1421.

Siess L., Dufour E., Forestini M., 2000, A&A, 358, 593.

Silverstone, M. D., Meyer, M. R., Mamajek, E. E. et al., 2006, ApJ, 639, 1138.

Smith, B. A. & Terrile, R. J., 1984, *Science*, 226, 1421.

Smith, P. L., Hines, D. C., Low, F. J. et al, 2006, ApJ, 644, 125.

Smith, R., Wyatt, M. C. & Dent, W. R. F, 2008, A&A, 485, 897.

Smith, R., Churcher, L. J., Wyatt, M. C. et al., 2009, A&A, 493, 299.

Smith, R., Wyatt, M. C. & Haniff, C. A., 2009b, A&A, 503, 265.

Smith, R. & Wyatt, M. C., 2010, A&A, 515, 95.

Smith, R., Jeffries, R. D., & Oliveira, J. M., 2011, MNRAS, 411, 2186.

Smith, R. & Jeffries, R. D., 2012, MNRAS, 420, 2884.

Soderblom, J. M., 2010, ARA&A, 48, 581.

Soderblom, J. M., Hillenbrand, L. A., Jeffries, R. D. et al., 2014, *Protostars and Planets IV*, ed. H. Beuther, R. Klessen, C. Dullemond, Th. Henning, Tucson, Univ. Ariz. Press, 1.

Song, I., Caillault, J.-P., Barrado y Navascues, D. et al., 2001, ApJ, 546, 352.

Song, I., Weinberger, A. J., Becklin, E. E. et al., 2002, AJ, 124, 514.

Song, I., Zuckerman, B. & Bessell, M. S., 2003, ApJ, 599, 342.

Song, I., Zuckerman, B. & Bessell, M. S., 2004, ApJ, 614, 125.

Song, I., Zuckerman, B., Weinberger, A. J. et al., 2005, *Nature*, 436, 363.

Soubiran, C., Le Campion, J. -F., Brouillet, N. et al., 2016, A&A, 591, 118.

Soummer, R., Perrin, M. D., Pueyo, L. et al., 2014, ApJ, 786, 23.

Spangler, S. R., Sargent, A. I., Silverstone, M. D. et al., 2001, ApJ, 555, 932.

Stauffer, J. R., Hartmann, L. W., Fazio, G. G. et al., 2007, ApJS, 172, 663.

Steele, A., Hughes, A. M., Carpenter, J. et al, 2016, ApJ, 816, 27.

Stock, N. D., Su, K. Y. L., Liu, W. et al., 2010, ApJ, 724, 1238.

Strassmeier, K., Washuettl, A., Granzer, Th. et al., 2000, A&AS, 142, 275.

Street, R. A., SuperWASP Consortium, 2004, *Baltic Astronomy*, 13, 707.

Strom, R. G., Malhotra, R., Ito, T. et al., 2005, *Science*, 309, 1847.

Su, K. Y. L., Rieke, G. H., Misselt, K. A. et al., 2005, ApJ, 628, 487.

Su, K. Y. L., Rieke, G. H., Stansberry, J. A. et al., 2006, ApJ, 653, 675.

Su, K. Y. L., Rieke, G. H., Stapelfeldt, K. R. et al., 2008, ApJ, 679, 125.

Su, K. Y. L., Rieke, G. H., Stapelfeldt, K. R. et al., 2009, ApJ, 705, 314.

Su, K. Y. L., Rieke, G. H., Malhotra, R. et al., 2013, ApJ, 763, 118.

Sylvester, R. J., Dunkin, S. K., & Barlow, M. J., 2001, MNRAS, 327, 133.

Tanner, A., Beichman, C., Bryden, G. et al., 2009, ApJ, 704, 109.

Taylor, B. J. & Joner, M. D., 2005, ApJS, 159, 100.

Thalmann, C., Janson, M., Buenzli, E. et al., 2013, ApJ, 763, 29.

Thalmann, C., Desidera, S., Bonavita, M. et al., 2014, A&A, 572, 91.

Theissen, C. & West, A., 2014, ApJ, 794, 146.

Thompson, M. A., Smith, D. J. B., Stevens, J. A. et al., 2010, A&A, 518, 134.

Thureau, N. D., Greaves, J. S., Matthews, B. C. et al., 2014, MNRAS, 445, 2558.

Trilling, D. E., Stansberry, J. A., Stapelfeldt, K. R. et al., 2007, ApJ, 658, 1289.

Trilling, D. E., Bryden, G., Beichman, C. A. et al., 2008, ApJ, 674, 1086.

Tsantaki, M., Sousa, S. G., Adibekyan, V. Zh. et al., 2013, A&A, 555, 150.

Urban, L. E., Rieke, G., Su, K. et al., 2012, ApJ, 750, 98.

van Leeuwen, F., 2007, A&A, 474, 653.

Vandenbussche, B., Sibthorpe, B., Acke, B. et al., 2010, A&A, 518, 133.

Vican, L., 2012, AJ, 143, 135.

Vican, L. & Schneider, A., 2014, ApJ, 780, 154.

Vitense, C., Krivov, A. V., Kobayashi, H. et al., 2012, A&A, 540, 30.

Voges, W., Aschenbach, B., Boller, T. et al., 1999, VizieR Online Data Catalog, 9010, 0.

Wahhaj, Z., Cieza, L., Koerner, D. W. et al., 2010, ApJ, 724, 835.

Wahhaj, Z., Liu, M. C., Nielsen, E. L. et al., 2013, ApJ, 773, 179.

Walker, H. J. & Wolstencroft, R. D., 1988, PASP, 100, 1509.

Weinberger, A. J., Becklin, E. E., Schneider, G. et al., 1999, ApJ, 525, 66.

Weinberger, A. J., Beklin, E. E. & Zuckerman, B., 2003, ApJ, 584, 33.

Weinberger, A. J., 2008, ApJ, 679, 41.

Weinberger, A. J., Becklin, E. E., Song, I. et al., 2011, ApJ, 726, 72.

White, R. J., Gabor, J. M. & Hillenbrand, L. A., 2007, AJ, 133, 2524.

White, J. A., Boley, A. C., Hughes, A. M. et al., 2016, ApJ, 829, 6.

Williams, J. P. & Andrews, S. M., 2006, ApJ, 653, 1480.

Williams, J. P. & Cieza, L. A., 2011, ARA&A, 49, 67.

Wilner, D. J., Andrews, S. M. & Hughes, A. M. et al., 2011, ApJ, 727, 42.

Wilson, O. C., 1968, ApJ, 153. 221.

Wilson, P. A., Hébrard, G., Santos, N. C. et al., 2016, A&A, 588, 144.

Wittenmyer, R. A., Tan, X., Lee, M. H. et al., 2014, ApJ, 780, 140.

Wright, J. T., Marcy, G. W., Butler, R. P. et al., 2004, ApJS, 152. 261.

Wright, E. L., Eisenhardt, P., Mainzer, A. et al., 2010, AJ, 140, 1868.

Wu, Chao-Jian, Wu, Hong, Lam, Man-I. et al., 2013, ApJS, 208, 29.

Wyatt, M. C., Dent, W. R. F. & Greaves, J. S., 2003, MNRAS, 342, 876.

Wyatt, M. C., Smith, R., Greaves, J. S. et al., 2007a, ApJ, 658, 569.

Wyatt, M. C., Smith, R., Su, K. Y. L. et al., 2007, ApJ, 663, 365.

Wyatt, Mark C., 2008, ARA&A, 46, 339.

Wyatt, M. C., Kennedy, G., Sibthorpe, B. et al., 2012, MNRAS, 424, 1206.

Wyatt, M. C., Pani, O, Kennedy, G. M. et al., 2015, *Ap&SS*, 357, 103.

Young, E. T., Beckline, E. E., Marcum, P. M. et al., 2012, ApJ, 749, 17.

Zorec, J. & Royer, F., 2012, A&A, 537, 120.

Zuckerman, B., 2001, ARA&A, 39, 549.

Zuckerman, B. & Song, I., 2004a, ApJ, 603, 738.

Zuckerman, B. & Song, I., 2004b, ARA&A, 42, 685.

Zuckerman, B., Rhee, J. H., Song, I. et al., 2011, ApJ, 732, 61.

Zuckerman, B., Melis, C., Rhee, J. H. et al., 2012, ApJ, 752, 58.

Zuckerman, B., & Song, I., 2012, ApJ, 758, 77.